CHRONIC INFLAMMATION AND NEURODEGENERATION IN RETINAL DISEASE, VOLUME II

EDITED BY: Settimio Rossi, Claudio Bucolo and Julie Sanderson
PUBLISHED IN: Frontiers in Pharmacology

frontiers Research Topics

ISSN 1664-8714
ISBN 978-2-88976-428-0
DOI 10.3389/978-2-88976-428-0

About Frontiers

Frontiers is more than just an open-access publisher of scholarly articles: it is a pioneering approach to the world of academia, radically improving the way scholarly research is managed. The grand vision of Frontiers is a world where all people have an equal opportunity to seek, share and generate knowledge. Frontiers provides immediate and permanent online open access to all its publications, but this alone is not enough to realize our grand goals.

Frontiers Journal Series

The Frontiers Journal Series is a multi-tier and interdisciplinary set of open-access, online journals, promising a paradigm shift from the current review, selection and dissemination processes in academic publishing. All Frontiers journals are driven by researchers for researchers; therefore, they constitute a service to the scholarly community. At the same time, the Frontiers Journal Series operates on a revolutionary invention, the tiered publishing system, initially addressing specific communities of scholars, and gradually climbing up to broader public understanding, thus serving the interests of the lay society, too.

Dedication to Quality

Each Frontiers article is a landmark of the highest quality, thanks to genuinely collaborative interactions between authors and review editors, who include some of the world's best academicians. Research must be certified by peers before entering a stream of knowledge that may eventually reach the public - and shape society; therefore, Frontiers only applies the most rigorous and unbiased reviews.
Frontiers revolutionizes research publishing by freely delivering the most outstanding research, evaluated with no bias from both the academic and social point of view. By applying the most advanced information technologies, Frontiers is catapulting scholarly publishing into a new generation.

What are Frontiers Research Topics?

Frontiers Research Topics are very popular trademarks of the Frontiers Journals Series: they are collections of at least ten articles, all centered on a particular subject. With their unique mix of varied contributions from Original Research to Review Articles, Frontiers Research Topics unify the most influential researchers, the latest key findings and historical advances in a hot research area! Find out more on how to host your own Frontiers Research Topic or contribute to one as an author by contacting the Frontiers Editorial Office: frontiersin.org/about/contact

CHRONIC INFLAMMATION AND NEURODEGENERATION IN RETINAL DISEASE, VOLUME II

Topic Editors:
Settimio Rossi, Second University of Naples, Italy
Claudio Bucolo, University of Catania, Italy
Julie Sanderson, University of East Anglia, United Kingdom

Citation: Rossi, S., Bucolo, C., Sanderson, J., eds. (2022). Chronic Inflammation and Neurodegeneration in Retinal Disease, Volume II. Lausanne: Frontiers Media SA. doi: 10.3389/978-2-88976-428-0

Table of Contents

frontiers | Frontiers in Pharmacology

EDITORIAL
published: 31 May 2022
doi: 10.3389/fphar.2022.915960

Editorial: Chronic Inflammation and Neurodegeneration in Retinal Disease, Volume II

Claudio Bucolo[1]*, *Julie Sanderson*[2] *and Settimio Rossi*[3]

[1]Department of Biomedical and Biotechnological Sciences, School of Medicine, University of Catania, Catania, Italy, [2]University of East Anglia, School of Pharmacy, Faculty of Science, Norwich, United Kingdom, [3]Multidisciplinary Department of Medical, Surgical and Dental Sciences, University of Campania "Luigi Vanvitelli", Naples, Italy

Keywords: inflammation, retinal diseases, diabetic retinopathy, age-related macular degeneration, retinitis pigmentosa

Editorial on the Research Topic

Chronic Inflammation and Neurodegeneration in Retinal Disease

Inflammation and neurodegeneration have a widely recognized role in the pathogenesis of the main retinal conditions. However, the exact mechanism through which inflammation causes alteration of the retinal structure—with consequent dysfunction of the retinal pigment epithelium, of neurons, and ultimately of photoreceptors—is not entirely known. This Research Topic "*Chronic Inflammation and Neurodegeneration in Retinal Disease, Volume II*" presents eight original research articles and one mini review from seven different countries with important contributions in the field of retinal inflammation. Most of the contributions are related to diabetic retinopathy (DR), the others cover age-related macular degeneration (AMD), retinitis pigmentosa, and the spontaneous polygenic model of inherited retinal dystrophy.

The review by Stravalaci et al. focused on long pentraxin 3 (PTX3), an emerging new player in ocular homeostasis and a potential pharmacological target in neurodegenerative disorders of the retina. Physiologically present in the human eye and induced in inflammatory conditions, this protein is strategically positioned at the blood retinal barrier interface, where it acts as a "molecular trap" for complement and modulates inflammation both in homeostatic and pathological conditions such as AMD and DR. Gesualdo et al. presented an interesting study on fingolimod and DR, investigating the interactions between fingolimod, a sphingosine 1-phosphate receptor (S1PR) agonist, and melanocortin receptors 1 and 5 (MCR1, MCR5). This Research Topic is a typical example of repurposing since fingolimod is a drug approved to treat relapsing-remitting multiple sclerosis. The authors demonstrated, in an *in vivo* model of DR, that fingolimod has anti-angiogenic activity mediated not only through S1P1R, but also by melanocortin receptors. Another interesting pre-clinical study on DR was provided by Canovai et al. The authors showed the efficacy of a novel substance containing cyanidin-3-glucoside (C3G), verbascoside, and zinc to maintain the integrity of the blood retinal barrier and retinal function in streptozotocin-induced diabetic rats.

Accumulating data provide evidence for a pivotal role of Müller cells in the pathogenesis of DR. In this regard the *in vitro* study by Schmalen et al. underlined the importance of Müller cell signaling in the inflamed retina, indicating an active role in chronic retinal inflammation. These authors demonstrated an intense signaling capacity of Müller cells, which reacted in a highly discriminating manner upon treatment with different cytokines, showing several characteristics of atypical antigen-presenting cells.

OPEN ACCESS

Edited and reviewed by:
Dieter Steinhilber,
Goethe University Frankfurt, Germany

***Correspondence:**
Claudio Bucolo
claudio.bucolo@unict.it

Specialty section:
This article was submitted to Inflammation Pharmacology, a section of the journal Frontiers in Pharmacology

Received: *08 April 2022*
Accepted: *20 April 2022*
Published: *31 May 2022*

Citation:
Bucolo C, Sanderson J and Rossi S (2022) Editorial: Chronic Inflammation and Neurodegeneration in Retinal Disease, Volume II. Front. Pharmacol. 13:915960. doi: 10.3389/fphar.2022.915960

An important clinical contribution on the Research Topic of DR has been provided by Parravano et al., where the authors carried out a randomized clinical trial on patients with diabetic macular edema (DME) treated with a special oral curcumin formulation with a polyvinylpyrrolidone-hydrophilic carrier and intravitreal injections of dexamethasone. They demonstrated a significant reduction in central retinal and inner retinal layer thickness with the combined therapy in patients affected by DME. This study also showed that the pharmacological combination therapy (curcumin and dexamethasone) was well-tolerated. On this regard, a good long-term safety profile of intravitreal dexamethasone has been demonstrated on real-world studies when used to manage DME (Bucolo et al., 2018). Further, these findings are in line with recent literature data that showed retinal protective effects by curcumin against high glucose damage (Bucolo et al., 2019). Another important contribution on the Research Topic of DME is the bibliometric study and visualization analysis by Lin et al.. They used CiteSpace and VOSviewer software to evaluate the Web of Science Core Collection publications and to build visualizing maps to describe the research progress on the use of steroids to treat DME. They concluded that while anti-VEGF therapy is the first-line treatment for DME and retinal vein occlusion (RVO)-induced macular edema, steroid implant is a valid option for DME patients not responding to anti-VEGF therapy and non-DME patients with macular edema. The final contribution on the topic of DME focused on the anti-inflammatory effects of subthreshold micropulse yellow laser (SMYL). The authors, Bonfiglio et al., demonstrated that SMYL may reduce macular thickening and improve best-corrected visual acuity in eyes with persistent macular edema after pars plana vitrectomy and membrane peeling for tractional DME.

A group of scientists from University of Tennessee (Hollingsworth et al.) have used systems genetics to identify possible models of spontaneous polygenic AMD by mining the BXD family of mice using single nucleotide polymorphism analyses of known genes associated with the human retinal disease. The goal of these scientists was to propose a pre-clinical mouse model (BXD32) to better understand the pathophysiology of progressive retinal dystrophies and discover efficacious treatments. Their study demonstrated that the BXD32 mouse strain exhibits a severe neurodegenerative phenotype accompanied by adverse effects on the retinal vasculature. Finally, Canto et al. showed that sulforaphane, a natural compound, modulates the inflammation and delays neurodegeneration in a retinitis pigmentosa (RP) mouse model. Specifically, they assessed the modulation of glial cells in the RP rd10 mouse model showing that sulforaphane treatment regulated the microglial activation state.

Overall, the contributions of the present Topic Research focused on inflammation and retinal degeneration, highlighting new insights in retinal diseases mechanisms and novel pharmacological approaches.

AUTHOR CONTRIBUTIONS

All authors listed have made a substantial, direct, and intellectual contribution to the work and approved it for publication.

REFERENCE

Bucolo, C., Gozzo, L., Longo, L., Mansueto, S., Vitale, D. C., and Drago, F. (2018). Long-term Efficacy and Safety Profile of Multiple Injections of Intravitreal Dexamethasone Implant to Manage Diabetic Macular Edema: A Systematic Review of Real-World Studies. *J. Pharmacol. Sci.* 138 (4), 219–232. doi:10.1016/j.jphs.2018.11.001

Bucolo, C., Drago, F., Maisto, R., Romano, G. L., D'Agata, V., and Maugeri, G. (2019). Curcumin Prevents High Glucose Damage in Retinal Pigment Epithelial Cells Through ERK1/2-Mediated Activation of the Nrf2/HO-1 Pathway. *J Cell Physiol* 234 (10), 17295–17304. doi:10.1002/jcp.28347

Conflict of Interest: The authors declare that the research was conducted in the absence of any commercial or financial relationships that could be construed as a potential conflict of interest.

frontiers in Pharmacology

ORIGINAL RESEARCH
published: 17 September 2021
doi: 10.3389/fphar.2021.718902

Fingolimod and Diabetic Retinopathy: A Drug Repurposing Study

Carlo Gesualdo[1†], Cornel Balta[2†], Chiara Bianca Maria Platania[3†], Maria Consiglia Trotta[4†], Hildegard Herman[2], Sami Gharbia[2], Marcel Rosu[2], Francesco Petrillo[5], Salvatore Giunta[3], Alberto Della Corte[1], Paolo Grieco[6], Rosa Bellavita[6], Francesca Simonelli[1], Michele D'Amico[4], Anca Hermenean[2,7‡], Settimio Rossi[1‡] and Claudio Bucolo[3‡]*

[1]Multidisciplinary Department of Medical, Surgical and Dental Sciences, University of Campania "Luigi Vanvitelli", Naples, Italy, [2]"Aurel Ardelean" Institute of Life Sciences, Vasile Godis Western University of Arad, Arad, Romania, [3]Department of Biomedical and Biotechnological Sciences, School of Medicine, University of Catania, Catania, Italy, [4]Department of Experimental Medicine, University of Campania "Luigi Vanvitelli", Naples, Italy, [5]Department of Ophthalmology, University of Catania, Catania, Italy, [6]Pharmacy Department, University of Naples Federico II, Naples, Italy, [7]Department of Histology, Faculty of Medicine, Vasile Goldis Western University of Arad, Arad, Romania

OPEN ACCESS

Edited by:
Galina Sud'ina,
Lomonosov Moscow State University, Russia

Reviewed by:
Kurt Neumann,
Independent researcher, Kerékteleki, Hungary
Ivan Senin,
Lomonosov Moscow State University, Russia

***Correspondence:**
Carlo Gesualdo
carlo.gesualdo@unicampania.it

†These authors share first authorship

‡These authors share last authorship

Specialty section:
This article was submitted to Inflammation Pharmacology, a section of the journal Frontiers in Pharmacology

Received: 01 June 2021
Accepted: 20 August 2021
Published: 17 September 2021

Citation:
Gesualdo C, Balta C, Platania CBM, Trotta MC, Herman H, Gharbia S, Rosu M, Petrillo F, Giunta S, Della Corte A, Grieco P, Bellavita R, Simonelli F, D'Amico M, Hermenean A, Rossi S and Bucolo C (2021) Fingolimod and Diabetic Retinopathy: A Drug Repurposing Study. Front. Pharmacol. 12:718902. doi: 10.3389/fphar.2021.718902

This study aimed to investigate the interactions between fingolimod, a sphingosine 1-phosphate receptor (S1PR) agonist, and melanocortin receptors 1 and 5 (MCR1, MCR5). In particular, we investigated the effects of fingolimod, a drug approved to treat relapsing-remitting multiple sclerosis, on retinal angiogenesis in a mouse model of diabetic retinopathy (DR). We showed, by a molecular modeling approach, that fingolimod can bind with good-predicted affinity to MC1R and MC5R. Thereafter, we investigated the fingolimod actions on retinal MC1Rs/MC5Rs in C57BL/6J mice. Diabetes was induced in C57BL/6J mice through streptozotocin injection. Diabetic and control C57BL/6J mice received fingolimod, by oral route, for 12 weeks and a monthly intravitreally injection of MC1R antagonist (AGRP), MC5R antagonist (PG20N), and the selective S1PR1 antagonist (Ex 26). Diabetic animals treated with fingolimod showed a decrease of retinal vascular endothelial growth factor A (VEGFA) and vascular endothelial growth factor receptors 1 and 2 (VEGFR1 and VEGFR2), compared to diabetic control group. Fingolimod co-treatment with MC1R and MC5R selective antagonists significantly ($p < 0.05$) increased retinal VEGFR1, VEGFR2, and VEGFA levels compared to mice treated with fingolimod alone. Diabetic animals treated with fingolimod plus Ex 26 (S1PR1 selective blocker) had VEGFR1, VEGFR2, and VEGFA levels between diabetic mice group and the group of diabetic mice treated with fingolimod alone. This vascular protective effect of fingolimod, through activation of MC1R and MC5R, was evidenced also by fluorescein angiography in mice. Finally, molecular dynamic simulations showed a strong similarity between fingolimod and the MC1R agonist BMS-470539. In conclusion, the anti-angiogenic activity exerted by fingolimod in DR seems to be mediated not only through S1P1R, but also by melanocortin receptors.

Keywords: fingolimod, sphingosine 1-phosphate receptor, melanocortin receptor 1, melanocortin receptor 5, diabetic retinopathy

INTRODUCTION

Fingolimod, an analog of myriocin (Mehling et al., 2011), is a sphingosine 1-phosphate receptors agonist (S1PRs), and it is used in monotherapy for the treatment of relapsing-remitting multiple sclerosis (RR-MS) (Cohen et al., 2010; Kappos et al., 2010). The modulation of the S1P1R activity could be useful for treatment of several diseases that share immune-inflammatory pathogenic mechanisms, such as rheumatoid arthritis, fibrosis, choroidal neovascularization (CNV), and diabetic retinopathy (DR) (Bing et al., 2009; Mehling et al., 2011; Yoshida et al., 2013; Fan and Yan, 2016). To this regard, recent studies have shown a protective role of fingolimod in a rat model of DR induced by intraperitoneal injection of streptozotocin (STZ): this anti-inflammatory action was exerted by a reduction of pro-inflammatory cytokines and molecules of adhesion to the vessel wall (Fan and Yan, 2016). Moreover, fingolimod was able to reduce vascular permeability, increasing tight junctions expression in the blood retinal barrier (Fan and Yan, 2016). Additionally, several studies reported a preserved macular structure and thickness over time in RR-MS patients treated with fingolimod (Fruschelli et al., 2019; d'Ambrosio et al., 2020). Worthy of note, although macular edema is reported as a side effect of fingolimod administration with an incidence of 0.3–1.2% (Nolan et al., 2013), two studies evidenced that RR-MS patients treated with fingolimod did not show any case of macular edema (Fruschelli et al., 2019; Rossi et al., 2020).

We have previously shown that activation of melanocortin receptors 1 and 5 (MC1R and MC5R) reduced retinal damage in mouse model of DR, preventing alterations of blood retinal barrier and reducing local pro-inflammatory and pro-angiogenic mediators such as cytokines, chemokines, and vascular endothelial growth factor (VEGF) (Maisto et al., 2017; Rossi et al., 2021). Interestingly, recent evidence showed that S1PR1 with melanocortin signaling pathway can play an important role in the regulation of energy homeostasis of hypothalamic neurons in rodents (Silva et al., 2014). With a virtual screening approach aimed at drug repurposing in DR, we first identified fingolimod as putative ligand for MC1R and MC5R. Indeed, we hypothesized that the interplay between sphingosine pathway and melanocortin pathway could also occur at the level of ocular structures. Therefore, we hypothesized that fingolimod may be protective in retinal degenerative diseases, such as DR, through binding at melanocortin receptors. Therefore, in the present study we investigated the interaction between fingolimod and melanocortin receptors in an animal model of DR, using pharmacological tools such as selective MC1R and MC5R antagonists.

MATERIALS AND METHODS

Molecular Modeling

Structural models of human melanocortin receptor 1 (hMC1R) and human melanocortin receptor 5 (hMC5R) were built with the Advanced Homology Modeling task of Schrödinger Maestro, using as primary sequences for hMC1R and the hMC5R, FASTA files from accession numbers Q01726.2 and NP_005904.1, respectively. Both models were built using as a template the x-ray structure of human melanocortin receptor 4 (PDB:6W25); because the Advance Homology Modeling Task gave, for this template, the highest scores for both the hMC1R (score 437, identity 43%, homology 60%, gaps 5%) and hMC5R (score 591, identity 60%, homology 75%, gaps 4%). The structural optimization (Prime energy minimization) of hMC1R and hMC5R led to similar structural models at least in the transmembrane domain (RMSD = 0.463Å). Therefore, as previously shown (Platania et al., 2012), in order to differentiate the two structural models, we carried out molecular dynamics simulation of hMC1R and hMC5R in an explicit water-membrane system, with Desmond Molecular Dynamics Simulation Task of Schrödinger Maestro. Specifically, an orthorhombic box has been created, the receptors were included in a 30 $Å^3$ POPC lipid membrane-water system according to output from OMP database (https://opm.phar.umich.edu/). TIP3P water molecules were added to the system, along with NaCl (150 mM). After membrane protein equilibration protocol, 6 ns NPγT ensemble production runs were carried out. After simulations of the two membrane receptor systems, molecular dynamics has been clustered in five clusters by means of Desmond Trajectory Analysis Clustering Task, based on RMSD values and applying the cut-off of 10 for frequency value. Therefore, we built for each 10 clusters (5 for hMC1R and 5 for hMC5R) a grid centered on pocket identified by SiteMap task. The grid was built tacking into account the peptide docking option. After that, selective active MCxR ligands were docked with Glide docking task, by taking advantage of ensemble docking option (i.e., multiple rigid receptor conformations). Ligand-receptor complexes were rescored with application of MM-GBSA calculation. Specifically, for MM-GBSA calculation, residues within 15 Å from ligands were free to move during minimization protocol, applying an implicit solvation and membrane model, according to protocol already published (Stark et al., 2020). Agouti related protein (AGRP) structure, an MC1R antagonist, was retrieved from the PDB: 1MR0, and subjected to energy minimization in implicit water model with Prime (Schrodinger Maestro). The BMS-470539 (BMS) is a MC1R agonist, and its 2D structure was built with the webserver https://cactus.nci.nih.gov/translate/. The. sdf files for two macrocycles PG901 (MC5R agonist) and PG20N (MC5R antagonist) were also built with https://cactus.nci.nih.gov/translate/. All ligands were then subjected to the LigPrep task and the ionization state was assigned at pH 7.4. Macrocycle conformation sampling task was applied to AGRP, PG901, and PG20N ligands, with the following settings: GB-SA electrostatic model, OPLS3e force-field, 5,000 simulation cycles, 5,000 Macrocycle specific LLMOD search step, and enhanced torsion sampling.

This preliminary docking step was used to rescore receptor clusters, on the basis of the docking scores and predicted $\Delta G_{binding}$ energy, relative to selective hMC1R and hMC5R ligands. After that, we carried out virtual screening of drugs already approved for several indications (Food and Drug

Administration–FDA-approved drugs database), according to our previous published protocol (Platania et al., 2020).

Fingolimod/hMC1, fingolimod/hMC5, BMS/hMC1, PG901/hMC5, AGRP/hMC1, and PG20N/hMC5 complexes were built through the molecular docking step as described above. Therefore, molecular dynamics simulations in explicit POPC membrane and TIP3P water were carried out as follows: membrane equilibration steps and 20 ns production runs, applying the same protocol described above for the unbound hMC1 and hMC5 receptors. Simulation Interaction task, within Schrödinger maestro environment, was used, providing information regarding ligand-receptor interactions. Salt-bridges of hMC1R and hMC5R ligand complexes were also analyzed with Visual Molecular Dynamics software (VMD version 1.9.3) (Humphrey et al., 1996). Differences between contact maps of ligand-receptor complexes, generated with Schrödinger Maestro, were analyzed applying Fuzzy Logic algorithm through access to the web server (https://online-image-comparison.com/). The fuzz option was set to 4 as cut-off value, to highlight the differences between contact maps.

Compounds

Fingolimod (FTY720) was purchased from MedChemExpress (Italy, catalog number HY-12005/CS-0114); Ex 26 [1-(5'-((1-(4-chloro-3-methylphenyl)ethyl)amino)-2′-fluoro-3,5-dimethyl-[1,1′-biphenyl]-4-ylcarboxamido cyclopropanecarboxylic acid)], a selective S1PR1 antagonist, from Tocris (Italy, catalog number 5833) and STZ from Santa Cruz Biotechnology (Italy, catalog number sc-200719). AGRP and PG20N, used respectively as MCR1 and MCR5 antagonists, were synthetized as previously described (Carotenuto et al., 2015; Merlino et al., 2018; Merlino et al., 2019).

Animals and Experimental Design

Animal care and experimental procedures were approved by the Institutional Ethical Committee of the "Vasile Goldis" Western University of Arad (number, 29/May 17, 2017) and were in line with the Association for Research in Vision and Ophthalmology (ARVO) Statement for the Use of Animals in Ophthalmic and Vision Research. Six-week-old C57BL/6J male mice (22.5 ± 1.6 g) (Cantacuzino National Research Institute of Bucharest, Romania) were housed in single standard cages with ad libitum access to mineral water and standard chow. They were exposed to 12 h light/12 h dark cycle, controlled humidity, and temperature. After an overnight fast, mice were intraperitoneally (i.p.) injected with a single dose of STZ (65 mgkg−1 of body weight) freshly dissolved in 50 mM sodium citrate buffer (pH 4.5) (STZ group) or with sodium citrate buffer alone as controls (CTR group). After 4 h fasting, a one-touch glucometer (Accu Chek Active, Roche Diagnostics, United States) was used to measure blood glucose levels. STZ mice showing fasting blood glucose levels higher than 2.5 gl−1 on two consecutive weeks were included in the experimental design as type 2 diabetic mice. Mice were randomized into the following experimental groups (N = 5 per group): I. control non-diabetic mice (CTR group); II. diabetic mice (STZ group) receiving intravitreally sterile phosphate saline buffer (PBS, p-H. 7.4); III. diabetic mice receiving per *os* fingolimod (STZ + Fingolimod group); IV. diabetic mice receiving per *os* fingolimod and intravitreally MC1 receptor antagonist AGRP (STZ + Fingolimod + AGRP group); V. diabetic mice receiving per *os* fingolimod and intravitreally PG20N (MC5R antagonist) (STZ + Fingolimod + PG20N group); VI. diabetic mice receiving per *os* fingolimod and intravitreally Ex 26 (selective S1PR1 receptor antagonist) (STZ + Fingolimod + Ex 26 group). Particularly, after 2 weeks from STZ injection, fingolimod was orally administered for 12 weeks at a dose of 0.3 mg/kg/day, contained in 20 ml of drinking water as calculated daily for each mouse intake (Bonfiglio et al., 2017). PBS, AGRP (14.3 μM in sterile PBS) (Rossi et al., 2021), PG20N (130 nM in sterile PBS) (Rossi et al., 2021), and Ex 26 (3 mg/kg in sterile PBS) (Cahalan et al., 2013) were administered by intravitreal injections (5 μL). These were performed after 2 weeks from STZ injection in mice with blood glucose levels higher than 2.5 gl−1 (baseline), then after 4 and 8 weeks.

Intravitreal Injections

To perform intravitreal injections, mice were anesthetized by pentobarbital (45 mg/kg in saline). To induce dilatation of pupils, tropicamide (5%) was instilled into the right eye of each animal plus tetracaine (1%) for local anesthesia. PBS, AGRP, PG20N, and EX 26 preparations (5 μL volume) were administered intravitreally into the right eye using a sterile syringe fitted with a 30-gauge needle (Microfine; Becton Dickinson AG, Meylan, France) (Rossi et al., 2021). Before the intravitreal injection, an anterior chamber paracentesis of similar volume was performed to avoid an increase of the intraocular pressure (Biswas et al., 2007).

Fluorescein Angiography

FA was performed by using a Topcon TRC-50DX apparatus (Topcon, Tokyo, Japan) after intraperitoneal injection of 10% fluorescein sterile solution (1 ml/kg body weight, AK-Fluor; Akorn, Inc.). To display the retinal vasculature and to evaluate the early DR typical alterations, C57BL/6J animals were monitored by FA over a 12-week period, with specific analyses at baseline and at weeks 4, 8, and 12. Particularly, mice were consecutively labelled from 1 to 5 in each group, to repeat FA to the same animal at each time point of the study. Vessel abnormalities (VA) were graded from 0 to 4 according to the following score: 0 = absence of vessel abnormalities; 1 = vessel thinning; 2 = vessel thinning and tortuosity; 3 = vessel thinning, tortuosity, and/or crushing; 4 = vessel thinning and tortuosity, venous beading, rosary-like vessels. The score was reported as a mean of the vascular alterations observed at the different time points during the follow-up. VA were scored by two different ophthalmologists (always the same) unaware of group labeling. At the end of the follow-up, animals were sacrificed and retina were dissected, placed in cooled PBS, then fixed by immersion in 10% neutral buffered formalin and paraffin-embedded for immunohistochemistry (Rossi et al., 2021).

Immunohistochemistry

The primary antibodies used for the immunohistochemical studies were the rabbit polyclonal anti-Vascular Endothelial Growth Factor Receptor 1 (VEGFR1) (ab32152, Abcam,

United Kingdom) and anti-Vascular Endothelial Growth Factor Receptor 2 (VEGFR2) (ab2349, Abcam, United Kingdom). Eye sections of 5 μm thickness were deparaffinized in Bond Dewax solution (Leica Biosystems, Germany) and rehydrated prior to epitope retrieval in Novocastra Epitope Retrieval solution (Leica Biosystems, Germany) (just in case of VEGFR1). After 10 min incubation with 3% H2O2, followed by the blocking solution (Novocastra Leica Biosystems, Germany) also for 10 min, the tissue sections were incubated overnight at 4 °C with anti-VEGFR1 and anti-VEGFR2 antibodies (1:100 dilution). Detection was performed using a polymer detection system (RE7280-K, Novolink max Polymer detection system, Novocastra Leica Biosystems) and 3,3′- diaminobenzidine (DAB, Novocastra Leica Biosystems) as chromogenic substrate, according to the manufacturer's instructions. Hematoxylin staining was applied before dehydration and mounting. Negative controls included substitution of the first antibody with normal rabbit serum. Images were acquired by light microscopy (Olympus BX43, Hamburg, Germany).

Enzyme-Linked Immunosorbent Assay

Vascular Endothelial Growth Factor A (VEGFA) levels were assessed in retinal lysates obtained from an adjunctive experimental set, in order to confirm IHC data on VEGFR1 and VEGFR2 expression. C57BL/6J male mice (N = 5 per group) were treated as previously described in section 2.3 and 2.4, by receiving bilateral intravitreal injections (N = 10 retinas per group). VEGFA levels were detected in retinal lysates by ELISA (MBS704351, MyBiosource, San Diego, CA, United States), following the manufacturer's instructions for tissue homogenates.

Statistical Analysis

Investigators that carried out FA and immunohistochemistry and ELISA analyses were blind to group labels. After graph design and rough statistical analysis, labels were unveiled by principal investigators. Statistical significance was assessed by one-way ANOVA, followed by Tukey's multiple comparisons test by using GraphPad Prism v.6 (GraphPad Software, La Jolla, CA, United States). Differences were considered statistically significant for p values <0.05.

RESULTS

Virtual Screening in Search of MC1R and MC5R Agonists, Repurposing of FDA Approved Drugs

Structural models of human MC1R and MC5R receptors were built with the Advanced Molecular modeling task of Schrödinger Maestro. Before virtual screening protocol, we carried out 6 ns molecular dynamics of hMC1 and hMC5 receptors embedded in an explicit water-membrane models. Then, we clustered MD trajectories on the basis of c-alpha carbons root mean square deviation (RMSD), then we carried out molecular docking of validated hMC1R and hMC5R agonists and antagonists (Merlino et al., 2019), in order to re-score the structural clusters of hMC1R and hMC5R, to be used for virtual screening of FDA approved drugs. Through the virtual screening approach, we identified several compounds (encoded with partial ATC codes) with putative activity on melanocortin receptors: diuretics (C03), anti-diabetic drugs (A10), anti-neoplastic agents (L01), anti-protozoal (P01), anti-hemorrhagic (B02), antibiotics and chemotherapeutics (D06), and anti-bacterial agents (J01). Interestingly, fingolimod (L04AA27) had the best scores for both hMC1R and hMC5R (**Table 1**); therefore, we tested the effects of fingolimod (FTY720) intravitreal administration in an *in vivo* model of diabetic retinopathy.

TABLE 1 | Virtual screening of FDA approved compounds to be repurposed as melanocortin ligands. Bold text within the table is referred to the predicted binding free energy of fingolimod, respectively to hMC1R and to hMC5R, as reported in round brackets.

Selective ligands	Re-score on hMCxR model kcal/mol (receptor)
BMS-470539	−85.2 (hMC1R)
AGRP	−197.9 (hMC1R)
PG901	−111.0 (hMC5R)
PG20N	−115.7 (hMC5R)
ATC of compounds	**$\Delta G_{binding}$ Kcal/mol (receptor)**
C03	−41.5 (hMC1R)
A10	−45 (hMC1R)
L01	−49.6 (hMC1R)
L01	−23 (hMC1R)
P01	−17 (hMC1R)
B02	−13 (hMC1R)
D06	−34 (hMC5R)
L04AA27	**−77 (hMC1R)**
	−85 (hMC5R)
J01	−50 (hMC5R)
A10	−66 (hMC5R)

Retinal Vascular Abnormalities Evidenced by FA Analysis

Three out of five eyes per group showed severe (2–4 score) retinal vascular abnormalities (VA) at FA exam. Particularly, an initial irregularity of the vessel size in diabetic mice (STZ group) was evident starting from 4 weeks. This became progressively more accentuated and associated with a vessel thinning both at 8 and 12 weeks. VA mean observed in STZ group was 2.6 ± 0.4 ($p < 0.01$ vs CTR) (**Figure 1**).

Similar to control group (CTR non-diabetic mice), no significant changes in retinal vascularity were observed during follow-up in diabetic mice treated with fingolimod (STZ + Fingolimod), which showed a VA score of 1.2 ± 0.3 ($p < 0.05$ vs STZ) (**Figure 1**).

Diabetic mice (STZ + Fingolimod + AGRP group) treated with fingolimod and AGRP, a MC1R antagonist, showed irregularity in vessel morphology and modification of vessel size, which did not significantly change over time. Diabetic mice (STZ + Fingolimod + PG20N group), treated with both fingolimod and PG20N, a MC5R antagonist, showed a slight progressive thinning of the vascular caliber at various time points. The above-

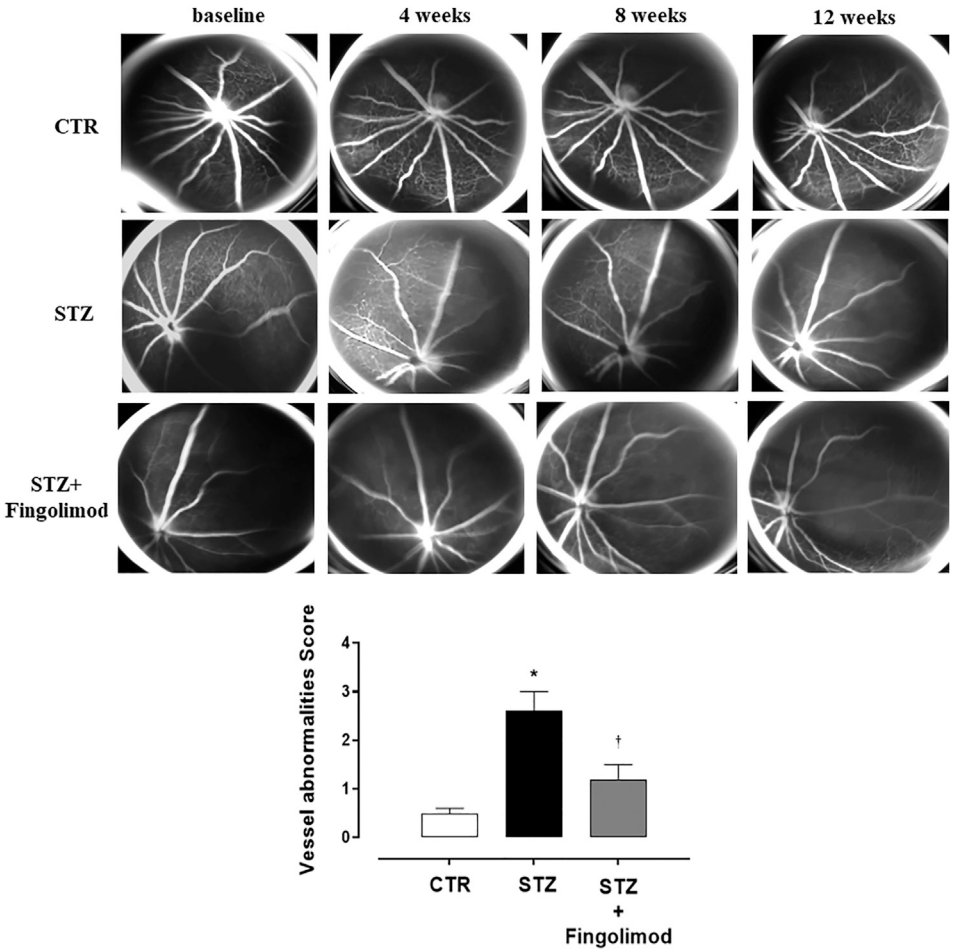

FIGURE 1 | Representative FA images of eyes of non-diabetic mice (CTR), diabetic mice (STZ), and diabetic mice treated with Fingolimod (STZ + Fingolimod) during the follow-up. In CTR mice no changes in retinal vascularity were noticed during follow-up. Instead, in STZ mice, there was an increase in the irregularity of the vessel size, which began at 4 weeks and looked appeared more evident at 8 weeks, in which a pattern of the "rosary-like" vessel was appreciated (red arrow). At 12 weeks there was a further thinning of the vascular caliber. In the STZ + Fingolimod group, no significant changes in retinal vascularity were seen during follow-up. Vessel abnormalities score (graded from 0 to 4) was calculated as the average of the vascular alterations observed (N = 5 animals per group). Vessel abnormalities were graded from 0 to 4 based on the presence of vessel thinning, tortuosity, venous beading, and rosary-like vessels. Each image represents the same retina of the same mouse but at different time points (at baseline, 4–12 weeks of treatment). Statistical significance was assessed by one-way ANOVA, followed by Tukey's multiple comparison test. *$p < 0.05$ vs CTR; †$p < 0.05$ *vs* STZ.

mentioned experimental groups showed a VA score significantly higher compared to STZ + Fingolimod mice (STZ + Fingolimod + AGRP = 2.2 ± 0.2; STZ + Fingolimod + PG20N = 2.0 ± 0.5, both $p < 0.05$ *vs* STZ + Fingolimod) (**Figure 2**).

On the contrary, in diabetic mice receiving fingolimod in combination with the selective S1P1R antagonist (STZ + Fingolimod + Ex 26 group), neither the appearance of DR typical signs nor a significant variation of the size, or of the vascular course was appreciated during the follow up. This was confirmed by the VA score, which was reduced to 1.8 ± 0.2 ($p < 0.05$ *vs* STZ) (**Figure 2**).

VEGFR1 and VEGFR2 Expression

VEGFR1 was expressed in all microvascular structures that were positive in retinas of both control non-diabetic (CTR group; 15 ± 8% expressing VEGFR1) and diabetic retinas (STZ group; 77 ± 12% expressing VEGFR1; $p < 0.05$ *vs* CTR) (**Figures 3A,B**, respectively). Staining was more intense in retinal microvessels of STZ mice, which displayed a hypertrophic morphology, compared to control retinas. In all diabetic retinas, granular VEGFR1 staining was also observed outside the retinal vasculature, in the inner limiting membrane (IML) (**Figure 3B**). Instead, the expression of VEGFR1 in the diabetic mice receiving fingolimod (STZ + Fingolimod group) was close to the control (22 ± 7% expressing VEGFR1; $p < 0.05$ vs STZ) (**Figure 3C**). Co-administration of fingolimod with either with MC1R or MC5R antagonists (STZ + Fingolimod + AGRP and STZ + Fingolimod + PG20N groups) led to a higher VEGFR1 immunostaining in the ganglion cell layer (GCL) and the inner plexiform and nuclear layer (INL), compared to STZ + Fingolimod treated group, but VEGFR1 staining was reduced compared to STZ

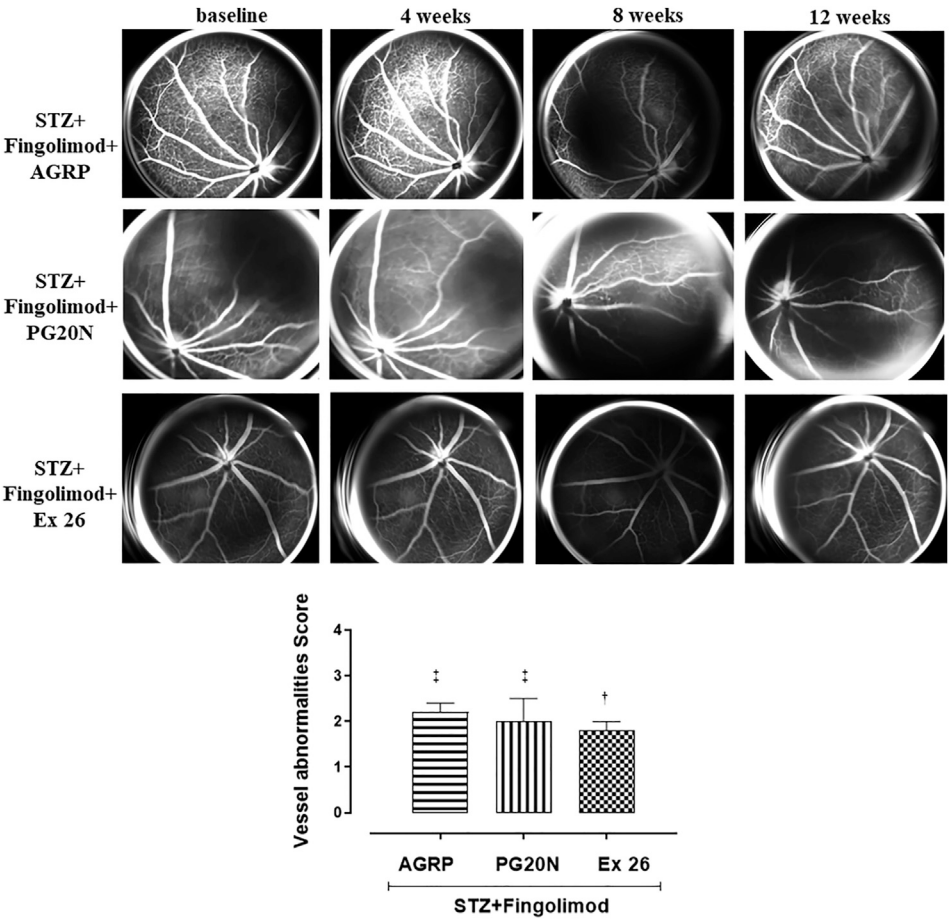

FIGURE 2 | Representative FA images of eyes from diabetic mice treated with Fingolimod and MC1R antagonist (STZ + Fingolimod + AGRP), MC5R antagonist (STZ + Fingolimod + PG20N), and SP1R1 antagonist (STZ + Fingolimod + Ex 26) during the follow-up. The STZ + Fingolimod + AGRP mice showed irregularity of the vessel size, which did not significantly change over time. The STZ + Fingolimod + PG20N group showed a slight progressive thinning of the vascular caliber during the follow-up. In the STZ + Fingolimod + Ex 26 group, neither the appearance of typical signs of RD nor a significant variation of the size or of the vascular course was appreciated, during the follow up. Vessel abnormalities score (graded from 0 to 4) was calculated as the average of the vascular alterations observed (N = 5 animals per group). Vessel abnormalities were graded from 0 to 4 based on the presence of vessel thinning, tortuosity, venous beading, and rosary-like vessels. Each image represents the same retina of the same mouse but at different time points (at baseline, 4–12 weeks of treatment). Statistical significance was assessed by one-way ANOVA, followed by Tukey's multiple comparison test. $^{\dagger}p < 0.05$ *vs* STZ; $^{\ddagger}p < 0.05$ *vs* STZ + Fingolimod.

group (49 ± 10% and 51 ± 8% expressing VEGFR1, respectively; both $p < 0.05$ vs STZ and $p < 0.05$ vs STZ + Fingolimod) (**Figures 3D,E**). In the retina of diabetic mice administered with fingolimod and SP1R1 selective antagonist (STZ + Fingolimod + Ex 26), some VEGFR1 positive retinal ganglion cells and amacrine and bipolar cells were detected (45 ± 11% expressing VEGFR1; $p < 0.05$ vs STZ and $p < 0.05$ vs STZ + Fingolimod) (**Figure 3F**).

Staining of VEGFR2 was weak in retina of control mice, with a patchy distribution pattern in retinal microvessels (CTR group; 24 ± 6% expressing VEGFR2) (**Figure 4A**). In diabetic retina (STZ group), staining of VEGFR-2 was observed in microvessels within the ganglion cell layer (GCL), inner plexiform (IPL), and nuclear layer (INL). Additionally, VEGFR2 granular staining was detected also in the non-vascular areas such as inner limiting membrane (ILM) and the outer part of the inner nuclear layer (INL) (75 ± 9% expressing VEGFR2; $p < 0.05$ vs CTR) (**Figure 4B**). Diabetic mice administered with fingolimod (STZ + Fingolimod) showed weak VEGFR2 retinal immunopositivity, similar to control (36 ± 10% expressing VEGFR2; $p < 0.05$ vs STZ) (**Figure 4C**). In the inner limiting membrane (ILM), ganglion cell layer (GCL) and the outer part of the inner nuclear layer (INL), retinas of groups STZ + Fingolimod + AGRP and STZ + Fingolimod + PG20N showed a VEGFR2 staining higher compared to diabetic mice treated only with fingolimod, but lower compared to STZ untreated mice ($p < 0.05$ vs STZ + Fingolimod and $p < 0.05$ vs STZ) (**Figures 4D,E**). Similarly, VEGFR2 labeling and localization was evidenced in diabetic mice treated with fingolimod and SP1R1 selective antagonist (STZ + Fingolimod + Ex 26; 45 ± 11% expressing VEGFR2, $p < 0.05$ vs STZ + Fingolimod and $p < 0.05$ vs STZ) (**Figure 4F**).

VEGFA Levels

VEGFR1 and VEGFR2 retinal immunostaining results were confirmed by retinal VEGFA levels assessment through ELISA.

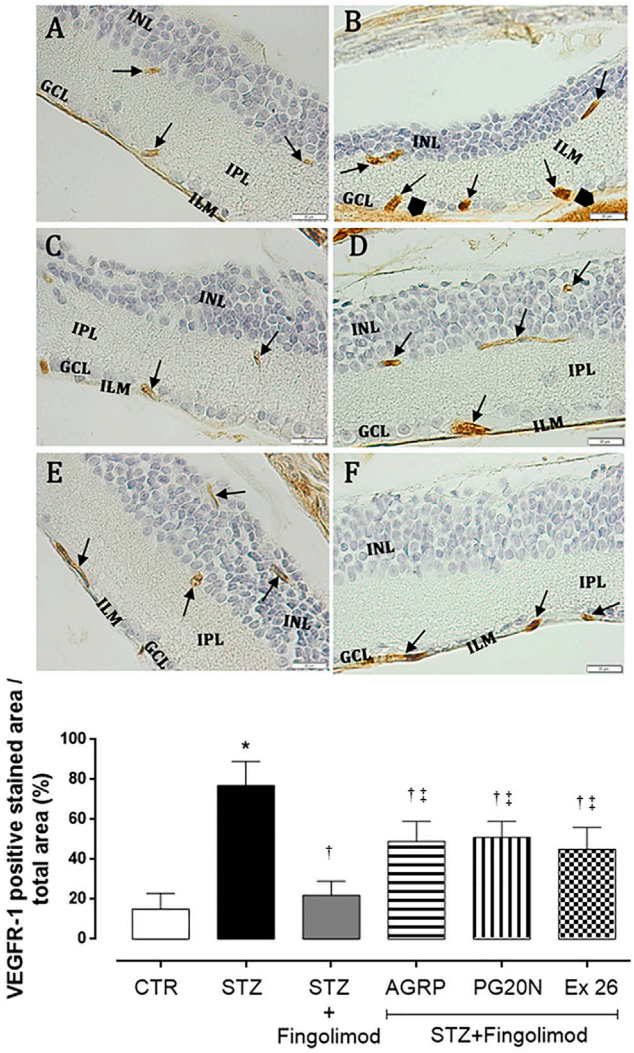

FIGURE 3 | VEGFR1 immunohistochemistry in the retina of non-diabetic mice [panel **(A)**, CTR], diabetic mice [panel **(B)** STZ], diabetic mice receiving Fingolimod alone [panel **(C)**, STZ + Fingolimod], or in combination with MC1R antagonist [panel **(D)**, STZ + Fingolimod + AGRP], MC5R antagonist [panel **(E)**, STZ + Fingolimod + PG20N], and SP1R1 antagonist [panel **(F)**, STZ + Fingolimod + Ex 26]. VEGFR1 positive stain (arrow). VEGFR1 protein levels are reported as percentage (%) ± standard deviation (S.D.) of positive stained area/total area. The images are representative of 10 histological observations per group. Statistical significance was assessed by one-way ANOVA, followed by Tukey's multiple comparison test. *$p < 0.05$ vs CTR; †$p < 0.05$ vs STZ; ‡$p < 0.05$ vs STZ + Fingolimod. INL, inner nuclear layer; IPL, inner plexiform layer; ILM, inner limiting membrane; GLC, ganglion cell layer; retinal microvessels staining of VEGFR1 (arrow), non-vascular staining of VEGFR-1 (arrowhead); magnification: 40X; scale bar: 20 μm. N = 5 retinas per group.

Particularly, the highest VEGFA levels were detected in diabetic retina (102 ± 8 pg/ml; $p < 0.01$ vs CTR group), while levels were significantly reduced by fingolimod treatment (48 ± 4 pg/ml; $p < 0.01$ vs STZ) (**Figure 5A**). The combination of fingolimod plus MC1R or MC5R antagonists significantly increased VEGFA levels compared to fingolimod alone (78 ± 9 pg/ml and 84 ± 6 pg/ml, both $p < 0.05$ vs STZ + Fingolimod), while diabetic mice receiving fingolimod and SP1R1 selective blocker exhibited intermediate VEGFA levels between STZ and STZ + Fingolimod groups (63 ± 6 pg/ml, $p < 0.05$ *vs* STZ) (**Figure 5B**).

Molecular Dynamics

The *in vivo* pharmacological studies, through co-administration of selective melanocortin antagonists, evidenced that fingolimod

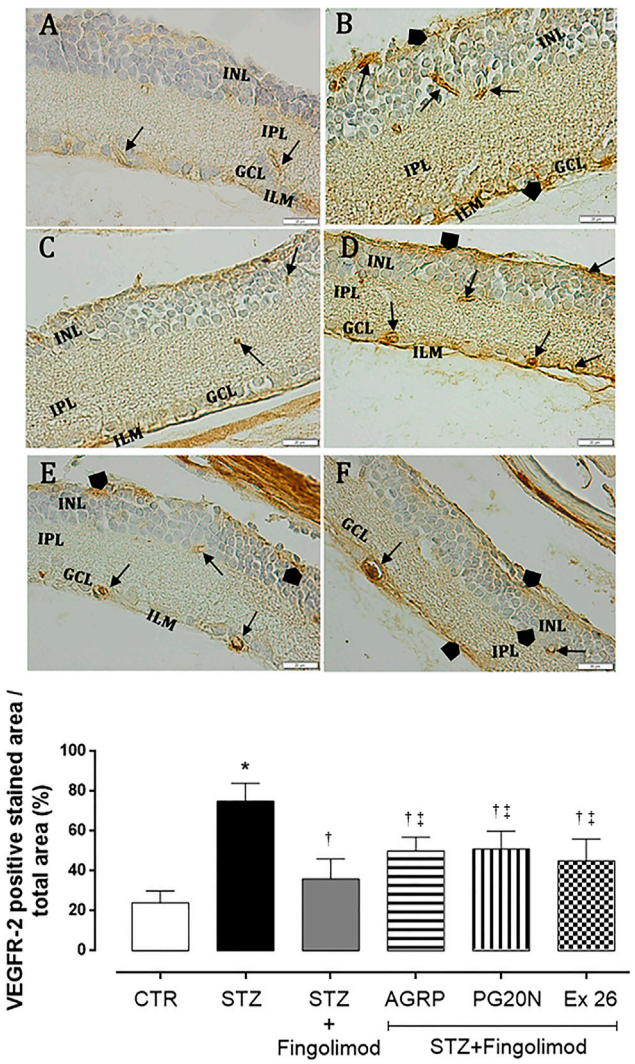

FIGURE 4 | VEGFR2 immunohistochemistry in the retina of non-diabetic mice [panel **(A)**, CTR], diabetic mice [panel **(B)**, STZ], diabetic mice receiving fingolimod alone [panel **(C)**, STZ + Fingolimod] or in combination with MC1R antagonist [panel **(D)**, STZ + Fingolimod + AGRP], MC5R antagonist [panel **(E)**, STZ + Fingolimod + PG20N], and SP1R1 antagonist [panel **(F)**, STZ + FTY720+Ex 26]. VEGFR2 positive stain (arrow). VEGFR2 protein levels are reported as percentage (%) ± S.D. of positive stained area/total area. The images are representative of 10 histological observations per group. Statistical significance was assessed by one-way ANOVA, followed by Tukey's multiple comparison test. *$p < 0.05$ vs CTR; †$p < 0.05$ vs STZ; ‡$p < 0.05$ vs STZ + Fingolimod. INL, inner nuclear layer; IPL, inner plexiform layer; ILM, inner limiting membrane; GLC, ganglion cell layer; retinal microvessels staining of VEGFR-2 (arrow), non-vascular staining of VEGFR-2 (arrowhead); magnification 40X; scale bar: 20 μm. N = 5 retinas per group.

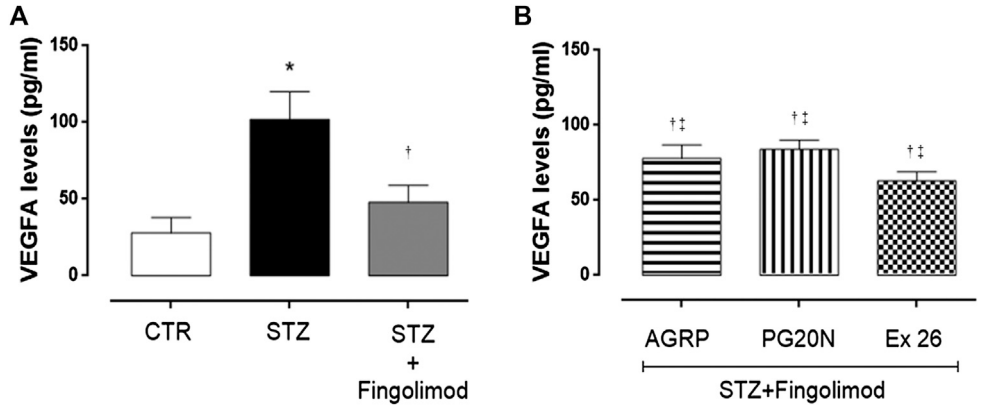

FIGURE 5 | VEGFA levels in retina of non-diabetic mice [panel **(A)**, CTR], diabetic mice [panel **(A)**, STZ], diabetic mice receiving fingolimod alone [panel **(A)**, STZ + Figolimod], or in combination with MC1R antagonist [panel **(B)**, STZ + Fingolimod + AGRP], MC5R antagonist [panel **(B)**, STZ + Fingolimod + PG20N], and SP1R1 antagonist [panel **(B)**, STZ + FTY720+Ex 26]. VEGFA levels, assayed by ELISA, are reported as pg/ml ± S.D. Statistical significance was assessed by one-way ANOVA, followed by Tukey's multiple comparison test. $^{*}p < 0.05$ vs CTR; $^{\dagger}p < 0.05$ vs STZ; $^{\ddagger}p < 0.05$ vs STZ + Fingolimod. N = 10 retinas per group.

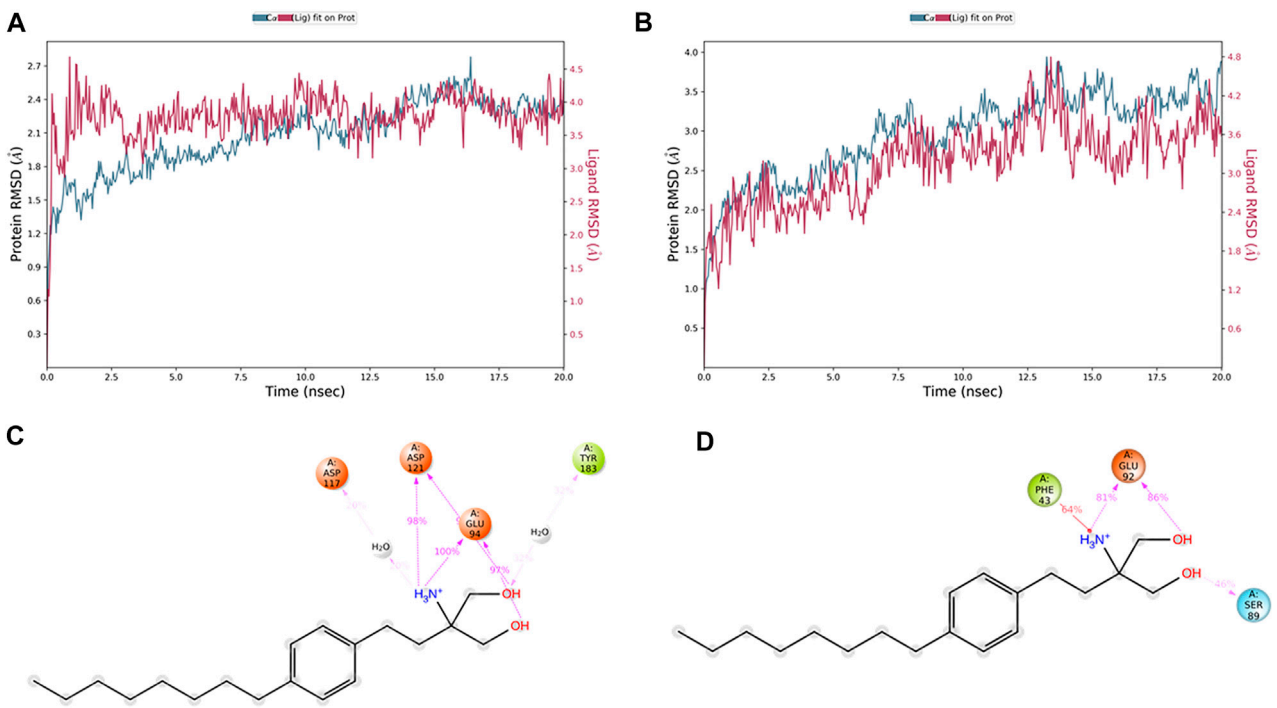

FIGURE 6 | Fingolimod stably bound to hMC1R and hMC5R during 20 ns MD simulation. **(A)** root mean square deviation (RMSD) of hMC1R (blue plot) and fingolimod (red blot) during 20 ns of MD simulation, of the complex embedded in a POPC membrane. **(B)** RMSD of hMC5R (blue plot) and fingolimod (red blot) during 20 ns of MD simulation, of the complex embedded in a POPC membrane. **(C)** Fingolimod interactions with hMC1R, and frequency (%) during 20 ns MD simulation. **(D)** Fingolimod interactions with hMC5R, and frequency (%) during 20 ns MD simulation.

exerted anti-angiogenic effects also by activation of MC1R and MC5R, besides its agonist activity on the S1PR1 receptor. Indeed, we explored the binding of fingolimod to hMC1R and hMC5R, by means of 20 ns molecular dynamics simulations, and compared it with simulation of hMC1R and hMC5R in complex with selective agonists (hMC1R/BMS-470539, hMC5R/PG901 complexes) and antagonists (hMC1R/Agrp, hMC1R/PG20N). Besides the greater predicted affinity for hMC5R (**table 1**) compared to hMC1R, during 20 ns simulation, fingolimod in complex with hMC1R receptor showed lower and more stable root mean square

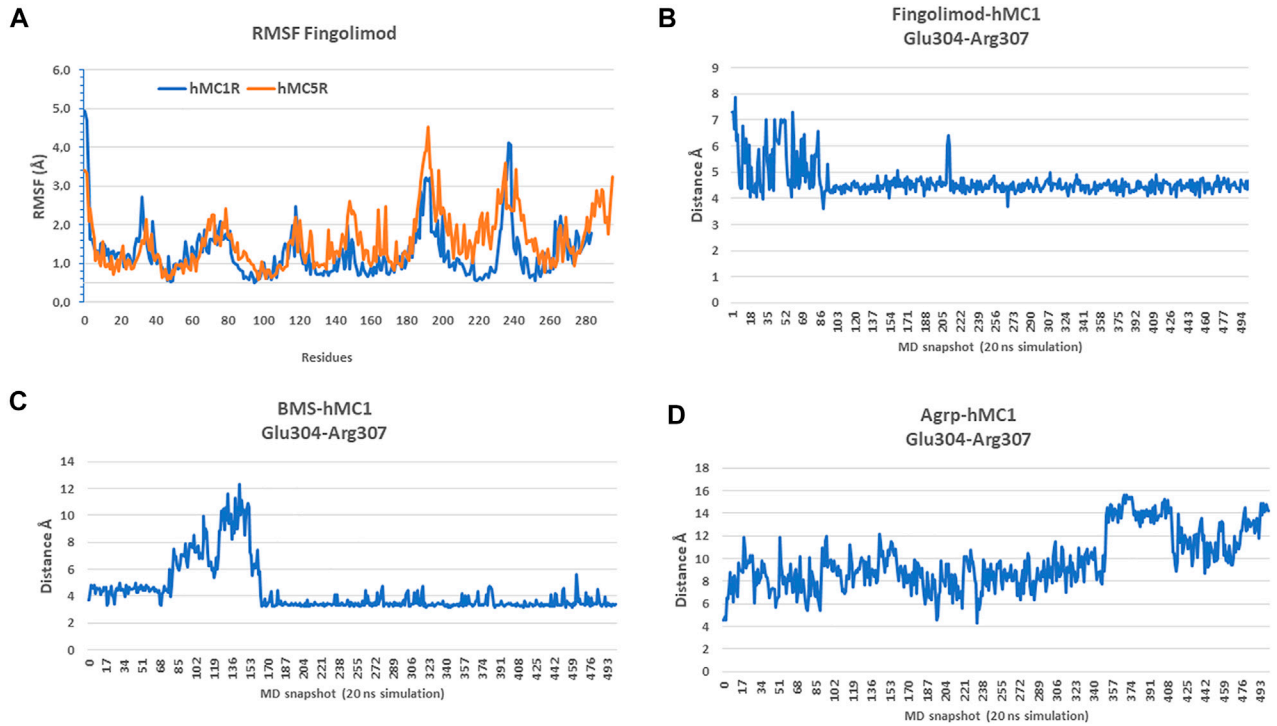

FIGURE 7 | Fingolimod stabilized hMC1R to lower root mean square fluctuations (RMSF), compared to hMC5R. **(A)** RMSF of fingolimod-hMC1R (blue) complex and fingolimod-hMC5R (orange) complex as mean of 20 ns simulations. **(B)** Glu304-Arg307 salt-bridge distance during 20 ns simulation of fingolimod-hMC1R complex. **(C)** Glu304-Arg307 salt bridge distance during 20 ns simulation of BMS-hMC1R complex. **(D)** Glu304-Arg307 salt bridge distance during 20 ns simulation of Agrp-hMC1R complex.

deviation (RMSD) plot, compared to fingolimod/hMC5R complex (**Figures 6A,B**). Additionally, fingolimod had a greater number of ligand-protein interactions, specifically stable H-bonds and a water bridge, with hMC1R receptor (**Figure 6C**) compared to hMC5R complex (**Figure 6D**).

Analysis of root mean square fluctuations (RMSF) showed that fingolimod stabilized hMC1R to lower RMSF values, compared to hMC5R RMSF values (**Figure 7A**). To confirm that fingolimod works as hMC1R and hMC5R agonist, we tried to shed light on receptor conformational modification induced by fingolimod, comparing salt-bridges of fingolimod/hMC1R and hMC5R complexes with correspondent salt-bridges in validated agonists and antagonists/hMC1R and hMC5R complexes. Data about salt-bridges at VIII of hMC1R, the amphipathic helix of GPCRs parallel to the cytosolic side of lipid membrane, have strengthened the hypothesis and the experimental results of the study hereby presented (**Figures 7B–D**). In fact, fingolimod bound to hMC1R (**Figure 7B**), during 20 ns simulation, stabilized to 4Å distance the salt-bridge between Glu304 and Arg307, similarly to BMS/hMC1R complex (**Figure 7C**). On the contrary, the hMC1R antagonist AGRP destroyed the Glu304-Arg307 salt-bridge (13 ± 0.5 Å, **Figure 7D**), during the 20 ns simulation. Unfortunately, salt-bridges analysis for hMC5R complexes gave inconclusive results.

As regards as overall conformational changes in hMCxR receptors, upon binding with agonists and antagonists, we built residue-residue contact maps. These contact maps were further analyzed to analyze the receptor conformational changes (i.e., differences between contact maps of unbound receptor compared to ligand-hMCxR complexes), by means of a web application (fuzzy logic algorithm for image differences analyses). We found that fingolimod induced in hMC1R a pattern of residue-residues interactions (i.e., conformational modification), very close to conformational changes induced by the selective hMC1 agonist BMS. The pattern of fingolimod-hMC1R complex was totally different from conformational modifications induced by the antagonist AGRP on hMC1R (**Figure 8**). These results are in accordance with data on salt-bridges in hMC1R complexes (**Figures 7B–D**). Contact map modifications (i.e., conformational changes) in hMC5R upon binding with fingolimod, PG901 (agonist) and PG20N (antagonist), gave ambiguous information (**Figure 9**). Specifically, contact maps on hMC5R upon binding with fingolimod gave a pattern of interactions different from conformational changes induced by PG901 and PG20N. Indeed, we can state that fingolimod would be a hMC5R agonist, only on the basis of *in vivo* pharmacological data.

DISCUSSION

Diabetic retinopathy, the most common complication of diabetes, is the leading cause of blindness in working-age adults (Cheloni

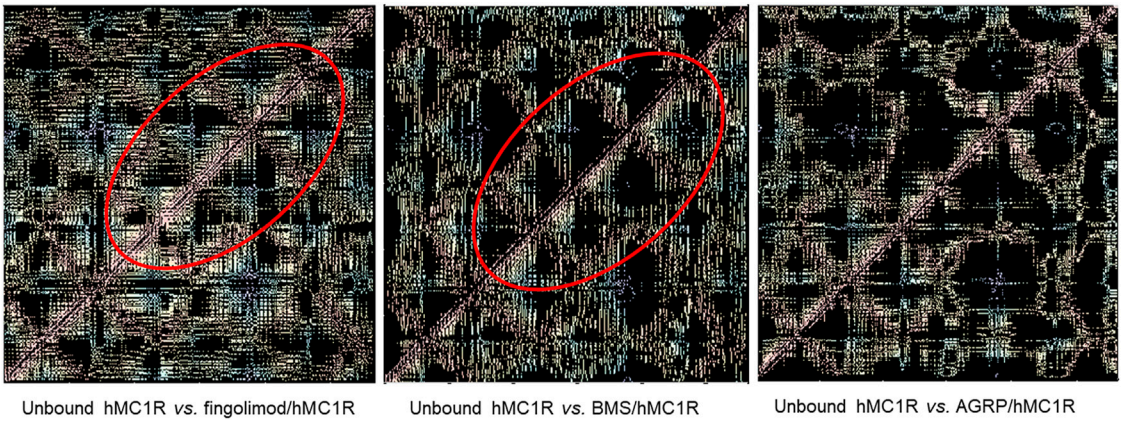

FIGURE 8 | Differences in residue-residues contact maps in hMC1R bound to fingolimod and selective agonist (BMS) and antagonist (AGRP).

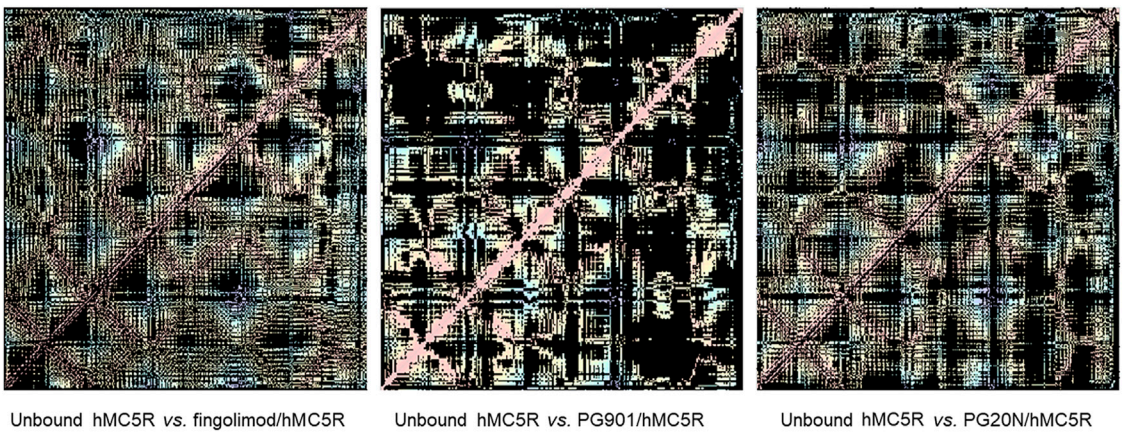

FIGURE 9 | Differences in residue-residues contact maps in hMC5R bound to fingolimod and selective agonist (PG901) and antagonist (PG20N).

et al., 2019). The role of chronic low-grade retinal inflammation in DR etiopathogenesis has been evidenced by several clinical and preclinical studies (Rübsam et al., 2018; Platania et al., 2019a; Lazzara et al., 2019; Lazzara et al., 2020; Trotta et al., 2019; Trotta et al., 2021; Bonfiglio et al., 2020; Rossi et al., 2021). Indeed, DR patients have shown high serum and ocular levels of pro-inflammatory cytokines and chemokines, such as interleukin 1β (IL-1β), interleukin 6 (IL-6), interleukin 8 (IL-8), Tumor Necrosis Factor α (TNF-α), and Monocyte Chemoattractant Protein-1 (MCP-1), transforming growth factor β (TGFβ) (Boss et al., 2017; Wu et al., 2017; Bonfiglio et al., 2020). The increase of these inflammatory mediators has been proposed to contribute to early neurovascular retinal dysfunction (Vujosevic and Simó, 2017; Rübsam et al., 2018; Fu et al., 2020). Particularly, by acting as a pro-inflammatory mediator, VEGFA plays a critical role in DR pathogenesis, by triggering the process of vascular proliferation (Zhao and Singh, 2018; Aguilar-Cazares et al., 2019). Particularly, VEGFA acts on VEGFR1, which generates vascular sprouting, and on VEGFR2, which mediates vao-permeability by activating endothelial nitric oxide synthase (eNOS) (Stuttfeld and Ballmer-Hofer, 2009; Ruszkowska-Ciastek et al., 2014). To this regard, ocular anti-VEGF therapy is the currently gold standard treatment for DR (Cheung et al., 2014), along with intravitreal steroids (Bucolo et al., 2018). Therefore, the modulation of the chronic inflammation, targeting several pathways (Bucolo et al., 2005; Shafiee et al., 2011), could be very useful in order to avoid the progression to the late state of DR, characterized by neuronal loss, increased vascular permeability with blood retinal barrier break, macular edema and finally retinal ischemia and neovascularization (Duh et al., 2017). To this regard, we have previously reported an emerging role of melanocortin receptors subtypes 1 and 5 (MC1R and MC5R), which when activated are able to counteract the retinal pro-inflammatory *milieu* induced by diabetes. In particular, MC1R and MC5R activation restored the levels of manganese-dependent superoxide dismutase (MnSOD) and glutathione peroxidase (GPx) antioxidant enzyme levels in primary retinal cell cultures exposed to high-glucose concentration, reducing pro-inflammatory cytokines and chemokines and consequently preserving photoreceptor integrity (Maisto et al., 2017). Moreover, MC1R and MC5R

agonists in diabetic mice reduced DR damage by increasing retinal occludin levels, leading to polarization of M2 macrophages levels and reducing retinal VEGF content (Rossi et al., 2021). Interestingly, melanocortin system has been recently shown to interact with S1P1Rs expressed by hypothalamic neurons in rodents. Particularly, a strong positive correlation was found among hypothalamic S1PR1 mRNA and MC3R and MC4R receptors (Silva et al., 2014). S1PRs modulate different cell functions such as proliferation, migration, angiogenesis, chemotaxis, and immune cell trafficking (Sharma et al., 2013). Particularly, 5 subtypes of S1PRs (S1P1–5) have been identified in humans. These G-protein coupled receptors are differentially expressed in various tissues and cell types, such as endothelial cells, T cells, B cells, macrophages, astrocytes, and neurons (Mehling et al., 2011; Bikbova et al., 2015). It has been demonstrated that, after oral administration, fingolimod is phosphorylated in the central nervous system and binds to S1P1R, S1P3R, S1P4R, and S1P5R with an affinity comparable to the affinity of sphingosine 1-phosphate (S1P) (Mehling et al., 2011). S1P1R is localized also on retinal neurons (Bikbova et al., 2015) and was found to be involved in cytokine production through signal transducer activator transcription 3 (STAT3), and it is also able to induce NOD-like receptor protein 3 (NLRP3) inflammasome, a multiprotein complex activated during diabetic retinal damage (Trotta et al., 2019; Weigert et al., 2019). After binding of FTY720 to S1P1R on lymphocytes and central nervous system (CNS) cells, S1P1R is internalized and degraded (Gräler and Goetzl, 2004), leading to decrease of S1P1R number on the cell surface and impairment of receptor signaling (Chiba et al., 1999). Particularly, fingolimod inhibited the lymphocytes egress from the lymph nodes; therefore, in this condition lymphocytes do not reach the CNS and cannot damage myelin of the nerve fibers (Chiba et al., 1999). Accordingly, S1P1R activation preserved blood brain barrier integrity and blocked peripheral blood mononuclear cells (PBMCs) transmigration (Spampinato et al., 2015; Yamamoto et al., 2017). Consequently, fingolimod action results in a reduction of inflammatory damage mediated by immune cells. Therefore, besides its approved clinical use in patients affected by relapsing-remitting multiple sclerosis (RR-MS) (Mehling et al., 2011), fingolimod effects have been investigated in other immune-inflammatory disorders (Bing et al., 2009; Yoshida et al., 2013). Fingolimod was able to exert an anti-inflammatory action and to increase blood retinal barrier tight junctions expression in a rodent model of DR, by ultimately reducing vascular permeability (Fan and Yan, 2016). To this regard, it is worthy of note that the examination of fingolimod ocular effects in RR-MS patients showed a preserved macular structure and thickness over the time, together with a complete absence of macular edema, even if it is reported as a fingolimod side effect (Fruschelli et al., 2019; d'Ambrosio et al., 2020; Rossi et al., 2020). In our study, a virtual screening approach evidenced that fingolimod, along with other FDA already approved drugs, can bind with good-predicted affinity to melanocortin receptors MC1R and MC5R. Therefore, we then tested fingolimod in an *in vivo* model of DR. Although our DR animal model shows some limitations in evidencing marked changes of retinal vascularity by FA evaluations, since it reproduces only alterations of DR early stages such as vascular caliber irregularity or microaneurysms, conversely immunohistochemical analysis showed a specific modulation of VEGFR1 and VEGFR2 expression, with consequent alterations in retinal neovascularization process, as evidenced by the increase of retinal VEGFA levels. Overall, diabetic C57BL/6J mice treated with fingolimod exhibited a reduction of retinal angiogenesis. Particularly, FA evaluations did not evidence any retinal vessel size irregularity in diabetic mice treated with fingolimod, which led to a reduced VEGFR1 and VEGFR2 retinal staining, compared to untreated diabetic mice. Also, retinal VEGFA levels were reduced by fingolimod treatment. This protective effect was less evident in mice receiving fingolimod combined with MC1R antagonist, showing an irregular retinal vessel size, which did not significantly change over time. Similarly, the combination of MC5R antagonist caused a slight progressive thinning of the vascular caliber. Furthermore, although VEGFR1 and VEGFR2 along with retinal VEGFA content were reduced in mice treated with fingolimod and MC1R or MC5R antagonists compared to the diabetic group, they were significantly higher when compared to diabetic mice treated with fingolimod alone. These results from our *in vivo* pharmacological study suggest that fingolimod acts as an agonist of MC1R and MC5R, as evidenced by our preliminary in-silico (virtual screening of FDA approved drugs) analysis. Particularly, we found that a similar trend was found in diabetic mice co-treated with fingolimod and a selective S1P1R antagonist. This may indicate that fingolimod influences independently melanocortin and SP1 pathways in the retina. These data were further confirmed through molecular dynamics simulations, showing that fingolimod stably binds to hMC1R and hMC5R. Structural analysis of simulation of hMC1R bound to fingolimod supported that fingolimod works as hMC1R agonist, similarly to the selective hMC1R agonist BMS-470539. Data on hMC5R molecular dynamics simulations are less straightforward compared to simulations on MC1R, and fingolimod effects on hMC5R structure are totally different from either antagonist or agonists effects. The present findings highlight that fingolimod is worthy of further pharmaceutical development such as optimization of drug formulations for ocular drug delivery (Conti et al., 1997; Platania et al., 2019b). In conclusion, despite the limitations of our experimental DR model, our data provided evidence that fingolimod exerted anti-angiogenic activity not only through the S1P1 receptor, but also activating MC1R and MC5R, confirming that these GPCRs are intriguing pharmacological targets to handle DR.

DATA AVAILABILITY STATEMENT

The original contributions presented in the study are included in the article/Supplementary Material, further inquiries can be directed to the corresponding author.

ETHICS STATEMENT

The animal study was reviewed and approved by the Institutional Ethical Committee of the "Vasile Goldis" Western University of Arad (number, 29/May 17, 2017).

AUTHOR CONTRIBUTIONS

"CG, CBu, CBMP, and MT contributed to conception and design of the study. CG, CBa, CBMP, MT, HH, SGh, MR, SGi, and AD performed the experimental analysis. FP, PG, RB, and FS performed the statistical analysis. MD and CBu wrote the first draft of the manuscript. AH and SR wrote sections of the manuscript. All authors contributed to manuscript revision, read, and approved the submitted version".

FUNDING

This study was supported by the Italian MIUR, Grant n. PRIN–2017TSHBXZ.

REFERENCES

Aguilar-Cazares, D., Chavez-Dominguez, R., Carlos-Reyes, A., Lopez-Camarillo, C., Hernadez de la Cruz, O. N., and Lopez-Gonzalez, J. S. (2019). Contribution of Angiogenesis to Inflammation and Cancer. *Front. Oncol.* 9, 1399. doi:10.3389/fonc.2019.01399

Bikbova, G., Oshitari, T., Baba, T., and Yamamoto, S. (2015). Altered Expression of NF- κ B and SP1 after Exposure to Advanced Glycation End-Products and Effects of Neurotrophic Factors in AGEs Exposed Rat Retinas. *J. Diabetes Res.* 2015, 543818. doi:10.1155/2015/543818

Biswas, S., Bhattacherjee, P., Paterson, C. A., Maruyama, T., and Narumiya, S. (2007). Modulation of Ocular Inflammatory Responses by EP1 Receptors in Mice. *Exp. Eye Res.* 84, 39–43. doi:10.1016/j.exer.2006.08.013

Bonfiglio, T., Olivero, G., Merega, E., Di Prisco, S., Padolecchia, C., Grilli, M., et al. (2017). Prophylactic Versus Therapeutic Fingolimod: Restoration of Presynaptic Defects in Mice Suffering from Experimental Autoimmune Encephalomyelitis. *PLoS One* 12, e0170825. doi:10.1371/journal.pone.0170825

Bonfiglio, V., Platania, C. B. M., Lazzara, F., Conti, F., Pizzo, C., Reibaldi, M., et al. (2020). TGF-β Serum Levels in Diabetic Retinopathy Patients and the Role of Anti-VEGF Therapy. *Int. J. Mol. Sci.* 21, 9558. doi:10.3390/ijms21249558

Boss, J. D., Singh, P. K., Pandya, H. K., Tosi, J., Kim, C., Tewari, A., et al. (2017). Assessment of Neurotrophins and Inflammatory Mediators in Vitreous of Patients with Diabetic Retinopathy. *Invest. Ophthalmol. Vis. Sci.* 58, 5594–5603. doi:10.1167/iovs.17-21973

Bucolo, C., Drago, F., Lin, L. R., and Reddy, V. N. (2005). Neuroactive Steroids Protect Retinal Pigment Epithelium against Oxidative Stress. *Neuroreport* 16, 1203–1207. doi:10.1097/00001756-200508010-00014

Bucolo, C., Gozzo, L., Longo, L., Mansueto, S., Vitale, D. C., and Drago, F. (2018). Long-Term Efficacy and Safety Profile of Multiple Injections of Intravitreal Dexamethasone Implant to Manage Diabetic Macular Edema: A Systematic Review of Real-World Studies. *J. Pharmacol. Sci.* 138, 219–232. doi:10.1016/j.jphs.2018.11.001

Cahalan, S. M., Gonzalez-Cabrera, P. J., Nguyen, N., Guerrero, M., Cisar, E. A., Leaf, N. B., et al. (2013). Sphingosine 1-Phosphate Receptor 1 (S1P(1)) Upregulation and Amelioration of Experimental Autoimmune Encephalomyelitis by an S1P(1) Antagonist. *Mol. Pharmacol.* 83, 316–321. doi:10.1124/mol.112.082958

Carotenuto, A., Merlino, F., Cai, M., Brancaccio, D., Yousif, A. M., Novellino, E., et al. (2015). Discovery of Novel Potent and Selective Agonists at the Melanocortin-3 Receptor. *J. Med. Chem.* 58, 9773–9778. doi:10.1021/acs.jmedchem.5b01285

Cheloni, R., Gandolfi, S. A., Signorelli, C., and Odone, A. (2019). Global Prevalence of Diabetic Retinopathy: Protocol for a Systematic Review and Meta-Analysis. *BMJ Open* 9, e022188. doi:10.1136/bmjopen-2018-022188

Cheung, N., Wong, I. Y., and Wong, T. Y. (2014). Ocular Anti-VEGF Therapy for Diabetic Retinopathy: Overview of Clinical Efficacy and Evolving Applications. *Diabetes Care* 37, 900–905. doi:10.2337/dc13-1990

Chiba, K., Yanagawa, Y., Kataoka, H., Kawaguchi, T., Ohtsuki, M., and Hoshino, Y. (1999). FTY720, a Novel Immunosuppressant, Induces Sequestration of Circulating Lymphocytes by Acceleration of Lymphocyte Homing. *Transpl. Proc* 31, 1230–1233. doi:10.1016/S0041-1345(98)01975-7

Cohen, J. A., Barkhof, F., Comi, G., Hartung, H. P., Khatri, B. O., Montalban, X., et al. (2010). Oral Fingolimod or Intramuscular Interferon for Relapsing Multiple Sclerosis. *N. Engl. J. Med.* 362, 402–415. doi:10.1056/NEJMoa0907839

Conti, B., Bucolo, C., Giannavola, C., Puglisi, G., Giunchedi, P., and Conte, U. (1997). Biodegradable Microspheres for the Intravitreal Administration of Acyclovir: *In Vitro/In Vivo* Evaluation. *Eur. J. Pharm. Sci.* 5, 287–293. doi:10.1016/S0928-0987(97)00023-7

d'Ambrosio, A., Capuano, R., Rossi, S., Bisecco, A., Lanza, M., Gesualdo, C., et al. (2020). Two-Year Macular Volume Assessment in Multiple Sclerosis Patients Treated with Fingolimod. *Neurol. Sci.* 42, 731–733. doi:10.1007/s10072-020-04802-x

Duh, E. J., Sun, J. K., and Stitt, A. W. (2017). Diabetic Retinopathy: Current Understanding, Mechanisms, and Treatment Strategies. *JCI insight* 2, e92751. doi:10.1172/jci.insight.93751

Fan, L., and Yan, H. (2016). FTY720 Attenuates Retinal Inflammation and Protects Blood-Retinal Barrier in Diabetic Rats. *Invest. Ophthalmol. Vis. Sci.* 57, 1254–1263. doi:10.1167/iovs.15-18658

Fruschelli, M., Capozzoli, M., Gelmi, M. C., Masi, G., and Annunziata, P. (2019). Longitudinal Quantitative Assessment of Macula during Therapy with Fingolimod in Relapsing-Remitting Multiple Sclerosis. *Int. Ophthalmol.* 39, 777–781. doi:10.1007/s10792-018-0870-x

Fu, Z., Sun, Y., Cakir, B., Tomita, Y., Huang, S., Wang, Z., et al. (2020). Targeting Neurovascular Interaction in Retinal Disorders. *Int. J. Mol. Sci.* 21, 1503. doi:10.3390/ijms21041503

Gräler, M. H., and Goetzl, E. J. (2004). The Immunosuppressant FTY720 Down-Regulates Sphingosine 1-Phosphate G-Protein-Coupled Receptors. *FASEB J.* 18, 551–553. doi:10.1096/fj.03-0910fje

Humphrey, W., Dalke, A., and Schulten, K. (1996). VMD: Visual Molecular Dynamics. *J. Mol. Graph.* 14 (33–38), 27–28. doi:10.1016/0263-7855(96)00018-5

Kappos, L., Radue, E. W., O'Connor, P., Polman, C., Hohlfeld, R., Calabresi, P., et al. (2010). A Placebo-Controlled Trial of Oral Fingolimod in Relapsing Multiple Sclerosis. *N. Engl. J. Med.* 362, 387–401. doi:10.1056/NEJMoa0909494

Lazzara, F., Fidilio, A., Platania, C. B. M., Giurdanella, G., Salomone, S., Leggio, G. M., et al. (2019). Aflibercept Regulates Retinal Inflammation Elicited by High Glucose via the PlGF/ERK Pathway. *Biochem. Pharmacol.* 168, 341–351. doi:10.1016/j.bcp.2019.07.021

Lazzara, F., Trotta, M. C., Platania, C. B. M., D'Amico, M., Petrillo, F., Galdiero, M., et al. (2020). Stabilization of HIF-1α in Human Retinal Endothelial Cells Modulates Expression of miRNAs and Proangiogenic Growth Factors. *Front. Pharmacol.* 11, 1063. doi:10.3389/fphar.2020.01063

Maisto, R., Gesualdo, C., Trotta, M. C., Grieco, P., Testa, F., Simonelli, F., et al. (2017). Melanocortin Receptor Agonists MCR1-5 Protect Photoreceptors from High-Glucose Damage and Restore Antioxidant Enzymes in Primary Retinal Cell Culture. *J. Cel. Mol. Med.* 21, 968–974. doi:10.1111/jcmm.13036

Mehling, M., Johnson, T. A., Antel, J., Kappos, L., and Bar-Or, A. (2011). Clinical Immunology of the Sphingosine 1-phosphate Receptor Modulator Fingolimod (FTY720) in Multiple Sclerosis. *Neurology* 76, S20–S27. doi:10.1212/WNL.0b013e31820db341

Merlino, F., Zhou, Y., Cai, M., Carotenuto, A., Yousif, A. M., Brancaccio, D., et al. (2018). Development of Macrocyclic Peptidomimetics Containing Constrained α,α-Dialkylated Amino Acids with Potent and Selective Activity at Human Melanocortin Receptors. *J. Med. Chem.* 61, 4263–4269. doi:10.1021/acs.jmedchem.8b00488

Merlino, F., Tomassi, S., Yousif, A. M., Messere, A., Marinelli, L., Grieco, P., et al. (2019). Boosting Fmoc Solid-Phase Peptide Synthesis by Ultrasonication. *Org. Lett.* 21, 6378–6382. doi:10.1021/acs.orglett.9b02283

Nolan, R., Gelfand, J. M., and Green, A. J. (2013). Fingolimod Treatment in Multiple Sclerosis Leads to Increased Macular Volume. *Neurology* 80, 139–144. doi:10.1212/WNL.0b013e31827b9132

Platania, C. B., Salomone, S., Leggio, G. M., Drago, F., and Bucolo, C. (2012). Homology Modeling of Dopamine D2 and D3 Receptors: Molecular Dynamics

Refinement and Docking Evaluation. *PLoS One* 7, e44316. doi:10.1371/journal.pone.0044316

Platania, C. B. M., Maisto, R., Trotta, M. C., D'Amico, M., Rossi, S., Gesualdo, C., et al. (2019a). Retinal and Circulating miRNA Expression Patterns in Diabetic Retinopathy: An In Silico and *In Vivo* Approach. *Br. J. Pharmacol.* 176, 2179–2194. doi:10.1111/bph.14665

Platania, C. B. M., Dei Cas, M., Cianciolo, S., Fidilio, A., Lazzara, F., Paroni, R., et al. (2019b). Novel Ophthalmic Formulation of Myriocin: Implications in Retinitis Pigmentosa. *Drug Deliv.* 26, 237–243. doi:10.1080/10717544.2019.1574936

Platania, C. B. M., Ronchetti, S., Riccardi, C., Migliorati, G., Marchetti, M. C., Di Paola, L., et al. (2020). Effects of Protein-Protein Interface Disruptors at the Ligand of the Glucocorticoid-Induced Tumor Necrosis Factor Receptor-Related Gene (GITR). *Biochem. Pharmacol.* 178, 114110. doi:10.1016/j.bcp.2020.114110

Rossi, S., Gesualdo, C., Gallo, A., Melillo, P., Martines, F., Colucci, R., et al. (2020). Oct Analysis in Patients with Relapsing-Remitting Multiple Sclerosis during Fingolimod Therapy: 2-Year Longitudinal Retrospective Study. *Appl. Sci.* 10, 7085. doi:10.3390/app10207085

Rossi, S., Maisto, R., Gesualdo, C., Trotta, M. C., Ferraraccio, F., Kaneva, M. K., et al. (2021). Corrigendum to "Activation of Melanocortin Receptors MC1 and MC5 Attenuates Retinal Damage in Experimental Diabetic Retinopathy". *Mediators Inflamm.* 2021, 9861434. doi:10.1155/2021/9861434

Rübsam, A., Parikh, S., and Fort, P. (2018). Role of Inflammation in Diabetic Retinopathy. *Int. J. Mol. Sci.* 19, 942. doi:10.3390/ijms19040942

Ruszkowska-Ciastek, B., Sokup, A., Socha, M. W., Ruprecht, Z., Hałas, L., Góralczyk, B., et al. (2014). A Preliminary Evaluation of VEGF-A, VEGFR1 and VEGFR2 in Patients with Well-Controlled Type 2 Diabetes Mellitus. *J. Zhejiang Univ. Sci. B.* 15, 575–581. doi:10.1631/jzus.B1400024

Shafiee, A., Bucolo, C., Budzynski, E., Ward, K. W., and López, F. J. (2011). *In Vivo* ocular Efficacy Profile of Mapracorat, a Novel Selective Glucocorticoid Receptor Agonist, in Rabbit Models of Ocular Disease. *Invest. Ophthalmol. Vis. Sci.* 52, 1422–1430. doi:10.1167/iovs.10-5598

Sharma, N., Akhade, A. S., and Qadri, A. (2013). Sphingosine-1-Phosphate Suppresses TLR-Induced CXCL8 Secretion from Human T Cells. *J. Leukoc. Biol.* 93, 521–528. doi:10.1189/jlb.0712328

Silva, V. R., Micheletti, T. O., Pimentel, G. D., Katashima, C. K., Lenhare, L., Morari, J., et al. (2014). Hypothalamic S1P/S1PR1 Axis Controls Energy Homeostasis. *Nat. Commun.* 5, 4859. doi:10.1038/ncomms5859

Spampinato, S. F., Obermeier, B., Cotleur, A., Love, A., Takeshita, Y., Sano, Y., et al. (2015). Sphingosine 1 Phosphate at the Blood Brain Barrier: Can the Modulation of S1P Receptor 1 Influence the Response of Endothelial Cells and Astrocytes to Inflammatory Stimuli? *PLoS One* 10, e0133392. doi:10.1371/journal.pone.0133392

Stark, T., Di Bartolomeo, M., Di Marco, R., Drazanova, E., Platania, C. B. M., Iannotti, F. A., et al. (2020). Altered Dopamine D3 Receptor Gene Expression in MAM Model of Schizophrenia Is Reversed by Peripubertal Cannabidiol Treatment. *Biochem. Pharmacol.* 177, 114004. doi:10.1016/j.bcp.2020.114004

Stuttfeld, E., and Ballmer-Hofer, K. (2009). Structure and Function of VEGF Receptors. *IUBMB Life* 61, 915–922. doi:10.1002/iub.234

Trotta, M. C., Maisto, R., Guida, F., Boccella, S., Luongo, L., Balta, C., et al. (2019). The Activation of Retinal HCA2 Receptors by Systemic Beta-Hydroxybutyrate Inhibits Diabetic Retinal Damage through Reduction of Endoplasmic Reticulum Stress and the NLRP3 Inflammasome. *PLoS One* 14, e0211005. doi:10.1371/journal.pone.0211005

Trotta, M. C., Gesualdo, C., Platania, C. B. M., De Robertis, D., Giordano, M., Simonelli, F., et al. (2021). Circulating miRNAs in Diabetic Retinopathy Patients: Prognostic Markers or Pharmacological Targets? *Biochem. Pharmacol.* 186, 114473. doi:10.1016/j.bcp.2021.114473

Vujosevic, S., and Simó, R. (2017). Local and Systemic Inflammatory Biomarkers of Diabetic Retinopathy: An Integrative Approach. *Invest. Ophthalmol. Vis. Sci.* 58, BIO68–BIO75. doi:10.1167/iovs.17-21769

Weigert, A., Olesch, C., and Brüne, B. (2019). Sphingosine-1-Phosphate and Macrophage Biology-How the Sphinx Tames the Big Eater. *Front. Immunol.* 10, 1706. doi:10.3389/fimmu.2019.01706

Wu, H., Hwang, D. K., Song, X., and Tao, Y. (2017). Association between Aqueous Cytokines and Diabetic Retinopathy Stage. *J. Ophthalmol.* 2017, 9402198. doi:10.1155/2017/9402198

Xie, B., Shen, J., Dong, A., Rashid, A., Stoller, G., and Campochiaro, P. A. (2009). Blockade of Sphingosine-1-Phosphate Reduces Macrophage Influx and Retinal and Choroidal Neovascularization. *J. Cel. Physiol.* 218, 192–198. doi:10.1002/jcp.21588

Yamamoto, R., Aoki, T., Koseki, H., Fukuda, M., Hirose, J., Tsuji, K., et al. (2017). A Sphingosine-1-Phosphate Receptor Type 1 Agonist, ASP4058, Suppresses Intracranial Aneurysm through Promoting Endothelial Integrity and Blocking Macrophage Transmigration. *Br. J. Pharmacol.* 174, 2085–2101. doi:10.1111/bph.13820

Yoshida, Y., Tsuji, T., Watanabe, S., Matsushima, A., Matsushima, Y., Banno, R., et al. (2013). Efficacy of Combination Treatment with Fingolimod (FTY720) Plus Pathogenic Autoantigen in a Glucose-6-Phosphate Isomerase Peptide (GPI325-339)-Induced Arthritis Mouse Model. *Biol. Pharm. Bull.* 36, 1739–1746. doi:10.1248/bpb.b13-00297

Zhao, Y., and Singh, R. P. (2018). The Role of Anti-Vascular Endothelial Growth Factor (Anti-VEGF) in the Management of Proliferative Diabetic Retinopathy. *Drugs Context* 7, 212532. doi:10.7573/dic.212532

Conflict of Interest: The authors declare that the research was conducted in the absence of any commercial or financial relationships that could be construed as a potential conflict of interest.

Publisher's Note: All claims expressed in this article are solely those of the authors and do not necessarily represent those of their affiliated organizations, or those of the publisher, the editors and the reviewers. Any product that may be evaluated in this article, or claim that may be made by its manufacturer, is not guaranteed or endorsed by the publisher.

frontiers in Pharmacology

ORIGINAL RESEARCH
published: 29 October 2021
doi: 10.3389/fphar.2021.771571

Proteomic Phenotyping of Stimulated Müller Cells Uncovers Profound Pro-Inflammatory Signaling and Antigen-Presenting Capacity

Adrian Schmalen[1,2], Lea Lorenz[2], Antje Grosche[3], Diana Pauly[4,5], Cornelia A. Deeg[2] and Stefanie M. Hauck[1]**

[1]Research Unit Protein Science and Metabolomics and Proteomics Core, Helmholtz Center Munich, German Research Center for Environmental Health (GmbH), Neuherberg, Germany, [2]Chair of Physiology, Department of Veterinary Sciences, LMU Munich, Martinsried, Germany, [3]Department of Physiological Genomics, Biomedical Center, LMU Munich, Martinsried, Germany, [4]Experimental Ophthalmology, Philipps-University Marburg, Marburg, Germany, [5]Department of Ophthalmology, University Hospital Regensburg, Regensburg, Germany

OPEN ACCESS

Edited by:
Settimio Rossi,
Second University of Naples, Italy

Reviewed by:
Karen Eastlake,
University College London, United Kingdom
Sandra M. Cardona,
University of Texas at San Antonio, United States
Ana Isabel Arroba,
Fundación Para la Gestión de la Investigación Biomédica de CádizCádiz, Spain

***Correspondence:**
Cornelia A. Deeg
deeg@tiph.vetmed.uni-muenchen.de
Stefanie M. Hauck
hauck@helmholtz-muenchen.de

Specialty section:
This article was submitted to Inflammation Pharmacology, a section of the journal Frontiers in Pharmacology

Received: 06 September 2021
Accepted: 12 October 2021
Published: 29 October 2021

Citation:
Schmalen A, Lorenz L, Grosche A, Pauly D, Deeg CA and Hauck SM (2021) Proteomic Phenotyping of Stimulated Müller Cells Uncovers Profound Pro-Inflammatory Signaling and Antigen-Presenting Capacity. Front. Pharmacol. 12:771571. doi: 10.3389/fphar.2021.771571

Müller cells are the main macroglial cells of the retina exerting a wealth of functions to maintain retinal homoeostasis. Upon pathological changes in the retina, they become gliotic with both protective and detrimental consequences. Accumulating data also provide evidence for a pivotal role of Müller cells in the pathogenesis of diabetic retinopathy (DR). While microglial cells, the resident immune cells of the retina are considered as main players in inflammatory processes associated with DR, the implication of activated Müller cells in chronic retinal inflammation remains to be elucidated. In order to assess the signaling capacity of Müller cells and their role in retinal inflammation, we performed in-depth proteomic analysis of Müller cell proteomes and secretomes after stimulation with INFγ, TNFα, IL-4, IL-6, IL-10, VEGF, TGFβ1, TGFβ2 and TGFβ3. We used both, primary porcine Müller cells and the human Müller cell line MIO-M1 for our hypothesis generating approach. Our results point towards an intense signaling capacity of Müller cells, which reacted in a highly discriminating manner upon treatment with different cytokines. Stimulation of Müller cells resulted in a primarily pro-inflammatory phenotype with secretion of cytokines and components of the complement system. Furthermore, we observed evidence for mitochondrial dysfunction, implying oxidative stress after treatment with the various cytokines. Finally, both MIO-M1 cells and primary porcine Müller cells showed several characteristics of atypical antigen-presenting cells, as they are capable of inducing MHC class I and MHC class II with co-stimulatory molecules. In line with this, they express proteins associated with formation and maturation of phagosomes. Thus, our findings underline the importance of Müller cell signaling in the inflamed retina, indicating an active role in chronic retinal inflammation.

Keywords: Müller cells, atypical antigen-presenting cell, immune response, diabetic retinopathy, oxidative phosphorylation, complement system, cytokines, retina

INTRODUCTION

Neurodegenerative diseases of the retina are characterized by progressive retinal damage eventually resulting in vision loss (Duncan et al., 2018). Accumulating evidence over the last years led to the recognition of chronic inflammation as an important part of the pathogenesis underlying this heterogeneous group of retinal diseases (Wooff et al., 2019; Forrester et al., 2020; Olivares-González et al., 2021). While the loss of photoreceptors in inherited retinal diseases such as retinitis pigmentosa originates in various genetic mutations (Broadgate et al., 2017), the driving force that leads to retinal degeneration and blindness in diabetic retinopathy (DR) is a disturbed metabolism with hyperglycemia and dyslipidemia, resulting in microvascular damage (Lechner et al., 2017). DR is among the most frequent causes of blindness worldwide with a rising prevalence (GBaVI, 2021). Chronic hyperglycemia in diabetes patients induces the activation of leukocytes in the periphery (Chen et al., 2019) as well as micro- and macroglial cells in the retina (Mizutani et al., 1998; Gerhardinger et al., 2005; Zeng et al., 2008). This results in the release of pro-inflammatory cytokines and eventually leads to photoreceptor cell death (Coughlin et al., 2017; Kinuthia et al., 2020). Microglial cells, the resident immune cells of the retina, are acknowledged as the main drivers of retinal immune responses (Karlstetter et al., 2015). However, growing evidence suggests that the interaction of micro- and macroglial cells essentially shapes retinal inflammation and photoreceptor degeneration (Wang et al., 2011; Di Pierdomenico et al., 2020).

Retinal Müller glial cells constitute the primary macroglial cells of the retina (Reichenbach and Bringmann, 2020). They span the entire width of the retina and are in close contact with the vitreous, the retinal blood-vessels and with all retinal neurons (Newman and Reichenbach, 1996). While they maintain retinal homeostasis during steady-state conditions, activation of Müller cells under pathological conditions results in gliosis, a cellular attempt to restore insulted tissue, with both protective and detrimental effects (Bringmann et al., 2006). It is known that Müller cells are an important source of neurotrophic factors but also of pro-inflammatory and angiogenetic cytokines (Bringmann et al., 2009; Ruzafa et al., 2018; von Toerne et al., 2014; Hauck et al., 2007). They play an important role in DR pathogenesis (Subirada et al., 2018; Ghaseminejad et al., 2020) and it was also suggested that they are involved in retinal immune responses (Roberge et al., 1988; Rutar et al., 2015; Natoli et al., 2017; Lorenz et al., 2021a; Lorenz et al., 2021b). However, the impact of their protective or detrimental effects on retinal inflammation in DR and other neurodegenerative retinal diseases remains elusive so far. Thus, we performed an in-depth-analysis of the Müller cell proteome and secretome after stimulation with various pro- and anti-inflammatory cytokines as well as growth factors. For our analysis, we used cells of the human Müller glia cell-line MIO-M1 as well as primary porcine retinal Müller Glia (pRMG), as porcine eyes resemble human eyes regarding their anatomy (Middleton S. Porcine ophthalmology, 2010). Furthermore, the pig is established as a useful model for research in diabetic retinopathy (Kleinwort et al., 2017; Renner et al., 2020). Comparative quantitative proteomic analysis allows to elucidate key proteins or pathways involved in disease pathogenesis. In addition, this approach enables the discovery of new biomarkers and has therefore proven as a valuable tool for deciphering pathophysiological key mechanisms (Konigsberg et al., 2021; Weigand et al., 2021). Our hypothesis-generating study yielded comprehensive data on the capacity of Müller cells to react in a very differentiated manner to varying stimulants. In addition to the secretion of pro-inflammatory cytokines, we observed expression of MHC class I and II molecules and proteins that are associated with the processing of antigens. We therefore propose that Müller cells are critical modulators of the retinal immune response and might exert an antigen-presenting function. Thus, attention should be paid to their implication in chronic inflammation underlying degenerative retinal diseases.

MATERIALS AND METHODS

Cell Preparation and Culture

Cells were maintained in Dulbecco's modified eagle medium (DMEM) containing 10% (v/v) inactivated fetal calf serum (FCS), 100 U/ml penicillin and 100 µg/ml streptomycin unless otherwise stated. Cell culture media and reagents were purchased from Gibco (Life Technologies GmbH, Darmstadt, Germany).

Ten porcine eyes from healthy pigs were kindly provided from a local abattoir. The use of porcine material from the abattoir was approved for purposes of scientific research by the appropriate board of the veterinary inspection office, Munich, Germany (registration number DE 09 162 0008-21). No experimental animals were involved in this study. Within 2 h after enucleation, eyes were processed under a laminar flow hood under sterile conditions as previously described (Lorenz et al., 2021b; Sagmeister et al., 2021). In short, periocular tissue was removed and the eyeballs were rinsed in 80% ethanol followed by washing with cold PBS. Afterwards, eyeballs were stored in DMEM until further processing. The eyeballs were opened circumferentially parallel to the limbus corneae, and anterior parts of the eyes were discarded. The retina was detached from the posterior eyeballs and transferred into a petri dish containing DMEM. After removal of vitreous and pigment epithelium residues, major blood-vessels were excised and the remaining retinal tissue was cut into very small fragments using micro-scissors. Resulting fragments were washed in Ringer's solution followed by enzymatic digestion at 37°C with papain previously activated by incubation with 1.1 mM EDTA, 0.067 mM mercaptoethanol and 5.5 mM cysteine-HCl. Enzymatic digestion was stopped after 12 min by adding serum-containing DMEM, followed by addition of Desoxyribonuclease I (Sigma-Aldrich Chemie GmbH, Taufkirchen, Germany) and trituration. After sedimentation of the cells, the supernatant was carefully removed using Pasteur pipettes. The remaining pellets were resuspended in DMEM, pooled and seeded into 6-well plates (Sarstedt, Nümbrecht, Germany). The following day, thorough panning of the plates and removal of the supernatant were performed in order to

eliminate non-attached cells, yielding pure Müller cell cultures as previously described (Hauck et al., 2003; Eberhardt et al., 2012). Cells were cultured at 37°C and 5% CO2 with regular exchange of medium and repeated microscopic control of cell density and purity according to previous reports (Limb et al., 2002; Eberhardt et al., 2012).

The human Müller cell line Moorfields/Institute of Ophthalmology-Müller 1 (MIO-M1; RRID:CVCL_0433) was a kind gift of G. A. Limb (Limb et al., 2002). They were tested negative for *mycoplasma* contamination. Two days before treatment, 1×10^5 MIO-M1 cells per well were seeded in 6-well plates and incubated at 37°C and 5% CO2 until further processing.

Cell Stimulation

The human cytokines Interleukin 10 (IL-10), Transforming Growth Factor beta-1 (TGFβ1), Transforming Growth Factor beta-2 (TGFβ2), Transforming Growth Factor beta-3 (TGFβ3), and Tumor Necrosis Factor Alpha (TNFα) were purchased from Sigma-Aldrich, Interleukin 4 (IL-4) and Interferon Gamma (IFNy) from R&D Systems/Bio-Techne (R&D Systems/Bio-Techne, Wiesbaden-Nordenstadt, Germany), and Interleukin 6 (IL-6) and Vascular Endothelial Growth Factor165 (VEGF) from PeproTech (PeproTech, Winterhude, Germany). Porcine TGFβ3 was purchased from Biozol (Biozol, Eching, Germany), whereas porcine TGFβ1, TGFβ2, IL-4, IL-6, IL-10, IFNy and TNFα were from R&D System/Bio-Techne. Since there was no porcine VEGF available, the above mentioned human VEGF was also used for stimulation of pRMG.

To diminish the influence of cytokines present in FCS, both confluent pRMG and MIO-M1 cells were rinsed two times with prewarmed serum-free medium, followed by starvation for 1 h at 37°C and 5% CO2 with serum-deprived medium. Afterwards, cells were treated over night with IFNy, IL-4, IL-6, IL-10, TGFβ1, TGFβ2, TGFβ3, TNFα or VEGF165, respectively, in a randomized plate design at a concentration of 5 ng/ml in 2 ml medium without FCS. Untreated cells cultured in serum-free medium served as a control. For this study, cells were treated with each cytokine separately, but not with multiple cytokines in combination.

Sample Collection and Proteolysis

Supernatants were collected 24 h after treatment, passed through medium equilibrated 0.2 µm Millex-GP filter units (Merck Chemicals GmbH, Darmstadt, Germany), and transferred into 2 ml Lo-Bind tubes (Eppendorf AG, Hamburg, Germany). Afterwards, cells were washed once with DPBS. 200 µl RIPA buffer containing Roche cOmplete Mini Protease Inhibitor Cocktail (Merck Chemicals GmbH) was applied directly into each well and cells were detached with a cell scraper. Cell supernatants for the secretome analysis and lysates for the proteome analysis were derived from the same experimental set. Lysates were transferred into freshly prepared 1.5 ml Lo-Bind tubes (Eppendorf AG). Protein concentration of the lysates was determined by Pierce BCA assay (Thermo Fisher Scientific). Ten µg protein per lysate or 400 µl supernatant per sample were digested with Lys-C and trypsin using a modified FASP procedure as described elsewhere (Wiśniewski et al., 2009; Grosche et al., 2016).

LC-MS/MS and Quantitative Analysis

LC-MSMS analysis was performed on a QExactive HF mass spectrometer (Thermo Fisher Scientific) online coupled to a UItimate 3000 RSLC nano-HPLC (Dionex, Sunnyvale, United States). Samples were automatically injected and loaded onto a C18 trap column for 5 min. Afterwards, samples were eluted and separated on a C18 analytical column (Acquity UPLC M-Class HSS T3 Column, 1.8 µm, 75 µm × 250 mm; Waters, Milford, United States). Samples were separated by a 95 min non-linear acetonitrile gradient at a flow rate of 250 nl/min. Resolution of the MS spectra was recorded at 60,000 with an AGC target of 3×10^6 and a maximum injection time of 50 ms from 300 to 1,500 m/z. The 10 most abundant peptide ions were selected from the MS scan and fragmented via HCD. Thereby, the normalized collision energy was 27 with an isolation window of 1.6 m/z, and a dynamic exclusion of 30 s. MS/MS spectra were recorded at a resolution of 15,000 with an AGC target of 105 and a maximum injection time of 50 ms. Spectra with unassigned charges, and charges of +1 and >8 were excluded from the precursor selection.

The four datasets (lysates of pRMG and MIO-M1 cells, and secretomes of pRMG and MIO-M1 cells) were analyzed separately. The Proteome Discoverer 2.4 SP1 software (version 2.4.1.15; Thermo Fisher Scientific) was used for peptide and protein identification via a database search (Sequest HT search engine) against the SwissProt Human (MIO-M1) and Ensembl Pig (pRMG). Database search was performed with full tryptic specificity, allowing for up to one missed tryptic cleavage site, a precursor mass tolerance of 10 ppm, and fragment mass tolerance of 0.02 Da. Carbamidomethylation of Cys was set as a static modification. Dynamic modifications included deamidation of Asn and Gln, oxidation of Met, and a combination of Met loss with acetylation on protein N-terminus. Peptide spectrum matches and peptides were validated with the Percolator algorithm (Käll et al., 2007). Each dataset was measured as triplicate. One control sample in the dataset of MIO-M1 secretomes had an unexpected low overall abundance and was excluded as an outlier. Only the top-scoring hits for each spectrum were accepted with a false discovery rate (FDR) < 1% (high confidence). The final list of proteins satisfying the strict parsimony principle included only protein groups passing an additional protein confidence filter FDR <5% filter (target/decoy concatenated search validation).

Quantification of proteins, after precursor recalibration, was based on intensity values (at RT apex) for all unique peptides per protein. Peptide abundances were normalized to the total peptide amount. The protein abundances were calculated summing the normalized abundance values of corresponding unique peptides. These protein abundances were used for calculation of enrichment ratios of proteins in the stimulated samples to the untreated samples, resulting in single ratios for every quantified protein in every treated sample. Significance of the ratios was tested using a background-based *t*-test with correction for multiple testing according to Benjamini-Hochberg (adjusted *p*-value) (Benjamini et al., 2001; Navarro et al., 2014).

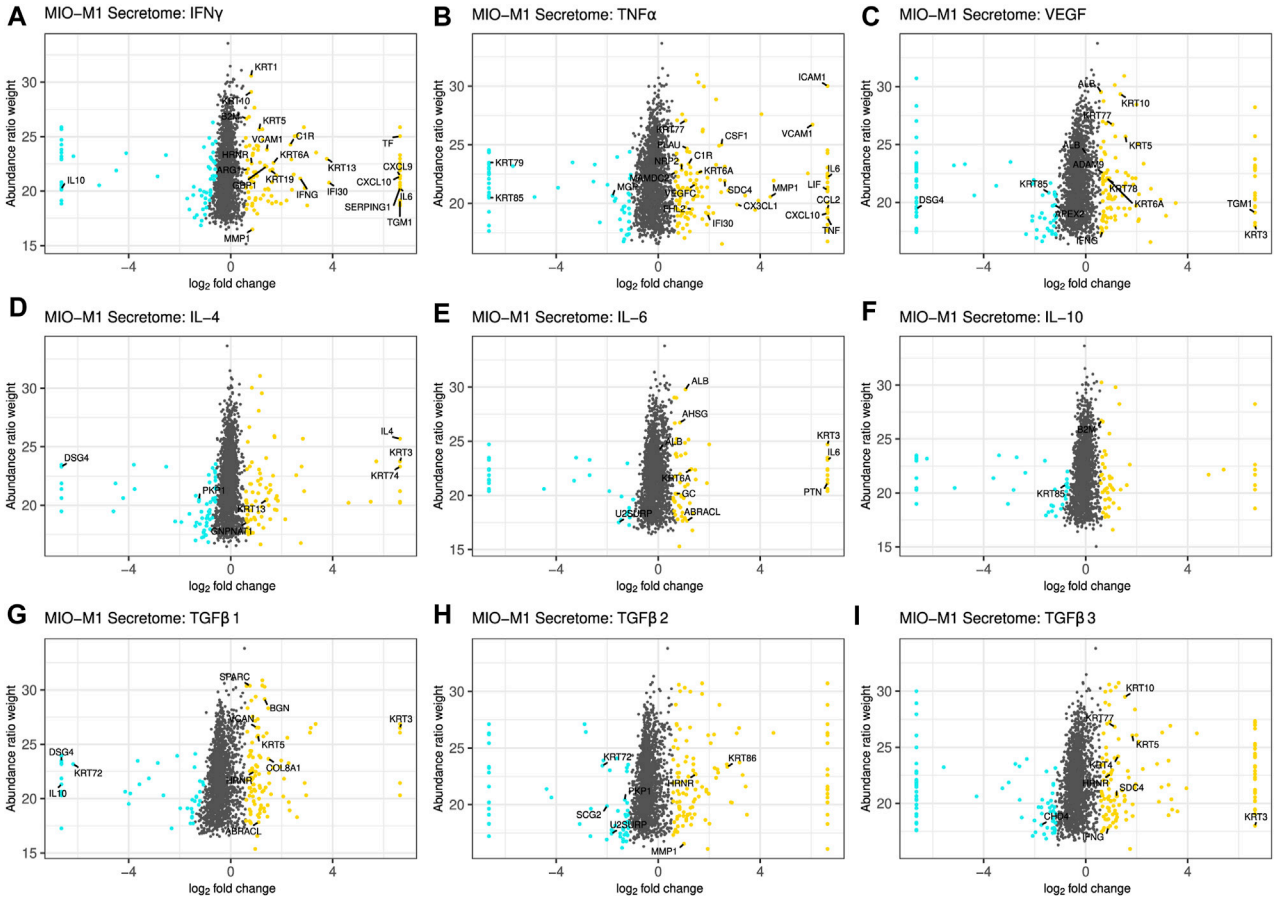

FIGURE 1 | Scatterplot of all identified proteins from MIO-M1 secretomes after treatment with the indicated cytokines for 24 h **(A–I)**. Proteins with significant changes in their abundance (±log2 (1.5) fold expression, corrected *p*-value ≤0.05) were colored, with upregulated proteins being depicted as yellow dots, while down-regulated proteins are colored cyan. Proteins with significantly altered abundance in both, MIO-M1 and pRMG secretomes, are labeled with their gene symbol. Keratins were excluded.

Data Analysis and Visualization

Calculation of the abundance ratio weight requires abundance values for both, the stimulated sample and the control. However, if a protein is exclusively expressed in one of these samples, the Proteome Discoverer software fails to calculate a respective abundance ratio weight. Since these extreme values were of special interest to us, the missing abundance ratio weights were imputed using the R package mice (version 3.13.0) and the "classification and regression trees" imputation method.

Ingenuity Pathway Analysis (IPA; Qiagen, Hilden, Germany) was used to analyze overrepresentation of proteins in canonical pathways of the IPA library, as described elsewhere (Krämer et al., 2014). IPA allows deducing potential physiological effects of the various separately tested cytokines. Analysis was performed based on the fold-change of the stimulated samples and the abundance ratio *p*-value. Fisher's exact test allowed testing for nonrandom associations of proteins in the datasets and the different canonical pathways (Fisher, 1922). Furthermore, the method of Benjamini-Hochberg (B-H *p*-value) corrected for multiple testing (Benjamini et al., 2001).

The euclidean distance for the heatmap analysis was calculated with the open source software Cluster 3.0 and hierarchically clustered by complete linkage clustering (Eisen et al., 1998). The resulting heat map was visualized with the open source software Java Treeview (version 1.2.0) (Saldanha, 2004).

RESULTS

Differential Secretion of Proteins After Stimulation of Müller Cells with Various Cytokines

Müller cells are in close contact to all retinal cells, the vitreous and the blood vessels (Reichenbach and Bringmann, 2020). To address, whether this privileged position within the retina also translates into extensive signaling between Müller cells and the surrounding cells, the secretomes of the human Müller cell-derived cell line MIO-M1 and of pRMG were quantitatively analyzed by mass spectrometry after stimulation for 24 h with the cytokines IFNγ, IL-10, IL-4, IL-6, TGFβ1, TGFβ2, TGFβ3,

TNFα and VEGF, respectively. By this means, we quantified 2,031 proteins in the supernatant of MIO-M1 cells (**Supplementary Table S1**) and 3,093 proteins in the supernatant of pRMG across all treatment groups (**Supplementary Table S2**).

Figure 1 and **Supplementary Figure S1** summarize changes in the secretome after treatment of Müller cells with the different cytokines. A log2 fold change of ±0.58 and a corrected *p*-value of equal or less than 0.05 served as cutoff to define significantly upregulated or downregulated genes, respectively. Proteins equally regulated in MIO-M1 cells and pRMG were labeled with their gene symbol. However, this was only possible for proteins with identical gene symbols in the human and the porcine protein database. After treatment with IFNγ, 107 proteins in the secretome of MIO-M1 cells and 176 proteins in the secretome of pRMG were significantly more abundant, while 67 proteins of MIO-M1 cells and 96 proteins of pRMG were significantly less abundant in the supernatants (**Figure 1A**; **Supplementary Figure S1A**). Intriguingly, MIO-M1 cells and pRMG shared 21 upregulated and one downregulated protein. Among these shared regulated proteins after treatment with IFNγ were many with immune system functions, like signaling molecules (e.g., C-X-C Motif Chemokine Ligand 9 (CXCL9), CXCL10, IL-6) and components of the complement system (e.g., C1r, Serpin Family G Member 1 (SERPING1)). Upon treatment with TNFα, 127 (MIO-M1) or 143 (pRMG) proteins were more abundant and 57 (MIO-M1) or 87 (pRMG) proteins were less abundant in the supernatant (**Figure 1B**; **Supplementary Figure S1B**). Within these groups, MIO-M1 cells and pRMG shared 20 upregulated and three downregulated proteins, again with many pro-inflammatory proteins like C-X3-C Motif Chemokine Ligand 1 (CX3CL1), CXCL10, C-C Motif Chemokine Ligand 2 (CCL2), IL-6, and C1r being upregulated. Thus, IFNγ and TNFα resulted in the most conserved changes of the secretome of Müller cells when comparing between stimulated MIO-M1 cells and pRMG. In contrast, MIO-M1 cells and pRMG only shared ten proteins that were more abundant and three which were less abundant after treatment with VEGF, with seven proteins being keratins (**Figure 1C**; **Supplementary Figure S1C**). Treatment of Müller cells with the three different interleukins had a subtle influence on secreted proteins with conserved regulation of seven (IL-4), nine (IL-6), and two (IL-10) proteins in the secretome of MIO-M1 cells and pRMG (**Figures 1D–F**; **Supplementary Figures S1D–F**).

Finally, TGFβs led to pronounced alterations in the secretome of MIO-M1 cells. TGFβ1 enhanced the secretion of 125 proteins while simultaneously reducing the abundance of 67 proteins, TGFβ2 increased the abundance of 131 proteins while impairing secretion of 69 proteins, and TGFβ3 raised abundance of 135 proteins and reduced the abundance of 76 proteins (**Figures 1G–I**). Furthermore, eleven proteins of MIO-M1 cells and pRMG were similarly regulated by TGFβ1, eight upregulated and three downregulated (**Supplementary Figure S1G**). After treatment with TGFβ2, three proteins were more abundant and four proteins less abundant in the secretome of both cell types (**Supplementary Figure S1H**). Additionally, the secretome of TGFβ3 treated MIO-M1 cells and pRMG shared one downregulated protein and eight upregulated proteins, with most proteins like Osteonectin (Secreted Protein Acidic And Rich In Cysteine; SPARC), Matrix Metallopeptidase 1 (MMP1), Biglycan (BGN) and various keratins being functionally related to extracellular matrix organization (**Supplementary Figure S1I**). Furthermore, stimulation with TGFβ3 evoked upregulation of pro-inflammatory cytokine IFNγ in both, the MIO-M1 cell line and pRMG. Overall, there are subtle, but intriguing differences in protein abundances after stimulation of Müller cells with the different TGFβ isoforms. Some of the proteins differentially induced by the TGFβ isoforms in MIO-M1 cells are pro-inflammatory cytokines, like IFNγ, TNFα, and CCL2 (**Supplementary Table S1**).

Next, we aimed to examine the physiological functions of proteins secreted by Müller cells. Therefore, we ordered secreted proteins in distinct clusters, grouped by similar expression patterns. From the identified proteins of the MIO-M1 supernatant, all cytosolic contaminants were removed, resulting in a list that exclusively contained extracellular proteins. Furthermore, only those proteins that showed a significant change of abundance (corrected *p*-value ≤0.05 and ±1.5-fold abundance) in at least one treatment were selected for further analysis. As a result, a hierarchical heat map and an associated dendrogram consisting of 171 proteins was generated using the log2 abundance ratio of treated and untreated control cells (**Supplementary Figure S2**). Furthermore, clusters were highlighted depending on their position on the dendrogram (**Figure 2**). To avoid single protein clusters, the proteins Polymeric Immunoglobulin Receptor (PIGR) and Lacritin (LACRT) were assigned to Cluster F, despite being on different branches of the dendrogram.

Notably, we identified proteins which were secreted by MIO-M1 cells exclusively after stimulation (cluster A), while another set of proteins was completely absent in MIO-M1 cells (cluster B) treated with VEGF. The largest cluster comprises proteins upregulated by at least one cytokine (cluster C). In contrast to cluster D, consisting of proteins downregulated by TGFβs, TGFβs induce secretion of proteins of cluster E. Finally, secretion of most proteins of cluster F is deterred by at least one cytokine.

The clusters A, C and E are large clusters with proteins upregulated by at least one cytokine, with cluster A being the cluster with the most pronounced changes in secretion of its members and cluster C being the most diffuse one. In order to deduce the physiological functions of the secreted proteins of each of these clusters, we performed gene ontology (GO) analysis. Thereby, redundant pathways were condensed to a single representative pathway and the top 10 pathways with the lowest enrichment FDR were displayed. Intriguingly, the top 10 pathways for cluster A were related to immune system processes, with "Humoral immune response" and "Immune system process" being the most significant pathways with an enrichment FDR of 3.6×10^{-9} and 6.9×10^{-9}, respectively (**Figure 3A**). Furthermore, cluster C contained the pathway "Immune system process", while most other pathways in this cluster C were involved in shaping the extracellular environment (**Figure 3B**). Besides further pathways involved in extracellular remodeling, the proteins of cluster E were also associated to the pathway "AGE-RAGE signaling pathway in diabetic complications" (**Figure 3C**).

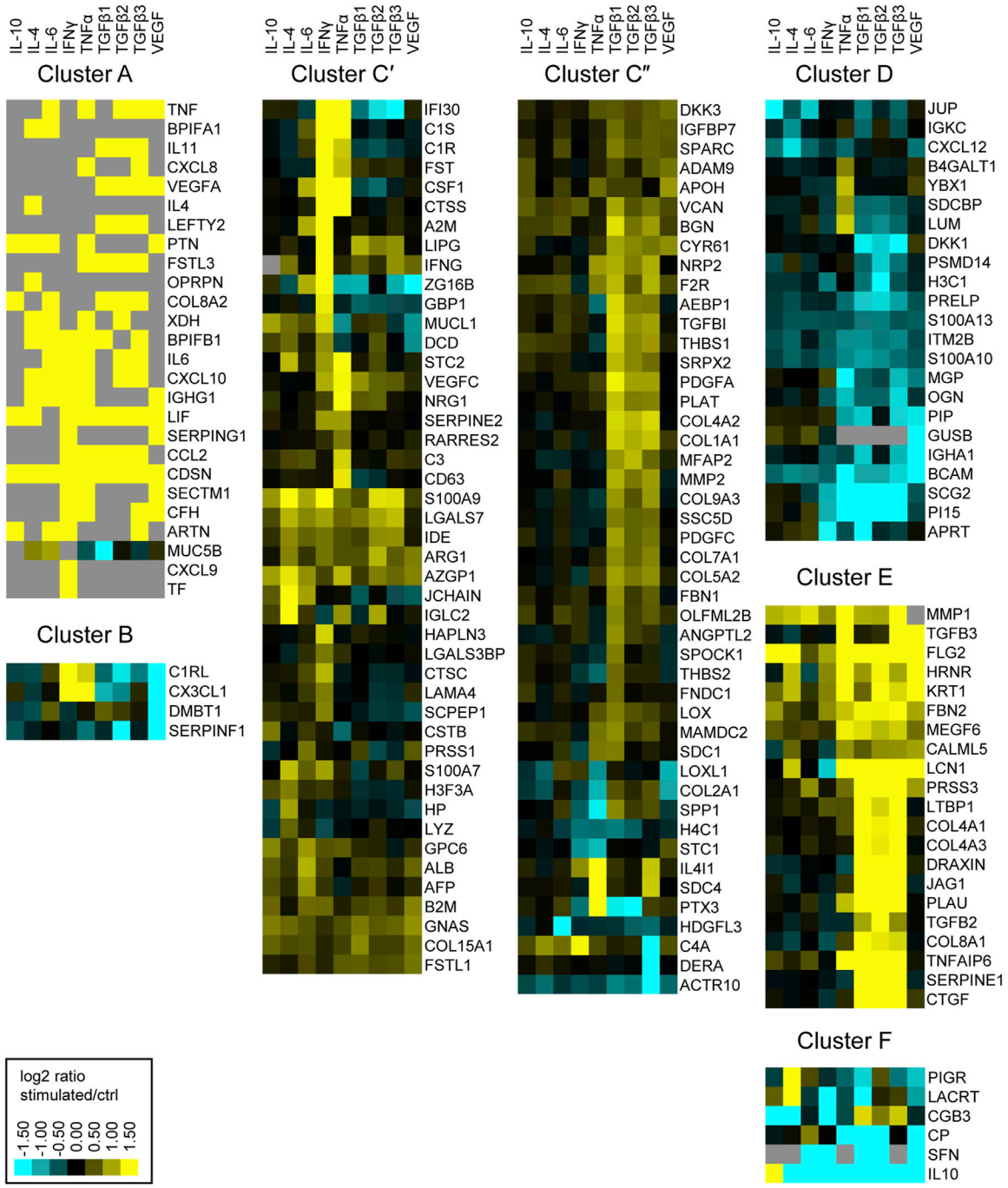

FIGURE 2 | Heatmap of hierarchical cluster analysis of proteins secreted by MIO-M1 cells after treatment with various cytokines separately. Identified proteins were filtered for extracellular proteins with significant changes in expression (±log2 (1.5) fold expression, corrected *p*-value ≤0.05). Down-regulated proteins are presented in cyan, while up-regulated proteins are depicted yellow for the respective treatments. Gray squares represent proteins that were neither identified in the untreated control, nor in the respective treatment. Clusters were defined using the branches of a dendrogram and shown as close up with the corresponding gene symbols.

In-Depth Analysis of the Müller Cell Proteome After Stimulation With a Selection of Cytokines

Our secretome analysis hints towards extensive signaling between Müller cells and their cellular environment, differentially induced upon treatment of Müller cells with various cytokines separately. To elucidate the underlying cellular alterations, we also investigated differences in the proteome of MIO-M1 cells and pRMG cells by mass spectrometry after treatment with these cytokines for 24 h. In total, 5,514 proteins were quantified in the lysates of MIO-M1 cells (**Supplementary Table S3**) and 4,187

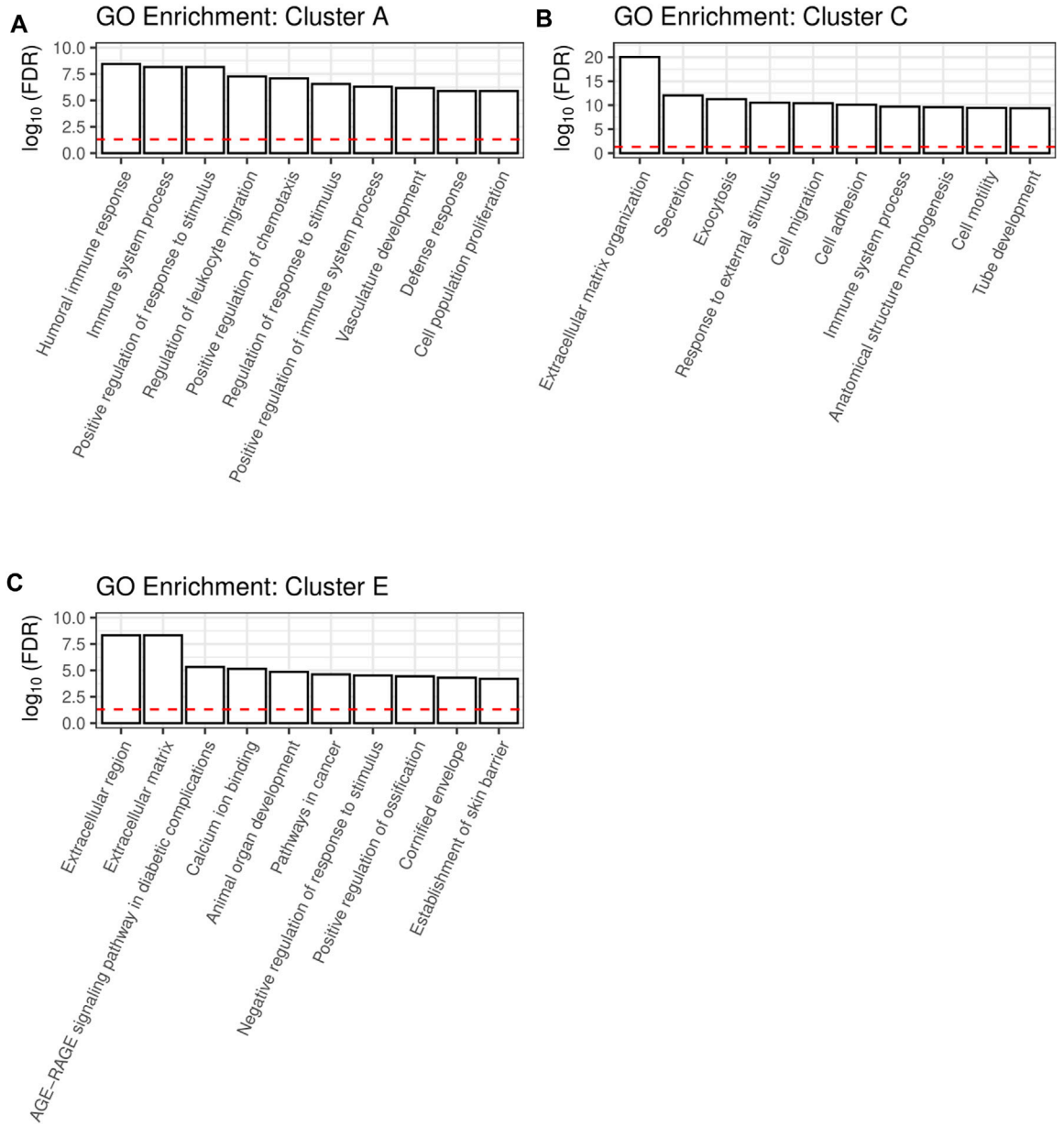

FIGURE 3 | A shiny GO enrichment analysis for the previously defined cluster A **(A)**, cluster C **(B)** and cluster E **(C)** was performed. Redundant pathways were reduced to show only one representative pathway. Depicted is the –log10(FDR) of the top 10 pathways for each cluster. The red dashed line indicates the significance threshold.

proteins in the lysates of pRMG cells (**Supplementary Table S4**) across all treatment groups.

The threshold for significant abundance changes was set using the same cutoff values as for the secretome, and equally regulated proteins in MIO-M1 cells and pRMG were labeled with their gene symbol, if they shared the same gene symbol in the human and the porcine database (**Figure 4**; **Supplementary Figure S3**). Although the porcine protein database contains mostly humanized gene symbols, the swine leukocyte antigens (SLA) genes show little sequence homology between the human and the porcine genome and cannot properly be humanized (Lunney et al., 2009). However, Human Leukocyte Antigen-C Alpha Chain (HLA-C) was part of the porcine protein database.

Treatment of Müller cells with IFNγ resulted in 206 more abundant and 88 less abundant proteins in MIO-M1 cells and 331 more abundant and 36 less abundant proteins in pRMG lysates (**Figure 4A**; **Supplementary Figure S3A**). Thereof, 29 proteins showed higher expression levels in both cells types. Among the overlapping proteins were restriction factors like SAM And HD Domain Containing Deoxynucleoside Triphosphate Triphosphohydrolase 1 (SAMHD1) and MX Dynamin Like GTPase 1 (MX1), transcription factors like Signal Transducer

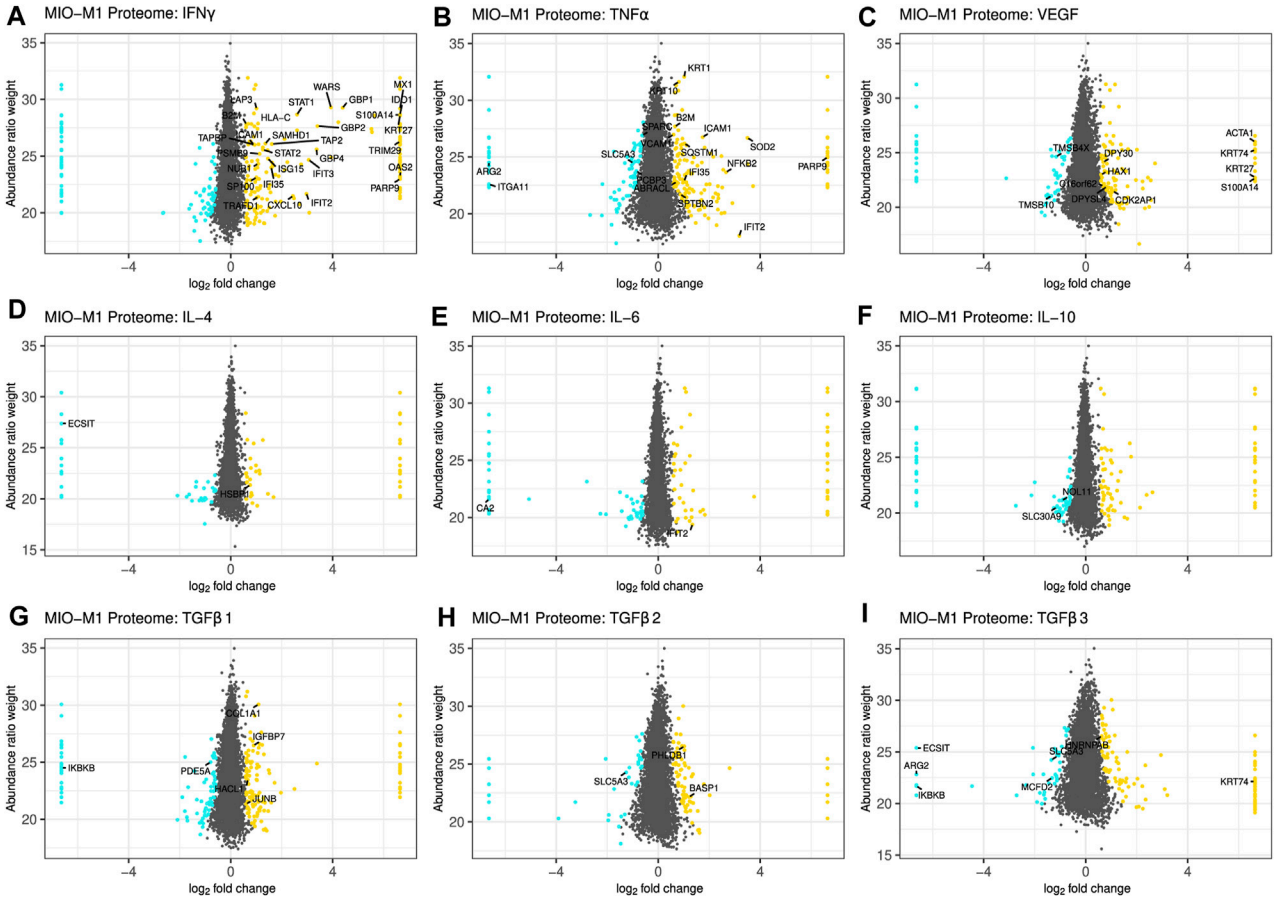

FIGURE 4 | Scatterplot of all identified proteins from MIO-M1 lysates after treatment with the indicated cytokines for 24 h **(A–I)**. Proteins with significant changes in their abundance (±log2 (1.5) fold expression, corrected *p*-value ≤0.05) were colored, with upregulated proteins being depicted as yellow dots, while down-regulated proteins are colored cyan. Proteins with significantly altered abundance in both, MIO-M1 and pRMG lysates, are labeled with their gene symbol. Keratins were excluded.

And Activator Of Transcription 1 (STAT1) and STAT2, regulators of protein homeostasis like Leucine Aminopeptidase 3 (LAP3) or the Proteasome 20S Subunit Beta 9 (PSMB9), and proteins associated with peptide transport and antigen presentation like Transporter 2, ATP Binding Cassette Subfamily B Member (TAP2), TAP Binding Protein (TAPBP), Beta-2-Microglobulin (B2M), as well as HLA-C. After treatment with TNFα, 204 proteins were more abundant in the proteome of MIO-M1 cells, while 119 proteins were less abundant (**Figure 4B**). In pRMG, 207 proteins with higher abundance and 285 proteins with lower abundance were identified upon treatment with TNFα, with 18 proteins that were differentially regulated in both cell types (**Supplementary Figure S3B**). Among shared proteins that were more abundant after treatment with TNFα were pro-inflammatory proteins like B2M and Nuclear Factor Kappa B Subunit 2 (NFKB2), or adhesion molecules like Intercellular Adhesion Molecule 1 (ICAM1) or Vascular Cell Adhesion Molecule 1 (VCAM1). VEGF led to 143 more and 102 less abundant proteins in MIO-M1 cells or 232 more and 224 less abundant proteins in pRMG, respectively (**Figure 4C**; **Supplementary Figure S3C**). Thereof, MIO-M1 cells and pRMG shared nine more abundant proteins, inter alia proteins associated with reorganization of the cortical cytoskeleton like Alpha-Actin-1 (ACTA1) or HCLS1 Associated Protein X-1 (HAX1), and two less abundant proteins, Thymosin Beta 10 (TMSB10) and Thymosin Beta 4 X-Linked (TMSB4X), both inhibitors of actin polymerization. Upon treatment with interleukins IL-4, IL-6 and IL-10, the Müller cell proteomes mirrored the subtle effects of these cytokines on the abundance of proteins observed for the Müller cell secretomes (**Figures 4D–F**; **Supplementary Figures S3D–F**). Also in line with the secretome data, the overlap between differentially abundant proteins of the MIO-M1 and pRMG proteome after treatment with the various interleukins contained only few proteins. In contrast, TGFβ1 increased the abundance of 143 proteins, while decreasing the abundance of 94 proteins in the proteome of MIO-M1 cells and increased the abundance of 203 proteins, while decreasing the abundance of 103 proteins in the proteome of pRMG (**Figure 4G**; **Supplementary Figure S3G**). In comparison to the lower abundant proteins Phosphodiesterase 5A (PDE5A) and Inhibitor Of Nuclear Factor Kappa B Kinase Subunit Beta (IKBKB), the proteins Collagen Type I Alpha 1 Chain (COL1A1),

FIGURE 5 | A comparative IPA analysis with the significantly regulated proteins identified in the pRMG lysates after stimulation with the indicated cytokines was performed. Canonical pathways related to signaling, cell death, immune system processes and oxidative stress were selected. Pathways with significant enrichment of genes after stimulation with at least one cytokine are presented. Significance of the gene enrichment for each pathway and treatment is indicated by purple squares in the left array. Thereby, treatments that did not meet the significance threshold (p-value ≤ 0.05) are marked with a dot. The z-score is indicated in the right array and represents a prediction of activation (orange) or inhibition (blue) of the pathway. Gray squares mark treatments where the activation state of a pathway could not be calculated.

Insulin Like Growth Factor Binding Protein 7 (IGFBP7), JunB Proto-Oncogene (JUNB), and 2-Hydroxyacyl-CoA Lyase 1 (HACL1) were more abundant in both, MIO-M1 cells and pRMG after treatment with TGFβ1. Following treatment with TGFβ2, 125 proteins of the proteome of MIO-M1 cells and 266 proteins of the proteome of pRMG were more abundant, whereas 67 proteins of the MIO-M1 proteome and 229 proteins of the pRMG proteome were less abundantly expressed (**Figure 4H**; **Supplementary Figure S3H**). In the case of treatment with TGFβ3, 130 proteins in the MIO-M1 proteome and 185 in the

pRMG proteome showed higher abundances, while 94 proteins in MIO-M1 proteome and 250 in the pRMG proteome were less abundant (**Figure 4I**; **Supplementary Figure S3I**). The overlap of MIO-M1 cells and pRMG treated with TGFβ2 comprised three proteins, and treatment with TGFβ3 resulted in an overlap of seven proteins. Overall, pRMG reacted more pronounced to treatment with the various cytokines compared to MIO-M1 cells.

Canonical Pathways Enriched in Müller Cells Upon Stimulation

Treatment with cytokines partly induced pronounced changes in the secretome and proteome of Müller cells. In the secretome, these changes primarily included the secretion of pro-inflammatory cytokines and proteins associated with organization of the extracellular matrix. To elucidate overrepresented mechanisms and pathways in stimulated Müller cells, we performed Ingenuity pathway analysis (IPA). We limited the IPA to significantly regulated proteins (p-value ≤ 0.05) identified in the MIO-M1 and pRMG lysates. Since IPA cannot handle porcine gene symbols, we replaced the only canonical SLA gene SLA-1 in our pRMG dataset by the canonical human HLA gene HLA-A. Hence, an IPA core analysis was performed with 1,543 proteins for pRMG and with 2,262 proteins for the MIO-M1 cells. IPA identified 338 canonical pathways within the proteome of MIO-M1 cells and 218 canonical pathways in the proteome of pRMG that were significantly enriched by at least one of the used cytokines (IPA p-value ≤ 0.05; **Supplementary Table S5**). Among the identified canonical pathways were many pathways associated with signaling, cell death, immune system processes and the cellular redox state (**Figure 5**; **Supplementary Figure S4**). A selection of canonical pathways enriched in pRMG cells after treatment with at least one of the tested cytokines is depicted in **Figure 5**. All presented pathways in **Figure 5** were also significantly enriched in MIO-M1 cells upon stimulation with at least one cytokine (**Supplementary Figure S4**).

Among the most significantly regulated pathways in MIO-M1 cells and pRMG were the canonical pathways "Mitochondrial Dysfunction" and "Oxidative Phosphorylation". These pathways were significantly induced by all examined cytokines in pRMG. The pathways "Ferroptosis Signaling Pathway", "iNOS Signaling", "NRF2-mediated Oxidative Stress Response", and "Production of Nitric Oxide and Reactive Oxygen Species in Macrophages" are closely linked to the cellular redox state and were among the enriched pathways in MIO-M1 cells and pRMG after treatment with various cytokines separately. Furthermore, proteins associated with the maturation of phagosomes were significantly enriched in pRMG. In line with this, "Caveolar-mediated Endocytosis Signaling" was significantly enriched in pRMG after treatment with IFNγ, TGFβ1, TNFα and VEGF, and "Clathrin-mediated Endocytosis Signaling" was significantly enriched in pRMG after treatment with all cytokines except IL-10. Besides these two pathways associated with the recycling of the extracellular environment, intracellular protein homeostasis and MHC class I peptide generation was facilitated by enrichment of the "Protein Ubiquitination Pathway" in pRMG after treatment with IFNγ, TGFβ3, TNFα and VEGF. Similarly, IFNγ, IL-4, TGFβ1, TGFβ3, TNFα and VEGF enriched "Protein Ubiquitination Signaling" in MIO-M1 cells. "Neuroinflammation Signaling" was induced by IFNγ, TNFα and VEGF in MIO-M1 cells and by IFNγ, TGFβ1, TGFβ3 and TNFα in pRMG, whereas TGFβ2 and VEGF led to a slight inhibition of this pathway in pRMG.

A Deeper Look Into Müller Cell Complement Secretion Upon Cytokine Stimulation

Because the enrichment analysis of the secretome yielded highly significant hits such as "humoral immune response" and "immune system process," we took a closer look at complement proteins in the secretome and cell lysates. Notably, most complement proteins are secreted as key components of the humoral immune system. The identified complement components include central complement proteins, regulators, and receptors. Consistent with their localization in the cell membrane, the latter (including ITGAM, ITGB2, C5aR1) were detected only in cell lysates, and here specifically in those of pRMGs. The complement regulators clusterin (CLU), vitronectin (VTN), CD59, and SERPING were found in most test samples. With regard to the central complement components, the pRMG secretome took a prominent position and showed results for complement components for all three different activation pathways (e.g., C1q, FD, MASP1) and the terminal pathway (e.g., C9). The central complement protein C3 was found in both the MIO-M1 and pRMG secretomes and in the MIO-M1 lysate. Interestingly, cytokine treatment induced changes in complement proteins and regulators but had no effect on complement receptor expression. We observed that C1q subunits, which initiate the classical complement pathway by binding to antibodies, were detectable only in pRMG but not in MIO-M1 cells. C1q levels in cell lysates and the corresponding secretome were consistently reduced after TNFα treatment but were increased by IFNγ. Moreover, complement proteases C1r and C1s, which bind to C1q therewith continuing the cascade of classical pathway activation, were enriched in the supernatants of MIO-M1 and pRMG cells treated with IFNγ (**Figure 2C**). In contrast, C1r concentration was significantly decrease in supernatants of MIO-M1 cells but not pRMG after VEGF and TGFβ2 application. Notably, C1s and C1r were not detected in cellular lysates. Interestingly, the abundance of the central complement proteins C3 and C4A were modified by the supplemented cytokines in MIO-M1 secretomes only and not in any other data set (**Figure 2C**). These proteins are cleaved upon complement activation as for example triggered by the C1q-mediated classical pathway and result in cleaved products which interact with cellular receptors (e.g., C3a/C3b, C4a). Here, complement protein C3 is mainly increased following TNFα addition and C4 upon exposure to IFNγ (**Figure 2C**). In fact, IFNγ was also the major player modulating the secreted complement components in pRMG: C2 and FI were significantly increased while C9, FD and MASP1 were clearly reduced in its presence. These complement components absent from any other sample.

Regarding the complement regulators factor H (FH), SERPING and CLU are of interest. Secretion of FH was not

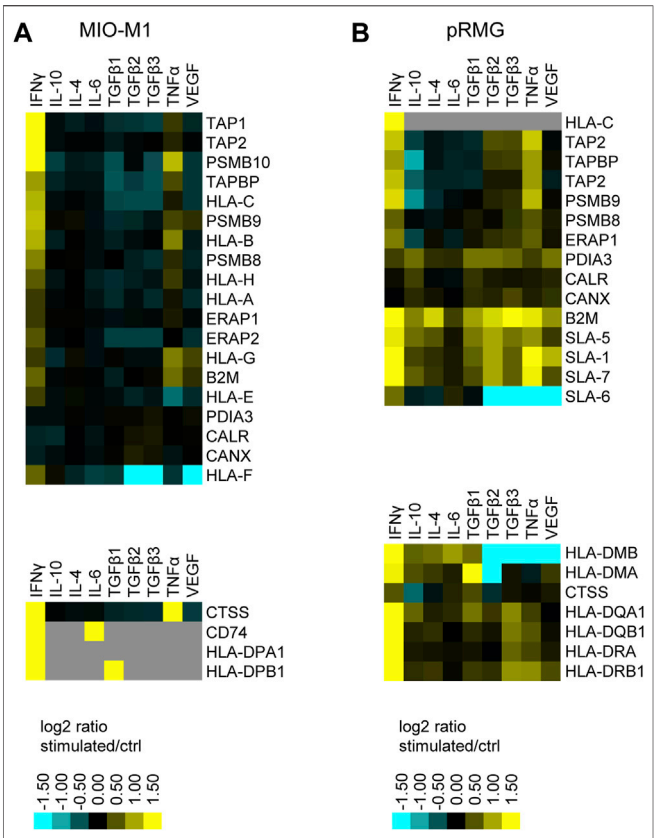

FIGURE 6 | Heatmap of hierarchical cluster analysis of proteins involved in MHC class I (upper panel) and MHC class II (lower panel) antigen presentation expressed by MIO-M1 cells **(A)** and pRMG cells **(B)** after treatment with various cytokines separately. Down-regulated proteins are presented in cyan, while up-regulated proteins are depicted yellow for the respective treatments. Gray squares represent proteins that were neither identified in the untreated control, nor in the respective treatment. The heatmap was generated on the basis of the log2 fold change of the respective proteins.

observed in untreated MIO-M1 and pRMG, but it was significantly upregulated in MIO-M1 secretomes following IFNγ, TNFα, TGFβ3, and VEGF treatment (**Figure 2A**). Similar results were obtained for SERPING, whose levels were increased by IFNγ in the MIO-M1 secretome, pRMG cell lysates and secretome. Remarkably, the MIO-M1 lysate showed decreased values for CLU following IFNγ, TGFβ1 and TNFα, and similar but not significant trends was observed for the respective secretome. Finally, while CLU was upregulated in pRMGs lysates upon IL-6 or VEGF treatment, no significant alterations could be found in corresponding secretomes.

In summary, IFNγ and TNFα seemed to be the most effective cytokines to modulate the Müller cell complement expression and secretion (**Figure 2**).

Müller Cells as Atypcial Antigen-Presenting Cells

Intriguingly, treatment of pRMG with IFNγ, TGFβ2, TGFβ3 and TNFα significantly enriched proteins associated with the "Antigen Presentation Pathway". Likewise, the "Antigen Presentation Pathway" was induced in MIO-M1 cells by treatment with IFNγ, TGFβ1, TNFα and VEGF. Thereby, antigen presentation is an umbrella term for two distinct processes. MHC class I antigen presentation is common to all nucleated cells and allows $CD8^+$ cytotoxic T cells (CTL) to assess whether cells are infected with an intracellular pathogen (Hewitt, 2003; Sigal, 2016). In contrast, MHC class II is presented to antigen specific $CD4^+$ T cells mainly by professional antigen-presenting cells inducing their activation and differentiation to T helper cells (Roche and Furuta, 2015).

To investigate the antigen presentation capacity of Müller cells, we constructed a hierarchical heatmap for MIO-M1 cells (**Figure 6A**) and pRMG (**Figure 6B**) challenged with various cytokines separately. Proteins linked to antigen presentation were selected and clustered hierarchically. Proteins associated with MHC class I antigen presentation are displayed in the upper panel and proteins correlated to MHC class II antigen presentation are depicted in the lower panel. In MIO-M1 cells, IFNγ induced the majority of proteins linked to both, MHC class I and II antigen presentation, whereas TNFα exerted its inductive effect exclusively on MHC class I antigen presentation. The only protein linked to MHC class II antigen presentation induced by TNFα in MIO-M1 cells was Cathepsin S (CTSS). Furthermore, the other cytokines did not induce proteins related to antigen presentation in MIO-M1 cells. Quite the contrary, TGFβ2 and TGFβ3 reduced the abundance of proteins linked to MHC class I antigen presentation in these cells. In contrast to MIO-M1 cells, pRMG reacted to all tested cytokines by induction of components of both MHC class I and II antigen presentation to varying degrees. IFNγ and TNFα induced proteins of MHC class I and II antigen presentation in pRMG, among others SLA-DQA1, SLA-DQB1, SLA-DRA and SLA-DRB1. Furthermore, class I and II antigen presentation was upregulated by TGFβ isoforms 1–3 in pRMG. While TGFβ2 and TGFβ3 induced the components of the MHC class I peptide loading complex TAP2 and TAPBP, TGFβ1 also increased the abundance of HLA-DMA and HLA-DMB, proteins involved in the peptide loading on MHC class II. We saw only a subtle induction of proteins related to antigen presentation by IL-10, IL-4 and IL-6. The smallest impact on antigen presentation proteins was seen after stimulation with IL-6. Furthermore, IFNγ significantly upregulated the expression of the co-stimulatory molecule CD40 in pRMG, while TGFβ2, TGFβ3, TNFα and VEGF resulted in lower abundance of CD40 (**Supplementary Table S4**).

Induction of the canonical MHC class I and MHC class II antigen presentation pathway as assessed by IPA for pRMG after treatment with IFNγ is summarized in **Figure 7**. This pathway was enriched in pRMG cells with a p-value of 4.15×10^{-12}. Besides MHC class I and MHC class II, also components of the peptide loading complex of MHC class I (TAP2 and TPN) were upregulated in pRMG after IFNγ treatment. Furthermore, IFNγ induces the Large Multifunctional Peptidase 2 (LMP2; synonymous to PSMB9) and Large Multifunctional Peptidase 7 (LMP7; synonymous to PSMB8) subunits of the immunoproteasome in MIO-M1 cells.

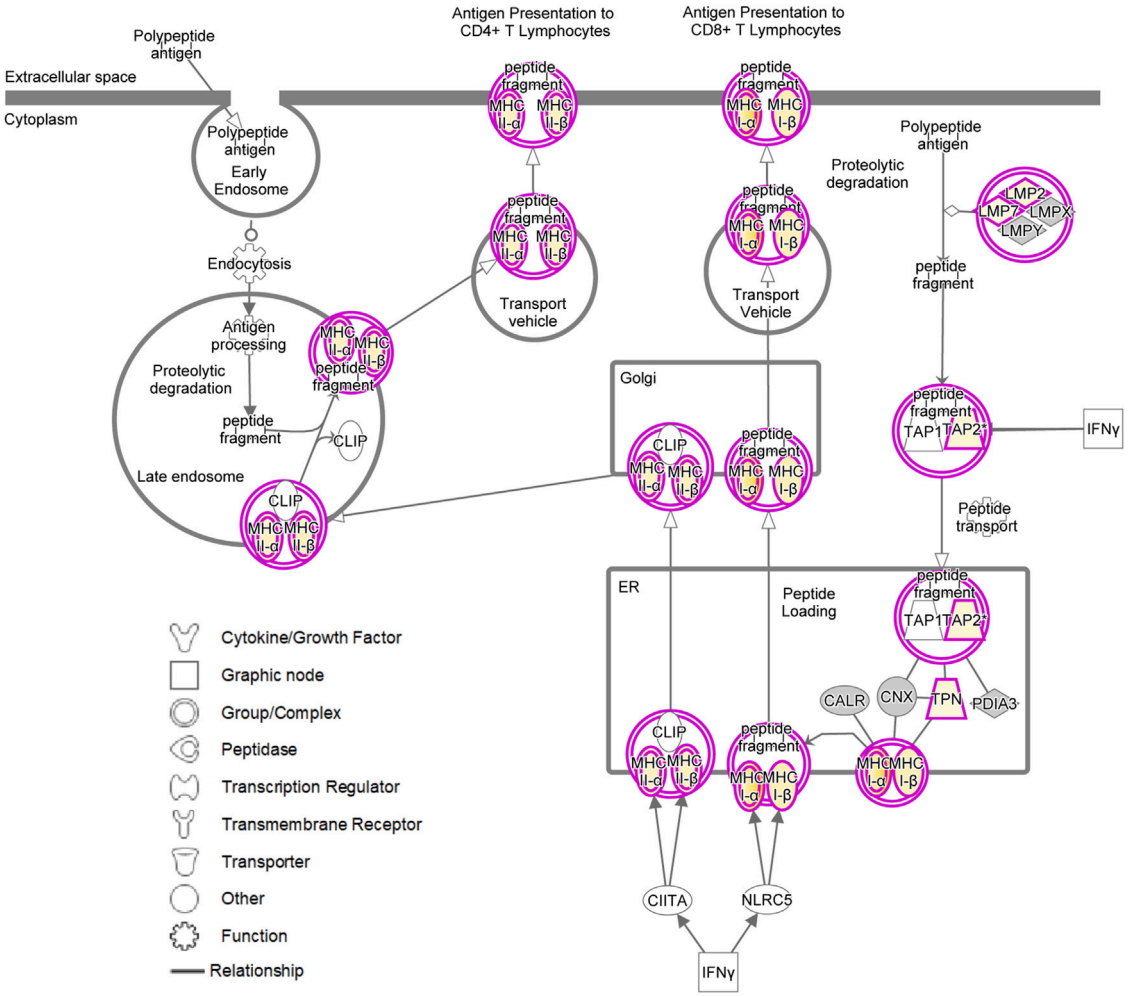

FIGURE 7 | IPA for pRMG cells after treatment with IFNγ was performed. Depicted is the canonical antigen presentation pathway. Yellow proteins are induced. The intensity of the yellow color indicates the degree of upregulation. Grey proteins are in the dataset but did not pass the analysis cutoffs of the pathway analysis. Purple circles highlight proteins (single circle) or complexes (double circles).

DISCUSSION

While microglial cells are considered as the main drivers of retinal immune responses (Karlstetter et al., 2015), increasing evidence suggests that excessive signaling between Müller cells and microglia also affects the inflammatory processes (Wang et al., 2011; Di Pierdomenico et al., 2020). In DR, a condition associated with microvascular degeneration, resulting in ocular inflammation and eventually in complete blindness (Lechner et al., 2017), the production of cytokines by Müller cells plays an essential role for disease pathogenesis, with both beneficial and detrimental effects (Coughlin et al., 2017). We show here that stimulation of Müller cells with pro-inflammatory cytokines like IFNγ or TNFα, but also with growth factors like TGFβ or VEGF resulted in profound, yet distinct response profiles in their secretomes, thus confirming their central role in cell-to-cell communication within the retina. In line with this, Müller cells have previously been shown to be an important source of retinal cytokines (Yoshida et al., 2001; Eastlake et al., 2016). Since the reported physiological concentrations of the tested cytokines is highly variable depending on the analyzed compartment or the method used for quantification, we decided to treat the cells with 5 ng/ml which is in the range of a previous *in vitro* cytokine study with human Müller cells (Yoshida et al., 2001). Furthermore, Yoshida and colleagues showed that the effect of IL-1 on human Müller cells is most pronounced after 24 h of treatment (Yoshida et al., 2001). However, different concentrations or treatment periods might affect the responses observed in Müller cells.

Previously, it has been shown that the conditional knock-out of VEGF in Müller cells of mice reduced the expression of inflammatory markers like TNFα or ICAM1 compared to diabetic control mice, indicating a pro-inflammatory effect of VEGF on Müller cells (Bai et al., 2009; Wang et al., 2010). Here we could show that VEGF induced the Müller cell line MIO-M1 to secrete proteins associated with immune effector processes like IFNγ, B2M, HRNR, and complement-associated proteins like

SERPING1 and complement factor H (FH). Furthermore, ICAM1 was more abundant in our proteome data of MIO-M1 cells and pRMG treated with VEGF compared to the respective control cells. Thus, we were able to confirm the pro-inflammatory role of VEGF in Müller cells.

Overall, we observed that MIO-M1 cells secreted TNFα upon stimulation with VEGF, IL-6, and the TGFβ isoforms 2 and 3. Increased levels of TNFα were previously identified in the vitreous of DR patients (Demircan et al., 2006). Furthermore, Müller cells have been reported to secrete increased amounts of VEGF and TNFα under stress conditions like inflammation or hyperglycemia, thereby promoting retinal inflammation (Zhang et al., 2006; Wang et al., 2010; Zhong et al., 2012; He et al., 2015; Kelly et al., 2018; Liu et al., 2021). Our results show that TNFα induced MIO-M1 cells to secrete inflammatory proteins but also proteins associated with tissue development like Leukemia Inhibitory Factor (LIF), Follistatin (FST), Neuregulin 1 (NRG1), or Pleiotrophin (PTN), to name but a few. Thus, our data suggest a pleotropic role of TNFα in Müller cells.

TGFβs regulate early embryogenesis, maintenance and regeneration of mature tissues, and various disease processes (Gilbert et al., 2016). TGFβ1 has been described to be anti-inflammatory, inducing immune tolerance in the periphery and preventing autoimmunity. Thus, knock out of TGFβ1 in mice induced autoantibodies and multifocal inflammatory disease in many tissues, eventually causing the mice to die within 4 weeks of age (Yaswen et al., 1996). In our *in vitro* model, treatment of MIO-M1 cells with TGFβ1 induced secretion of CCL2 and therefore might result in the recruitment of leukocytes. Simultaneously, TGFβ1 enhanced the secretion of anti-inflammatory proteins like TNF Alpha Induced Protein 6 (TNFAIP6) or LIF in Müller cells. In contrast, TGFβ2 and TGFβ3 also promoted immune system processes in MIO-M1 cells by inducing secretion of pro-inflammatory cytokines TNFα, CXCL8, CXCL10 and IFNγ. It has been shown that TGFβ2 acts immunomodulatory in aqueous humor by decreasing the expression of IL-6, CXCL1, CCL2, G-CSF and IGFBP-5 (Yamagami et al., 2004). However, we demonstrated that treatment of Müller cells with TGFβ2 induced expression of IL-6 and CCL2, suggesting a complex and diverse role of TGFβ2 signaling in the eye. Although TGFβ isoforms are closely related (sharing 71–79% sequence identity), have similar three-dimensional structures and signal canonically through the same receptor (Huang et al., 2014), our secretome analyses provide evidence that they affect Müller cells differentially Latent TGFβ binds Thrombospondin 1 (THBS1), augmenting its activation (Schultz-Cherry and Murphy-Ullrich, 1993; Schultz-Cherry et al., 1994; Murphy-Ullrich and Downs, 2015). Intriguingly, in our study, all three TGFβs elevate the abundance of THBS1 indicating a positive feedback loop. Recently, transcriptome analysis linked the expression of TGFβ isoforms of mice to activation of different signaling cascades. While TGFβ1 and TGFβ2 evoked the non-canonical p38MAPK signaling pathway, which has been linked to gliosis, TGFβ3 induced the SMAD canonical signaling pathway for TGFβs in mice (Kaminska et al., 2009; Conedera et al., 2021). During glaucoma, the aqueous humor contains elevated levels of TGFβ2, exceeding levels for homeostatic signaling (Tripathi et al., 1994; Murphy-Ullrich and Downs, 2015). Thereby, TGFβ2 has been associated with pathological remodeling of the trabecular meshwork and the optical nerve head (Murphy-Ullrich and Downs, 2015). Furthermore, it stimulated secretion of extracellular matrix proteins by astrocytes and cells of the lamina cribrosa (Fuchshofer et al., 2005; Fuchshofer, 2011; Zode et al., 2011; Fuchshofer and Tamm, 2012). Our data suggest that Müller cells also contribute to the remodeling of the extracellular matrix as stimulation with TGFβ1 and TGFβ3 resulted in enhanced secretion of extracellular matrix proteins like Fibrillin-2 (FBN2), various keratins, and collagens. Furthermore, they simultaneously enhanced the turnover of extracellular matrix by inducing the secretion of the Matrix Metalloprotease-1 (MMP1) and MMP2. Previously, MMP2 has been described to be elevated in DR patients and to promote the pathogenesis of DR by inducing mitochondrial dysfunction and apoptosis of retinal capillary cells (Mohammad and Kowluru, 2010). Intriguingly, our IPA also indicates that the canonical pathway for mitochondrial dysfunction is enriched in Müller cells upon stimulation with all TGFβ isoforms. However, this is not solely due to the enhanced secretion of MMP2, since mitochondrial dysfunction is enriched in Müller cells by all tested cytokines, whereas TGFβs exclusively induce MMP2.

Although our data show no contribution of Müller cells to elevated IL-10 secretion upon stimulation with the tested cytokines, IL-10 induced proteins associated with tissue development, cell adhesion, and angiogenesis in MIO-M1 cells, namely Corneodesmosin (CDSN), LIF, PTN, and various collagens, to name a few. In line with this, it has been shown that IL-10 is involved in the pathological angiogenesis during the postnatal development by modulating the macrophage response to hypoxia (Dace et al., 2008). Thus, we hypothesize that IL-10 might also be involved in the abnormal angiogenesis during DR.

Previously, it has been shown that the canonically anti-inflammatory IL-4 can potentiate cytokine and chemokine production in macrophages following a pro-inflammatory stimulus (Major et al., 2002; Gadani et al., 2012; Luzina et al., 2012). In line with this, we observed increased abundances of many pro-inflammatory proteins like IFNγ, S100A9, S100A7, CXCL10, and Lysozyme C (LYZ) upon stimulation of MIO-M1 cells with IL-4, indicating that IL-4 does not exert an anti- but a pro-inflammatory influence in these cells. Thus, IL-4 might potentiate pro-inflammatory secretion in Müller cells similar to pro-inflammatory stimulated macrophages (Major et al., 2002; Gadani et al., 2012; Luzina et al., 2012). The similarities of Müller cells and macrophages upon IL-4 treatment should be investigated in more detail in future studies. Interestingly, MIO-M1 cells did not secrete the anti-inflammatory interleukin IL-4 upon treatment with the various tested cytokines. Secretion of pro-inflammatory IL-6 by Müller cells has been described upon treatment with IL-1β or LPS (Yoshida et al., 2001). Furthermore, elevated levels of IL-6 were found in the vitreous and serum of DR patients and even further increased in patients suffering from proliferative DR (Yao et al., 2019). Here we show that IFNγ, TNFα, TGFβ2, and TGFβ3 also induced the secretion of IL-6 in MIO-M1 cells. Previously, it was shown that IL1β induced IL-6

through activation of the p38MAPK signaling pathway (Liu et al., 2015). The murine TGFβ isoforms 1 and 2 also activated the p38MAPK signaling in Müller cells of mice (Conedera et al., 2021). Thus, the involvement of p38MAPK signaling in secretion of IL-6 by Müller cells should be addressed in further studies. Brandon and colleagues demonstrated induction of VEGF by IL-6 in Müller cells, especially under hyperglycemic conditions, preventing Müller cells from glucose toxicity (Coughlin et al., 2019). In contrast, our analysis revealed no VEGF secretion by MIO-M1 cells upon IL-6 treatment. High glucose concentrations of 25 mM potentiated the induction of VEGF by IL-6 (Coughlin et al., 2019). However, by default the standard culture medium used in our study has a D-glucose concentration of 25 mM. Thus, an adaption of MIO-M1 cells to these conditions might have occurred negating the induction of VEGF by IL-6.

Elevated levels of IFNγ in the vitreous of DR patients have been described previously (Wu et al., 2017; Ucgun et al., 2020). In our study, we could observe distinctly elevated INFγ secretion only after stimulation with INFγ. Treatment with IFNγ furthermore induced the secretion of CXCL9, CXCL10, IL-6 and complement subcomponent C1r in MIO-M1 cells and pRMG.

Interestingly, we observed an induction of CX3CL1 in the whole-cell lysates and in the secretomes. Specifically, except for TGFβ1 and TGFβ2, all stimulants used in this study induced expression of CX3CL1 in the cell proteome of MIO-M1 cells, while only IFNγ and TNFα treatment resulted in significantly higher abundance of CX3CL1 in the secretome as well. CX3CL1 is a membrane-bound chemokine, which functions as an adhesion molecule for leukocytes, but can also be proteolytically cleaved, resulting in a soluble form with chemotactic function (Bazan et al., 1997; Imai et al., 1997). Circulating CD11b+ leukocytes that are involved in leukostasis in DR express higher levels of CX3CR1 in diabetic mice compared to controls (Serra et al., 2012). Thus, membrane-bound CX3CL1 on the surface of Müller cells might be involved in leukostasis in DR. In a previous study, incubation of microglia with Müller cell supernatant containing secreted CX3CL1 resulted in the upregulation of the respective receptor CX3CR1 in microglia. The authors proposed that Müller cells might be able to promote microglial motility via the chemotactic effect of CX3CL1 (Zhang et al., 2018). Thus, secretion of CX3CL1 from Müller cells might contribute to chronic retinal inflammation by recruiting peripheral inflammatory cells and microglia. Another route of communication between microglia/macrophages and Müller cells could be local changes in complement expression. We recently demonstrated, that Müller cells in the mouse retina are the main producers of complement components of the classical (C1s, C4), the alternative pathway (FB) and C3 as the central component to all pathways under homeostatic, but also under ischemic stress conditions (Pauly et al., 2019). In the retina, it is the microglia that by far express highest levels of complement receptors including ITGAM (alias CD11b), C3aR, C5aR1 and C5aR2 (Pauly et al., 2019). In our present study, TNFα and INFγ triggerd the most prominent effects on complement expression consistently in MIO-M1 and pRMG. Given that *in vivo* microglia and potentially other immune cell serve as major source of TNFα and INFγ (Kaczmarek-Hajek et al., 2018) (resource data from Cowan et al. (2020) at https://data.iob.ch), the strong effect of these cytokines on Müller cells could be central to coordinate the tissue immune homeostasis in pathologies. In this context, the enhanced expression of activating complement components by Müller cells could serve as feedback mechanisms towards microglia in turn modulating their activation profile. Taken together, our results point towards a pro-inflammatory phenotype of Müller cells, which is in line with a previous study, where we analyzed the surfaceome of primary equine Müller cells and MIO-M1 cells after stimulation with Lipopolysaccharide (Lorenz et al., 2021b). While the surfaceome of Müller cells in this previous study revealed expression of MHC class I and II as well as costimulatory molecules especially in primary equine Müller cells, we could now further complement these results with LC-MS/MS-analyses of whole cell lysates and of cell supernatants, confirming an antigen-presenting phenotype of Müller cells. While stimulation with LPS resulted in enhanced expression of MHC class II molecules in primary equine Müller cells, no MHC class II molecules could be identified in MIO-M1 cells upon LPS treatment (Lorenz et al., 2021b). In contrast, stimulation with IFNγ in this study induced the expression of proteins that are associated with both MHC class I and MHC class II antigen presentation in pRMG as well as in MIO-M1 cells. This is in accordance with an early study that demonstrated the induction of MHC class I and MHC class II molecules in primary human Müller cells by IFNγ *in vitro* (Mano et al., 1991). In contrast to MIO-M1 cells, pRMG also showed basal expression of MHC class II without stimulation. Thus, our data demonstrate that Müller cells exhibit several criteria for atypical antigen-presenting cells (Kambayashi and Laufer, 2014). Furthermore, our proteomic analysis revealed significantly higher abundance of the costimulatory molecule CD40 in pRMG after stimulation with IFNγ. In contrast to the porcine dataset, we could not identify CD40 in the MIO-M1 cells. As CD40 expression has already been shown in primary human Müller cells, our result might be due to the dedifferentiation of immortalized cells in culture (Portillo et al., 2014). Our data confirm that Müller cells are crucially involved in immunological processes in the retina as well, as they possess an antigen processing and presenting machinery and secrete pro-inflammatory cytokines (Karlstetter et al., 2015). We have previously shown that the cultivation of primary porcine Müller cells under hyperglycemic conditions resulted in higher expression levels of MHC class II molecules, pointing towards an immunologically activated state of Müller cells in DR (Sagmeister et al., 2021).

Pro-inflammatory stimulation of Müller cells resulted in the enrichment of proteins and pathways that are associated with the formation and maturation of phagosomes. Previously, Müller cells have been described to be phagocytic cells, capable of phagocytosing cell debris, dead photoreceptor cells and even bacteria (Singh et al., 2014; Bejarano-Escobar et al., 2017; Sakami et al., 2019). Our IPA showed that proteins of phagocytosis pathways in Müller cells are induced upon stimulation with various cytokines. Furthermore, phagocytosis is not only clathrin- but also caveolar-mediated. Since our data showed enrichment of phagocytic pathways, as well as the

canonical antigen presentation pathway, it is possible that Müller cells present exogenous peptides on MHC class II to $CD4^+$ T helper cells. Intriguingly, phagocytosis of dead photoreceptors would also allow Müller cells to present proteins expressed by photoreceptors on MHC class II, and via cross-presentation on MHC class I (Larsson et al., 2001; Gutiérrez-Martínez et al., 2015). Further studiesshould address, whether Müller cells are sufficient to stimulate alloreactive naïve T cells or memory T cells (Kambayashi and Laufer, 2014).

Oxidative stress and reactive oxygen species (ROS) are known to play a central role during the pathogenesis of DR (Cecilia et al., 2019). Rat-derived Müller cells under hyperglycemic conditions developed mitochondrial dysfunction and oxidative stress, causing swelling and eventually apoptosis of the cells (Krügel et al., 2011; Tien et al., 2017). Mitochondrial dysfunction can lead to ROS production, which then promotes inflammatory response by activation of NF-κB and release of pro-inflammatory cytokines (Behl and Kotwani, 2015; Homme et al., 2018). Our analysis revealed that proteins associated with mitochondrial dysfunction were enriched after treatment of pRMG with all tested cytokines. Furthermore, two significantly enriched pathways in our data sets are associated with reactive oxygen species, namely "NRF2 mediated Oxidative Stress Response" and "Production of Nitric Oxide and Reactive Oxygen Species in Macrophages". Intriguingly, Müller cells have previously been found to regulate the ROS levels via Nrf2 and to be more resistant to ROS formation compared to photoreceptor cells or bipolar cells (Wang et al., 2015; Grosche et al., 2016). In line with this, we showed that treatment with IL-4, TGFβ2, TGFβ3, TNFα and VEGF inhibited death receptor signaling in pRMG. Phagocytic cells often produce ROS to protect themselves from pathogens (Geng et al., 2015). Furthermore, macrophages stabilize cytosolic Nrf2 to be more resistant against ROS (Wang et al., 2019). Since Müller cells have been shown to by phagocytic, we propose that induction of ROS in these cells also serves as a defense mechanism (Singh et al., 2014; Bejarano-Escobar et al., 2017; Sakami et al., 2019).

Our hypothesis generating approach indicates the release of many pro-inflammatory cytokines *in vitro* by Müller cells, as well as Müller cells with the potential to present peptides on MHC class I and II to T cells. This might have implications for the pathogenesis of DR or, in a broader context, on chronic retinal inflammation in general. However, further studies using diseased retinas are necessary in order to show the influence of pro-inflammatory Müller cells on retinal inflammations.

In this study, we used both primary porcine Müller cells and the spontaneously immortalized human Müller cell line MIO-M1 that was established and described in the Moorfields Institute of Ophthalmology 2002 (Limb et al., 2002). Although MIO-M1 cells largely retain the phenotypic and functional characteristics of Müller cells *in vitro*, previous studies documented some characteristics of neuronal stem cells and expression of postmitotic neuronal cell markers in MIO-M1 cells (Limb et al., 2002; Lawrence et al., 2007; Hollborn et al., 2011). Furthermore, it has been shown that Müller cells tend to adapt to cell culture conditions by reduced secretion of neurotrophic factors (Hauck et al., 2008; Merl et al., 2012). Our analysis revealed many proteins commonly regulated in pRMG and MIO-M1 cells, as well as pathways similarly enriched and regulated in both cells. However, we also observed effects specific for either MIO-M1 cells or pRMG. Thus, for example our IPA revealed that MIO-M1 cells decrease the activity of the significantly enriched canonical pathway oxidative phosphorylation, while it is amongst the most induced pathways of pRMG following treatment with the majority of tested cytokines. While these differences might originate from different adaption of MIO-M1 cells and pRMG to the cell culture conditions or the immortalization of MIO-M1 cells, it might as well be possible that they originate from differences in human and porcine Müller cells. Further studies should elaborate similarities and differences between freshly prepared primary human and porcine Müller cells.

Taken together, our in-depth proteomic profiling of MIO-M1 cells and pRMG revealed the capacity of Müller cells to react in a differentiated manner upon treatment with various growth factors and cytokines. Furthermore, we demonstrated a primarily pro-inflammatory phenotype of Müller cells, as they secreted a variety of pro-inflammatory cytokines, complement components and upregulated proteins associated with antigen processing and presentation, suggesting a function as atypical antigen-presenting cell in the course of retinal inflammation. Furthermore, we observed enrichment of proteins connected to mitochondrial dysfunction, as well as proteins related to the formation and maturation of phagosomes. Thus, Müller cells are capable of modulating immune responses in the retina, and may significantly contribute to chronic inflammation during DR.

DATA AVAILABILITY STATEMENT

The datasets presented in this study can be found in an online repository. The repository and accession number can be found below: https://www.ebi.ac.uk/pride; PXD028390.

AUTHOR CONTRIBUTIONS

Conceptualization, SH and CD; Formal analysis, SH; Funding acquisition, SH and CD; Investigation, AS, LL, CD, and SH; Project administration, SH; Supervision, SH; Visualization, AS; Writing–original draft, AS, LL, AG, and DP; Writing–review and editing, CD and SH. All authors have read and agreed to the published version of the manuscript.

FUNDING

This work was funded by Deutsche Forschungsgemeinschaft in the SPP 2127, grant numbers DFG DE 719/7-1 to CD, HA 6014/5-1 to SH, GR 4403/5-1 to AG and PA 1844/3-1 to DP.

ACKNOWLEDGMENTS

The authors would like to thank Adrian Sandbiller for providing porcine eye samples as well as Juliane Merl-Pham for critical discussions.

SUPPLEMENTARY MATERIAL

The Supplementary Material for this article can be found online at: https://www.frontiersin.org/articles/10.3389/fphar.2021.771571/full#supplementary-material

REFERENCES

Bai, Y., Ma, J. X., Guo, J., Wang, J., Zhu, M., Chen, Y., et al. (2009). Müller Cell-Derived VEGF Is a Significant Contributor to Retinal Neovascularization. *J. Pathol.* 219 (4), 446–454. doi:10.1002/path.2611

Bazan, J. F., Bacon, K. B., Hardiman, G., Wang, W., Soo, K., Rossi, D., et al. (1997). A New Class of Membrane-Bound Chemokine with a CX3C Motif. *Nature* 385 (6617), 640–644. doi:10.1038/385640a0

Behl, T., and Kotwani, A. (2015). Exploring the Various Aspects of the Pathological Role of Vascular Endothelial Growth Factor (VEGF) in Diabetic Retinopathy. *Pharmacol. Res.* 99, 137–148. doi:10.1016/j.phrs.2015.05.013

Bejarano-Escobar, R., Sánchez-Calderón, H., Otero-Arenas, J., Martín-Partido, G., and Francisco-Morcillo, J. (2017). Müller Glia and Phagocytosis of Cell Debris in Retinal Tissue. *J. Anat.* 231 (4), 471–483. doi:10.1111/joa.12653

Benjamini, Y., Drai, D., Elmer, G., Kafkafi, N., and Golani, I. (2001). Controlling the False Discovery Rate in Behavior Genetics Research. *Behav. Brain Res.* 125 (1-2), 279–284. doi:10.1016/s0166-4328(01)00297-2

Bringmann, A., Iandiev, I., Pannicke, T., Wurm, A., Hollborn, M., Wiedemann, P., et al. (2009). Cellular Signaling and Factors Involved in Müller Cell Gliosis: Neuroprotective and Detrimental Effects. *Prog. Retin. Eye Res.* 28 (6), 423–451. doi:10.1016/j.preteyeres.2009.07.001

Bringmann, A., Pannicke, T., Grosche, J., Francke, M., Wiedemann, P., Skatchkov, S. N., et al. (2006). Müller Cells in the Healthy and Diseased Retina. *Prog. Retin. Eye Res.* 25 (4), 397–424. doi:10.1016/j.preteyeres.2006.05.003

Broadgate, S., Yu, J., Downes, S. M., and Halford, S. (2017). Unravelling the Genetics of Inherited Retinal Dystrophies: Past, Present and Future. *Prog. Retin. Eye Res.* 59, 53–96. doi:10.1016/j.preteyeres.2017.03.003

Cecilia, O. M., José Alberto, C. G., José, N. P., Ernesto Germán, C. M., Ana Karen, L. C., Luis Miguel, R. P., et al. (2019). Oxidative Stress as the Main Target in Diabetic Retinopathy Pathophysiology. *J. Diabetes Res.* 2019, 8562408. doi:10.1155/2019/8562408

Chen, M., Obasanmi, G., Armstrong, D., Lavery, N. J., Kissenpfennig, A., Lois, N., et al. (2019). STAT3 Activation in Circulating Myeloid-Derived Cells Contributes to Retinal Microvascular Dysfunction in Diabetes. *J. Neuroinflammation* 16 (1), 138. doi:10.1186/s12974-019-1533-1

Conedera, F. M., Quintela Pousa, A. M., Presby, D. M., Mercader, N., Enzmann, V., and Tschopp, M. (2021). Diverse Signaling by TGFβ Isoforms in Response to Focal Injury Is Associated with Either Retinal Regeneration or Reactive Gliosis. *Cell Mol Neurobiol* 41 (1), 43–62. doi:10.1007/s10571-020-00830-5

Coughlin, B. A., Feenstra, D. J., and Mohr, S. (2017). Müller Cells and Diabetic Retinopathy. *Vis. Res* 139, 93–100. doi:10.1016/j.visres.2017.03.013

Coughlin, B. A., Trombley, B. T., and Mohr, S. (2019). Interleukin-6 (IL-6) Mediates protection against Glucose Toxicity in Human Müller Cells via Activation of VEGF-A Signaling. *Biochem. Biophys. Res. Commun.* 517 (2), 227–232. doi:10.1016/j.bbrc.2019.07.044

Cowan, C. S., Renner, M., De Gennaro, M., Gross-Scherf, B., Goldblum, D., Hou, Y., et al. (2020). Cell Types of the Human Retina and its Organoids at Single-Cell Resolution. *Cell* 182 (6), 1623–e34. doi:10.1016/j.cell.2020.08.013

Dace, D. S., Khan, A. A., Kelly, J., and Apte, R. S. (2008). Interleukin-10 Promotes Pathological Angiogenesis by Regulating Macrophage Response to Hypoxia during Development. *PLoS One* 3 (10), e3381. doi:10.1371/journal.pone.0003381

Demircan, N., Safran, B. G., Soylu, M., Ozcan, A. A., and Sizmaz, S. (2006). Determination of Vitreous Interleukin-1 (IL-1) and Tumour Necrosis Factor (TNF) Levels in Proliferative Diabetic Retinopathy. *Eye (Lond)* 20 (12), 1366–1369. doi:10.1038/sj.eye.6702138

Di Pierdomenico, J., Martínez-Vacas, A., Hernández-Muñoz, D., Gómez-Ramírez, A. M., Valiente-Soriano, F. J., Agudo-Barriuso, M., et al. (2020). Coordinated Intervention of Microglial and Müller Cells in Light-Induced Retinal Degeneration. *Invest. Ophthalmol. Vis. Sci.* 61 (3), 47. doi:10.1167/iovs.61.3.47

Duncan, J. L., Pierce, E. A., Laster, A. M., Daiger, S. P., Birch, D. G., Ash, J. D., et al. (2018). Inherited Retinal Degenerations: Current Landscape and Knowledge Gaps. *Transl Vis. Sci. Technol.* 7 (4), 6. doi:10.1167/tvst.7.4.6

Eastlake, K., Banerjee, P. J., Angbohang, A., Charteris, D. G., Khaw, P. T., and Limb, G. A. (2016). Müller Glia as an Important Source of Cytokines and Inflammatory Factors Present in the Gliotic Retina during Proliferative Vitreoretinopathy. *Glia* 64 (4), 495–506. doi:10.1002/glia.22942

Eberhardt, C., Amann, B., Stangassinger, M., Hauck, S. M., and Deeg, C. A. (2012). Isolation, Characterization and Establishment of an Equine Retinal Glial Cell Line: a Prerequisite to Investigate the Physiological Function of Müller Cells in the Retina. *J. Anim. Physiol. Anim. Nutr. (Berl)* 96 (2), 260–269. doi:10.1111/j.1439-0396.2011.01147.x

Eisen, M. B., Spellman, P. T., Brown, P. O., and Botstein, D. (1998). Cluster Analysis and Display of Genome-wide Expression Patterns. *Proc. Natl. Acad. Sci. U S A.* 95 (25), 14863–14868. doi:10.1073/pnas.95.25.14863

Fisher, R. A. (1922). On the Interpretation of χ 2 from Contingency Tables, and the Calculation of P. *J. R. Stat. Soc.* 85 (1), 87–94. doi:10.2307/2340521

Forrester, J. V., Kuffova, L., and Delibegovic, M. (2020). The Role of Inflammation in Diabetic Retinopathy. *Front. Immunol.* 11, 583687. doi:10.3389/fimmu.2020.583687

Fuchshofer, R., Birke, M., Welge-Lussen, U., Kook, D., and Lütjen-Drecoll, E. (2005). Transforming Growth Factor-Beta 2 Modulated Extracellular Matrix Component Expression in Cultured Human Optic Nerve Head Astrocytes. *Invest. Ophthalmol. Vis. Sci.* 46 (2), 568–578. doi:10.1167/iovs.04-0649

Fuchshofer, R., and Tamm, E. R. (2012). The Role of TGF-β in the Pathogenesis of Primary Open-Angle Glaucoma. *Cell Tissue Res* 347 (1), 279–290. doi:10.1007/s00441-011-1274-7

Fuchshofer, R. (2011). The Pathogenic Role of Transforming Growth Factor-B2 in Glaucomatous Damage to the Optic Nerve Head. *Exp. Eye Res.* 93 (2), 165–169. doi:10.1016/j.exer.2010.07.014

Gadani, S. P., Cronk, J. C., Norris, G. T., and Kipnis, J. (2012). IL-4 in the Brain: a Cytokine to Remember. *J. Immunol.* 189 (9), 4213–4219. doi:10.4049/jimmunol.1202246

GBaVI, Collaborators. (2021). Causes of Blindness and Vision Impairment in 2020 and Trends over 30 years, and Prevalence of Avoidable Blindness in Relation to VISION 2020: the Right to Sight: an Analysis for the Global Burden of Disease Study. *Lancet Glob. Health* 9 (2), e144–e60.

Geng, J., Sun, X., Wang, P., Zhang, S., Wang, X., Wu, H., et al. (2015). Kinases Mst1 and Mst2 Positively Regulate Phagocytic Induction of Reactive Oxygen Species and Bactericidal Activity. *Nat. Immunol.* 16 (11), 1142–1152. doi:10.1038/ni.3268

Gerhardinger, C., Costa, M. B., Coulombe, M. C., Toth, I., Hoehn, T., and Grosu, P. (2005). Expression of Acute-phase Response Proteins in Retinal Müller Cells in Diabetes. *Invest. Ophthalmol. Vis. Sci.* 46 (1), 349–357. doi:10.1167/iovs.04-0860

Ghaseminejad, F., Kaplan, L., Pfaller, A. M., Hauck, S. M., and Grosche, A. (2020). The Role of Müller Cell Glucocorticoid Signaling in Diabetic Retinopathy. *Graefes Arch. Clin. Exp. Ophthalmol.* 258 (2), 221–230. doi:10.1007/s00417-019-04521-w

Gilbert, R. W. D., Vickaryous, M. K., and Viloria-Petit, A. M. (2016). Signalling by Transforming Growth Factor Beta Isoforms in Wound Healing and Tissue Regeneration. *J. Dev. Biol.* 4 (2). doi:10.3390/jdb4020021

Grosche, A., Hauser, A., Lepper, M. F., Mayo, R., von Toerne, C., Merl-Pham, J., et al. (2016). The Proteome of Native Adult Müller Glial Cells from Murine Retina. *Mol. Cel Proteomics* 15 (2), 462–480. doi:10.1074/mcp.M115.052183

Gutiérrez-Martínez, E., Planès, R., Anselmi, G., Reynolds, M., Menezes, S., Adiko, A. C., et al. (2015). Cross-Presentation of Cell-Associated Antigens by MHC

Class I in Dendritic Cell Subsets. *Front. Immunol.* 6, 363. doi:10.3389/fimmu.2015.00363

Hauck, S. M., Gloeckner, C. J., Harley, M. E., Schoeffmann, S., Boldt, K., Ekstrom, P. A., et al. (2008). Identification of Paracrine Neuroprotective Candidate Proteins by a Functional Assay-Driven Proteomics Approach. *Mol. Cel Proteomics* 7 (7), 1349–1361. doi:10.1074/mcp.M700456-MCP200

Hauck, S. M., Schoeffmann, S., Amann, B., Stangassinger, M., Gerhards, H., Ueffing, M., et al. (2007). Retinal Mueller Glial Cells Trigger the Hallmark Inflammatory Process in Autoimmune Uveitis. *J. Proteome Res.* 6 (6), 2121–2131. doi:10.1021/pr060668y

Hauck, S. M., Suppmann, S., and Ueffing, M. (2003). Proteomic Profiling of Primary Retinal Müller Glia Cells Reveals a Shift in Expression Patterns upon Adaptation to *In Vitro* Conditions. *Glia* 44 (3), 251–263. doi:10.1002/glia.10292

He, J., Wang, H., Liu, Y., Li, W., Kim, D., and Huang, H. (2015). Blockade of Vascular Endothelial Growth Factor Receptor 1 Prevents Inflammation and Vascular Leakage in Diabetic Retinopathy. *J. Ophthalmol.* 2015, 605946. doi:10.1155/2015/605946

Hewitt, E. W. (2003). The MHC Class I Antigen Presentation Pathway: Strategies for Viral Immune Evasion. *Immunology* 110 (2), 163–169. doi:10.1046/j.1365-2567.2003.01738.x

Hollborn, M., Ulbricht, E., Rillich, K., Dukic-Stefanovic, S., Wurm, A., Wagner, L., et al. (2011). The Human Müller Cell Line MIO-M1 Expresses Opsins. *Mol. Vis.* 17, 2738–2750.

Homme, R. P., Singh, M., Majumder, A., George, A. K., Nair, K., Sandhu, H. S., et al. (2018). Remodeling of Retinal Architecture in Diabetic Retinopathy: Disruption of Ocular Physiology and Visual Functions by Inflammatory Gene Products and Pyroptosis. *Front. Physiol.* 9, 1268. doi:10.3389/fphys.2018.01268

Huang, T., Schor, S. L., and Hinck, A. P. (2014). Biological Activity Differences between TGF-B1 and TGF-B3 Correlate with Differences in the Rigidity and Arrangement of Their Component Monomers. *Biochemistry* 53 (36), 5737–5749. doi:10.1021/bi500647d

Imai, T., Hieshima, K., Haskell, C., Baba, M., Nagira, M., Nishimura, M., et al. (1997). Identification and Molecular Characterization of Fractalkine Receptor CX3CR1, Which Mediates Both Leukocyte Migration and Adhesion. *Cell* 91 (4), 521–530. doi:10.1016/s0092-8674(00)80438-9

Kaczmarek-Hajek, K., Zhang, J., Kopp, R., Grosche, A., Rissiek, B., Saul, A., et al. (2018). Re-evaluation of Neuronal P2X7 Expression Using Novel Mouse Models and a P2X7-specific Nanobody. *Elife* 7. doi:10.7554/eLife.36217

Käll, L., Canterbury, J. D., Weston, J., Noble, W. S., and MacCoss, M. J. (2007). Semi-supervised Learning for Peptide Identification from Shotgun Proteomics Datasets. *Nat. Methods* 4 (11), 923–925. doi:10.1038/nmeth1113

Kambayashi, T., and Laufer, T. M. (2014). Atypical MHC Class II-Expressing Antigen-Presenting Cells: Can Anything Replace a Dendritic Cell. *Nat. Rev. Immunol.* 14 (11), 719–730. doi:10.1038/nri3754

Kaminska, B., Gozdz, A., Zawadzka, M., Ellert-Miklaszewska, A., and Lipko, M. (2009). MAPK Signal Transduction Underlying Brain Inflammation and Gliosis as Therapeutic Target. *Anat. Rec. (Hoboken)* 292 (12), 1902–1913. doi:10.1002/ar.21047

Karlstetter, M., Scholz, R., Rutar, M., Wong, W. T., Provis, J. M., and Langmann, T. (2015). Retinal Microglia: Just Bystander or Target for Therapy. *Prog. Retin. Eye Res.* 45, 30–57. doi:10.1016/j.preteyeres.2014.11.004

Kelly, K., Wang, J. J., and Zhang, S. X. (2018). The Unfolded Protein Response Signaling and Retinal Müller Cell Metabolism. *Neural Regen. Res.* 13 (11), 1861–1870. doi:10.4103/1673-5374.239431

Kinuthia, U. M., Wolf, A., and Langmann, T. (2020). Microglia and Inflammatory Responses in Diabetic Retinopathy. *Front. Immunol.* 11, 564077. doi:10.3389/fimmu.2020.564077

Kleinwort, K. J. H., Amann, B., Hauck, S. M., Hirmer, S., Blutke, A., Renner, S., et al. (2017). Retinopathy with central Oedema in an INS C94Y Transgenic Pig Model of Long-Term Diabetes. *Diabetologia* 60 (8), 1541–1549. doi:10.1007/s00125-017-4290-7

Konigsberg, I. R., Borie, R., Walts, A. D., Cardwell, J., Rojas, M., Metzger, F., et al. (2021). Molecular Signatures of Idiopathic Pulmonary Fibrosis. *Am. J. Respir. Cel Mol Biol.* doi:10.1165/rcmb.2020-0546oc

Krämer, A., Green, J., Pollard, J., Jr., and Tugendreich, S. (2014). Causal Analysis Approaches in Ingenuity Pathway Analysis. *Bioinformatics* 30 (4), 523–530. doi:10.1093/bioinformatics/btt703

Krügel, K., Wurm, A., Pannicke, T., Hollborn, M., Karl, A., Wiedemann, P., et al. (2011). Involvement of Oxidative Stress and Mitochondrial Dysfunction in the Osmotic Swelling of Retinal Glial Cells from Diabetic Rats. *Exp. Eye Res.* 92 (1), 87–93. doi:10.1016/j.exer.2010.11.007

Larsson, M., Fonteneau, J. F., and Bhardwaj, N. (2001). Dendritic Cells Resurrect Antigens from Dead Cells. *Trends Immunol.* 22 (3), 141–148. doi:10.1016/s1471-4906(01)01860-9

Lawrence, J. M., Singhal, S., Bhatia, B., Keegan, D. J., Reh, T. A., Luthert, P. J., et al. (2007). MIO-M1 Cells and Similar Muller Glial Cell Lines Derived from Adult Human Retina Exhibit Neural Stem Cell Characteristics. *Stem Cells* 25 (8), 2033–2043. doi:10.1634/stemcells.2006-0724

Lechner, J., O'Leary, O. E., and Stitt, A. W. (2017). The Pathology Associated with Diabetic Retinopathy. *Vis. Res* 139, 7–14. doi:10.1016/j.visres.2017.04.003

Limb, G. A., Salt, T. E., Munro, P. M., Moss, S. E., and Khaw, P. T. (2002). *In Vitro* characterization of a Spontaneously Immortalized Human Müller Cell Line (MIO-M1). *Invest. Ophthalmol. Vis. Sci.* 43 (3), 864–869.

Liu, X., Ye, F., Xiong, H., Hu, D. N., Limb, G. A., Xie, T., et al. (2015). IL-1β Induces IL-6 Production in Retinal Müller Cells Predominantly through the Activation of P38 MAPK/NF-κB Signaling Pathway. *Exp. Cel Res* 331 (1), 223–231. doi:10.1016/j.yexcr.2014.08.040

Liu, Y., Li, L., Pan, N., Gu, J., Qiu, Z., Cao, G., et al. (2021). TNF-α Released from Retinal Müller Cells Aggravates Retinal Pigment Epithelium Cell Apoptosis by Upregulating Mitophagy during Diabetic Retinopathy. *Biochem. Biophys. Res. Commun.* 561, 143–150. doi:10.1016/j.bbrc.2021.05.027

Lorenz, L., Amann, B., Hirmer, S., Degroote, R. L., Hauck, S. M., and Deeg, C. A. (2021). NEU1 Is More Abundant in Uveitic Retina with Concomitant Desialylation of Retinal Cells. *Glycobiology*. doi:10.1093/glycob/cwab014

Lorenz, L., Hirmer, S., Schmalen, A., Hauck, S. M., and Deeg, C. A. (2021). Cell Surface Profiling of Retinal Müller Glial Cells Reveals Association to Immune Pathways after LPS Stimulation. *Cells* 10 (3). doi:10.3390/cells10030711

Lunney, J. K., Ho, C. S., Wysocki, M., and Smith, D. M. (2009). Molecular Genetics of the Swine Major Histocompatibility Complex, the SLA Complex. *Dev. Comp. Immunol.* 33 (3), 362–374. doi:10.1016/j.dci.2008.07.002

Luzina, I. G., Keegan, A. D., Heller, N. M., Rook, G. A., Shea-Donohue, T., and Atamas, S. P. (2012). Regulation of Inflammation by Interleukin-4: a Review of "alternatives". *J. Leukoc. Biol.* 92 (4), 753–764. doi:10.1189/jlb.0412214

Major, J., Fletcher, J. E., and Hamilton, T. A. (2002). IL-4 Pretreatment Selectively Enhances Cytokine and Chemokine Production in Lipopolysaccharide-Stimulated Mouse Peritoneal Macrophages. *J. Immunol.* 168 (5), 2456–2463. doi:10.4049/jimmunol.168.5.2456

Mano, T., Tokuda, N., and Puro, D. G. (1991). Interferon-gamma Induces the Expression of Major Histocompatibility Antigens by Human Retinal Glial Cells. *Exp. Eye Res.* 53 (5), 603–607. doi:10.1016/0014-4835(91)90219-5

Merl, J., Ueffing, M., Hauck, S. M., and von Toerne, C. (2012). Direct Comparison of MS-based Label-free and SILAC Quantitative Proteome Profiling Strategies in Primary Retinal Müller Cells. *Proteomics* 12 (12), 1902–1911. doi:10.1002/pmic.201100549

Middleton S. Porcine ophthalmology (2010). Veterinary Clinics of North America: Food Animal Practice. *Porcine Ophthalmol.* 26 (3), 557–572. doi:10.1016/j.cvfa.2010.09.002

Mizutani, M., Gerhardinger, C., and Lorenzi, M. (1998). Müller Cell Changes in Human Diabetic Retinopathy. *Diabetes* 47 (3), 445–449. doi:10.2337/diabetes.47.3.445

Mohammad, G., and Kowluru, R. A. (2010). Matrix Metalloproteinase-2 in the Development of Diabetic Retinopathy and Mitochondrial Dysfunction. *Lab. Invest.* 90 (9), 1365–1372. doi:10.1038/labinvest.2010.89

Murphy-Ullrich, J. E., and Downs, J. C. (2015). The Thrombospondin1-TGF-β Pathway and Glaucoma. *J. Ocul. Pharmacol. Ther.* 31 (7), 371–375. doi:10.1089/jop.2015.0016

Natoli, R., Fernando, N., Madigan, M., Chu-Tan, J. A., Valter, K., Provis, J., et al. (2017). Microglia-derived IL-1β Promotes Chemokine Expression by Müller Cells and RPE in Focal Retinal Degeneration. *Mol. Neurodegener* 12 (1), 31. doi:10.1186/s13024-017-0175-y

Navarro, P., Trevisan-Herraz, M., Bonzon-Kulichenko, E., Núñez, E., Martínez-Acedo, P., Pérez-Hernández, D., et al. (2014). General Statistical Framework for Quantitative Proteomics by Stable Isotope Labeling. *J. Proteome Res.* 13 (3), 1234–1247. doi:10.1021/pr4006958

Newman, E., and Reichenbach, A. (1996). The Müller Cell: a Functional Element of the Retina. *Trends Neurosci.* 19 (8), 307–312. doi:10.1016/0166-2236(96)10040-0

Olivares-González, L., Velasco, S., Campillo, I., and Rodrigo, R. (2021). Retinal Inflammation, Cell Death and Inherited Retinal Dystrophies. *Int. J. Mol. Sci.* 22 (4). doi:10.3390/ijms22042096

Pauly, D., Agarwal, D., Dana, N., Schäfer, N., Biber, J., Wunderlich, K. A., et al. (2019). Cell-Type-Specific Complement Expression in the Healthy and Diseased Retina. *Cell Rep* 29 (9), 2835–e4. doi:10.1016/j.celrep.2019.10.084

Portillo, J. A., Greene, J. A., Okenka, G., Miao, Y., Sheibani, N., Kern, T. S., et al. (2014). CD40 Promotes the Development of Early Diabetic Retinopathy in Mice. *Diabetologia* 57 (10), 2222–2231. doi:10.1007/s00125-014-3321-x

Reichenbach, A., and Bringmann, A. (2020). Glia of the Human Retina. *Glia* 68 (4), 768–796. doi:10.1002/glia.23727

Renner, S., Blutke, A., Clauss, S., Deeg, C. A., Kemter, E., Merkus, D., et al. (2020). Porcine Models for Studying Complications and Organ Crosstalk in Diabetes Mellitus. *Cel Tissue Res.* doi:10.1007/s00441-019-03158-9

Roberge, F. G., Caspi, R. R., and Nussenblatt, R. B. (1988). Glial Retinal Müller Cells Produce IL-1 Activity and Have a Dual Effect on Autoimmune T Helper Lymphocytes. Antigen Presentation Manifested after Removal of Suppressive Activity. *J. Immunol.* 140 (7), 2193–2196.

Roche, P. A., and Furuta, K. (2015). The Ins and Outs of MHC Class II-Mediated Antigen Processing and Presentation. *Nat. Rev. Immunol.* 15 (4), 203–216. doi:10.1038/nri3818

Rutar, M., Natoli, R., Chia, R. X., Valter, K., and Provis, J. M. (2015). Chemokine-mediated Inflammation in the Degenerating Retina Is Coordinated by Müller Cells, Activated Microglia, and Retinal Pigment Epithelium. *J. Neuroinflammation* 12 (1), 8. doi:10.1186/s12974-014-0224-1

Ruzafa, N., Pereiro, X., Lepper, M. F., Hauck, S. M., and Vecino, E. (2018). A Proteomics Approach to Identify Candidate Proteins Secreted by Müller Glia that Protect Ganglion Cells in the Retina. *PROTEOMICS* 18 (11), e1700321. doi:10.1002/pmic.201700321

Sagmeister, S., Merl-Pham, J., Petrera, A., Deeg, C. A., and Hauck, S. M. (2021). High Glucose Treatment Promotes Extracellular Matrix Proteome Remodeling in Mller Glial Cells. *PeerJ* 9, e11316. doi:10.7717/peerj.11316

Sakami, S., Imanishi, Y., and Palczewski, K. (2019). Müller Glia Phagocytose Dead Photoreceptor Cells in a Mouse Model of Retinal Degenerative Disease. *FASEB J.* 33 (3), 3680–3692. doi:10.1096/fj.201801662R

Saldanha, A. J. (2004). Java Treeview-Eextensible Visualization of Microarray Data. *Bioinformatics* 20 (17), 3246–3248. doi:10.1093/bioinformatics/bth349

Schultz-Cherry, S., Lawler, J., and Murphy-Ullrich, J. E. (1994). The Type 1 Repeats of Thrombospondin 1 Activate Latent Transforming Growth Factor-Beta. *J. Biol. Chem.* 269 (43), 26783–26788. doi:10.1016/s0021-9258(18)47087-1

Schultz-Cherry, S., and Murphy-Ullrich, J. E. (1993). Thrombospondin Causes Activation of Latent Transforming Growth Factor-Beta Secreted by Endothelial Cells by a Novel Mechanism. *J. Cel Biol* 122 (4), 923–932. doi:10.1083/jcb.122.4.923

Serra, A. M., Waddell, J., Manivannan, A., Xu, H., Cotter, M., and Forrester, J. V. (2012). CD11b+ Bone Marrow-Derived Monocytes Are the Major Leukocyte Subset Responsible for Retinal Capillary Leukostasis in Experimental Diabetes in Mouse and Express High Levels of CCR5 in the Circulation. *Am. J. Pathol.* 181 (2), 719–727. doi:10.1016/j.ajpath.2012.04.009

Sigal, L. J. (2016). Activation of CD8 T Lymphocytes during Viral Infections. *Encyclopedia of Immunobiology*, 286–290. doi:10.1016/b978-0-12-374279-7.14009-3

Singh, P. K., Shiha, M. J., and Kumar, A. (2014). Antibacterial Responses of Retinal Müller Glia: Production of Antimicrobial Peptides, Oxidative Burst and Phagocytosis. *J. Neuroinflammation* 11, 33. doi:10.1186/1742-2094-11-33

Subirada, P. V., Paz, M. C., Ridano, M. E., Lorenc, V. E., Vaglienti, M. V., Barcelona, P. F., et al. (2018). A Journey into the Retina: Müller Glia Commanding Survival and Death. *Eur. J. Neurosci.* 47 (12), 1429–1443. doi:10.1111/ejn.13965

Tien, T., Zhang, J., Muto, T., Kim, D., Sarthy, V. P., and Roy, S. (2017). High Glucose Induces Mitochondrial Dysfunction in Retinal Müller Cells: Implications for Diabetic Retinopathy. *Invest. Ophthalmol. Vis. Sci.* 58 (7), 2915–2921. doi:10.1167/iovs.16-21355

Tripathi, R. C., Li, J., Chan, W. F., and Tripathi, B. J. (1994). Aqueous Humor in Glaucomatous Eyes Contains an Increased Level of TGF-Beta 2. *Exp. Eye Res.* 59 (6), 723–727. doi:10.1006/exer.1994.1158

Ucgun, N. I., Zeki-Fikret, C., and Yildirim, Z. (2020). Inflammation and Diabetic Retinopathy. *Mol. Vis.* 26, 718–721.

von Toerne, C., Menzler, J., Ly, A., Senninger, N., Ueffing, M., and Hauck, S. M. (2014). Identification of a Novel Neurotrophic Factor from Primary Retinal Müller Cells Using Stable Isotope Labeling by Amino Acids in Cell Culture (SILAC). *Mol. Cel Proteomics* 13 (9), 2371–2381. doi:10.1074/mcp.M113.033613

Wang, J., Shanmugam, A., Markand, S., Zorrilla, E., Ganapathy, V., and Smith, S. B. (2015). Sigma 1 Receptor Regulates the Oxidative Stress Response in Primary Retinal Müller Glial Cells via NRF2 Signaling and System Xc(-), the Na(+)-independent Glutamate-Cystine Exchanger. *Free Radic. Biol. Med.* 86, 25–36. doi:10.1016/j.freeradbiomed.2015.04.009

Wang, J., Xu, X., Elliott, M. H., Zhu, M., and Le, Y. Z. (2010). Müller Cell-Derived VEGF Is Essential for Diabetes-Induced Retinal Inflammation and Vascular Leakage. *Diabetes* 59 (9), 2297–2305. doi:10.2337/db09-1420

Wang, M., Ma, W., Zhao, L., Fariss, R. N., and Wong, W. T. (2011). Adaptive Müller Cell Responses to Microglial Activation Mediate Neuroprotection and Coordinate Inflammation in the Retina. *J. Neuroinflammation* 8, 173. doi:10.1186/1742-2094-8-173

Wang, P., Geng, J., Gao, J., Zhao, H., Li, J., Shi, Y., et al. (2019). Macrophage Achieves Self-protection against Oxidative Stress-Induced Ageing through the Mst-Nrf2 axis. *Nat. Commun.* 10 (1), 755. doi:10.1038/s41467-019-08680-6

Weigand, M., Hauck, S. M., Deeg, C. A., and Degroote, R. L. (2021). Deviant Proteome Profile of Equine Granulocytes Associates to Latent Activation Status in Organ Specific Autoimmune Disease. *J. Proteomics* 230, 103989. doi:10.1016/j.jprot.2020.103989

Wiśniewski, J. R., Zougman, A., Nagaraj, N., and Mann, M. (2009). Universal Sample Preparation Method for Proteome Analysis. *Nat. Methods* 6 (5), 359–362. doi:10.1038/nmeth.1322

Wooff, Y., Man, S. M., Aggio-Bruce, R., Natoli, R., and Fernando, N. (2019). IL-1 Family Members Mediate Cell Death, Inflammation and Angiogenesis in Retinal Degenerative Diseases. *Front. Immunol.* 10, 1618. doi:10.3389/fimmu.2019.01618

Wu, H., Hwang, D. K., Song, X., and Tao, Y. (2017). Association between Aqueous Cytokines and Diabetic Retinopathy Stage. *J. Ophthalmol.* 2017, 9402198. doi:10.1155/2017/9402198

Yamagami, S., Yokoo, S., Mimura, T., and Amano, S. (2004). Effects of TGF-Beta2 on Immune Response-Related Gene Expression Profiles in the Human Corneal Endothelium. *Invest. Ophthalmol. Vis. Sci.* 45 (2), 515–521. doi:10.1167/iovs.03-0912

Yao, Y., Li, R., Du, J., Long, L., Li, X., and Luo, N. (2019). Interleukin-6 and Diabetic Retinopathy: A Systematic Review and Meta-Analysis. *Curr. Eye Res.* 44 (5), 564–574. doi:10.1080/02713683.2019.1570274

Yaswen, L., Kulkarni, A. B., Fredrickson, T., Mittleman, B., Schiffman, R., Payne, S., et al. (1996). Autoimmune Manifestations in the Transforming Growth Factor-Beta 1 Knockout Mouse. *Blood* 87 (4), 1439–1445. doi:10.1182/blood.v87.4.1439.bloodjournal8741439

Yoshida, S., Sotozono, C., Ikeda, T., and Kinoshita, S. (2001). Interleukin-6 (IL-6) Production by Cytokine-Stimulated Human Müller Cells. *Curr. Eye Res.* 22 (5), 341–347. doi:10.1076/ceyr.22.5.341.5498

Zeng, H. Y., Green, W. R., and Tso, M. O. (2008). Microglial Activation in Human Diabetic Retinopathy. *Arch. Ophthalmol.* 126 (2), 227–232. doi:10.1001/archophthalmol.2007.65

Zhang, S., Zhang, S., Gong, W., Zhu, G., Wang, S., Wang, Y., et al. (2018). Müller Cell Regulated Microglial Activation and Migration in Rats with N-Methyl-N-Nitrosourea-Induced Retinal Degeneration. *Front. Neurosci.* 12, 890. doi:10.3389/fnins.2018.00890

Zhang, S. X., Wang, J. J., Gao, G., Shao, C., Mott, R., and Ma, J. X. (2006). Pigment Epithelium-Derived Factor (PEDF) Is an Endogenous Antiinflammatory Factor. *FASEB J.* 20 (2), 323–325. doi:10.1096/fj.05-4313fje

Zhong, Y., Li, J., Chen, Y., Wang, J. J., Ratan, R., and Zhang, S. X. (2012). Activation of Endoplasmic Reticulum Stress by Hyperglycemia Is Essential for Müller Cell-Derived Inflammatory Cytokine Production in Diabetes. *Diabetes* 61 (2), 492–504. doi:10.2337/db11-0315

Zode, G. S., Sethi, A., Brun-Zinkernagel, A. M., Chang, I. F., Clark, A. F., and Wordinger, R. J. (2011). Transforming Growth Factor-B2 Increases Extracellular Matrix Proteins in Optic Nerve Head Cells via Activation of the Smad Signaling Pathway. *Mol. Vis.* 17, 1745–1758.

Conflict of Interest: The authors declare that the research was conducted in the absence of any commercial or financial relationships that could be construed as a potential conflict of interest.

Publisher's Note: All claims expressed in this article are solely those of the authors and do not necessarily represent those of their affiliated organizations, or those of the publisher, the editors, and the reviewers. Any product that may be evaluated in this article, or claim that may be made by its manufacturer, is not guaranteed or endorsed by the publisher.

frontiers in Pharmacology

ORIGINAL RESEARCH
published: 03 January 2022
doi: 10.3389/fphar.2021.811818

Preventive Efficacy of an Antioxidant Compound on Blood Retinal Barrier Breakdown and Visual Dysfunction in Streptozotocin-Induced Diabetic Rats

Alessio Canovai[1], Rosario Amato[1], Alberto Melecchi[1], Massimo Dal Monte[1,2], Dario Rusciano[3], Paola Bagnoli[1] and Maurizio Cammalleri[1,2]**

[1]Department of Biology, University of Pisa, Pisa, Italy, [2]Interdepartmental Research Center Nutrafood "Nutraceuticals and Food for Health", University of Pisa, Pisa, Italy, [3]Research Center, Sooft Italia SpA, Catania, Italy

In diabetic retinopathy (DR), high blood glucose drives chronic oxidative stress and inflammation that trigger alterations of the neurovascular balance finally resulting in vascular abnormalities and retinal cell death, which converge towards altered electroretinogram (ERG). In the last years, a growing body of preclinical evidence has suggested that nutrients with anti-inflammatory/antioxidant properties can be able to hamper DR progression since its very early stages. In the present study, we used a streptozotocin-induced rat model of DR, which mimics most aspects of the early stages of human DR, to test the preventive efficacy of a novel compound containing cyanidin-3-glucoside (C3G), verbascoside and zinc as nutrients with antioxidant and anti-inflammatory properties. Western blot, immunofluorescence and electroretinographic analyses demonstrated a dose-dependent inhibition of oxidative stress- and inflammation-related mechanisms, with a significant counterpart in preventing molecular mechanisms leading to DR-associated vasculopathy and its related retinal damage. Preventive efficacy of the compound on dysfunctional a- and b-waves was also demonstrated by electroretinography. The present demonstration that natural compounds, possibly as a consequence of vascular rescue following ameliorated oxidative stress and inflammation, may prevent the apoptotic cascade leading to ERG dysfunction, adds further relevance to the potential application of antioxidants as a preventive therapy to counteract DR progression.

Keywords: oxidative stress, inflammation, gliosis, vasopermeability, apoptosis, electroretinogram

OPEN ACCESS

Edited by:
Claudio Bucolo, University of Catania, Italy

Reviewed by:
Sebastiano Alfio Torrisi, University of Catania, Italy
Yvette Wooff, Australian National University, Australia

****Correspondence:***
Rosario Amato
rosario.amato@biologia.unipi.it ;
Maurizio Cammalleri
maurizio.cammalleri@unipi.it

Specialty section:
This article was submitted to Inflammation Pharmacology, a section of the journal Frontiers in Pharmacology

Received: *09 November 2021*
Accepted: *06 December 2021*
Published: *03 January 2022*

Citation:
Canovai A, Amato R, Melecchi A, Dal Monte M, Rusciano D, Bagnoli P and Cammalleri M (2022) Preventive Efficacy of an Antioxidant Compound on Blood Retinal Barrier Breakdown and Visual Dysfunction in Streptozotocin-Induced Diabetic Rats. Front. Pharmacol. 12:811818. doi: 10.3389/fphar.2021.811818

INTRODUCTION

Diabetic retinopathy (DR) is a leading cause of acquired visual impairment in developed countries. DR is characterized by a chronic progression, which might result asymptomatic for several years before the occurrence of overt clinical evidence (Al-Kharashi, 2018). Major signs of DR are morpho functional alterations of retinal vascularization, primarily manifested as a significant increase in vascular leakage, and macular oedema deriving from the blood retinal barrier (BRB) breakdown (Klaassen et al., 2013). Noteworthy, the onset of relevant clinical signs of DR corresponds to advanced stages of the disease that marks a point of no return (Sinclair and Schwartz, 2019). These aspects render the clinical management of DR a challenging topic

and feeds the research of treatment approaches to intervene on the early stages of the disease in order to prevent or delay DR progression.

Although the clinical symptoms of DR are almost exclusively attributed to dysfunctional vascularization, DR consists in a complex interplay of pathological processes affecting the integrity of the neurovascular unit since its early stages (Simó et al., 2018; Rossino et al., 2019). In fact, prolonged exposure to high glucose leads to metabolic stress that affects the BRB and the highly specialized neural connections, responsible for vision processes (Feng et al., 2012; Mi et al., 2014). In particular, hyperglycemia initiates an early increase of reactive oxygen species (ROS), which triggers the activation of endogenous antioxidant response through increased levels of nuclear factor erythroid 2-related factor 2 (Nrf2) leading to the transcription of antioxidant enzymes such as heme oxygenase-1 (HO-1) (Kang and Yang, 2020). However, antioxidant defenses are overwhelmed by ROS accumulation thus producing the onset of oxidative stress (Kowluru and Chan, 2007).

Oxidative stress activates inflammation that exacerbates ROS production, both events converging on retinal cell degeneration and altered vascularization (Tang and Kern 2011). Among the several players that participate to the early vascular pathology that characterizes DR, vascular endothelial growth factor (VEGF) and its regulatory transcription factor hypoxia inducible factor-1 (HIF-1) play an important role and their increase takes place in response to hyperglycemia-induced hypoxic environment (Gu et al., 2019). VEGF overexpression induces the loss of tight-junction proteins and subsequent alterations in the BRB integrity (Qaum et al., 2001). Therefore, the early neurovascular dysfunction appears to be strictly related to a series of metabolic unbalances deriving from the hyperglycemic condition of which common denominators are oxidative stress and inflammation (Al-Kharashi, 2018). Their importance along the progression of DR is further corroborated by the fact that strategies already approved for the management of advanced DR, such as treatments with anti-VEGF drugs and the use of steroids, have been found to interfere on inflammatory pathways (Giurdanella et al., 2015; Bucolo et al., 2018). On the other hand, the efficacy of dietary compounds with antioxidant/anti-inflammatory properties has been largely studied for their extensive bioactivity and limited risk of side effects (Rossino and Casini, 2019). However, clinical trials using antioxidants in DR have provided controversial results and much preclinical evidence is still needed to demonstrate the efficacy of antioxidant compounds to counteract the multifactorial nature of DR (Garcia-Medina et al., 2020). In this respect, the use of a multicomponent formula may further improve antioxidant efficacy as the different compounds contained in the mixture may exert multi-target and multifunctional effects by acting at different levels of the same signaling cascade or by modulating different cascades (Leena et al., 2020).

Among natural compounds exerting antioxidant/anti-inflammatory properties, anthocyanin subcomponents, and in particular cyanidins, have been shown to display a good uptake rate, a low decay and a significant clinical relevance, thus resulting one of the most pharmaceutically promising class of nutrients (Khoo et al., 2017). Among cyanidins, cyanidin-3-glucoside (C3G), the most abundant anthocyanin, has a predominant antioxidant capacity that has been reported in several diabetic complications including DR (Sasaki et al., 2007; Wang et al., 2016; Li et al., 2018; Qin et al., 2018).

Additional antioxidant/anti-inflammatory compounds belong to the extensive family of phenylpropanoids, a class of plant-derived polyphenols, which are biosynthesized from the amino acid phenylalanine (Alipieva et al., 2014). Of them verbascoside exerts an anti-inflammatory role due to its ROS scavenging, antioxidant and iron chelating properties (Perron and Brumaghim, 2009; Burgos et al., 2020) although its potential role in DR remains to be established. In addition to plant-derived antioxidant compounds, the activation of enzymes involved in antioxidant defenses has been related to the activity of zinc (Kamińska et al., 2021). Zinc itself is not redox active but is a cofactor that exerts an indirect redox activity by regulating mitochondrial function and, therefore, the rate of ROS generation (Marreiro et al., 2017).

The individual antioxidant efficacy of C3G, verbascoside and zinc has been demonstrated in several experimental models of ocular diseases including DR, glaucoma and age-related macular degeneration (Miao et al., 2013; Chen et al., 2019; Nomi et al., 2019; Oliveira et al., 2020), but information is lacking about their combined efficacy in preventing the early signs of experimental DR.

In the present study, we investigated the efficacy of a compound including C3G, verbascoside and zinc using the chemically induced streptozotocin (STZ) rat model of diabetes, which has been routinely used in preclinical studies and therapeutic drug investigations. This model that mimics the early stages of DR in humans, is characterized by an increased expression of oxidative stress and inflammation markers resulting in VEGF-induced retinal vasopermeability that causes BRB breakdown and retinal dysfunction (Naderi et al., 2019). In STZ rats, we evaluated the preventive efficacy of the compound on oxidative stress, inflammation, gliotic responses and apoptotic markers. In addition, its preventive efficacy on neuroretinal components responsible for vision processes was also assessed by electroretinography.

MATERIALS AND METHODS

Reagents

Rabbit polyclonal anti-NRF2 (catalog n. ab92946), rabbit polyclonal anti-HO-1 (catalog n. ab13243), rabbit polyclonal anti-NF-kB p65 (catalog n. ab16502), rabbit monoclonal anti-HIF-1α (catalog n. ab179483), rabbit monoclonal anti-Bax (catalog n. ab182733), rabbit polyclonal anti-Bcl-2 (catalog n. ab194583), rabbit polyclonal anti-cleaved caspase 3 (catalog n. ab2302), rabbit monoclonal anti-GFAP (catalog n. ab207165), goat polyclonal anti-rabbit conjugated with either Alexa-Fluor 555 (catalog n. ab150078) or Alexa-Fluor 488 (catalog n. ab150077) antibodies were purchased from Abcam (Cambridge, United Kingdom). Rabbit polyclonal anti-pNF-kB p65 (Ser 536) (catalog n. sc-33020), mouse monoclonal anti-IL-6

(catalog n. sc-57315), rabbit polyclonal anti-VEGF (catalog n. sc-507) antibodies were purchased from Santa Cruz Biotechnology, Inc (Dallas, TX, United States). Rabbit polyclonal anti-ZO-1 (catalog n. 40-2200), mouse monoclonal anti-Claudin 5 (catalog n. 35-2500) antibodies were purchased from Invitrogen (Waltham MA, United States). Mouse monoclonal anti-β-actin (catalog n. A2228), rabbit polyclonal anti-mouse HRP-conjugated (catalog n. A9044) antibody were purchased from Sigma-Aldrich (St. Louis, MO, United States). Rabbit monoclonal anti-cleaved caspase 3 (catalog n. 9664S) antibody used for immunofluorescence was purchased from Cell Signaling Technology (Danvers, MA, United States). Goat polyclonal anti-rabbit HRP-conjugated (catalog n. 170-6515) antibody was purchased from Bio-Rad Laboratories, Inc (Hercules, CA, United States).

Animals

Animals were managed in accordance with the Association for Research in Vision and Ophthalmology statement for the Use of Animals in Ophthalmic and Vision Research. The present study is also in agreement with the European Communities Council Directive (2010/63/UE) and the Italian guidelines for animal care (DL 26/14). The experimental protocol was authorized by the Commission for Animal Wellbeing of the University of Pisa (protocol no. 133/2019-PR, February 14, 2019). Efforts to reduce both the number and suffering of the animals were made in accordance with the 3Rs principles for ethical use of animals in scientific research. Male Sprague Dawley rats (8 weeks old, about 200 g weight) were purchased from Envigo Italy (San Pietro al Natisone, Italy). Animals were housed in a regulated environment (23 ± 1°C, 50 ± 5% humidity) with 12 h light/dark cycles (lights on at 08:00 a.m.) and fed with a standard diet and water ad libitum. Thirty-two rats were used. They were divided in four groups of eight rats each: control, STZ untreated, STZ-treated with the low dose of the mixture and STZ-treated with the high dose (see below). To evaluate the effect of the compound on weight, glycemia and visual function of healthy rats, additional six rats were supplemented with the compound.

STZ-Induced Model of Diabetes and Treatments

STZ (Sigma-Aldrich, St. Louis, MO, United States) diluted in citrate buffer, pH 4.5, was intraperitoneally injected at 65 mg/kg. Age-matched rats treated with vehicle were considered as the control group. Blood glucose was measured 3 days after the injection by tail sampling using a OneTouch Ultra glucometer (LifeScan Inc, Milpitas, CA, United States) to confirm the diabetic induction. Animals were considered diabetic if glycemia was ≥250 mg/dl. Blood glucose level was then regularly checked once a week for the entire experimental period. Among diabetic rats, 16 animals for each group were treated with a compound including *Oryza sativa* L. seeds (C3G titrated at 20%), *Verbascum thapsus* L (verbascoside titrated at 10%) and zinc gluconate (zinc titrated at 13.23%) with a content ratio of 60:30:10, respectively. The compound was diluted in water at 84 mg/ml and administered at low dose (100 µL containing 1.0 mg of C3G, 0.25 mg of verbascoside and 0.125 mg of zinc) or high dose (300 µL containing 3.0 mg of C3G, 0.75 mg of verbascoside and 0.375 mg of zinc). Dosage range corresponds to that recommended in humans, normalized by the body surface area for interspecies drug dosage translation (Nair and Jacob, 2016). Rats were treated once daily by oral gavage for 30 days after STZ administration. Thirty days after STZ administration, the animals underwent to electroretinography. In **Table 1**, the experimental groups, the schedule of treatment, the amount of daily administered components and the number of rats for each experimental group are shown.

Electroretinogram

In the four groups, retinal function was examined with scotopic full-field electroretinogram (ERG). Before ERG, rats underwent overnight dark-adaptation and subsequent anesthesia with intraperitoneal injection of 30 mg/kg sodium pentobarbital. Pupils were dilated with a topical drop of 1% tropicamide (Allergan S.p.A.) and the body temperature was kept constantly at 37.5°C by a heating pad. The electrophysiological signals were recorded using silver/silver chloride corneal ring electrodes inserted under the lower eyelids to avoid visual field obstruction. In order to prevent dryness and clouding of the ocular surface, saline solution drops were intermittently instilled. Each corneal electrode was referred to a needle electrode inserted subcutaneously at the level of the corresponding frontal region, and the ground electrode was inserted subcutaneously at the tail root. Scotopic ERG, which primarily measures rod function, was evoked by flashes of increasing light intensities ranging from −3.4 to one log cd-s/m^2 generated through a Ganzfeld stimulator (Biomedica Mangoni, Pisa, Italy). An interval of 20 s between light flashes was adjusted to allow response recovery. Scotopic responses were collected simultaneously from both eyes, amplified at 10000x gain, filtered with a 0.2–500 Hz bandpass and digitized at 5 kHz rate with a data acquisition device (Biomedica Mangoni). ERG waveforms were analyzed using a customized program (Biomedica Mangoni). In the absence of light stimulation, the electrical activity was measured to evaluate noise amplitude. In accordance with the International Society for Clinical Electrophysiology guidelines, the a-wave amplitude was measured from the pre-stimulus baseline to the negative through of the a-wave while the b-wave amplitude was retrieved from the through of the a-wave to the peak of the b-wave. Data were pooled and reported as mean amplitude ±SEM (in µV). Intensity-response function of the b-wave was fitted to the following modified Naka-Rushton function (Naka and Rushton, 1966):

$$V(I) = V0 + \frac{Vmax \times In}{In + kn}$$

In this equation, V is the amplitude of the b-wave (in µV), I is the stimulus intensity (in log cd-s/m^2), V0 is the nonzero baseline effect, Vmax is the saturated amplitude of the b-wave (in µV) and k is the stimulus intensity that evokes b-waves of half-maximum amplitude (in log cd-s/m^2); n, which was constrained to unity, is a dimensionless constant that controls the slope of the function and represents the degree of heterogeneity of retinal sensitivity.

TABLE 1 | Experimental groups and schedule of treatments.

Group	N	Treatment	Daily amount	Days of treatment
Control	8	None	—	—
	3	+ low dose	C3G (1.0 mg), verbascoside (0.25 mg), zinc (0.125 mg)	30
	3	+ high dose	C3G (3.0 mg), verbascoside (0.75 mg), zinc (0.375 mg)	30
STZ	8	None	—	—
	8	+ low dose	C3G (1.0 mg), verbascoside (0.25 mg), zinc (0.125 mg)	30
	8	+ high dose	C3G (3.0 mg), verbascoside (0.75 mg), zinc (0.375 mg)	30

Detection of Vascular Leakage by Evans Blue Dye Perfusion

After electroretinography, two rats per group were anesthetized with an intraperitoneal injection of 30 mg/kg sodium pentobarbital and perfused through the left ventricle with 0.5% Evans blue dye (Sigma-Aldrich) in phosphate-buffer saline (PBS) that was allowed to circulate for 10 min. The animals were then sacrificed, and retinas were dissected and flat mounted onto microscope slides. Retinas were then examined by an epifluorescence microscope (Ni-E; Nikon Europe, Amsterdam, Netherlands) and the images were acquired using a 10x plan apochromat objective and a digital camera (DS-Fi1c camera; Nikon-Europe).

Western Blot

In six rats per group, eyes were enucleated and alternatively used for Western blot analysis in explanted retinas or immunohistochemistry (see below). For Western blot, retinas were lysed with RIPA lysis buffer (Santa Cruz Biotechnology, Dallas, TX, United States) implemented with phosphatase and proteinase inhibitor cocktails (Roche Applied Science, Indianapolis, IN, United States). Protein content was evaluated by Micro BCA protein assay (Thermo Fisher Scientific, Waltham, MA, United States). Fourty micrograms of proteins per sample were separated by SDS-PAGE (4–20%; Bio-Rad Laboratories, Inc., Hercules, CA, United States) and gels were subsequently transblotted onto nitrocellulose membranes (Bio-Rad Laboratories, Inc.). Membranes were blocked with 5% skim milk for 1 h at room temperature and then incubated overnight at 4°C with the solutions of primary anti-NRF2 (1:1,000), anti-HO-1 (1:500), anti-pNF-kB p65 (Ser 536) (1:100), anti-NF-kB p65 (1:1,000), anti-IL-6 (1:100), anti-HIF-1α (1:1,000), anti-VEGF (1:100), anti-ZO-1 (1:500), anti-Claudin 5 (1:500), anti-Bax (1:500), anti-Bcl-2 (1:500), anti-cleaved caspase 3 (1:500), anti-β-actin (1:2500) antibodies. Thereafter, membranes were incubated for 2 h at room temperature with appropriate HRP-conjugated secondary anti-mouse or anti-rabbit (1:5,000) antibodies. Blots were developed using the Clarity western enhanced chemiluminescence substrate (Bio-Rad Laboratories, Inc.) and the images were acquired by the ChemiDoc XRS+ (Bio-Rad Laboratories, Inc.). The optical density (OD) relative to the target bands (Image Lab 3.0 software; Bio-Rad Laboratories, Inc.) was normalized to the corresponding OD of β-actin as loading control or nuclear factor kappa-light-chain-enhancer of activated B cells (NF-kB) p65 as appropriate.

Measurement of ROS Levels

ROS levels were measured using the general oxidative stress probe 2′,7′-dichlorodihydrofluorescein diacetate (DCFH-DA) (Invitrogen, CA, United States). DCFH-DA, a nonfluorescent dye, is cleaved by esterase activity to yield dichlorodihydrofluorescein (DCFH), which is subsequently oxidized by ROS to form fluorescent dichlorofluorescein (DCF). Retinal samples containing 20 μg proteins were incubated with 50 μM DCFHDA in 96-well plates. After 60 min at 37°C, fluorescence intensity was detected over 60 min using a microplate reader (FLUOstar Omega, BMG Labtech, Ortenberg, Germany) at excitation 488 nm and emission 525 nm. The relative ROS levels were expressed as arbitrary fluorescence units per μg of protein.

Immunofluorescence

Enucleated eyes were immersion-fixed in 4% paraformaldehyde in 0.1 M PBS for 2 h at room temperature. Fixed eyes were transferred to 25% sucrose in 0.1 M PBS and stored at 4°C. Following the inclusion in cryo-gel medium, fixed samples were cut into 10 μm thick coronal sections and mounted onto glass slides. Mounted sections were then incubated with the solutions of primary anti-HO-1 (1:500), anti-GFAP (1:400) or anti-cleaved caspase 3 (1:400) antibodies diluted in 0.1 M PBS containing 0.1% v/v Triton X-100, overnight at 4°C. Mounted sections were incubated with goat polyclonal anti-rabbit secondary antibodies conjugated with Alexa-Fluor 555 (ab150078, Abcam, Cambridge, United Kingdom; dilution: 1: 200) or Alexa-Fluor 488 (ab150077, Abcam; dilution: 1:200) diluted in 0.1 M PBS containing 0.1% v/v Triton X-100 for 2 h at room temperature. Finally, retinal sections were coverslipped with Fluoroshield mounting medium containing 4′, 6-diamidino-2-phenylindole (DAPI; Abcam). In order to analyze the outer BRB, the retinal pigmented epithelium (RPE)-choroid complexes were isolated from fixed eyes and incubated for 72 h at 4°C in anti-ZO-1 antibody (1:100 in 0.1 M PB containing 1.0% Triton X-100). Subsequently, they were incubated for 48 h at 4 °C in anti-rabbit secondary antibody conjugated with Alexa-Fluor 488 (1: 200) followed by 0.1 M PB rinsing. Four radial incisions were made in the RPE-choroid complexes that were flat-mounted on gelatin-coated glass slides. Images of retinal sections or RPE-choroid flatmounts were acquired through an epifluorescence microscope (Nikon-Europe) at 20× and 40x,

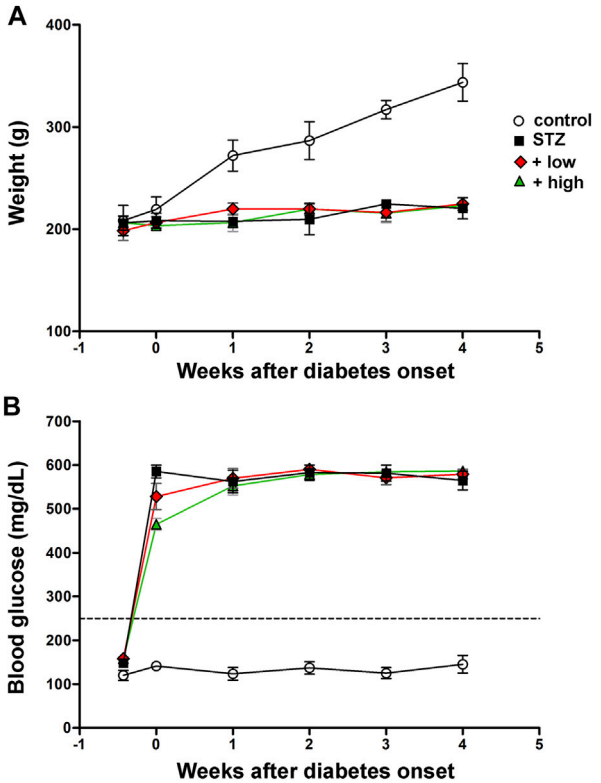

FIGURE 1 | Longitudinal evaluation of body weight **(A)** and blood glucose **(B)** in controls, STZ-untreated rats or STZ rats treated with either the low dose (C3G, 1.0 mg; verbascoside, 0.25 mg and zinc, 0.125 mg) or the high dose (C3G, 3.0 mg; verbascoside, 0.75 mg and zinc, 0.375 mg) of the compound. Data are expressed as mean ± SEM. Statistical significance was assessed by two-ways ANOVA followed by Bonferroni's multiple comparison post-hoc test (N = 8).

respectively using a digital camera (Nikon-Europe). The quantification of the GFAP immunostaining was performed by averaging the fluorescence intensity of five coronal sections (4 images per section) randomly chosen from each retina (6 retinas per group). Fluorescence intensity was calculated on grayscale images normalized for the background by measuring the mean gray level using the analysis tool of Adobe Photoshop. The thickness of the outer nuclear layer (ONL) was measured as the interface between the outer plexiform layer and photoreceptor inner segment, while the thickness of the inner nuclear layer (INL) was measured as the interface between the outer plexiform layer and the inner plexiform layer. The quantification of ONL and INL thickness was performed by averaging measurements from five coronal sections (4 images per section) randomly chosen from each retina (6 retinas per group).

Statistical Analysis

Graph Pad Prism 8.0.2 software (Graph-Pad Software, Inc., San Diego, CA, United States) was used for the statistical analyses. Differences among groups were assessed through one-way or two-ways ANOVA followed by Tukey's or Bonferroni's multiple comparison post hoc test, respectively. Differences with $p < 0.05$ were considered significant. All data are expressed as means ± SEM of the indicated n values.

RESULTS

The Compound Does Not Affect Body Weight and Glycemia

Control rats displayed a significant age-dependent gain of weight. In line with previous findings (Furman, 2015), STZ injection resulted in markedly lower body weight as compared to controls ($p < 0.01$, **Figure 1A**). Following STZ administration, blood glucose levels were significantly increased and remained higher than in controls until the animals underwent to ERG recordings and were subsequently sacrificed ($p < 0.0001$ vs control, **Figure 1B**). Blood glucose levels did not significantly differ between STZ rats either untreated or treated with the compound at both doses. Control rats treated with the compound displayed an age-dependent gain of weight and blood glucose levels comparable to those of untreated controls (**Supplementary Figure S1**).

The Compound Protects the Retina From Oxidative Stress and Inflammation

The preventive efficacy of the compound was tested on ROS generation. Levels of specific markers of oxidative stress and inflammation known to play a crucial role in the early progression of DR (Al-Kharashi, 2018) were also measured. As shown in **Figure 2A,,** STZ rats displayed a significant increase in ROS generation as compared to controls ($p < 0.001$ vs control). STZ rats treated with the compound at low dose showed lower levels of ROS as compared to untreated STZ ($p < 0.01$ vs STZ), although still resulting significantly higher than in controls ($p < 0.01$ vs control). In STZ rats treated with the compound at high dose, ROS levels were comparable to those measured in controls ($p > 0.05$ vs control). Oxidative stress was evaluated by analyzing the protein levels of NRF2, a ROS-sensitive transcriptional factor, and HO-1, one of the antioxidant enzymes involved in defensive responses to oxidative stress (Kang and Yang., 2020). As shown in **Figures 2B, C**, the densitometric analysis of immunoblots revealed a significant increment in both Nrf2 and HO-1 in STZ rats as compared to controls ($p < 0.01$ vs control). This increment was partially attenuated by the compound at low dose ($p < 0.05$ vs STZ), but completely prevented by the high dose ($p < 0.001$ vs STZ; $p < 0.05$ vs low dose). As shown in **Figure 2D**, immunofluorescence analysis revealed a faint HO-1 immunoreactivity in control retinas mainly confined to the ganglion cell layer (GCL). In retinas of STZ rats, HO-1 immunoreactivity was significantly increased in the GCL and expanded toward the outer retina, clearly depicting vertical processes in the inner plexiform layer (IPL) and cellular profiles localized in the inner nuclear layer (INL). Retinas of rats treated with compound at low dose displayed a less evident HO-1 immunostaining as compared to untreated STZ rats, with rare spots in the GCL and residual labeling in the IPL and INL. HO-1 immunostaining was not detectable in the IPL and INL

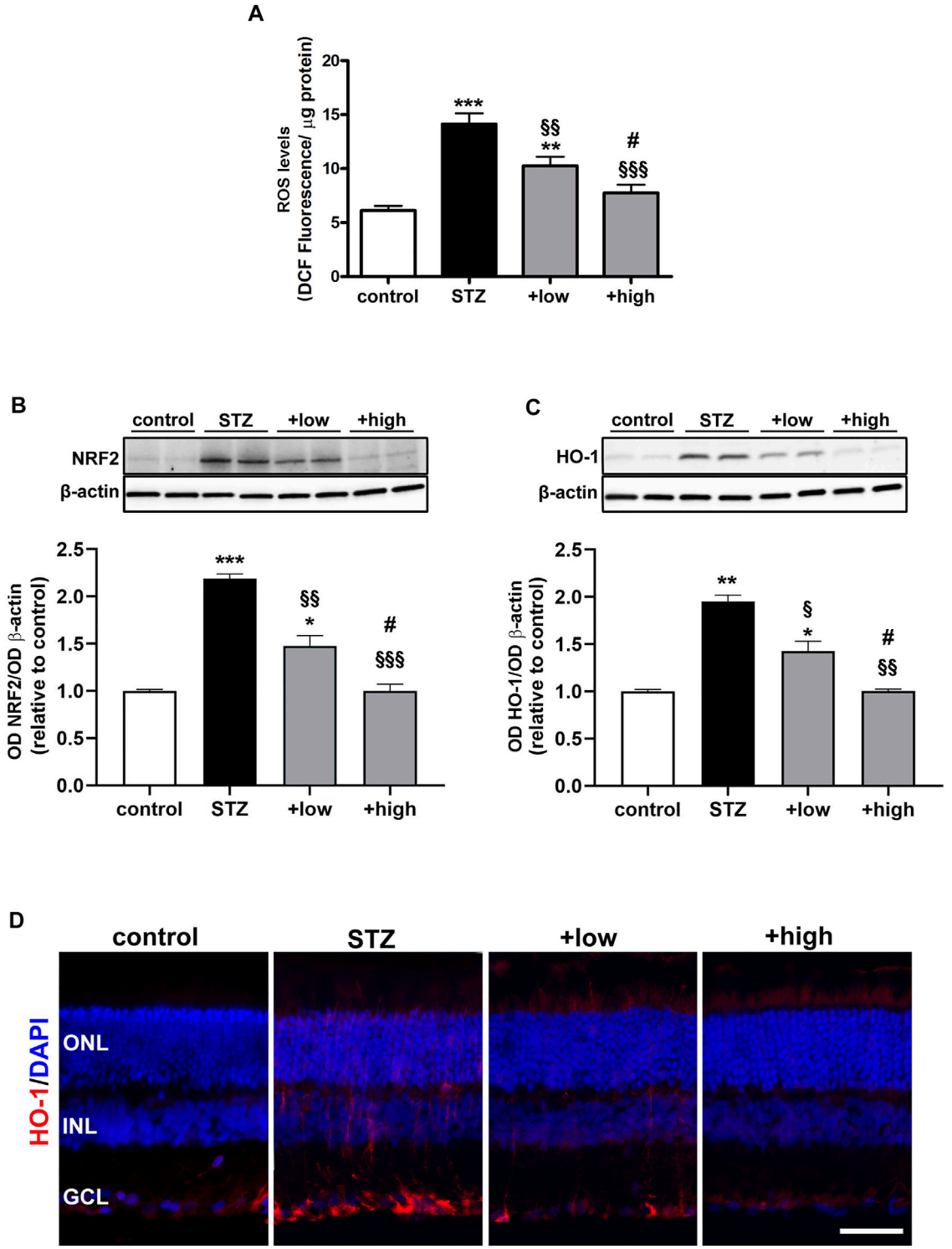

FIGURE 2 | Effects of the compound on ROS levels and markers of oxidative stress **(A)** ROS levels in controls, STZ untreated or STZ treated with either the low dose (C3G, 1.0 mg; verbascoside, 0.25 mg and zinc, 0.125 mg) or the high dose (C3G, 3.0 mg; verbascoside, 0.75 mg and zinc, 0.375 mg) of the compound. Representative Western blots and densitometric analysis of NRF2 **(B)** and HO-1 **(C)** in controls, STZ untreated or STZ rats treated with either the low dose or the high dose. β-actin was used as loading control. Data are expressed as mean ± SEM. Statistical significance was assessed by one-way ANOVA followed by Tukey's multiple comparison post-hoc test (N = 6). $^{*}p < 0.05$, $^{**}p < 0.01$ and $^{***}p < 0.001$ vs control; $^{\S}p < 0.05$, $^{\S\S}p < 0.01$ and $^{\S\S\S}p < 0.001$ vs STZ; $^{\#}p < 0.05$ vs low dose-treated STZ **(D)** Representative images of retinal cross sections immunolabeled for HO-1 (red) and counterstained with DAPI (blue). Scale bar, 50 µm. GCL, ganglion cell layer; INL, inner nuclear layer; ONL, outer nuclear layer.

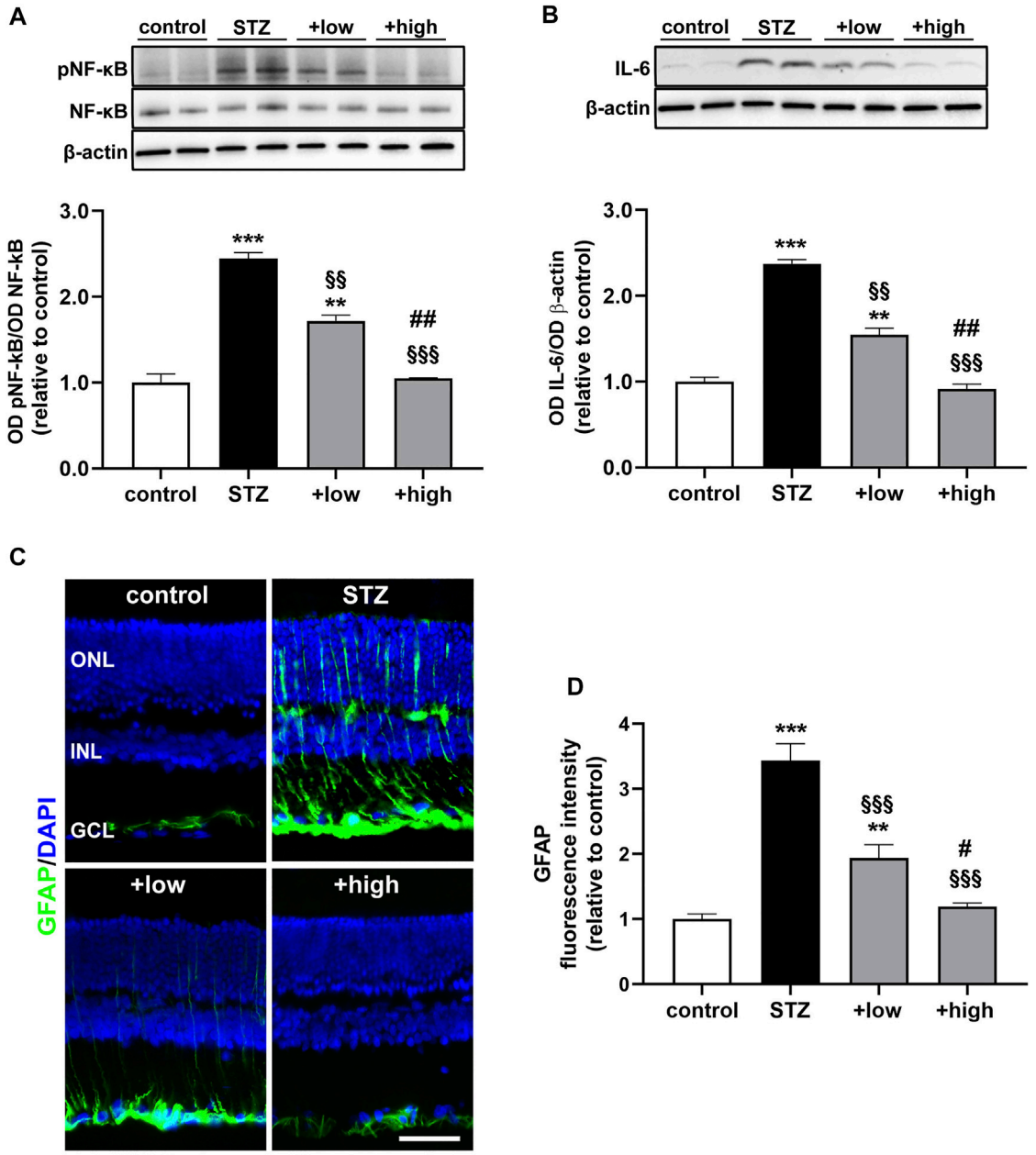

FIGURE 3 | Effects of the compound on inflammatory and gliosis markers. Representative Western blots and densitometric analysis of levels of pNF-kB **(A)** and IL-6 **(B)** in controls, STZ untreated or STZ rats treated with either the low dose (C3G, 1.0 mg; verbascoside, 0.25 mg and zinc, 0.125 mg) or the high dose (C3G, 3.0 mg; verbascoside, 0.75 mg and zinc, 0.375 mg) of the compound. Levels of pNF-kB were normalized to NF-kB levels, while IL-6 was normalized to the loading control β-actin. Data are expressed as mean ± SEM. Statistical significance was assessed by one-way ANOVA followed by Tukey's multiple comparison post-hoc test (N = 6). $^{**}p < 0.01$ and $^{***}p < 0.001$ vs control; $^{§§}p < 0.01$ and $^{§§§}p < 0.001$ vs STZ; $^{##}p < 0.01$ vs low dose treated STZ **(C)** Representative images of retinal cross sections immunolabeled for GFAP (green) and counterstained with DAPI (blue). Scale bar, 50 µm. GCL, ganglion cell layer; INL, inner nuclear layer; ONL, outer nuclear layer **(D)** Quantitative analysis of GFAP immunofluorescence intensity. Data are expressed as mean ± SEM. Statistical significance was assessed by one-way ANOVA followed by Tukey's multiple comparison post-hoc test (N = 6). $^{**}p < 0.01$ and $^{***}p < 0.001$ vs control; $^{§§}p < 0.01$ and $^{§§§}p < 0.001$ vs STZ; $^{#}p < 0.05$ and $^{##}p < 0.01$ vs low dose treated STZ.

following the treatment with high dose, while a basal labeling was observed in the GCL similarly to what found in the control retina.

The protein levels of the phosphorylated form of the p65 subunit of NF-kB, a master transcriptional regulator of pro-inflammatory factors and interleukin 6 (IL-6), a related pro-inflammatory cytokine (Liu et al., 2017), were also measured. As shown in **Figures 3A, B**, STZ rats displayed a marked increase in pNF-KB and IL-6 as compared to controls ($p < 0.001$ vs control). STZ rats treated with the compound at low dose showed lower levels of both markers as compared to untreated STZ ($p < 0.01$ vs

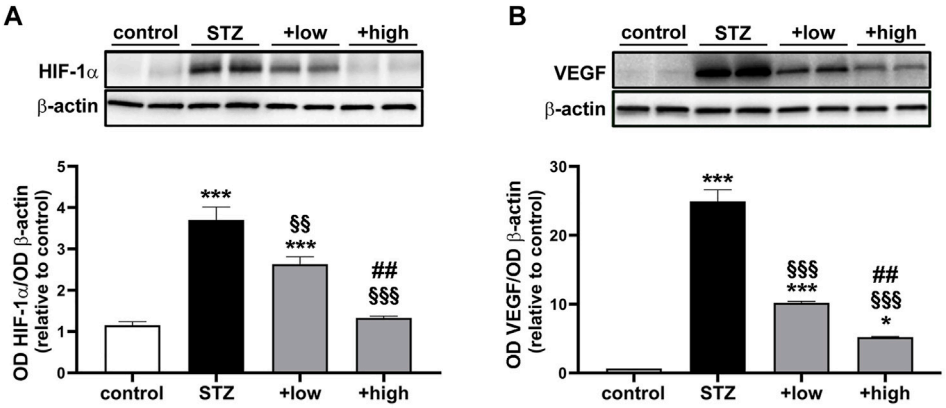

FIGURE 4 | Effects of the compound on vascular-related markers. Representative Western blots and densitometric analysis of HIF-1α **(A)** and VEGF **(B)** in controls, STZ untreated or STZ rats treated with either the low dose (C3G, 1.0 mg; verbascoside, 0.25 mg and zinc, 0.125 mg) or the high dose (C3G, 3.0 mg; verbascoside, 0.75 mg and zinc, 0.375 mg) of the compound. β-actin was used as loading control. Data are expressed as mean ± SEM. Statistical significance was assessed by one-way ANOVA followed by Tukey's multiple comparison post-hoc test (N = 6). $^{*}p < 0.05$ and $^{***}p < 0.001$ vs control; $^{§§}p < 0.01$ and $^{§§§}p < 0.001$ vs STZ; $^{##}p < 0.01$ vs low dose treated STZ.

STZ), although still resulting significantly higher than in controls ($p < 0.01$ vs control). On the other hand, in STZ rats treated with the high dose, the levels of pNF-kB and IL-6 were comparable to those measured in controls ($p > 0.05$ vs control). The activation of inflammatory processes triggers glial reactivity, which participates to the chronic inflammatory response (Rübsam et al., 2018). The reactive phenotype of glial cells was analyzed by immunostaining with glial fibrillary acidic protein (GFAP), a well-established marker of gliosis (**Figure 3C**). In control retinas, basal GFAP labeling was confined to the GCL. In contrast, STZ retinas showed an evident increment of GFAP immunoreactivity in the GCL together with densely immunopositive processes spreading across retinal layers as a typical hallmark of Müller cell reactivity. Comparable immunostaining could be detected in retinas of low dose-treated rats, although GFAP immunoreactivity was less prominent both in the GCL and in Müller cell processes. On the other hand, retinas of rats treated with the high dose displayed a GFAP immunostaining almost similar to that of controls, with the usual basal staining and barely detectable immunoreactive vertical processes. As shown in **Figure 3D**, quantitative analysis of fluorescence intensity showed a marked increment in GFAP immunoreactivity in STZ rat as compared to controls ($p < 0.001$). In STZ rats treated with the low dose, GFAP immunoreactivity was significantly lower than in untreated STZ rats ($p < 0.001$ vs STZ), while STZ rats treated with the high dose displayed GFAP immunofluorescence intensity comparable to that of controls ($p > 0.05$ vs control).

VEGF-Induced Vascular Permeability and BRB Breakdown Are Prevented by the Compound

Oxidative and inflammatory processes have a direct impact on molecular mechanisms regulating the vascular homeostasis through the alteration of the HIF-1-dependent pathway and the consequent dysregulation of angiogenic factors such as VEGF (Semeraro et al., 2015). As shown in **Figure 4**, HIF-1α levels were significantly increased in STZ rats as compared to controls ($p < 0.0001$). The increment in HIF-1α was significantly attenuated by the compound in a dose-dependent fashion (low dose $p < 0.001$ vs STZ; high dose $p < 0.0001$ vs STZ), with the high dose maintaining HIF-1α to control levels ($p > 0.05$ vs control; **Figure 4A**). Similarly, STZ rats displayed a marked increase in VEGF levels as compared to controls ($p < 0.0001$). The administration of the compound dose-dependently prevented VEGF accumulation with increased efficacy of the high dose ($p < 0.0001$ vs low dose), although VEGF levels were still higher than in controls (high dose $p < 0.05$ vs control; **Figure 4B**).

BRB dysfunction resulting from altered HIF-1α-VEGF axis was evaluated by analyzing the levels of zonula occludens 1 (ZO-1) and Claudin 5 as components of the inter-endothelial tight junctions. The BRB integrity was also assessed with the Evans Blue dye perfusion of retinal vessels (for inner BRB) and with ZO-1 immunostaining in RPE-choroid flatmounts (for outer BRB). As shown in **Figures 5A, B**, the levels of ZO-1 and Claudin five were drastically decreased in STZ retinas ($p < 0.0001$ vs control). The treatment with the compound was found to prevent protein loss with dose-dependent efficacy (low dose $p < 0.05$ vs STZ; high dose $p < 0.0001$ vs STZ), with the high dose displaying ZO-1 and Claudin five levels comparable to those of controls ($p > 0.05$ vs control). As shown in **Figure 5C**, in STZ rats, the dysregulation of BRB markers was correlated with inner BRB breakdown. In fact, Evans blue, a dye that binds to plasma proteins, was restricted to the vascular lumen in control retinas. Contrariwise, several focal points of extravasation were visible in STZ retinas. The vascular leakage was still evident in STZ rats treated with the compound at low dose, while the extravasation appeared more contained or even absent in retinas of rats treated with the high dose. ZO-1 immunostaining in RPE-choroid flatmounts from STZ rats revealed the presence of large holes between RPE cells indicating a significant loss of tight junctions leading to outer

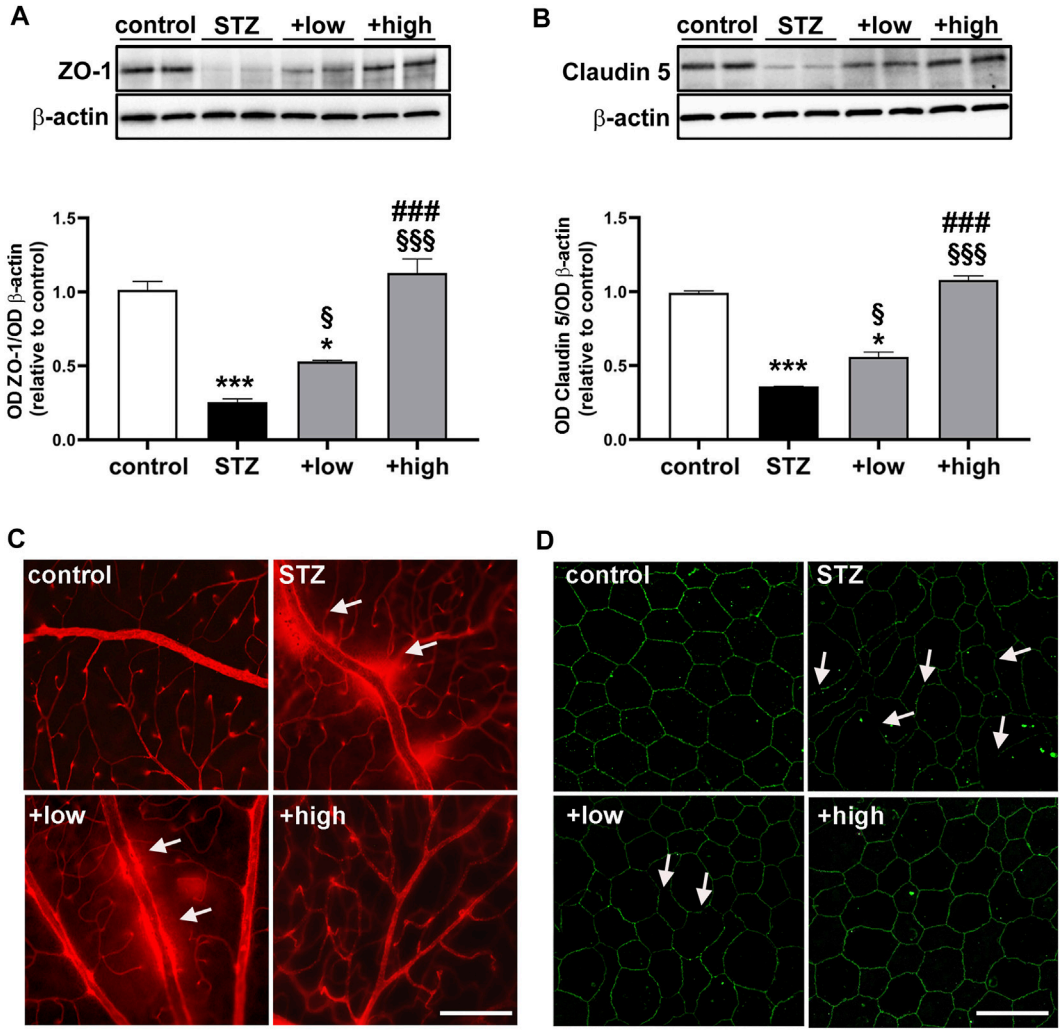

FIGURE 5 | Effects of the compound on BRB markers and vascular leakage. Representative Western blots and densitometric analysis of ZO-1 **(A)** and Claudin 5 **(B)** in controls, STZ untreated or STZ rats treated with either the low dose (C3G, 1.0 mg; verbascoside, 0.25 mg and zinc, 0.125 mg) or the high dose (C3G, 3.0 mg; verbascoside, 0.75 mg and zinc, 0.375 mg) of the compound. β-actin was used as loading control. Data are expressed as mean ± SEM. Statistical significance was assessed by one-way ANOVA followed by Tukey's multiple comparison post-hoc test (N = 6). $^{*}p < 0.05$ and $^{***}p < 0.001$ vs control; $^{§}p < 0.05$ and $^{§§§}p < 0.001$ vs STZ; $^{###}p < 0.001$ vs low dose treated STZ **(C)** Representative images of whole-mounted retinas after Evans blue dye perfusion. Vascular leakage is indicated by the white arrows. Scale bar, 200 μm **(D)** Representative images of RPE-choroid flatmounts stained with ZO-1. White arrows indicate large holes appeared between the RPE cells Scale bar, 20 μm.

BRB breakdown (**Figure 5D**). Supplementation with the compound dose-dependently prevented tight junction loss with no apparent differences between controls and STZ rats treated with the high dose.

The Compound Protects the Retina From Apoptosis and ERG Dysfunction

A growing body of evidence has underlined that early DR is characterized by apoptosis-related degenerative processes and vascular abnormalities that concur to ERG dysfunction (Barber and Baccouche, 2017). Whether the compound might influence the levels of proapoptotic markers was assessed by evaluating the ratio of pro-apoptotic Bax to anti-apoptotic Bcl-2 proteins as a major checkpoint in the apoptotic pathway. Downstream to the Bax/Bcl-2 ratio, levels of activated caspase 3 as the major effector protease driving the programmed cell death were also determined. As shown by the representative blots and the densitometric analysis in **Figures 6A, B**, the Bax/Bcl-2 ratio and the levels of caspase 3 were significantly increased in STZ rats as compared to controls ($p < 0.0001$). Treatment with the compound dose-dependently prevented the STZ-induced increase in Bax/Bcl-2 ratio and caspase 3, with a partial efficacy of the low dose ($p < 0.001$ vs STZ), while their increase was completely prevented by the high dose ($p < 0.0001$ vs STZ; $p > 0.05$ vs control). The evidence of attenuated levels of caspase 3 was further supported by immunofluorescence analysis (**Figure 6C**). In STZ rats,

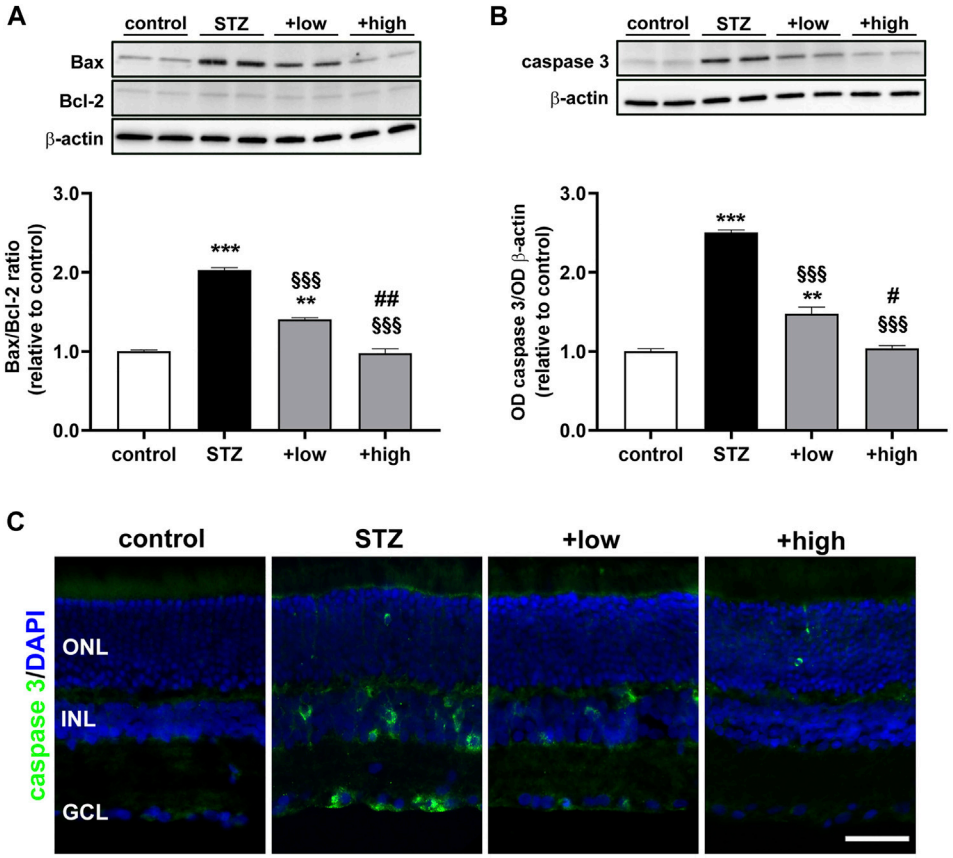

FIGURE 6 | Effects of the compound on apoptotic markers. Representative Western blots and densitometric analysis of Bax/Bcl-2 ratio **(A)** and cleaved caspase 3 **(B)** in controls, STZ untreated or STZ rats treated with either the low dose (C3G, 1.0 mg; verbascoside, 0.25 mg and zinc, 0.125 mg) or the high dose (C3G, 3.0 mg; verbascoside, 0.75 mg and zinc, 0.375 mg) of the compound. The levels of cleaved caspase 3 were normalized to the loading control β-actin. Data are expressed as mean ± SEM. Statistical significance was assessed by one-way ANOVA followed by Tukey's multiple comparison post-hoc test (N = 6). $^{**}p < 0.01$ and $^{***}p < 0.001$ vs control; $^{§§§}p < 0.001$ vs STZ; $^{\#}p < 0.05$ and $^{\#\#}p < 0.01$ vs low dose treated STZ **(C)** Representative images of retinal cross sections immunolabeled for cleaved caspase 3 (green) and counterstained with DAPI (blue). Scale bar, 50 μm. GCL, ganglion cell layer; INL, inner nuclear layer; ONL, outer nuclear layer.

increased caspase 3 was localized to cellular profiles in the GCL and INL as compared to controls in which caspase 3 immunostaining was absent. After the low dose, caspase 3-immunopositive cells were less evident and faintly stained, although some cellular profiles localized to the GCL and INL were still visible. Conversely, no caspase 3-immunopositive cell profiles could be observed after the high dose.

To evaluate whether protective efficacy of the compound might be reflected on preventing STZ-induced visual dysfunction, we analyzed the outer and inner retinal activity using scotopic ERG recordings. Under scotopic condition, a-wave reflects the activity of rods, while b-wave reflects the activity of bipolar cells and Müller glia. **Figure 7A** shows representative mixed a- and b-waves recorded at light intensities of one log cd-s/m^2. As shown in **Figures 7B, C**, In STZ rats treated with the low dose, ERG responses were partially preserved. In fact, at maximal stimulus intensity of 1 log cd-s/m^2, the a-wave amplitude, although not significantly different from that measured in STZ rats (196.5 ± 10.8, $p > 0.05$ vs STZ), showed a tendency toward an increase, while the b-wave amplitude was significantly higher than in STZ rats (518.2 ± 15.7, $p < 0.01$ vs STZ). After treatment with the high dose, a-and b-wave amplitudes were significantly higher than in STZ rats (a-wave 251.2 ± 12.8; b-wave 682.2 ± 24.8 $p < 0.001$ vs STZ) and in low dose-treated rats ($p < 0.01$ vs low dose), but still lower than in controls ($p < 0.05$). No significant effects on ERG responses were found in control rats treated with the compound either at low or high dose (**Supplementary Figure S2**). As shown in **Figures 7D, E**, a- and b-wave amplitude increased with increasing stimulus intensity. A clear a-wave developed at a light intensity of approximately −1.6 log cd-s/m^2. Compared to controls, STZ rats showed a reduction in the amplitude of both the a-wave and the b-wave at light intensities ranging from −1.6 to one log cd-s/m^2 ($p < 0.001$ vs control) although the thickness of both ONL and INL measured in untreated STZ rats did not differ from that measured in controls (**Supplementary Figure S3**). As shown in **Figure 7E**, b-wave amplitudes over increasing light intensities were fitted using the Naka-Rushton equation to evaluate the post-

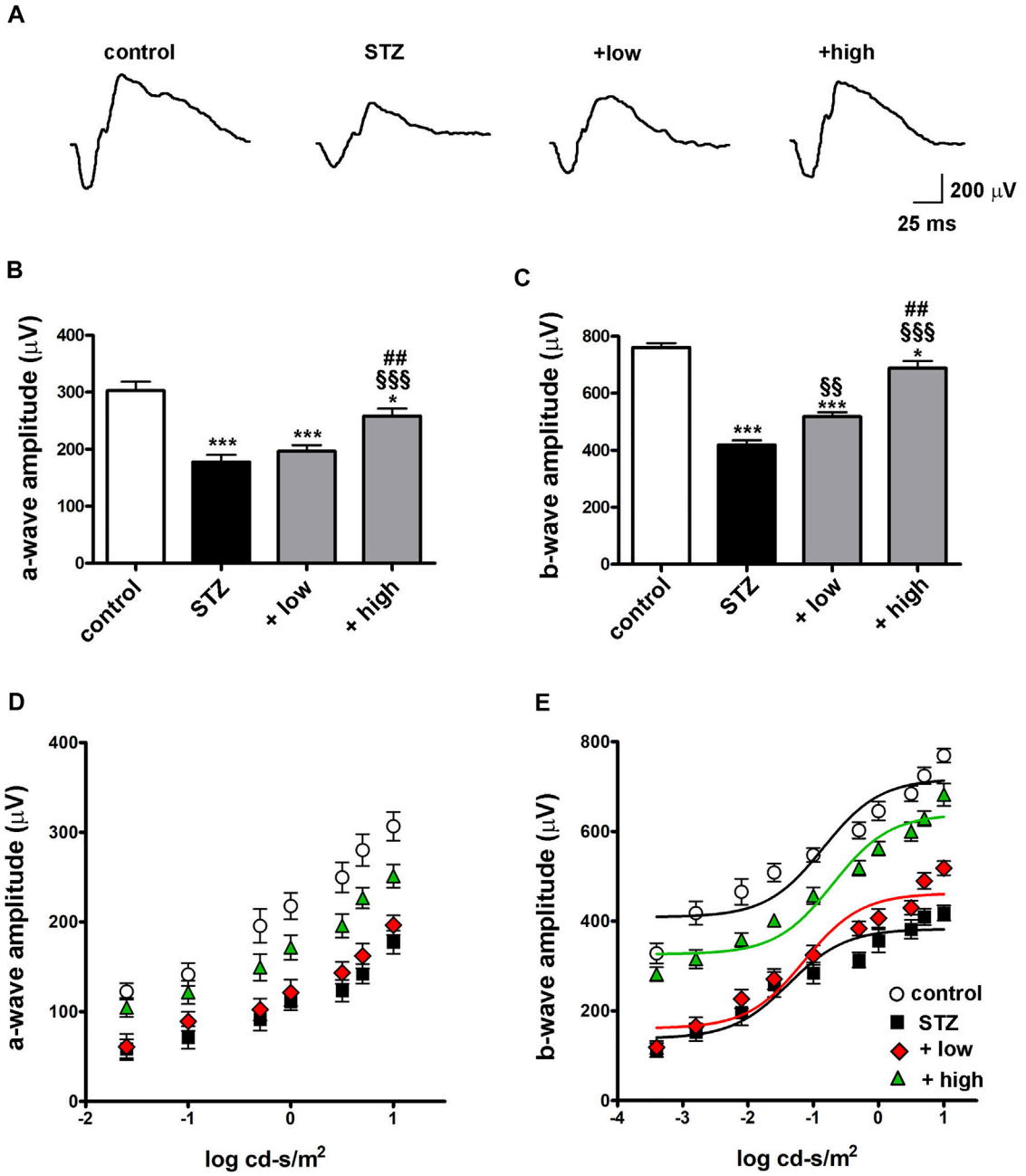

FIGURE 7 | Effects of the compound on scotopic ERG responses **(A)** Representative scotopic ERG waveforms recorded at one log cd-s/m^2 light intensity. Quantitative analysis of the scotopic a- **(B)** and b-wave **(C)** amplitudes recorded at one log cd-s/m^2 light intensity in controls, STZ-untreated rats or STZ rats treated with either the low dose (C3G, 1.0 mg; verbascoside, 0.25 mg and zinc, 0.125 mg) or the high dose (C3G, 3.0 mg; verbascoside, 0.75 mg and zinc, 0.375 mg) of the compound. Statistical significance was assessed by one-way ANOVA followed by Tukey's multiple comparison post-hoc test (N = 8). *$p < 0.05$ and ***$p < 0.001$ vs control; $^{§§}p < 0.01$ and $^{§§§}p < 0.001$ vs STZ; $^{##}p < 0.01$ vs low dose treated STZ. Quantitative analysis of the scotopic a- **(D)** and b-wave **(E)** amplitudes recorded at increasing light intensities. Lines indicate the Naka-Rushton fit of the variation of the b-wave amplitude depending on stimulus intensity. Statistical significance was assessed by two-ways ANOVA followed by Bonferroni's multiple comparison post-hoc test (N = 8).

receptor response amplitude (Vmax) and the retinal sensitivity (k). As shown in **Table 2**, in STZ rats, the values of Vmax and k were significantly lower than in controls ($p < 0.001$). In STZ rats treated with the low dose, Vmax values were significantly higher than those in untreated STZ rats, whereas k values were almost comparable. On the contrary, in STZ rats treated with the high dose, the values of both Vmax and k were significantly higher than in untreated STZ rats.

TABLE 2 | Parameters obtained from b-wave amplitude using the Naka-Rushton function.

	Control	STZ	+ Low	+ High
Vmax (μV)	717.5 ± 16.5	382.9 ± 11.7***	462.4 ± 12.5***,§	638.7 ± 14.2**,§§,##
k (log cd-s/m^2)	−0.87 ± 0.12	−1.40 ± 0.11**	−1.31 ± 0.12*	−0.75 ± 0.11§§,#

*$p < 0.05$, **$p < 0.0$, ***$p < 0.001$ vs control, §$p < 0.01$, §§$p < 0.001$ vs STZ, #$p < 0.01$, ##$p < 0.001$ vs low dose.

DISCUSSION

Recently, much effort has been devoted to preclinical studies in which preventive treatments have been tested in order to stop/delay DR progression. Here, preclinical data on the efficacy of antioxidant compounds in preventing the occurrence of pathological signs that characterize DR have been collected and discussed in light of their possible application to humans.

Currently, the recommended treatment for severe non-proliferative or proliferative DR is photocoagulation and intravitreal injections of anti-VEGF associated, or not, with focal laser for diabetic macular oedema (DME). Anti-VEGF therapy not only counteracts new vessel proliferation but also interferes with inflammatory processes that have a considerable role in the pathogenesis of DME. In particular, VEGF accumulation induced by high blood glucose triggers major inflammatory processes and several drugs are already approved in clinical practice to handle DME. Anti-VEGF agents act also with mechanisms that interfere with inflammatory pathways. In particular, inflammation-induced dropout of pericytes leads to the formation of aberrant capillaries through VEGF accumulation, which reverberates on inflammatory pathways thus contributing to further compromise pericyte viability (Giurdanella et al., 2015). The complex network of pro-inflammatory factors involved in DME represents the rationale for its treatment by intravitreal steroids. In particular, repeated dexamethasone implants have been found to correlate well with DME duration with a better efficacy than anti-VEGF treatments (Bucolo et al., 2018).

Among the major limitations of treatments against vascular complications that characterize DR, late beginning of therapy is the greatest obstacle to cure the disease. In fact, in a high percentage of diabetic patients, inadequate control of metabolic parameters is a major cause of chronic complications including progressive DR. Approximately 15% of patients may show some degree of DR at the time of diabetes first diagnosis although severe microvascular complications will develop many years later. Early diagnosis of DR is the best tool to prevent or delay vision loss, but DR has been long considered as an asymptomatic disease and its progression to advanced stages has reduced the effectiveness of treatments (Corcóstegui et al., 2017; Rodríguez et al., 2019). Current work using subtle analysis of ERG waveforms in diabetic patients has allowed ophthalmologists to reach early diagnosis of non-proliferative DR and to evaluate the possibility to intervene at early stages when the retinal neuro-vascular unit is not yet seriously compromised (Ahmadieh et al., 2021). In this respect, natural plant extracts or their naturally occurring components have been shown to be very proficient in the prevention and treatment of DR. In preclinical studies, treatments with protective compounds that inhibit oxidative stress and inflammation have been shown to counteract the pathological signs of DR although clinical trials dealing with the effect of antioxidants on human DR have provided limited results that are often controversial (Garcia-Medina et al., 2020).

At the preclinical level, the STZ model of diabetes is a well-established and useful tool to investigate complications of diabetes including DR, although its progression to visual dysfunction, which in humans take years to be established, in rodents occur early after STZ injection. However, some limitations need to be considered when approaching the translation to clinics. The induction of diabetes with STZ consists in the acute disruption of pancreatic beta cells and the drastic interruption of insulin production. Therefore, it results in an all-or-nothing phenomenon in which different predispositions or risks of diabetes and, subsequently, different risks of developing DR, are not reproducible.

After STZ injection, elevated blood glucose concentration induced by pancreatic β-cell disruption, initiates an early increase of ROS, which overwhelms endogenous antioxidant defences and leads to early inflammation, increased levels of both HIF-1α and VEGF, increased vascular permeability that causes BRB breakdown leading to decreased visual function (Rodríguez et al., 2019).

There is convincing evidence that throughout the pathologic process of DR, oxidative stress plays an important role. In fact, a series of metabolic pathways altered by the exposure to high glucose concurrently result in the increment of ROS production in the retina. The excess in glucose undergoing glycolysis and citric acid cycle compels the increment in mitochondrial electron transport reaching the maximum threshold, and thus forcing the electron transfer to molecular oxygen generating radical species. In addition, chronic exposure to hyperglycemia favors the nonenzymatic glycation of proteins and lipids leading to the accumulation of advanced glycation end products (AGEs). Besides causing the loss of protein structure and function, AGEs can bind their receptors driving the downstream activation of NADPH oxidases, thus enhancing ROS generation. ROS accumulation triggers the endogenous antioxidant response masterly regulated by the redox sensitive transcriptional factor NRF2, which in turn mediates the increment in antioxidant enzymes such as HO-1 (Kang and Yang, 2020). However, the high glucose-driven ROS accumulation overcomes the endogenous capacity of antioxidant enzymes, which is further hindered by the high-glucose mediated activation of metabolic pathways driving the depletion of enzymatic cofactors. Both the ROS increment and

the antioxidant depotentiation initiate a cascade of events leading to retinal damage (Kowluru and Chan, 2007).

ROS increase also reverberates on the stimulation of the inflammatory response that further promotes oxidative damage. Indeed, ROS accumulation triggers the activation of NF-kB, a transcription factor involved in the modulation of the inflammatory response, which in turn regulates the expression of pro-inflammatory cytokines, such as IL-6 (Liu et al., 2017). In particular, inflammatory cytokines contribute to further amplify retinal cell damage by recruiting and activating immune cells as well as by increasing the levels of mediators responsible for the BRB dysfunction (Semeraro et al., 2015).

Pro-inflammatory stimuli result in macroglia activation as identified by GFAP overexpression, which can be considered as a marker for gliosis. In the healthy retina, GFAP is expressed only in astrocytes and not in Müller cells, whereas in the diseased retina, Müller cells exhibit dense GFAP immunostaining that has been widely used as a cellular marker for retinal pathological injury (Vecino et al., 2016).

Inflammation and gliosis lead to cell injury both in the neuroretina and in retinal blood vessels, thus promoting neuronal and vascular dysfunction. In particular, capillary closure and non-perfusion that develop relatively early after the onset of diabetes participate to establish hypoxic condition in the retina. Hypoxia causes the upregulation of HIF-1α, although HIF-1α increase may also occur as a direct consequence of hyperglycaemia independently on hypoxia (Xiao et al., 2013). HIF-1α accumulation leads to an increased production of VEGF that is a target of HIF-1. Upregulation of the VEGF signalling pathway ultimately leads to the dysfunction of inner and outer BRB with the loss of tight junctions integrity between neighbouring endothelial cells of both retinal microvasculature endothelium and RPE cells (Antonetti et al., 1999). Tight junction proteins including Claudin five and ZO-1, play a pivotal role in maintaining the BRB function through the regulation of the transport of solutes and molecules (Eshaq et al., 2017). The BRB breakdown results in the leakage of blood contents from retinal and choroidal vessels to the surrounding tissue which reverberate on inflammatory and ischemic processes leading to neuroretinal cell damage and ERG dysfunction (Xu and Le, 2011; Klaassen et al., 2013).

Retinal cell death is driven by the activation of apoptotic cascade, as also confirmed here by the altered Bax/Bcl-2 ratio, ultimately leading to the activation of caspase 3, a critical enzyme involved in apoptosis execution. As shown by the present findings, active caspase 3 is mostly localized to the inner retina in agreement with previous results indicating a significant involvement of inner retinal cells in apoptotic processes that characterize DR (Li et al., 2008; Sasaki et al., 2010; Thounaojam et al., 2017; Amato et al., 2018) while the outer retina is rather preserved at least soon after blood glucose increase (Park et al., 2003).

As a consequence of retinal damage, ERG becomes dysfunctional as demonstrated by the decreased amplitude of the scotopic a-wave arising from photoreceptor hyperpolarization, and the b-wave that reflects bipolar cell depolarization leading to potassium outflux that is buffered by Muller cells, which produce a transretinal current participating to b-wave generation (Dong and Hare, 2000 PMID 10824262). ERG dysfunction occurs at 4 weeks after STZ injection in agreement with previous longitudinal studies demonstrating that in the STZ model, ERG responses are unaffected by hyperglycemia up to 3 weeks after diabetes onset (Li et al., 2002; Shinoda et al., 2007; Cammalleri et al., 2017; Amato et al., 2018).

Impairment of scotopic ERG components might be reconducted to alterations of the activity of both photoreceptors and inner retinal cells. In this respect, despite no evidence of reduced thickness of the outer retina in which no apoptotic activity was detected, decreased amplitude of the a-wave is indicative of early photoreceptor suffering in line with previous reports demonstrating early degenerative changes of photoreceptors and pigment epithelium prior to apoptotic events (Énzsöly et al., 2014; Liu et al., 2016). On the other hand, the increased apoptotic activity in the inner retina as demonstrated by the presence of caspase 3-positive cells together with Müller cell gliosis, correlates well with altered b-waves that are known to be early and extensively affected in DR as a sign of inner retina dysfunction (Li et al., 2002).

Ongoing apoptotic processes in the inner retina were not correlated with reduced thickness of the INL in line with previous findings demonstrating that apoptosis becomes manifest as early as 4 weeks after STZ injection to then progress over an extended period of time, eventually leading to a later reduction in the retinal layer thickness (Barber et al., 1998).

As shown by the present results hyperglycaemia-induced cascade leading to ERG dysfunction is prevented by diet administration with antioxidant compounds including C3G, verbascoside and zinc starting on the day of STZ injection and persisting until the fourth week after, when the rats have undergone to ERG recording.

Most chronic diseases including diabetes are worsened by a deficiency of essential antioxidant nutrients, a condition that is further impaired by deficits in their absorption and utilization (Shi et al., 2020). Although major efforts to support the clinical benefits of vitamin and antioxidant interventions to reduce the risk and severity of vision loss, nutraceutical therapy is still limited and more large scales studies in DR are needed to overcome the limitations of clinical trials. Large clinical trials such as the AREDS2 formulation was a major improvement, bringing together natural antioxidants for the treatment of macular degeneration (AREDS2 Research Group et al., 2012; Shi et al., 2020). In this respect, decreased incidence of blindness in patients with macular degeneration have been observed in the zinc supplemented elderly (Prasad and Bao, 2019). Results from clinical trials about the efficacy of natural antioxidants in DR patients are highly variable and, in some cases, controversial. However, a general tendency towards the efficacy of antioxidants in combination has been reported to match the need of counteracting the wide spectrum of pathogenic mechanisms characterizing DR (Garcia-Medina et al., 2020). For instance, the supplementation with lutein, alpha-tocopherol, niacin, beta-carotene, zinc and selenium has been found to delay DR progression in patients with type 2 diabetes, although no effects on visual acuity have been detected (Garcia-Medina

et al., 2011). In contrast, ameliorated visual acuity, but no efficacy on retinal thickness have been determined in patients with type 2 diabetes following the treatment with combined antioxidants including carotenoids, racemic compounds, vitamins and botanical extracts (Chous et al., 2016).

Still, major limitation to the conflicting results of clinical trials in DR depends on the fact that antioxidant efficacy of natural compounds is generally tested on patients who already experienced disorders of visual processing at various levels. Instead, the specific interest would be to test the antioxidant efficacy of nutraceutical compounds by intervening on the early stages of DR to prevent/delay its progression to proliferative DR. In this respect, there is an increasing body of evidence about the role of antioxidants in the control of DR in animal models.

The present results in the STZ model of DR demonstrate the preventive efficacy of a novel compound containing C3G, verbascoside and zinc as nutrients with antioxidant and anti-inflammatory properties. The PK profile of C3G has been characterized by de Ferrars et al. (2014) demonstrating C3G retention in the plasma up to 6 h post-oral administration. In a recent work, C3G has been detected in the plasma from which it reaches the ocular tissue following oral administration (Amato et al., 2021) also in line with previous findings (Matsumoto et al., 2006). Orally administered verbascoside appears to be distributed to most tissues including the brain suggesting its ability to cross the blood-brain barrier (Wen et al., 2016). In addition, verbascoside, has been found to protect ocular tissues and fluids from naturally occurring oxidation (Mosca et al., 2014). The PK profile and biodistribution of zinc have been established in previous studies (Nève et al., 1991; Gilbert et al., 2019). Recently, zinc, orally administered, has been found to accumulate in the retina where it acts as cofactor for antioxidant enzymes (Kamińska et al., 2021). C3G is a potent inhibitor of oxidative stress and its antioxidant properties include the activation of endogenous anti-oxidant enzymes, quenching singlet oxygen, chelation of trace metals involved in free radical production, inhibition of ROS-promoting enzymes, ROS scavenger properties (Tena et al., 2020). ROS scavenging activates a downstream anti-inflammatory cascade leading to the inhibition of the NF-kB activity, the reduced release of pro-inflammatory cytokines and the inhibition of inflammasome activity (Min et al., 2010; Jin et al., 2018). Additional efficacy of C3G includes its capacity to counteract pathological neoangiogenesis by contrasting VEGF overexpression in response to high glucose (Matsunaga et al., 2010; Oliveira et al., 2020). Verbascoside has been reported to exert a major anti-inflammatory activity through the inhibition of NF-kB signalling and nitric oxide pathway, thus resulting in decreased inflammatory response (Wu et al., 2020). Interestingly, verbascoside has also been shown to directly interact with cell survival mechanisms by inhibiting autophagy-induced apoptosis (Chen et al., 2019). In diabetic condition, verbascoside has been established to inhibit endoplasmic reticulum stress and advanced glycation end-product formation (Liu et al., 2013; Galli et al., 2020). Zinc is known as a fundamental trace element involved in the structure and function of numerous enzymes regulating cellular processes and signalling pathways. Zinc potentiates the endogenous antioxidant response by increasing the activity of antioxidant proteins and enzymes that are transcribed by NRF2 (Jarosz et al., 2017). Zinc deficiency has been shown to correlate with ocular abnormalities such as cataract and retinal diseases including age-related macular degeneration and DR (Miao et al., 2013). In line with the negative effects of zinc deficiency, the supplementation of zinc, in combination with additional functional nutrients, has provided promising results to establish its potential for counteracting retinal diseases (Miao et al., 2013; Vishwanathan et al., 2013). However, the boundary line between the activity and the contribution of these hypothetical classes of natural molecules is complicated by the fact that many of the properties of each molecule are shared with the others. For instance, C3G may also activate endogenous antioxidant defenses, as played by zinc. In addition, verbascoside may exert an anti-inflammatory activity leading to reduced ROS generation thus amplifying the effect of zinc and C3G. In this respect, although a theoretical classification of the molecules could be done based on their individual bioactivity, an actual discrimination of each component activity in the context of a compound is difficult to retrieve. The efficacy of C3G, verbascoside and zinc has already been established in a model of light induced retinal damage in which the combined formula has been shown to exert marked antioxidant and anti-inflammatory effects resulting in a significant protection of photoreceptor morpho-functional integrity (Amato et al., 2021). Its application to DR is further stressed by the hypoglycaemic properties of the compounds included in the formula (Sasaki et al., 2007; Xiong et al., 2013; Sadri et al., 2017). However, as shown by the present results, glycemia is not affected by the formula presumably because the serious destruction of islet function by STZ renders the blood glucose difficult to control (Pang et al., 2020). Although the efficacy of the compound supplementation on pathological signs of DR is independent on glycemia control, oxidative stress- and inflammation-related mechanisms downstream hyperglycaemia are markedly counteracted with a significant counterpart in preventing BRB leakage, retinal cell death and retinal dysfunction.

CONCLUSION

One the major clinical problems of late stages of DR is irreversible visual loss due to the scarce availability of drugs restoring visual function once proliferative DR is established. Therefore, research work to investigate possible strategies to prevent DR progression should be accurately pursued. The fact that antioxidant/anti-inflammatory compounds, possibly through their protective efficacy on vascular damage may prevent the apoptotic cascade leading to ERG dysfunction, adds further relevance to their potential application as a preventive therapy to counteract DR progression. On the other hand, the glycemic control is the milestone for the management of diabetes and its related complications including DR. However, a significant number of diabetic patients undergoing glycemic control therapies still develop DR symptoms, thus highlighting the need of

complementary therapies, other than those dedicated to blood glucose lowering. The present study demonstrates that antioxidant supplementation could represent a non-invasive solution to prevent or delay DR signs. Therefore, the translational goal of the present approach consists in its potential complementary role in combination with hypoglycemic drugs in order to further reduce the risk of DR onset and progression. However, the extrapolation of these experimental findings to the clinic is not straightforward as animal models of DR may not faithfully recapitulate all the pathologic signs seen in human DR. In this respect, neither macular edema nor proliferative retinopathy ever develop in STZ-rats, indicating that they are a suitable model for the early phase of human DR.

DATA AVAILABILITY STATEMENT

The raw data supporting the conclusions of this article will be made available by the authors, without undue reservation.

ETHICS STATEMENT

The animal study was reviewed and approved by the Commission for Animal Wellbeing of the University of Pisa.

AUTHOR CONTRIBUTIONS

Conceptualization, DR, PB and MC; methodology, AC, RA and AM; validation, AC and AM; formal analysis, AC and RA; investigation, AC, RA and AM, resources, MD; data curation, RA and MC; writing-original draft preparation, RA, PB and MC.; writing-review and editing, RA, MD, DR, PB and MC; supervision, MC; project administration, DR, PB and MC; funding acquisition, MD. All authors have read and agreed to the published version of the manuscript.

FUNDING

This research was funded by grants from Sooft Italia, SpA (Montegiorgio, FM, Italy) to MDM.

ACKNOWLEDGMENTS

The authors wish to thank Prof. Giuseppe Guarnaccia, Director, ESASO, Switzerland and Prof. Giacomo Panozzo, board coordinator, ESASO Plus, Switzerland, for the critical reading of the manuscript and Marco Pellegrini (Ophthalmology Unit, S.Orsola-Malpighi University Hospital, University of Bologna) for his critical advise on the current state of the art about the use of natural antioxidant compounds in ophthalmology. The authors also wish to thank Tiziana Cintio for animal assistance.

SUPPLEMENTARY MATERIAL

The Supplementary Material for this article can be found online at: https://www.frontiersin.org/articles/10.3389/fphar.2021.811818/full#supplementary-material

REFERENCES

Ahmadieh, H., Behbahani, S., and Safi, S. (2021). Continuous Wavelet Transform Analysis of ERG in Patients with Diabetic Retinopathy. *Doc. Ophthalmol.* 142 (3), 305–314. doi:10.1007/s10633-020-09805-9

Al-Kharashi, A. S. (2018). Role of Oxidative Stress, Inflammation, Hypoxia and Angiogenesis in the Development of Diabetic Retinopathy. *Saudi J. Ophthalmol.* 32 (4), 318–323. doi:10.1016/j.sjopt.2018.05.002

Alipieva, K., Korkina, L., Orhan, I. E., and Georgiev, M. I. (2014). Verbascoside--a Review of its Occurrence, (Bio)synthesis and Pharmacological Significance. *Biotechnol. Adv.* 32 (6), 1065–1076. doi:10.1016/j.biotechadv.2014.07.001

Amato, R., Canovai, A., Melecchi, A., Pezzino, S., Corsaro, R., Dal Monte, M., et al. (2021). Dietary Supplementation of Antioxidant Compounds Prevents Light-Induced Retinal Damage in a Rat Model. *Biomedicines* 9 (9), 1177. doi:10.3390/biomedicines9091177

Amato, R., Rossino, M. G., Cammalleri, M., Locri, F., Pucci, L., Dal Monte, M., et al. (2018). Lisosan G Protects the Retina from Neurovascular Damage in Experimental Diabetic Retinopathy. *Nutrients* 10 (12), 1932. doi:10.3390/nu10121932

Antonetti, D. A., Barber, A. J., Hollinger, L. A., Wolpert, E. B., and Gardner, T. W. (1999). Vascular Endothelial Growth Factor Induces Rapid Phosphorylation of Tight junction Proteins Occludin and Zonula Occluden 1. A Potential Mechanism for Vascular Permeability in Diabetic Retinopathy and Tumors. *J. Biol. Chem.* 274 (33), 23463–23467. doi:10.1074/jbc.274.33.23463

AREDS2 Research GroupChew, E. Y., Chew, E. Y., Clemons, T., SanGiovanni, J. P., Danis, R., et al. (2012). The Age-Related Eye Disease Study 2 (AREDS2): Study Design and Baseline Characteristics (AREDS2 Report Number 1). *Ophthalmology* 119 (11), 2282–2289. doi:10.1016/j.ophtha.2012.05.027

Barber, A. J., and Baccouche, B. (2017). Neurodegeneration in Diabetic Retinopathy: Potential for Novel Therapies. *Vis. Res.* 139, 82–92. doi:10.1016/j.visres.2017.06.014

Barber, A. J., Lieth, E., Khin, S. A., Antonetti, D. A., Buchanan, A. G., and Gardner, T. W. (1998). Neural Apoptosis in the Retina during Experimental and Human Diabetes. Early Onset and Effect of Insulin. *J. Clin. Invest.* 102 (4), 783–791. doi:10.1172/JCI2425

Bucolo, C., Gozzo, L., Longo, L., Mansueto, S., Vitale, D. C., and Drago, F. (2018). Long-term Efficacy and Safety Profile of Multiple Injections of Intravitreal Dexamethasone Implant to Manage Diabetic Macular Edema: A Systematic Review of Real-World Studies. *J. Pharmacol. Sci.* 138 (4), 219–232. doi:10.1016/j.jphs.2018.11.001

Burgos, C., Muñoz-Mingarro, D., Navarro, I., Martín-Cordero, C., and Acero, N. (2020). Neuroprotective Potential of Verbascoside Isolated from Acanthus Mollis L. Leaves through its Enzymatic Inhibition and Free Radical Scavenging Ability. *Antioxidants (Basel)* 9 (12), 1207. doi:10.3390/antiox9121207

Cammalleri, M., Locri, F., Marsili, S., Dal Monte, M., Pisano, C., Mancinelli, A., et al. (2017). The Urokinase Receptor-Derived Peptide UPARANT Recovers Dysfunctional Electroretinogram and Blood-Retinal Barrier Leakage in a Rat Model of Diabetes. *Invest. Ophthalmol. Vis. Sci.* 58 (7), 3138–3148. doi:10.1167/iovs.17-21593

Chen, Q., Xi, X., Zeng, Y., He, Z., Zhao, J., and Li, Y. (2019). Acteoside Inhibits Autophagic Apoptosis of Retinal Ganglion Cells to rescue Glaucoma-Induced Optic Atrophy. *J. Cel Biochem.* 120 (8), 13133–13140. doi:10.1002/jcb.28586

Chous, A. P., Richer, S. P., Gerson, J. D., and Kowluru, R. A. (2016). The Diabetes Visual Function Supplement Study (DiVFuSS). *Br. J. Ophthalmol.* 100 (2), 227–234. doi:10.1136/bjophthalmol-2014-306534

Corcóstegui, B., Durán, S., González-Albarrán, M. O., Hernández, C., Ruiz-Moreno, J. M., Salvador, J., et al. (2017). Update on Diagnosis and Treatment of Diabetic Retinopathy: A Consensus Guideline of the Working Group of Ocular Health (Spanish Society of Diabetes and Spanish Vitreous and Retina Society). *J. Ophthalmol.* 2017, 8234186. doi:10.1155/2017/8234186

de Ferrars, R. M., Czank, C., Zhang, Q., Botting, N. P., Kroon, P. A., Cassidy, A., et al. (2014). The Pharmacokinetics of Anthocyanins and Their Metabolites in Humans. *Br. J. Pharmacol.* 171 (13), 3268–3282. doi:10.1111/bph.12676

Dong, C. J., and Hare, W. A. (2000). Contribution to the Kinetics and Amplitude of the Electroretinogram B-Wave by Third-Order Retinal Neurons in the Rabbit Retina. *Vis. Res.* 40 (6), 579–589. doi:10.1016/s0042-6989(99)00203-5

Énzsöly, A., Szabó, A., Kántor, O., Dávid, C., Szalay, P., Szabó, K., et al. (2014). Pathologic Alterations of the Outer Retina in Streptozotocin-Induced Diabetes. *Invest. Ophthalmol. Vis. Sci.* 55 (6), 3686–3699. doi:10.1167/iovs.13-13562

Eshaq, R. S., Aldalati, A. M. Z., Alexander, J. S., and Harris, N. R. (2017). Diabetic Retinopathy: Breaking the Barrier. *Pathophysiology* 24 (4), 229–241. doi:10.1016/j.pathophys.2017.07.001

Feng, Y., Busch, S., Gretz, N., Hoffmann, S., and Hammes, H. P. (2012). Crosstalk in the Retinal Neurovascular Unit - Lessons for the Diabetic Retina. *Exp. Clin. Endocrinol. Diabetes* 120 (4), 199–201. doi:10.1055/s-0032-1304571

Furman, B. L. (2015). Streptozotocin-Induced Diabetic Models in Mice and Rats. *Curr. Protoc. Pharmacol.* 70, 5.47.1–5.47.20. doi:10.1002/0471141755.ph0547s70

Galli, A., Marciani, P., Marku, A., Ghislanzoni, S., Bertuzzi, F., Rossi, R., et al. (2020). Verbascoside Protects Pancreatic β-Cells against ER-Stress. *Biomedicines* 8 (12), 582. doi:10.3390/biomedicines8120582

Garcia-Medina, J. J., Pinazo-Duran, M. D., Garcia-Medina, M., Zanon-Moreno, V., and Pons-Vazquez, S. (2011). A 5-year Follow-Up of Antioxidant Supplementation in Type 2 Diabetic Retinopathy. *Eur. J. Ophthalmol.* 21 (5), 637–643. doi:10.5301/EJO.2010.6212

Garcia-Medina, J. J., Rubio-Velazquez, E., Foulquie-Moreno, E., Casaroli-Marano, R. P., Pinazo-Duran, M. D., Zanon-Moreno, V., et al. (2020). Update on the Effects of Antioxidants on Diabetic Retinopathy: *In Vitro* Experiments, Animal Studies and Clinical Trials. *Antioxidants (Basel)* 9 (6), 561. doi:10.3390/antiox9060561

Gilbert, R., Peto, T., Lengyel, I., and Emri, E. (2019). Zinc Nutrition and Inflammation in the Aging Retina. *Mol. Nutr. Food Res.* 63 (15), e1801049. doi:10.1002/mnfr.201801049

Giurdanella, G., Anfuso, C. D., Olivieri, M., Lupo, G., Caporarello, N., Eandi, C. M., et al. (2015). Aflibercept, Bevacizumab and Ranibizumab Prevent Glucose-Induced Damage in Human Retinal Pericytes *In Vitro*, through a PLA2/COX-2/VEGF-A Pathway. *Biochem. Pharmacol.* 96 (3), 278–287. doi:10.1016/j.bcp.2015.05.017

Gu, L., Xu, H., Zhang, C., Yang, Q., Zhang, L., and Zhang, J. (2019). Time-dependent Changes in Hypoxia- and Gliosis-Related Factors in Experimental Diabetic Retinopathy. *Eye (Lond)* 33 (4), 600–609. doi:10.1038/s41433-018-0268-z

Jarosz, M., Olbert, M., Wyszogrodzka, G., Młyniec, K., and Librowski, T. (2017). Antioxidant and Anti-inflammatory Effects of Zinc. Zinc-dependent NF-κB Signaling. *Inflammopharmacology* 25 (1), 11–24. doi:10.1007/s10787-017-0309-4

Jin, X., Wang, C., Wu, W., Liu, T., Ji, B., and Zhou, F. (2018). Cyanidin-3-glucoside Alleviates 4-Hydroxyhexenal-Induced NLRP3 Inflammasome Activation via JNK-C-Jun/AP-1 Pathway in Human Retinal Pigment Epithelial Cells. *J. Immunol. Res.* 2018, 5604610. doi:10.1155/2018/5604610

Kamińska, A., Romano, G. L., Rejdak, R., Zweifel, S., Fiedorowicz, M., Rejdak, M., et al. (2021). Influence of Trace Elements on Neurodegenerative Diseases of the Eye-The Glaucoma Model. *Int. J. Mol. Sci.* 22 (9), 4323. doi:10.3390/ijms22094323

Kang, Q., and Yang, C. (2020). Oxidative Stress and Diabetic Retinopathy: Molecular Mechanisms, Pathogenetic Role and Therapeutic Implications. *Redox Biol.* 37, 101799. doi:10.1016/j.redox.2020.101799

Khoo, H. E., Azlan, A., Tang, S. T., and Lim, S. M. (2017). Anthocyanidins and Anthocyanins: Colored Pigments as Food, Pharmaceutical Ingredients, and the Potential Health Benefits. *Food Nutr. Res.* 61 (1), 1361779. doi:10.1080/16546628.2017.1361779

Klaassen, I., Van Noorden, C. J., and Schlingemann, R. O. (2013). Molecular Basis of the Inner Blood-Retinal Barrier and its Breakdown in Diabetic Macular Edema and Other Pathological Conditions. *Prog. Retin. Eye Res.* 34, 19–48. doi:10.1016/j.preteyeres.2013.02.001

Kowluru, R. A., and Chan, P. S. (2007). Oxidative Stress and Diabetic Retinopathy. *Exp. Diabetes Res.* 2007, 43603. doi:10.1155/2007/43603

Leena, M. M., Silvia, M. G., Vinitha, K., Moses, J. A., and Anandharamakrishnan, C. (2020). Synergistic Potential of Nutraceuticals: Mechanisms and Prospects for Futuristic Medicine. *Food Funct.* 11 (11), 9317–9337. doi:10.1039/d0fo02041a

Li, Q., Zemel, E., Miller, B., and Perlman, I. (2002). Early Retinal Damage in Experimental Diabetes: Electroretinographical and Morphological Observations. *Exp. Eye Res.* 74 (5), 615–625. doi:10.1006/exer.2002.1170

Li, W., Chen, S., Zhou, G., Li, H., Zhong, L., and Liu, S. (2018). Potential Role of Cyanidin 3-glucoside (C3G) in Diabetic Cardiomyopathy in Diabetic Rats: An *In Vivo* Approach. *Saudi J. Biol. Sci.* 25 (3), 500–506. doi:10.1016/j.sjbs.2016.11.007

Li, Y. H., Zhuo, Y. H., Lü, L., Chen, L. Y., Huang, X. H., Zhang, J. L., et al. (2008). Caspase-dependent Retinal Ganglion Cell Apoptosis in the Rat Model of Acute Diabetes. *Chin. Med. J. (Engl)* 121 (24), 2566–2571. doi:10.1097/00029330-200812020-00018

Liu, H., Tang, J., Du, Y., Saadane, A., Tonade, D., Samuels, I., et al. (2016). Photoreceptor Cells Influence Retinal Vascular Degeneration in Mouse Models of Retinal Degeneration and Diabetes. *Invest. Ophthalmol. Vis. Sci.* 57 (10), 4272–4281. doi:10.1167/iovs.16-19415

Liu, T., Zhang, L., Joo, D., and Sun, S. C. (2017). NF-κB Signaling in Inflammation. *Signal. Transduct. Target. Ther.* 2, 17023. doi:10.1038/sigtrans.2017.23

Liu, Y. H., Lu, Y. L., Han, C. H., and Hou, W. C. (2013). Inhibitory Activities of Acteoside, Isoacteoside, and its Structural Constituents against Protein Glycation *In Vitro*. *Bot. Stud.* 54 (1), 6. doi:10.1186/1999-3110-54-6

Marreiro, D. D., Cruz, K. J., Morais, J. B., Beserra, J. B., Severo, J. S., and de Oliveira, A. R. (2017). Zinc and Oxidative Stress: Current Mechanisms. *Antioxidants (Basel)* 6 (2), 24. doi:10.3390/antiox6020024

Matsumoto, H., Nakamura, Y., Iida, H., Ito, K., and Ohguro, H. (2006). Comparative Assessment of Distribution of Blackcurrant Anthocyanins in Rabbit and Rat Ocular Tissues. *Exp. Eye Res.* 83 (2), 348–356. doi:10.1016/j.exer.2005.12.019

Matsunaga, N., Tsuruma, K., Shimazawa, M., Yokota, S., and Hara, H. (2010). Inhibitory Actions of Bilberry Anthocyanidins on Angiogenesis. *Phytother Res.* 24 (Suppl. 1), S42–S47. doi:10.1002/ptr.2895

Mi, X. S., Yuan, T. F., Ding, Y., Zhong, J. X., and So, K. F. (2014). Choosing Preclinical Study Models of Diabetic Retinopathy: Key Problems for Consideration. *Drug Des. Devel. Ther.* 8, 2311–2319. doi:10.2147/DDDT.S72797

Miao, X., Sun, W., Miao, L., Fu, Y., Wang, Y., Su, G., et al. (2013). Zinc and Diabetic Retinopathy. *J. Diabetes Res.* 2013, 425854. doi:10.1155/2013/425854

Min, S. W., Ryu, S. N., and Kim, D. H. (2010). Anti-inflammatory Effects of Black rice, Cyanidin-3-O-Beta-D-Glycoside, and its Metabolites, Cyanidin and Protocatechuic Acid. *Int. Immunopharmacol.* 10 (8), 959–966. doi:10.1016/j.intimp.2010.05.009

Mosca, M., Ambrosone, L., Semeraro, F., Casamassima, D., Vizzarri, F., and Costagliola, C. (2014). Ocular Tissues and Fluids Oxidative Stress in Hares Fed on Verbascoside Supplement. *Int. J. Food Sci. Nutr.* 65 (2), 235–240. doi:10.3109/09637486.2013.836742

Naderi, A., Zahed, R., Aghajanpour, L., Amoli, F. A., and Lashay, A. (2019). Long Term Features of Diabetic Retinopathy in Streptozotocin-Induced Diabetic Wistar Rats. *Exp. Eye Res.* 184, 213–220. doi:10.1016/j.exer.2019.04.025

Nair, A. B., and Jacob, S. (2016). A Simple Practice Guide for Dose Conversion between Animals and Human. *J. Basic Clin. Pharm.* 7 (2), 27–31. doi:10.4103/0976-0105.177703

Naka, K. I., and Rushton, W. A. (1966). S-potentials from Colour Units in the Retina of Fish (Cyprinidae). *J. Physiol.* 185 (3), 536–555. doi:10.1113/jphysiol.1966.sp008001

Nève, J., Hanocq, M., Peretz, A., Abi Khalil, F., Pelen, F., Famaey, J. P., et al. (1991). Pharmacokinetic Study of Orally Administered Zinc in Humans: Evidence for an Enteral Recirculation. *Eur. J. Drug Metab. Pharmacokinet.* 16 (4), 315–323. doi:10.1007/BF03189977

Nomi, Y., Iwasaki-Kurashige, K., and Matsumoto, H. (2019). Therapeutic Effects of Anthocyanins for Vision and Eye Health. *Molecules* 24 (18), 3311. doi:10.3390/molecules24183311

Oliveira, H., Fernandes, A., F Brás, N., Mateus, N., de Freitas, V., and Fernandes, I. (2020). Anthocyanins as Antidiabetic Agents-In Vitro and In Silico Approaches of Preventive and Therapeutic Effects. *Molecules* 25 (17), 3813. doi:10.3390/molecules25173813

Pang, B., Ni, Q., Di, S., Du, L. J., Qin, Y. L., Li, Q. W., et al. (2020). Luo Tong Formula Alleviates Diabetic Retinopathy in Rats through Micro-200b Target. *Front. Pharmacol.* 11, 551766. doi:10.3389/fphar.2020.551766

Park, S. H., Park, J. W., Park, S. J., Kim, K. Y., Chung, J. W., Chun, M. H., et al. (2003). Apoptotic Death of Photoreceptors in the Streptozotocin-Induced Diabetic Rat Retina. *Diabetologia* 46 (9), 1260–1268. doi:10.1007/s00125-003-1177-6

Perron, N. R., and Brumaghim, J. L. (2009). A Review of the Antioxidant Mechanisms of Polyphenol Compounds Related to Iron Binding. *Cell Biochem. Biophys.* 53 (2), 75–100. doi:10.1007/s12013-009-9043-x

Prasad, A. S., and Bao, B. (2019). Molecular Mechanisms of Zinc as a Pro-antioxidant Mediator: Clinical Therapeutic Implications. *Antioxidants (Basel)* 8 (6), 164. doi:10.3390/antiox8060164

Qaum, T., Xu, Q., Joussen, A. M., Clemens, M. W., Qin, W., Miyamoto, K., et al. (2001). VEGF-initiated Blood-Retinal Barrier Breakdown in Early Diabetes. *Invest. Ophthalmol. Vis. Sci.* 42 (10), 2408–2413.

Qin, Y., Zhai, Q., Li, Y., Cao, M., Xu, Y., Zhao, K., et al. (2018). Cyanidin-3-O-glucoside Ameliorates Diabetic Nephropathy through Regulation of Glutathione Pool. *Biomed. Pharmacother.* 103, 1223–1230. doi:10.1016/j.biopha.2018.04.137

Rodríguez, M. L., Pérez, S., Mena-Mollá, S., Desco, M. C., and Ortega, Á. L. (2019). Oxidative Stress and Microvascular Alterations in Diabetic Retinopathy: Future Therapies. *Oxid. Med. Cel. Longev.* 2019, 4940825. doi:10.1155/2019/4940825

Rossino, M. G., and Casini, G. (2019). Nutraceuticals for the Treatment of Diabetic Retinopathy. *Nutrients* 11 (4), 771. doi:10.3390/nu11040771

Rossino, M. G., Dal Monte, M., and Casini, G. (2019). Relationships between Neurodegeneration and Vascular Damage in Diabetic Retinopathy. *Front. Neurosci.* 13, 1172. doi:10.3389/fnins.2019.01172

Rübsam, A., Parikh, S., and Fort, P. E. (2018). Role of Inflammation in Diabetic Retinopathy. *Int. J. Mol. Sci.* 19 (4), 942. doi:10.3390/ijms19040942

Sadri, H., Larki, N. N., and Kolahian, S. (2017). Hypoglycemic and Hypolipidemic Effects of Leucine, Zinc, and Chromium, Alone and in Combination, in Rats with Type 2 Diabetes. *Biol. Trace Elem. Res.* 180 (2), 246–254. doi:10.1007/s12011-017-1014-2

Sasaki, M., Ozawa, Y., Kurihara, T., Kubota, S., Yuki, K., Noda, K., et al. (2010). Neurodegenerative Influence of Oxidative Stress in the Retina of a Murine Model of Diabetes. *Diabetologia* 53 (5), 971–979. doi:10.1007/s00125-009-1655-6

Sasaki, R., Nishimura, N., Hoshino, H., Isa, Y., Kadowaki, M., Ichi, T., et al. (2007). Cyanidin 3-glucoside Ameliorates Hyperglycemia and Insulin Sensitivity Due to Downregulation of Retinol Binding Protein 4 Expression in Diabetic Mice. *Biochem. Pharmacol.* 74 (11), 1619–1627. doi:10.1016/j.bcp.2007.08.008

Semeraro, F., Cancarini, A., dell'Omo, R., Rezzola, S., Romano, M. R., and Costagliola, C. (2015). Diabetic Retinopathy: Vascular and Inflammatory Disease. *J. Diabetes Res.* 2015, 582060. doi:10.1155/2015/582060

Shi, C., Wang, P., Airen, S., Brown, C., Liu, Z., Townsend, J. H., et al. (2020). Nutritional and Medical Food Therapies for Diabetic Retinopathy. *Eye Vis. (Lond)* 7, 33. doi:10.1186/s40662-020-00199-y

Shinoda, K., Rejdak, R., Schuettauf, F., Blatsios, G., Völker, M., Tanimoto, N., et al. (2007). Early Electroretinographic Features of Streptozotocin-Induced Diabetic Retinopathy. *Clin. Exp. Ophthalmol.* 35 (9), 847–854. doi:10.1111/j.1442-9071.2007.01607.x

Simó, R., Stitt, A. W., and Gardner, T. W. (2018). Neurodegeneration in Diabetic Retinopathy: Does it Really Matter? *Diabetologia* 61 (9), 1902–1912. doi:10.1007/s00125-018-4692-1

Sinclair, S. H., and Schwartz, S. S. (2019). Diabetic Retinopathy-An Underdiagnosed and Undertreated Inflammatory, Neuro-Vascular Complication of Diabetes. *Front. Endocrinol. (Lausanne)* 10, 843. doi:10.3389/fendo.2019.00843

Tang, J., and Kern, T. S. (2011). Inflammation in Diabetic Retinopathy. *Prog. Retin. Eye Res.* 30 (5), 343–358. doi:10.1016/j.preteyeres.2011.05.002

Tena, N., Martín, J., and Asuero, A. G. (2020). State of the Art of Anthocyanins: Antioxidant Activity, Sources, Bioavailability, and Therapeutic Effect in Human Health. *Antioxidants (Basel)* 9 (5), 451. doi:10.3390/antiox9050451

Thounaojam, M. C., Powell, F. L., Patel, S., Gutsaeva, D. R., Tawfik, A., Smith, S. B., et al. (2017). Protective Effects of Agonists of Growth Hormone-Releasing Hormone (GHRH) in Early Experimental Diabetic Retinopathy. *Proc. Natl. Acad. Sci. U S A.* 114 (50), 13248–13253. doi:10.1073/pnas.1718592114

Vecino, E., Rodriguez, F. D., Ruzafa, N., Pereiro, X., and Sharma, S. C. (2016). Glia-neuron Interactions in the Mammalian Retina. *Prog. Retin. Eye Res.* 51, 1–40. doi:10.1016/j.preteyeres.2015.06.003

Vishwanathan, R., Chung, M., and Johnson, E. J. (2013). A Systematic Review on Zinc for the Prevention and Treatment of Age-Related Macular Degeneration. *Invest. Ophthalmol. Vis. Sci.* 54 (6), 3985. doi:10.1167/iovs.12-11552

Wang, Y., Huo, Y., Zhao, L., Lu, F., Wang, O., Yang, X., et al. (2016). Cyanidin-3-glucoside and its Phenolic Acid Metabolites Attenuate Visible Light-Induced Retinal Degeneration *In Vivo* via Activation of Nrf2/HO-1 Pathway and NF-κB Suppression. *Mol. Nutr. Food Res.* 60 (7), 1564–1577. doi:10.1002/mnfr.201501048

Wen, Y., Huo, S., Zhang, W., Xing, H., Qi, L., Zhao, D., et al. (2016). Pharmacokinetics, Biodistribution, Excretion and Plasma Protein Binding Studies of Acteoside in Rats. *Drug Res. (Stuttg)* 66 (3), 148–153. doi:10.1055/s-0035-1555896

Wu, L., Georgiev, M. I., Cao, H., Nahar, L., El-Seedi, H. R., Sarker, S. D., et al. (2020). Therapeutic Potential of Phenylethanoid Glycosides: A Systematic Review. *Med. Res. Rev.* 40 (6), 2605–2649. doi:10.1002/med.21717

Xiao, H., Gu, Z., Wang, G., and Zhao, T. (2013). The Possible Mechanisms Underlying the Impairment of HIF-1α Pathway Signaling in Hyperglycemia and the Beneficial Effects of Certain Therapies. *Int. J. Med. Sci.* 10 (10), 1412–1421. doi:10.7150/ijms.5630

Xiong, W. T., Gu, L., Wang, C., Sun, H. X., and Liu, X. (2013). Anti-hyperglycemic and Hypolipidemic Effects of Cistanche Tubulosa in Type 2 Diabetic Db/db Mice. *J. Ethnopharmacol.* 150 (3), 935–945. doi:10.1016/j.jep.2013.09.027

Xu, H. Z., and Le, Y. Z. (2011). Significance of Outer Blood-Retina Barrier Breakdown in Diabetes and Ischemia. *Invest. Ophthalmol. Vis. Sci.* 52 (5), 2160–2164. doi:10.1167/iovs.10-6518

Conflict of Interest: MM received a study grant from Sooft Italia SpA. DR is an employee of Sooft Italia SpA. Sooft Italia SpA had no direct role in the collection, analyses or interpretation of data or in the decision to publish the results.

The remaining authors declare that the research was conducted in the absence of any commercial or financial relationships that could be construed as a potential conflict of interest.

The reviewer ST declared a past collaboration with one of the authors MC to the handling editor.

frontiers in Pharmacology

ORIGINAL RESEARCH
published: 04 January 2022
doi: 10.3389/fphar.2021.726104

Effectiveness of a Hydrophilic Curcumin-Based Formulation in Coadjuvating the Therapeutic Effect of Intravitreal Dexamethasone in Subjects With Diabetic Macular Edema

Mariacristina Parravano[1], Davide Allegrini[2], Adriano Carnevali[3], Eliana Costanzo[1], Giuseppe Giannaccare[3], Paola Giorno[1], Vincenzo Scorcia[3], Giorgio Alfredo Spedicato[4], Monica Varano[1] and Mario R Romano[2,5]*

[1]IRCCS-Fondazione Bietti, Rome, Italy, [2]Department of Ophthalmology, Bergamo, Italy, [3]Ophthalmology Unit, Department of Medical and Surgical Sciences, University Magna Graecia of Catanzaro, Catanzaro, Italy, [4]Catholic University of Milan, Milan, Italy, [5]Department of Biomedical Sciences, Humanitas University, Milan, Italy

OPEN ACCESS

Edited by:
Julie Sanderson,
University of East Anglia,
United Kingdom

Reviewed by:
Giustino Orlando,
University of Studies G d'Annunzio
Chieti and Pescara, Italy
Maria Consiglia Trotta,
Università della Campania Luigi
Vanvitelli, Italy

***Correspondence:**
Mariacristina Parravano
mcparravano@gmail.com

Specialty section:
This article was submitted to
Inflammation Pharmacology,
a section of the journal
Frontiers in Pharmacology

Received: 16 June 2021
Accepted: 19 November 2021
Published: 04 January 2022

Citation:
Parravano M, Allegrini D, Carnevali A, Costanzo E, Giannaccare G, Giorno P, Scorcia V, Spedicato GA, Varano M and Romano MR (2022) Effectiveness of a Hydrophilic Curcumin-Based Formulation in Coadjuvating the Therapeutic Effect of Intravitreal Dexamethasone in Subjects With Diabetic Macular Edema. Front. Pharmacol. 12:726104. doi: 10.3389/fphar.2021.726104

Purpose: This study evaluates if the addition of a curcumin formulation with a polyvinylpyrrolidone-hydrophilic carrier (CHC; Diabec®, Alfa Intes, Italy) to intravitreal injections of dexamethasone (DEX-IVT) can affect the morphological retinal characteristics, extending the steroid re-treatment period in patients with diabetic macular edema (DME).

Methods: A randomized controlled clinical trial was carried out in DME patients, randomly assigned to receive DEX-IVT or DEX-IVT and a CHC. The evaluation of the mean difference of central retinal thickness (CRT) was the primary aim. Secondary aims were the evaluations of best-corrected visual acuity, differences in the predetermined retinal layer thickness, the number/time of re-treatment, and the assessment of safety.

Results: A total of 73 DME patients were included (35 in the control group and 38 in the combined therapy group). In both the control and combined therapy groups, the mean CRT change from T_0 to the 6 months' evaluation was significant ($p = 0.00$). The mean CRT result was significantly different at month 4 ($p = 0.01$) between the control and combined therapy groups, with a greater reduction in the combined therapy group, in particular, in patients with ≤10 years of diabetes. A trend of CRT reduction in the combined therapy group has been observed also considering patients with subfoveal neuroretinal detachment. In addition, we observed that the reduction of inner retinal layer thickness was greater in the combination group, in comparison with controls.

Conclusion: The combination of a CHC to DEX-IVT is a promising therapeutic option in case of DME, in particular, for patients with early-stage diabetes and with an inflammatory phenotype. Further studies will be necessary to confirm these findings.

Keywords: diabetic macular edema, dexamethasone, curcumin in hydrophilic carrier, CurcuWIN, central retinal thickness

INTRODUCTION

Diabetic macular edema (DME) is the leading cause of vision loss in diabetic patients (Daruich et al., 2018).

The treatment of DME still appears difficult. Even if the destruction of the blood–retinal barrier (BRB) is the primary pathological feature, the inflammatory component plays a crucial role in the development of this condition. Consequently, the administration of steroids or anti-vascular endothelial growth factor (anti-VEGF) drugs associated (or not) with laser therapy is a widely used therapeutic approach (Dugel et al., 2015; Berco et al., 2017; Mukkamala et al., 2017). It is worthy of note that anti-VEGF agents and steroids, used in clinical practice, are considerably different in terms of molecular interactions when they bind with VEGF (Platania et al., 2015); therefore, characterization of such features can improve the design of novel drugs in reducing the intravitreal (IVT) injection.

IVT corticosteroids and, among them, slow-release dexamethasone IVT injection (DEX-IVT) have been shown to block the production of several inflammatory mediators, such as VEGF and intercellular adhesion molecule 1 (ICAM-1), and to inhibit leukostasis (Tamura et al., 2005; Platania et al., 2015).

The beneficial effects of DEX-IVT therapy on functional and retinal morphological parameters have been demonstrated in DME (Wang et al., 2008).

To significantly improve the therapeutic approach based on anti-VEGF drugs and steroid IVT injections, the reduction of the administration frequency represents a therapeutic need.

Slow-release IVT implants have been used for this purpose (Regillo et al., 2017), leading to re-treatment times that may vary subjectively from 4 to over 6 months (Scaramuzzi et al., 2015; Pacella et al., 2016; He et al., 2018). To further extend the re-treatment time, some studies are evaluating nutraceutical agents in addition to standard therapies.

In particular, the role of curcumin as an adjuvating therapeutic agent in retinal diseases has been extensively reviewed in the past years (Wang et al., 2013; Riva et al., 2017) and was supported by a recent study on experimental models of diabetic retinopathy (DR) (Li et al., 2016a). Curcumin showed *in vitro* and *in vivo* solid evidence of antioxidant, anti-inflammatory, and antiproliferative activities by suppressing the transcription factor NF-kB (nuclear factor kappa-light-chain-enhancer of activated B cells) activity and thus downregulating the activity of cyclooxygenase-2 (COX-2), nitric oxide synthase (NOS), and others (Muangnoi et al., 2019; López-Malo et al., 2020). Curcumin can also upregulate many factors involved in vessel wall damage and hyperpermeability and can downregulate the expression of pro-inflammatory cytokines (interleukins (ILs) and tumor necrosis factor-α [TNF-α]) and proteins. It also inhibits the VEGF release, which downregulates vascular permeability and retinal neo-angiogenesis (Sarao et al., 2017; Platania et al., 2018).

However, the therapeutic use of curcumin in humans presents some limitations such as poor adsorption, degradation, metabolism, and excretion rates. Consequently, several efforts have been carried out to increase the oral bioavailability of curcumin (Li et al., 2016b).

Among them, the combination of a curcumin formulation (CurcuWIN® Dry Powder 20%) with a polyvinylpyrrolidone-hydrophilic carrier (CHC; Diabec®, Alfa Intes, Arpino, Italy) compared with other formulations resulted in its bioavailability in the blood and retina after a single oral administration (Jäger et al., 2014; Sarao et al., 2017; Dei Cas and Ghidoni, 2019).

The efficacy and safety of this formulation for macular edema (ME) of various uncommon etiologies have been recently demonstrated in a retrospective interventional case series, resulting in significant improvement of both functional and anatomical outcomes, with the complete resolution of the edema in most cases (Ferrara et al., 2020).

Based on this background, the aim of the present study is to explore if the addition of a CHC to a DEX-IVT can affect the morphological retinal characteristics, extending the steroid re-treatment period in patients with DME.

PATIENTS AND METHODS

Study Design and Participants

This is a single-blind, randomized controlled clinical trial carried out between February 2018 and March 2020 at three experimental centers in Italy: IRCCS–Fondazione Bietti; Department of Biomedical Sciences, Humanitas Gavazzeni University, Bergamo; and the Department of Ophthalmology of the University of Magna Graecia, Catanzaro. This study was conducted in accordance with the ICH E6 guidelines: "Good Clinical Practice: Consolidated Guidance" and related applicable laws and in accordance with the Declaration of Helsinki.

This study has been approved by the ethics committee of the three experimental centers involved in the study (ClinicalTrials.gov ID: NCT03598205).

The study involved patients with DME in non-proliferative DR, diagnosed by fluorescein angiography and optical coherence tomography (OCT) examination, being treated with DEX-IVT.

Naive patients, patients not treated with anti-VEGF therapy for more than 3 months or with DEX-IVT for more than 6 months, with central retinal thickness (CRT) >300 μm and best-corrected visual acuity (BCVA) evaluated with ETDRS (Early Treatment Diabetic Retinopathy Study) charts at 4 m not <20/400 were included.

Exclusion criteria were considered retinal pathologies other than DME, media opacities limiting the execution and interpretation of diagnostic tests, surgery or para-surgery in the study eye within 3 months prior to the start of treatment, pregnancy, and breastfeeding.

Included patients have been randomly assigned to two groups of treatment:

- Control group: DEX-IVT (0.7 mg)
- Combined therapy group: DEX-IVT (0.7 mg) and 2 tablets/die of CHC. This dosage was reported to be safe and effective in patients with ME, with no reported adverse effects during the follow-up period (Ferrara et al., 2020).

The duration of the study was 6 months.

All patients underwent a comprehensive ophthalmic examination at the baseline (T_0) and monthly. The ophthalmic examination included the BCVA assessment with ETDRS charts at 4 m, slit lamp biomicroscopy, intraocular pressure measurement, dilated fundus examination, and structural OCT image acquisition with RTVue XR spectral domain (SD)-OCT device (Optovue, Inc., Fremont, CA, USA). This instrument has an A-scan rate of 70,000 scans/s and uses a light source centered at 840 nm and a bandwidth of 45 nm.

Moreover, the thickness of the retinal layers was measured on the structural map, and CRT was analyzed. The OCT software automatically allows measurement of the thickness of individual retinal layers, in particular of the foveal inner retinal layer (IRL) thickness (from the inner limiting membrane to the outer border of the inner plexiform layer) and outer retinal layer thickness, from the inner plexiform layer to Bruch membrane.

DEX-IVT was performed at T_0 for all included patients. Following the first DEX-IVT, patients were re-treated according to a pro re nata regimen, starting from month 3 if there was a persistence/recurrence of DME, defined as the presence of intraretinal or subretinal fluid on SD-OCT, also in the absence of visual impairment.

Study Measures

The evaluation of the mean difference of CRT values measured by structural OCT between the two study groups has been considered the primary aim.

Secondary aims were the evaluation of the mean difference of BCVA values, the differences in the predetermined retinal layer thickness detected by structural OCT, the number and the time of re-treatment, and the evaluation of safety.

All measures have been assessed at the baseline (T_0) and at 1, 3, 4, 5, and 6 months of treatment.

Statistical Analysis

Descriptive statistics were used to summarize relevant study information. ANOVA for repeated measures followed by *post-hoc* comparisons has been applied to evaluate the experimental results. The statistical software R (R Core Team, 2017), the packages R nlme (Pinheiro and Bates, 2017) and lsmeans (Lenth, 2016) for ANOVA, and *post-hoc* tests have been used. The first- and second-type error thresholds were respectively α = 5% and β = 20% (i.e., implying a power of 80%).

The primary outcome has been analyzed for the overall population and for the following subgroups: patients with ≤10 years of diabetes and those presenting a subfoveal neuroretinal detachment (SND). The secondary outcomes have been analyzed for the overall population only.

RESULTS

Participants

A total of 73 DME patients were included in the study, of whom 35 were randomly assigned to the control group and 38 to the combined therapy group. Baseline characteristics of patients were summarized in **Table 1**.

Analysis of Central Retinal Thickness Values

Overall Population

The CRT values are comparable at the baseline between groups (p = 0.07). In both treatment groups, the mean CRT change from T_0 to the 6 months' evaluation is significant (p = 0.00) and with a decrease in values from 526 ± 108 to 377 ± 155 μm in the control group and from 488 ± 122 to 344 ± 104 μm in the combined therapy group.

The mean CRT values have been compared between the two study groups at the baseline and at each follow-up visit, and the mean CRT result was significantly different at month 4 (p = 0.01; **Figure 1A**), with a greater reduction of the thickness in the combined therapy group in comparison with controls (**Figure 1B**). Reduction corresponds to 24% in the combined therapy group and to 12% in the control group, compared with baseline values.

Patients With ≤10 Years of Diabetes

The mean CRT values of patients with ≤10 years of diabetes have been compared between the two treatment groups, with the aim of verifying whether the adjuvant effect of the CHC therapy was more evident in the early stage of diabetes.

The statistical analysis indicated a significant difference in the mean CRT values between groups at month 4 (p = 0.002) (**Figure 2A**).

These data are strengthened by the lack of significance found in the same analysis carried out on patients with diabetes for >10 years (n = 43) (**Figure 2B**).

Patients With Subfoveal Neuroretinal Detachment

The mean CRT values have been compared between the two treatments group considering only patients who present SND at the baseline and for each follow-up visit. A trend of greater reduction of CRT values can be observed in patients treated with combined therapy compared with those in the control group (**Figure 3**), despite not being statistically significant. At each follow-up visit, the mean number of patients with an SND was

TABLE 1 | Baseline characteristics.

Parameters	Overall	Combined group	Control group
All patients	**n = 73**	**n = 38**	**n = 35**
Age (years), mean ± SD	67 ± 9	66 ± 7	67 ± 10
Diabetes length (years), mean ± SD	13 ± 7	13 ± 7	13 ± 6
Patients with previous IVT, n (%)	38 (52)	20 (52)	18 (51)
Phakic patients, n (%)	43 (58)	24 (63)	19 (66)
Previous laser intervention, n (%)	31 (42)	15 (39)	16 (45)
Patients with ≤10 years diabetes	**n = 30 (41%)**	**n = 14**	**n = 16**
Age (years), mean ± SD	62 ± 8	62 ± 7	61 ± 9
Diabetes length (years), mean ± SD	7 ± 2	7 ± 2	7 ± 2
Patients with previous IVT, n (%)	16 (53)	8 (57)	8 (50)
Phakic patients, n (%)	22 (73)	10 (71)	12 (75)
Previous laser intervention, n (%)	8 (26)	3 (21)	5 (31)
Patients with SND at the baseline	**n = 20 (27%)**	**n = 11**	**n = 9**
Age (years), mean ± SD	69 ± 9	72 ± 6	66 ± 12
Diabetes length (years), mean ± SD	14 ± 7	16 ± 7	13 ± 6
Patients with previous IVT, n (%)	13 (65)	6 (54)	7 (77)
Phakic patients, n (%)	12 (60)	5 (45)	7 (78)
Previous laser intervention, n (%)	8 (40)	5 (45)	3 (34)

Note. IVT, intravitreal; SND, subfoveal neuroretinal detachment.

17% (n = 6) of total patients in the control group and 10% (n = 4) in the combined therapy group.

Secondary Outcomes

Best-Corrected Visual Acuity Analysis

The BCVA values are non-homogeneous at the baseline between groups ($p = 0.00$).

The comparison between the mean BCVA values at each follow-up between the two study groups did not show any significant difference (baseline BCVA = 50.0 ± 18.7 in the control group and 48.5 ± 17.7 in combined therapy group; 6 months BCVA = 54.8 ± 17.0 in the control group and 48.9 ± 19.8 in combined therapy group).

Anatomical Findings on Optical Coherence Tomography

Among the different retinal layer thickness measured by structural OCT, a significant difference between the two study groups was detected in IRL thickness values with a significantly greater reduction at month 4 in the combined group in comparison with the control group (**Figure 4A**). Compared with T_0 values, at T4, the IRL thickness variation is equal to −28% in the combined therapy group and +1% in the control group.

At baseline, this parameter was homogeneous between groups ($p = 0.78$).

Otherwise, the mean outer retinal layer thickness values were not significantly different between the two study groups in any follow-up visit (**Figure 4B**).

Comparison Between Dexamethasone Intravitreal Injection Number and Reinjection Time

During the study period, there was no significant difference in the mean number of treatments (1.4 ± 0.5 in the control group and 1.6 ± 0.5 in the combined treatment group) nor a significant difference in the re-injection mean time (4.5 ± 0.8 months in the control group, 4.6 ± 0.5 months in the combined therapy group) between the two study groups.

During the study, 31 patients out of 73 (42%) were treated with only one DEX-IVT: 15 in the control group and 16 in the combined therapy. Otherwise, most of the patients were re-treated (n = 42, 58%): two control patients within the first 3 months, the others after the 4 months' follow-up, 19 in the control group, and 21 in the combined treatment.

Safety Assessment

No events of hypertonia, endophthalmitis, or retinal detachment were reported by patients during the study period.

DISCUSSION

In this study, we aimed to verify if the addition of a CHC to a DEX-IVT in DME patients, compared with DEX-IVT alone, can affect the morphological retinal response at 6 months.

The efficacy of DEX-IVT therapy in DME on functional and retinal morphological parameters has been widely demonstrated (Wang et al., 2008), by exerting specific effects on the inflammatory component in DME. To further extend the re-treatment time, some studies are evaluating nutraceutical agents in addition to standard therapies.

In particular, emerging evidence of the pharmacological effects of curcumin led to this compound being considered as a potentially beneficial treatment of various retinal diseases, including those complicated by DME (Peddada et al., 2019). DME is recognized as a neurovascular complication of DR, and the involvement of inflammatory processes in this pathology particularly characterizes the early stages of DR (Rossino et al., 2019).

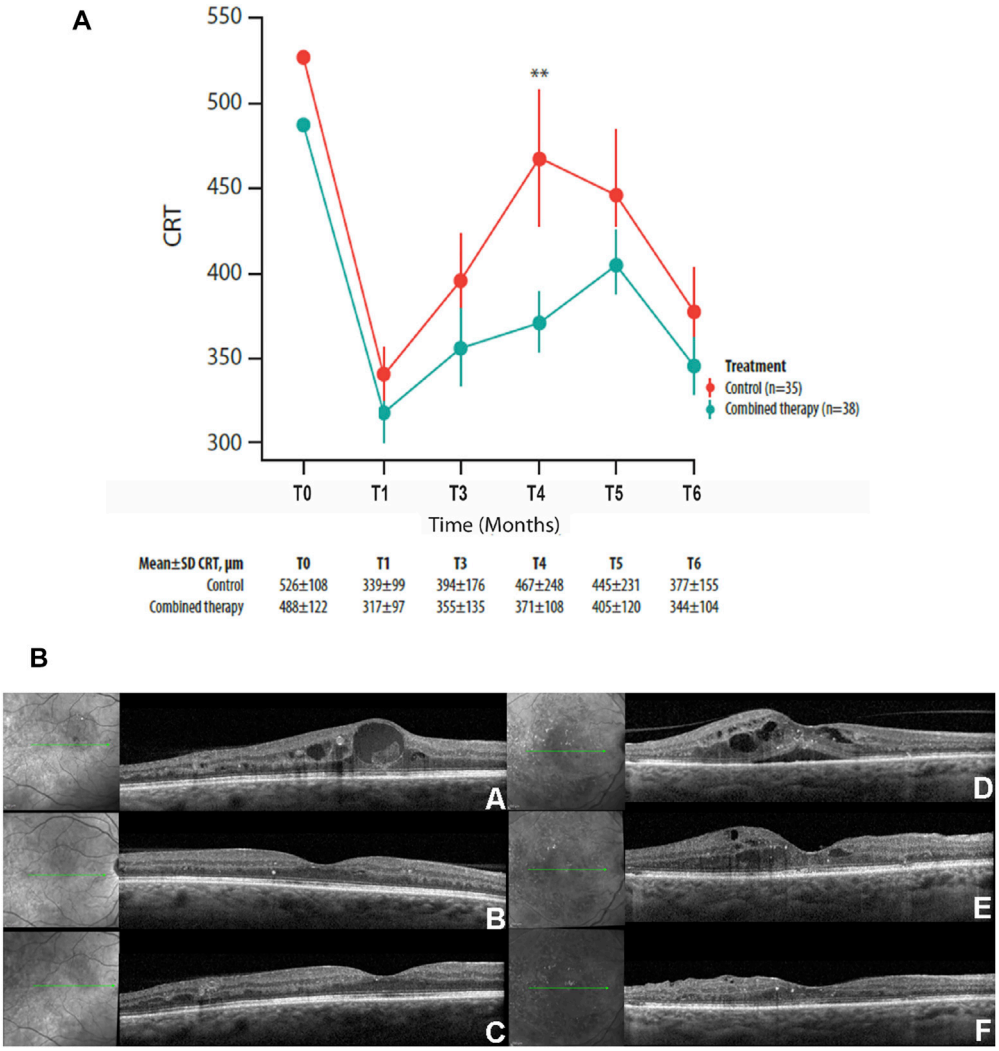

FIGURE 1 | (A) Mean ± SD central retinal thickness (CRT) values collected at T_0 and at each follow-up visit in control and combined therapy groups, considering the overall population. **(B)** Representative OCT scans collected at T_0 **(A, D)**, at the 4-month follow-up **(B, E)**, and at the 6-month follow-up visits **(C, F)** in combined therapy **(left panel)** and control **(right panel)** patients. In the combined therapy group (left side, A), macular edema, characterized by intraretinal fluid and hyperreflective material inside the cyst, was present at T_0; macular edema was completely resolved after combined therapy at the 4- and 6-month follow-up **(left side, B** and **C)**. In the control group **(right side, D)**, macular edema, characterized by intraretinal and subretinal fluid, was present at T_0; after DEX-IVT at the 4-month follow-up **(right side, E)**, complete reabsorption of subretinal fluid with persistence of intraretinal fluid was observed; complete reabsorption of intraretinal fluid was recorded at the 6-month follow-up **(right side, F).** $^{**}p = 0.01$.

Curcumin shows anti-inflammatory, antioxidant, antiangiogenic, and neuronal- and vascular-protective properties due to its capability to target and regulate multiple signaling pathways (Rossino et al., 2019). An inhibitory effect has also been documented of curcumin on cyclooxygenase, NF-κB, TNF-α, IL-1, IL-6, IL-8, and free radical production.

Moreover, curcumin shows an inhibitory activity on lipoteichoic acid-activated microglial cells. Neuroinflammation plays a key role in the pathogenesis of DR, where the microglia become activated, producing inflammatory mediators (Malchiodi-Albedi et al., 2008; Abcouwer, 2013; Farajipour et al., 2018).

However, the clinical use of curcumin has been limited by its pharmacokinetics, being poorly soluble and rapidly metabolized and eliminated (Yu et al., 2018).

To increase the oral bioavailability of curcumin, a CHC has been conjugated (CHC, Diabec®). This combination was demonstrated to be bioavailable in the human blood with a concentration that is 46 times higher than that of other curcumins formulations and reached the retinal target after a single administration in a rabbit model (Sarao et al., 2017; Dei Cas and Ghidoni, 2019).

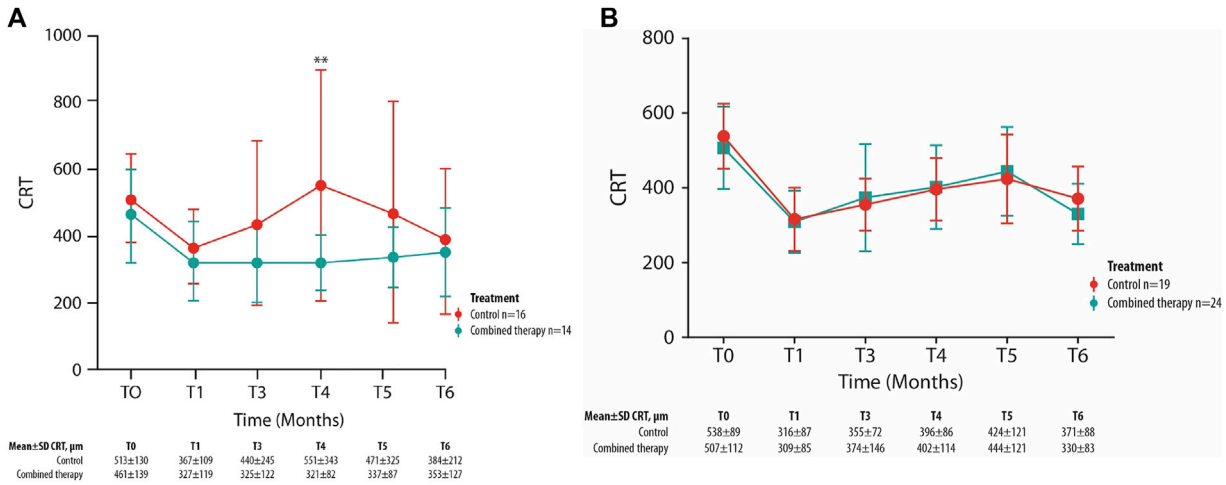

FIGURE 2 | Mean ± SD central retinal thickness (CRT) values collected at T_0 and up to the 6-month follow-up visit in control and combined therapy groups, considering patients with ≤10 years of diabetes **(A)** or >10 years of diabetes **(B)**. $^{**}p = 0.002$.

The results of the study show a significant reduction of the mean CRT values in both groups after treatment. In addition, a significant CRT reduction has been observed in the combined therapy group at month 4 in comparison with controls, concomitant with the reduction of the dexamethasone effect, administered by DEX-IVT at the baseline to all patients.

Of note, the reduction of the mean CRT values at month 4 is more evident in the combined therapy group if we consider patients with early-stage diabetes (<10 years of diabetes duration) or patients who present an SND.

In addition, we observed that the reduction of intra/subretinal fluid was greater in the combination group and more evident in the IRL.

These results could be related to the complex properties of a CHC that exert a synergic anti-inflammatory effect with DEX-IVT and by reducing the glia activation in the inner retina.

To better understand this result, we can speculate about its correlation with the pathogenesis of DME in the early stages. The BRB breakdown is a typical event in early-stage DR, and the underlying mechanisms causing this vascular dysfunction result in the increased vascular permeability and degeneration of retinal capillaries (Anand et al., 2007).

The breakdown of both the inner BRB (iBRB) and outer BRB triggers the development of DME at any stage of DR (Shin et al., 2014). In particular, the breakdown of the iBRB especially is a hallmark of DME (Das, 2016).

The iBRB is composed of the endothelium cells on the basal lamina, enveloped by the processes of Müller cells and pericytes, which are responsible for the activity of retinal endothelial cells transmitting regulatory signals (Vinores, 2010) in the inner retina.

Several cytokines and growth factors are responsible for BRB breakdown in the early stages through multiple signaling pathways, leading to the loss of adherents and tight-junction proteins between endothelial cells, responsible for the regulation of vascular permeability (Hosoya and Tachikawa, 2012).

This suggests that the adjuvant efficacy of a CHC is enhanced especially in the earliest stages of the retinal pathology when the structural damage is still limited and the vascular network is not completely compromised.

In addition, our results showed a trend of greater reduction of CRT values among patients with SND treated with combined therapy as compared with those in the control group, with the smallest percentage of SND in the combined therapy at each follow-up visit. DME with SND has been considered as a distinct DME pattern associated with a major ocular inflammatory condition, including higher levels of IL-6 in the vitreous and increased number of hyperreflective retinal spots, considered as signs of activated microglial cells in the retina. These results corroborate a possible relevant role of curcumin on the inflammation process mitigation.

In our population, no differences in the mean number of IVT and in the re-treatment time have been observed. This could be related to the defined study period of 6 months, and a longer one could allow a better evaluation of this parameter. In addition, the re-treatment was performed by evaluating not only the reduction of intra/subretinal fluid related to the CRT parameter but also the BCVA, a functional parameter that often does not correlate with the anatomical variations (Förster, 2008; Browning and Fraser, 2008).

This study presents some limitations such as the small size of the sample, the short duration of the follow-up, and the inclusion of naïve and previously treated patients. In addition, not considering the metabolic parameters as influencing factors for the morphological and functional outcomes could be another limitation.

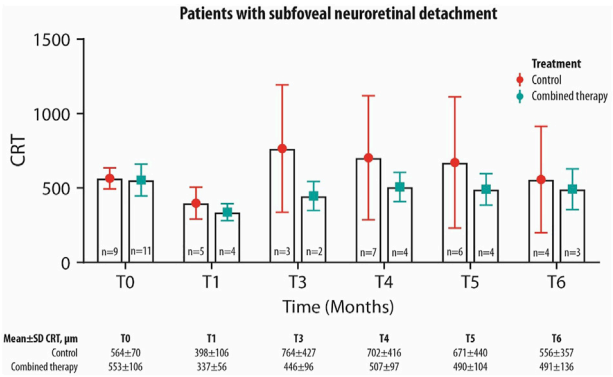

FIGURE 3 | Mean ± SD central retinal thickness (CRT) values collected at T_0 and up to the 6-month follow-up visit in control and combined therapy groups, considering patients with SND.

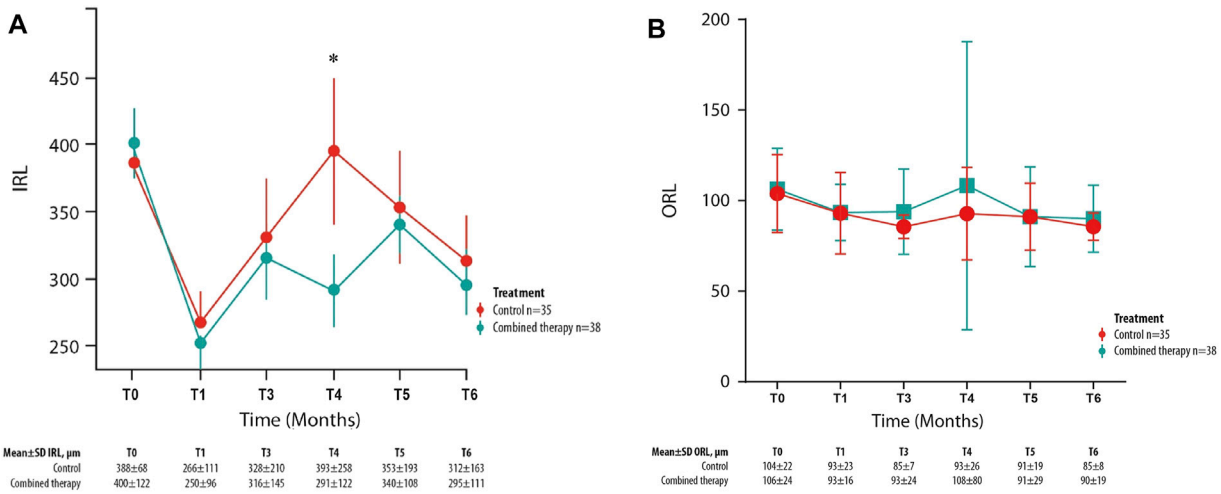

FIGURE 4 | Mean ± SD inner retinal layer (IRL) **(A)** and outer retinal layer **(B)** values collected at T_0 and for each follow-up visit in control and combined therapy groups. *p = 0.045.

CONCLUSION

The oral administration of a CHC in addition to DEX-IVT in patients affected by DME is well-tolerated and resulted in a greater improvement of morphological findings (significant reduction of CRT and IRL values), suggesting a major effect on DME. The beneficial effect of the additional treatment with a CHC is even more evident when considering the subpopulation of patients with ≤10 years of diabetes or who present an SND.

In conclusion, the combination of a CHC to DEX-IVT has promising results as a therapeutic option in case of DME, in particular for patients with early-stage diabetes and with an inflammatory phenotype. Further studies will be necessary to validate this therapeutic strategy and confirm our findings.

The treatment of DME still appears difficult. Considering the solid *in vitro* and *in vivo* evidence about the antioxidant, anti-inflammatory, and antiproliferative activities of curcumin, its potential as an adjuvating therapeutic agent in retinal diseases has been extensively reviewed, and a recent study on experimental models of DR supported this hypothesis. This study demonstrates that the oral administration of a curcumin formulation (CurcuWINÂ® Dry Powder 20%) with a CHC (DiabecÂ®, Alfa Intes, Italy) in addition to slow-release DEX-IVT in DME patients is well-tolerated and resulted in a greater improvement of morphological findings (significant reduction of CRT and IRL), suggesting a major effect on DME. The beneficial effect of the additional treatment with a CHC was more evident when considering the subpopulation of patients with ≤10 years of diabetes or who present an inflammatory phenotype, further increasing our knowledge about this therapeutic approach.

DATA AVAILABILITY STATEMENT

The raw data supporting the conclusions of this article will be made available by the authors, without undue reservation.

ETHICS STATEMENT

The studies involving human participants were reviewed and approved by the ethics committee of the three experimental centers involved in the study (ClinicalTrials.gov ID: NCT03598205). The patients/participants provided their written informed consent to participate in this study.

AUTHOR CONTRIBUTIONS

Concept and study design: MP and MR. Data collection, analysis, and interpretation: all. Manuscript writing: MP and MR. Manuscript editing and approval to submit: all.

FUNDING

This research concerning IRCCS–Fondazione Bietti was in part financially supported by the Italian Ministry of Health and Fondazione Roma. The funders had no role in study design, data collection, and analysis, decision to publish, or preparation of the manuscript.

ACKNOWLEDGMENTS

The authors would like to thank Dr Anna Rita Blanco (Medical Liaison, Alfa Intes) for the scientific support. Editorial assistance was provided by Simonetta Papa, PhD, and Aashni Shah (Polistudium SRL, Milan, Italy). Graphical assistance was provided by Massimiliano Pianta (Polistudium SRL, Milan, Italy). This assistance was supported by Alfa Intes.

REFERENCES

Abcouwer, S. F. (2013). Angiogenic Factors and Cytokines in Diabetic Retinopathy. *J. Clin. Cel Immunol.* 1, 1–12. doi:10.4172/2155-9899

Anand, P., Kunnumakkara, A. B., Newman, R. A., and Aggarwal, B. B. (2007). Bioavailability of Curcumin: Problems and Promises. *Mol. Pharm.* 4, 807–818. doi:10.1021/mp700113r

Berco, E., Rappoport, D., and Pollack, A. (2017). Treatment Options for Diabetic Macular Edema. *Harefuah* 156, 109–113.

Browning, D. J., and Fraser, C. M. (2008). The Predictive Value of Patient and Eye Characteristics on the Course of Subclinical Diabetic Macular Edema. *Am. J. Ophthalmol.* 145, 149–154. doi:10.1016/j.ajo.2007.08.038

Daruich, A., Matet, A., Moulin, A., Kowalczuk, L., Nicolas, M., Sellam, A., et al. (2018). Mechanisms of Macular Edema: Beyond the Surface. *Prog. Retin. Eye Res.* 63, 20–68. doi:10.1016/j.preteyeres.2017.10.006

Das, A. (2016). Diabetic Retinopathy: Battling the Global Epidemic. *Invest. Ophthalmol. Vis. Sci.* 57, 6669–6682. doi:10.1167/iovs.16-21031

Dei Cas, M., and Ghidoni, R. (2019). Dietary Curcumin: Correlation between Bioavailability and Health Potential. *Nutrients* 11, 2147. doi:10.3390/nu11092147

Dugel, P. U., Bandello, F., and Loewenstein, A. (2015). Dexamethasone Intravitreal Implant in the Treatment of Diabetic Macular Edema. *Clin. Ophthalmol.* 9, 1321–1335. doi:10.2147/OPTH.S79948

Farajipour, H., Rahimian, S., and Taghizadeh, M. (2018). Curcumin: A New Candidate for Retinal Disease Therapy? *J. Cel Biochem* 120, 6886–6893. Online ahead of print. doi:10.1002/jcb.28068

Ferrara, M., Allegrini, D., Sorrentino, T., Sborgia, G., Parmeggiani, F., Borgia, A., et al. (2020). Curcumin-based Treatment for Macular Edema from Uncommon Etiologies: Efficacy and Safety Assessment. *J. Med. Food* 23, 834–840. doi:10.1089/jmf.2019.0241

Förster, C. (2008). Tight Junctions and the Modulation of Barrier Function in Disease. *Histochem. Cel Biol* 130, 55–70. doi:10.1007/s00418-008-0424-9

He, Y., Ren, X. J., Hu, B. J., Lam, W. C., and Li, X. R. (2018). A Meta-Analysis of the Effect of a Dexamethasone Intravitreal Implant versus Intravitreal Anti-vascular Endothelial Growth Factor Treatment for Diabetic Macular Edema. *BMC Ophthalmol.* 18, 121. doi:10.1186/s12886-018-0779-1

Hosoya, K., and Tachikawa, M. (2012). The Inner Blood-Retinal Barrier: Molecular Structure and Transport Biology. *Adv. Exp. Med. Biol.* 763, 85–104.

Jäger, R., Lowery, R. P., Calvanese, A. V., Joy, J. M., Purpura, M., and Wilson, J. M. (2014). Comparative Absorption of Curcumin Formulations. *Nutr. J.* 13, 11. doi:10.1186/1475-2891-13-11

Lenth, R. V. (2016). Least-squares Means: the R Package Lsmeans. *J. Stat. Softw.* 69, 1–33. doi:10.18637/jss.v069.i01

Li, J., Wang, P., Ying, J., Chen, Z., and Yu, S. (2016). Curcumin Attenuates Retinal Vascular Leakage by Inhibiting Calcium/calmodulin-dependent Protein Kinase II Activity in Streptozotocin-Induced Diabetes. *Cell Physiol Biochem* 39, 1196–1208. doi:10.1159/000447826

Li, Q., Wang, Z., Wang, R., Tang, H., Chen, H., and Feng, Z. (2016). A Prospective Study of the Incidence of Retinopathy of Prematurity in China: Evaluation of Different Screening Criteria. *J. Ophthalmol.* 2016, 5918736. doi:10.1155/2016/5918736

López-Malo, D., Villarón-Casares, C. A., Alarcón-Jiménez, J., Miranda, M., Díaz-Llopis, M., Romero, F. J., et al. (2020). Curcumin as a Therapeutic Option in Retinal Diseases. *Antioxidants* 9 (1), 48. doi:10.3390/antiox9010048

Malchiodi-Albedi, F., Matteucci, A., Bernardo, A., and Minghetti, L. (2008). PPAR-gamma, Microglial Cells, and Ocular Inflammation: New Venues for Potential Therapeutic Approaches. *PPAR Res.* 2008, 295784. doi:10.1155/2008/295784

Muangnoi, C., Sharif, U., Ratnatilaka Na BhuketBhuket, P. P., Rojsitthisak, P., and Paraoan, L. (2019). Protective Effects of Curcumin Ester Prodrug, Curcumin Diethyl Disuccinate against H2O2-Induced Oxidative Stress in Human Retinal Pigment Epithelial Cells: Potential Therapeutic Avenues for Age-Related Macular Degeneration. *Ijms* 20, 3367. doi:10.3390/ijms20133367

Mukkamala, L., Bhagat, N., and Zarbin, M. (2017). Practical Lessons from Protocol T for the Management of Diabetic Macular Edema. *Dev. Ophthalmol.* 60, 109–124. doi:10.1159/000459694

Pacella, F., Ferraresi, A. F., Turchetti, P., Lenzi, T., Giustolisi, R., Bottone, A., et al. (2016). Intravitreal Injection of Ozurdex(®) Implant in Patients with Persistent Diabetic Macular Edema, with Six-Month Follow-Up. *Ophthalmol. Eye Dis.* 8, 11–16. doi:10.4137/OED.S38028

Peddada, K. V., Brown, A., Verma, V., and Nebbioso, M. (2019). Therapeutic Potential of Curcumin in Major Retinal Pathologies. *Int. Ophthalmol.* 39, 725–734. doi:10.1007/s10792-018-0845-y

Pinheiro, J., and Bates, D. (2017). Available at: http://cran.rapporter.net/web/packages/nlme/nlme.pdf.

Platania, C. B., Di Paola, L., Leggio, G. M., Romano, G. L., Drago, F., Salomone, S., et al. (2015). Molecular Features of Interaction between VEGFA and Anti-angiogenic Drugs Used in Retinal Diseases: a Computational Approach. *Front. Pharmacol.* 6, 248. doi:10.3389/fphar.2015.00248

Platania, C. B. M., Fidilio, A., Lazzara, F., Piazza, C., Geraci, F., Giurdanella, G., et al. (2018). Retinal protection and Distribution of Curcumin *In Vitro* and *In Vivo*. *Front. Pharmacol.* 9, 670. doi:10.3389/fphar.2018.00670

R Core Team (2017). Available at: https://www.R-project.org/.

Regillo, C. D., Callanan, D. G., Do, D. V., Fine, H. F., Holekamp, N. M., Kuppermann, B. D., et al. (2017). Use of Corticosteroids in the Treatment of Patients with Diabetic Macular Edema Who Have a Suboptimal Response to Anti-VEGF: Recommendations of an Expert Panel. *Ophthalmic Surg. Lasers Imaging Retina* 48, 291–301. doi:10.3928/23258160-20170329-03

Riva, A., Togni, S., Giacomelli, L., Franceschi, F., Eggenhoffner, R., Feragalli, B., et al. (2017). Effects of a Curcumin-Based Supplementation in Asymptomatic Subjects with Low Bone Density: a Preliminary 24-week Supplement Study. *Eur. Rev. Med. Pharmacol. Sci.* 21, 1684–1689.

Rossino, M. G., Dal Monte, M., and Casini, G. (2019). Relationships between Neurodegeneration and Vascular Damage in Diabetic Retinopathy. *Front. Neurosci.* 13, 1172. doi:10.3389/fnins.2019.01172

Sarao, V., Veritti, D., Furino, C., Giancipoli, E., Alessio, G., Boscia, F., et al. (2017). Dexamethasone Implant with Fixed or Individualized Regimen in the Treatment of Diabetic Macular Oedema: Six-Month Outcomes of the UDBASA Study. *Acta Ophthalmol.* 95, e255–e260. doi:10.1111/aos.13395

Scaramuzzi, M., Querques, G., Spina, C. L., Lattanzio, R., and Bandello, F. (2015). Repeated Intravitreal Dexamethasone Implant (Ozurdex) for Diabetic Macular Edema. *Retina* 35, 1216–1222. doi:10.1097/IAE.0000000000000443

Shin, E. S., Sorenson, C. M., and Sheibani, N. (2014). Diabetes and Retinal Vascular Dysfunction. *J. Ophthalmic Vis. Res.* 9, 362–373. doi:10.4103/2008-322X.143378

Tamura, H., Miyamoto, K., Kiryu, J., Miyahara, S., Katsuta, H., Hirose, F., et al. (2005). Intravitreal Injection of Corticosteroid Attenuates Leukostasis and Vascular Leakage in Experimental Diabetic Retina. *Invest. Ophthalmol. Vis. Sci.* 46, 1440–1444. doi:10.1167/iovs.04-0905

Vinores, S. A. (2010). "Breakdown of the Blood–Retinal Barrier," in *Encyclopedia of the Eye*. Elsevier, 216222.

Wang, K., Wang, Y., Gao, L., Li, X., Li, M., and Guo, J. (2008). Dexamethasone Inhibits Leukocyte Accumulation and Vascular Permeability in Retina of Streptozotocin-Induced Diabetic Rats via Reducing Vascular Endothelial Growth Factor and Intercellular Adhesion Molecule-1 Expression. *Biol. Pharm. Bull.* 31, 1541–1546. doi:10.1248/bpb.31.1541

Wang, L. L., Sun, Y., Huang, K., and Zheng, L. (2013). Curcumin, a Potential Therapeutic Candidate for Retinal Diseases. *Mol. Nutr. Food Res.* 57, 1557–1568. doi:10.1002/mnfr.201200718

Yu, Y., Shen, Q., Lai, Y., Park, S. Y., Ou, X., Lin, D., et al. (2018). Anti-inflammatory Effects of Curcumin in Microglial Cells. *Front. Pharmacol.* 9, 386. doi:10.3389/fphar.2018.00386

Conflict of Interest: The authors declare that the research was conducted in the absence of any commercial or financial relationships that could be construed as a potential conflict of interest.

Publisher's Note: All claims expressed in this article are solely those of the authors and do not necessarily represent those of their affiliated organizations, or those of the publisher, the editors, and the reviewers. Any product that may be evaluated in this article, or claim that may be made by its manufacturer, is not guaranteed or endorsed by the publisher.

frontiers in Pharmacology

MINI REVIEW
published: 07 January 2022
doi: 10.3389/fphar.2021.811344

The Long Pentraxin PTX3 as a New Biomarker and Pharmacological Target in Age-Related Macular Degeneration and Diabetic Retinopathy

*Matteo Stravalaci[1], Mariantonia Ferrara[2], Varun Pathak[3], Francesca Davi[1], Barbara Bottazzi[1], Alberto Mantovani[1,4,5], Reinhold J. Medina[3], Mario R. Romano[2,4] and Antonio Inforzato[1,4]**

[1]IRCCS Humanitas Research Hospital, Rozzano, Italy, [2]Eye Center, Humanitas Gavazzeni-Castelli, Bergamo, Italy, [3]School of Medicine, Dentistry, and Biomedical Sciences, Wellcome-Wolfson Institute for Experimental Medicine, Queen's University Belfast, Belfast, United Kingdom, [4]Department of Biomedical Sciences, Humanitas University, Rozzano, Italy, [5]The William Harvey Research Institute, Queen Mary University of London, London, United Kingdom

OPEN ACCESS

Edited by:
Julie Sanderson,
University of East Anglia,
United Kingdom

Reviewed by:
Mario Damiano Toro,
Medical University of Lublin, Poland

***Correspondence:**
Antonio Inforzato
antonio.inforzato@
humanitasresearch.it

Specialty section:
This article was submitted to Inflammation Pharmacology, a section of the journal Frontiers in Pharmacology

Received: 08 November 2021
Accepted: 20 December 2021
Published: 07 January 2022

Citation:
Stravalaci M, Ferrara M, Pathak V, Davi F, Bottazzi B, Mantovani A, Medina RJ, Romano MR and Inforzato A (2022) The Long Pentraxin PTX3 as a New Biomarker and Pharmacological Target in Age-Related Macular Degeneration and Diabetic Retinopathy. Front. Pharmacol. 12:811344. doi: 10.3389/fphar.2021.811344

Age related macular degeneration (AMD) and diabetic retinopathy (DR) are multifactorial, neurodegenerative and inflammatory diseases of the eye primarily involving cellular and molecular components of the outer and inner blood-retina barriers (BRB), respectively. Largely contributed by genetic factors, particularly polymorphisms in complement genes, AMD is a paradigm of retinal immune dysregulation. DR, a major complication of diabetes mellitus, typically presents with increased vascular permeability and occlusion of the retinal vasculature that leads, in the proliferative form of the disease, to neovascularization, a pathogenic trait shared with advanced AMD. In spite of distinct etiology and clinical manifestations, both pathologies share common drivers, such as chronic inflammation, either of immune (in AMD) or metabolic (in DR) origin, which initiates and propagates degeneration of the neural retina, yet the underlying mechanisms are still unclear. As a soluble pattern recognition molecule with complement regulatory functions and a marker of vascular damage, long pentraxin 3 (PTX3) is emerging as a novel player in ocular homeostasis and a potential pharmacological target in neurodegenerative disorders of the retina. Physiologically present in the human eye and induced in inflammatory conditions, this protein is strategically positioned at the BRB interface, where it acts as a "molecular trap" for complement, and modulates inflammation both in homeostatic and pathological conditions. Here, we discuss current viewpoints on PTX3 and retinal diseases, with a focus on AMD and DR, the roles therein proposed for this pentraxin, and their implications for the development of new therapeutic strategies.

Keywords: age-related macular degeneration, diabetic retinopathy, complement, inflammation, PTX3

INTRODUCTION

Diabetic retinopathy (DR) and age-related macular degeneration (AMD) are leading causes of vision loss in working-age and elderly individuals, respectively, in developed countries (Cheung et al., 2010; Wong et al., 2014). In spite of distinctive clinical presentations and pathogenetic mechanisms, both diseases are multifactorial and neurodegenerative, and have in chronic inflammation a common driver. Cellular and molecular components of the outer blood-retinal barrier (oBRB) in AMD and inner BRB (iBRB) in DR are primarily involved in these pathologies. AMD manifests itself with accumulation of retinal pigment epithelium (RPE) abnormalities and drusen, extracellular deposits located between the RPE and Bruch's membrane (BrM) (Parmeggiani et al., 2013). On the other hand, DR is characterized by capillary occlusion, decreased retinal perfusion, microvascular destabilization, and increased vascular permeability, which collectively lead to retinal ischemia and vascular abnormalities (e.g., microaneurysms, retinal hemorrhages) (Semeraro et al., 2015). In both cases, a status of chronic and local inflammation sets in place that propels and sustains progression to advanced pathology. In this regard, exudative macular edema, neovascularization and hemorrhages, responsible for structural damage to the retina and fibrosis, are characteristic of DR and neovascular AMD (Govetto et al., 2020), whereas geographic atrophy, degeneration of the RPE and photoreceptors are typical processes of dry AMD (Parmeggiani et al., 2013). Interestingly, among the optical coherence tomography (OCT) biomarkers identified for these diseases (Ceravolo et al., 2020; Sitnilska et al., 2021), intraretinal hyperreflective foci in optical coherence tomography (OCT), representative of microglial activation and, thus, intraretinal inflammation, have been proposed as biomarkers of AMD and DR (Schreur et al., 2020; Sitnilska et al., 2021; Wu et al., 2021), indicating that local inflammatory reactions in the eye might have diagnostic potential (e.g., to monitor disease progression and/or response to therapy) in addition to play a direct role as pathogenetic mechanisms.

AMD is regarded as the paradigm of retinal immune dysregulation, in that local overactivation of the complement system (and the following inflammation) is a primary pathogenetic mechanism of AMD (Ambati et al., 2013; Clark and Bishop, 2018). In this regard, many factors contribute to the risk of disease, including age-related changes in structure/function of the RPE and BrM, oxidative stress, lifestyle, and, more importantly, genetics (Armento et al., 2021). Most of the polymorphisms associated with onset and progression of AMD map in or nearby genes of the complement system, particularly those of the alternative pathway (AP) (Fritsche et al., 2016). Of these, the Y402H polymorphism in the factor H gene (*CFH*) is the greatest (single) genetic risk factor of developing AMD (Hageman et al., 2005; Fritsche et al., 2016). This polymorphism affects the coding sequence of factor H (major soluble inhibitor of the AP) and its truncated form factor H-like protein 1 (FHL-1), and alters the binding of these proteins to sulfated glycosaminoglycans (GAGs) of the BrM (Clark et al., 2010). This extracellular matrix is devoid of any other inhibitor of the AP, therefore the restricted binding specificity of the pathological variant of factor H (and FHL-1) is believed to cause dysregulated complement activation (Clark and Bishop, 2018). This leads to generation of the anaphylatoxins C3a and C5a and the sub-lytic C5b-9 complexes, which induce the RPE to express inflammatory cytokines and growth factors (e.g., vascular endothelial growth factor, VEGF) (Lueck et al., 2011; Lueck et al., 2015). Complement fragments and RPE-derived factors cooperatively promote recruitment and activation of immune cells (Behnke et al., 2020; Ogura et al., 2020) that propagate the inflammatory reaction in the eye, eventually leading to damage and dysfunction of the oBRB (Natoli et al., 2017). In addition to inflammation, complement overactivation has been associated with impaired antioxidant potential and energy metabolism in the RPE cells (Sivapathasuntharam et al., 2019; Armento et al., 2020), and accumulation of retinal lipids in the drusen (Acar et al., 2020). Furthermore, age-related changes in the RPE and BrM, and smoking both contribute to complement activation, retinal inflammation and oxidative stress, pointing to a close interaction between diverse risk factors (Pietkiewicz et al., 2008; Wang et al., 2014; Woodell and Rohrer, 2014; Clark et al., 2017; Fields et al., 2017; Brown et al., 2019).

In DR, hyperglycemia promotes vascular dysfunction and neuroinflammation through multiple biochemical mechanisms, including activation of the polyol pathway, increased expression of cytokines and growth factors (e.g., tumor necrosis factor-alpha, TNF-α, pro-inflammatory interleukins, adiponectin, erythropoietin, VEGF, angiopoietin-2), oxidative stress, enhanced production of advanced glycation and lipoxidation end-products (AGE, ALE, respectively), hemodynamic changes, and leukostasis and oxidative stress (the latter also involved in AMD and other retinal pathologies) (Lorenzi, 2007; Costagliola et al., 2013; Semeraro et al., 2014; Semeraro et al., 2015; Khalaf et al., 2017; Toro et al., 2019; Kinuthia et al., 2020; Pietras-Baczewska et al., 2021). In particular, reactive oxygen species (ROS), AGE, ALE, and pro-inflammatory molecules collectively lead to activation of microglia, which is considered a major mechanism of neuroinflammation (Sharma et al., 2012; Semeraro et al., 2015; Subedi et al., 2020). Activated microglial cells in turn synthesize and release pro-inflammatory cytokines (e.g., TNF-α, IL-1β, and IL-6) and cytotoxic molecules (e.g., ROS and reactive nitrogen species, RNS) that propagate the local inflammatory response with endothelial damage, loss of pericytes, iBRB disruption, and vascular dysfunction (Scholz et al., 2015; Kinuthia et al., 2020). Neuroinflammation is further amplified by overactivation of the complement system and other glial cells, such as retinal astrocytes (Kinuthia et al., 2020; Shahulhameed et al., 2020). Moreover, breakdown of the iBRB favors the transfer of circulating pro-inflammatory factors, including chemokines, cytokines, and immune cells, into the inner retina which further promotes local immune dysregulation and retinal neurovascular damage, thus leading to DR progression (Kinuthia et al., 2020).

AMD and DR share cellular and molecular components of major inflammatory pathways, including the long pentraxin 3 (PTX3), long-known as a key mediator of vascular (Presta et al.,

TABLE 1 | Studies describing expression and localization of PTX3 in AMD and DR.

References	Source	Treatment	Localization	Main findings
An et al. (2008), Woo et al. (2013), Juel et al. (2015), Stravalaci et al. (2020)	ARPE-19 cell line	TNF-α[a] IL-1β	secreted	PTX3 was overexpressed by ARPE-19 cells in inflammatory conditions, and the released protein had complement-inhibiting properties
Yamada et al. (2008), Wang et al. (2016)	ARPE-19 cell line	ox-LDL 4-HNE	secreted	PTX3 expression was induced by oxidative stress
Hwang et al. (2019)	ARPE-19 cell line primary H-RPE cells	$NaIO_3$	secreted	PTX3 expression was correlated with cell death caused by oxidative stress
Wang et al. (2016)	Mouse retina	4-HNE	RPE/inner BrM	In a mouse model of AMD, PTX3 was found to co-localize with factor H and control complement activation
Yamada et al. (2008)	Human retina	—	BrM/ choriocapillaris	PTX3 immunohistochemical staining was documented in tissues obtained from AMD donors
Swinkels et al. (2018)	Human retina	—	BrM/ choriocapillaris	PTX3 immunofluorescence staining was reported in tissues obtained both from AMD and non-AMD subjects, suggesting a role in retina homeostasis
Stravalaci et al. (2020)	Human vitreous	—	secreted	PTX3 was detected and quantitated in the humor vitreous of AMD and non-AMD donors, suggesting that other cell types of the retina (in addition to the RPE) can make the protein
Yang et al. (2014), Zhou and Hu. (2016), Erdenen et al. (2018), Elbana et al. (2019)	Human plasma/ serum	—	circulating	Plasma/serum PTX3 levels were associated with DR
Chodkowski et al. (2018), Hokazono et al. (2018), Güngel et al. (2021)	Human plasma	—	circulating	No differences were found in the plasma levels of PTX3 measured in DR patients and diabetics without retinopathy
Mutlu et al. (2017)	Aqueous humor	—	secreted	PTX3 levels in the aqueous humor were associated with DR

[a]*TNF-α, tumor necrosis factor-α; IL-1β, interleukin-1β; ox-LDL, oxidized low-density lipoprotein; 4-HNE, 4-Hydroxynonenal; $NaIO_3$, sodium iodate.*

2018; Ristagno et al., 2019) and complement-dependent (Doni et al., 2019; Haapasalo and Meri, 2019) inflammation, and recently emerging as a novel player in retinal neurodegeneration (Wang et al., 2016; Stravalaci et al., 2020). Here, we revisit available clinical and preclinical evidence on the role(s) of PTX3 in AMD and DR, with major regard to current hypotheses on the involvement of this pentraxin in their pathogenesis, and its potential as a diagnostic/prognostic biomarker (see **Table 1**).

STRUCTURE/FUNCTION OF THE LONG PENTRAXIN PTX3

Originally cloned in the early 1990s, PTX3 is the prototype of long pentraxins, which, along with the short pentraxins C reactive protein (CRP) and Serum Amyloid P component (SAP), make up a superfamily of evolutionary conserved proteins with distinctive structures and functions [reviewed in (Daigo et al., 2016)]. As opposed to CRP and SAP, whose synthesis is primarily induced in the liver by IL-6, PTX3 is expressed by a number of immune and non-immune cells (including RPE, endothelial and myeloid cells) at sites of inflammation and infection upon stimulation with inflammatory cytokines, microbial moieties, and intact microorganisms (Doni et al., 2019). Of relevance to AMD and DR, oxidative conditions [e.g., oxidized low density lipoproteins, ox-LDL (Norata et al., 2008; Yamada et al., 2008)], in addition to inflammatory cytokines (Breviario et al., 1992; An et al., 2008; Woo et al., 2013; Juel et al., 2015; Stravalaci et al., 2020), induce the synthesis of PTX3 both in RPE and endothelial cells (see below). Furthermore, expression of the human protein is controlled both in physiological and pathological conditions by epigenetic mechanisms (Rubino et al., 2017) and genetic polymorphisms (Garlanda et al., 2018).

Like other long pentraxins, the human PTX3 protomer is a multidomain glycoprotein (Inforzato et al., 2006) with a C-terminal pentraxin domain and an N-terminal region that fold into homo-octamers stabilized by noncovalent (coiled coils) and covalent (disulfide bonds) interactions (Inforzato et al., 2008; Inforzato et al., 2010). This structural organization mediates the protein's interactions with a broad spectrum of ligands, which results into diverse functions in innate immunity (Porte et al., 2019), inflammation (Bottazzi et al., 2016), vascular biology (Presta et al., 2018; Ristagno et al., 2019) and tissue remodeling (Doni et al., 2016). In particular, PTX3 is a ligand of key complement activators [i.e., C1q (Nauta et al., 2003; Bally et al., 2019), ficolin-1 (Ma et al., 2013), ficolin-2 (Ma et al., 2009), mannose binding lectin, MBL (Ma et al., 2011), and C3b (Stravalaci et al., 2020)] and inhibitors [i.e., factor H (Deban et al., 2008), and C4 binding protein, C4BP (Braunschweig and Józsi, 2011)], and therefore modulates all three complement pathways. Also, PTX3 regulates the extravasation of leukocytes at sites of inflammation *via* its interaction with P-selectin, thus controlling the inflammatory response *via* complement-independent mechanisms (Deban et al., 2010). Interestingly, PTX3 binds selected fibroblast growth factors (FGFs), including FGF2 and FGF8b, and inhibits FGF-dependent angiogenic responses (Rusnati et al., 2004; Camozzi et al., 2006). Finally, this pentraxin is a key component of the hyaluronic acid-rich extracellular matrix (ECM) that forms in inflammatory and inflammation-like conditions (Scarchilli et al., 2007; Baranova et al., 2014). These properties, particularly the engagement of factor H and FGF2, might be relevant in the pathogenesis of AMD and DR, as discussed below.

PTX3 AS AN ENDOGENOUS RHEOSTAT OF COMPLEMENT ACTIVATION IN AMD

Initial evidence of an involvement of PTX3 in the pathogenesis of AMD dates back to 2008, when Yamada et al. documented the presence of this protein in the macula of an 81-year-old male with early AMD by means of immunohistochemistry on post-mortem human eye specimens (Yamada et al., 2008). Using fluorescence microscopy techniques, we have afterward recapitulated these findings in an independent cohorts of AMD donors, and demonstrated that PTX3 is expressed in the eye of non-AMD donors too, where it localizes at the interface between the RPE and choroid, particularly in the intercapillary septa of the choriocapillaris (Swinkels et al., 2018). Also, we found the protein in the humor vitreous of both AMD and non-AMD donors (Stravalaci et al., 2020), suggesting that PTX3 is constitutively expressed in the human eye, where it might contribute to tissue homeostasis both in physiological and pathological conditions. Current literature indicates that PTX3 is locally made by the RPE in the presence of pro-inflammatory cytokines, such as TNF-α or IL-1β (An et al., 2008; Woo et al., 2013; Juel et al., 2015; Stravalaci et al., 2020), peroxidized lipids (i.e., 4-hydroxinonenanl, 4-HNE) (Wang et al., 2016), and ox-LDL (Hwang et al., 2019). Based on the notion that human leukocytes express PTX3 (Doni et al., 2019), it is plausible that eye-resident phagocytes (in addition to the RPE) might make the protein, including retinal microglia and Müller cells. Regardless of the cellular sources of PTX3 in the eye, this organ marginally contributes to the protein's plasmatic pool, which therefore cannot predict the AMD status (Juel et al., 2015). Conceivably, it is the locally made protein (i.e., in the posterior segment of the eye) that contributes to AMD pathogenesis. So far, no large study has been conducted to assess associations between the ocular levels of PTX3 and AMD, however, in small cohorts of donors; trends of increasing protein concentration in the vitreous (Stravalaci et al., 2020) and staining intensity in the choriocapillaris (Swinkels et al., 2018) have been documented in AMD subjects. Also, it is interesting to notice that transcription of the *PTX3* gene in the human RPE/choroid region increases with age, although in an AMD-independent fashion (Juel et al., 2015).

The role of PTX3 in AMD has been investigated in diverse experimental settings. Hwang et al. reported that in the presence of sodium iodate (that induces oxidative stress), primary human H-RPE and ARPE-19 cells cultured *in vitro* increased PTX3 expression, and the newly synthesized protein impaired the transcription of antioxidant enzymes, while inducing that of AMD-associated genes (Hwang et al., 2019). These findings might suggest that PTX3 contributes to AMD development by accelerating RPE cell death, however a non-physiological chemical stimulus (i.e., sodium iodate) was used throughout the study, and the applied experimental setting did not consider the effect of PTX3 on activation of the complement system [a primary pathogenetic mechanism of AMD (Clark and Bishop, 2018)]. In this regard, PTX3 is a well-known ligand of complement factor H (CFH) (Deban et al., 2008), and genetic variations in the *CFH* gene, particularly the Y402H polymorphism in the complement control protein (CCP) module seven of the protein, are strongly associated with the risk of developing AMD, as anticipated above (Parente et al., 2017). PTX3 binds factor H at CCP7 and CCPs19-20, *via* its C- and N-terminal domains, respectively (Deban et al., 2008). Therefore, assembly and control of the factor H/PTX3 complex might be of functional relevance in retinal physiology and pathology. In this regard, in an animal model of AMD, genetic deficiency of PTX3 amplified complement activation induced by 4-HNE (a product of lipid peroxidation found in the AMD eye), with increased C3a levels and inflammasome activation, leading to IL-1β production by the RPE, and enhanced accumulation of macrophages in the choroid (Wang et al., 2016). These findings indicate that PTX3 mediates retinal homeostasis *in vivo*, especially in inflammatory conditions, whereby it promotes the recruitment of factor H and tames complement overactivation. Consistent with this view, PTX3 has been shown to co-localize with factor H in the murine inner BrM and RPE, where it controls factor H distribution and protects the RPE from complement dysregulation and inflammasome activation (Wang et al., 2016).

We have recently reported that PTX3 binds RPE cells in physiological conditions *in vitro*, however this interaction is impaired when these cells are stimulated with IL-1β and, to a lesser extent, TNF-α (to mimic the inflammatory microenvironment of AMD) (Stravalaci et al., 2020). Therefore, PTX3 cannot restrain complement on the RPE surface during inflammation, when expression of the AP-activating genes (*C3* and factor B, *FB*, but not *CFH*) is upregulated (Stravalaci et al., 2020). However, we have demonstrated that PTX3 recruits both factor H and C3b onto non-cellular surfaces (simulating the basement membrane of RPE and choroid, and the BrM), where it forms a stable ternary complex that acts as a "molecular brake" for complement activation (Stravalaci et al., 2020). This mechanism is likely relevant in the presence of the AMD-associated 402H variant of factor H, which has a more restricted specificity for sulfated GAGs compared to 402Y, and likely has decreased ability to control complement activation at ECM sites, such as the BrM (Clark and Bishop, 2018). Also, we have reported that PTX3 interacts with FHL-1 (in addition to factor H), and the Y402H polymorphism (that is retained in FHL-1) affects the binding of FHL-1 (but not factor H) to PTX3 (Swinkels et al., 2018). Immunolocalization studies indicate that FHL-1 is the major complement inhibitor in the BrM and intercapillary septa of the choriocapillaris, and passively diffuses through the BrM, whereas factor H cannot (Clark et al., 2014). Therefore, PTX3 might act as an ECM anchoring site for FHL-1 (in addition to factor H), and a "hot spot" for complement inhibition in the eye. Furthermore, the interaction of PTX3 with factor H has been proposed to promote complement-mediated phagocytosis [including

clearance of apoptotic debris (Deban et al., 2008)], suggesting that this long pentraxin might take part in the RPE-dependent turnover of photoreceptor outer segments (POS), a fundamental process of retinal physiology (Kwon and Freeman, 2020). Overall, available *in vitro* and *in vivo* evidence points to a protective (rather than pathological) role of PTX3 in response to complement dysregulation in AMD.

EMERGING ROLES OF PTX3 IN DR

Diabetes is underpinned by sterile, chronic, low-grade inflammation characterized by mildly elevated circulating levels of IL-1β (Donath and Shoelson, 2011). In line with this view, anti-inflammatory drugs, such as interleukin one receptor antagonist (Larsen et al., 2007), anti-IL-1β antibody (Cavelti-Weder et al., 2012), and salsalate (Goldfine et al., 2013) have been shown to lower hyperglycemia in type 2 diabetes patients. Most diabetic complications, including retinal diseases, are associated with endotheliopathy (endothelial dysfunction), which points to inflammatory vascular pathology as a major point of attention in the clinical management of diabetes (Rask-Madsen and King, 2013). Interestingly, PTX3 is produced by endothelial cells during inflammation (Breviario et al., 1992), and has been consistently proposed as a biomarker of vascular inflammation (Ristagno et al., 2019). This has prompted investigations into the role of PTX3 as a marker of disease in DR, with conflicting outcomes. In fact, higher PTX3 levels have been documented in the plasma (or serum) of DR patients, compared to that of diabetics with no retinopathy or non-diabetic volunteers (Yang et al., 2014; Zhou and Hu, 2016; Erdenen et al., 2018; Elbana et al., 2019), however these findings have not been recapitulated in other studies (Chodkowski et al., 2018; Hokazono et al., 2018; Güngel et al., 2021). Such lack of consistency is likely due to high variability in the plasmatic concentration of PTX3 in diabetic patients, as a reflection of varying extents of hyperglycemia-dependent damage to tissues and vascular beds. This makes it problematic to detect differences across small cohorts of patients (like those investigated so far). We propose that PTX3 is involved in the local rather than systemic inflammatory reaction to hyperglycemia. Our view is supported by a study reporting higher levels of the protein in the aqueous humor of patients with DR than in that of diabetics with no retinopathy or non-diabetic volunteers (Mutlu et al., 2017). This suggests that the diabetic damage to the retinal endothelium is perhaps more evident in adjacent tissues (like the vitreous) than is in the blood, where any PTX3 contribution from the retinal tissue is likely to be highly diluted. In line with this, no correlation has been found between serum hemoglobin A1c (HbA1c) and vitreous PTX3 levels (Mutlu et al., 2017).

PTX3 is produced by myeloid and endothelial cells in response to inflammatory stimuli, including TNF-α or IL-1β (Doni et al., 2019). The inner retina is a complex tissue that comprises various cells able to synthesize and release PTX3, and the diabetic microenvironment provides relevant pro-inflammatory triggers. DR is associated with endothelial dysfunction, microglia activation, and neurodegeneration (Stitt et al., 2016). In this context, microglia, endothelial cells, and neural cells are tissue-resident candidate producers of PTX3 within the retina. Retinal endothelial cells are particularly sensitive to damage by hyperglycemia. Indeed, early glycemia control is a primary therapeutic goal to avoid the development of DR complications (Yau et al., 2012). Poor control of glycemia and longer duration of diabetes are associated with loss of pericytes, thickening of the basement membrane, and pathological neovascularization in the vitreoretinal interphase, leading to proliferative DR. Since PTX3 binds to FGF2 (Camozzi et al., 2006), and inhibits its proangiogenic functions (Rusnati et al., 2004; Presta et al., 2018), there is potential for this pentraxin to provide an alternative to current anti-VEGF therapies for treatment of DR (and wet AMD), especially in non-responsive cases. Although inhibition of pathological preretinal neovascularization is the goal in the clinical management of advanced proliferative DR, it is important to underscore that in early-stage DR, intraretinal reparative angiogenesis is a desired biological outcome (Sapieha, 2012). Therefore, PTX3-dependent inhibition of angiogenesis (e.g., *via* binding and sequestration of FGF2) in the ischemic DR may drive disease progression (rather than regression) to proliferative retinopathy.

As outlined above, inflammation plays a major role in DR. In this regard, microglia are resident cells of the retina that modulate tissue inflammation. In physiological conditions, retinal microglia patrol the inner retina and maintain tissue homeostasis. However, in conditions of prolonged hyperglycemia and hypoxic stress, an activated microglial status is induced that promotes inflammation, including complement activation, and disease progression (Fumagalli et al., 2015). In this context, PTX3 might exert complement-modulating in addition to angiogenesis-inhibiting properties, with a more complex role in DR-associated retinal inflammation.

CONCLUDING REMARKS

Clinical and pre-clinical evidence corroborates the inflammatory nature of AMD (Parmeggiani et al., 2013) and DR (Semeraro et al., 2019), and new molecules and processes are proposed that take part in their pathogenesis (Forrester et al., 2020). The inflammatory mediator PTX3 is emerging as a novel player in neurodegenerative disorders of the retina (summarized in **Table 1**). Endowed with modulatory properties towards complement (Haapasalo and Meri, 2019) and angiogenesis (Presta et al., 2018), this pentraxin is ideally positioned at the interface between immune and metabolic inflammation. In this regard, *in vivo* and *in vitro* data suggest that PTX3 acts as an endogenous inhibitor of complement overactivation and

neovascularization in the human eye, thus holding promise as a pharmacological target for the treatment of AMD (Wang et al., 2016; Stravalaci et al., 2020). Available information points to this pentraxin as a biomarker and, possibly, a pathogenetic player of DR too, however more research is needed to address these hypotheses, with major regard to animal modelling of the disease and clinical investigations. Human data, in particular, are fragmented, likely due to small size of the studies so far conducted. Larger cohorts of patients are needed to overcome this limitation that integrate biochemical (e.g., protein concentration) and genetic (e.g., polymorphisms) information, perhaps accounting for epistatic interactions between this pentraxin and other pathogenetic drivers of DR (and AMD), including FGFs (and complement proteins).

AUTHOR CONTRIBUTIONS

MS wrote the "PTX3 as an endogenous rheostat of complement activation in AMD" chapter. FD prepared the table. VP and RJM wrote the "Emerging roles of PTX3 in DR" chapter. MF and MRR wrote the "Introduction" chapter. AI wrote the Abstract and the "Structure/function of the long pentraxin PTX3" and "Concluding remarks" chapters, conceptualized, outlined, and revised the manuscript. BB and AM contributed to critical revision of the manuscript. All authors contributed to manuscript revision, read, and approved the submitted version.

FUNDING

The article's publication fees are funded by Fondazione Beppe and Nuccy Angiolini. MRR is recipient of a Prize Project for Scientific Research from the Italian Society of Ophthalmology (SOI) that funded a technician (FD) and the most recent work on PTX3 and AMD (Stravalaci et al., 2020). The financial support of Fondazione Beppe and Nuccy Angiolini to AI is greatly acknowledged. VP is recipient of a Research Fellowship from the Wellcome Trust Institutional Strategic Support Fund QUB-ISSF-204835/Z/16/Z. RJM is funded by Diabetes UK 20/0006162, the Dunhill Medical Trust RPFG 1910/199, MRC MR/S036695/, and BBSRC BB/T000805/1.

REFERENCES

Acar, İ. E., Lores-Motta, L., Colijn, J. M., Meester-Smoor, M. A., Verzijden, T., Cougnard-Gregoire, A., et al. (2020). Integrating Metabolomics, Genomics, and Disease Pathways in Age-Related Macular Degeneration: The EYE-RISK Consortium. *Ophthalmology* 127 (12), 1693–1709. doi:10.1016/j.ophtha.2020.06.020

Ambati, J., Atkinson, J. P., and Gelfand, B. D. (2013). Immunology of Age-Related Macular Degeneration. *Nat. Rev. Immunol.* 13 (6), 438–451. doi:10.1038/nri3459

An, E., Gordish-Dressman, H., and Hathout, Y. (2008). Effect of TNF-Alpha on Human ARPE-19-Secreted Proteins. *Mol. Vis.* 14, 2292–2303.

Armento, A., Honisch, S., Panagiotakopoulou, V., Sonntag, I., Jacob, A., Bolz, S., et al. (2020). Loss of Complement Factor H Impairs Antioxidant Capacity and Energy Metabolism of Human RPE Cells. *Sci. Rep.* 10 (1), 10320. doi:10.1038/s41598-020-67292-z

Armento, A., Ueffing, M., and Clark, S. J. (2021). The Complement System in Age-Related Macular Degeneration. *Cell Mol Life Sci* 78 (10), 4487–4505. doi:10.1007/s00018-021-03796-9

Bally, I., Inforzato, A., Dalonneau, F., Stravalaci, M., Bottazzi, B., Gaboriaud, C., et al. (2019). Interaction of C1q with Pentraxin 3 and IgM Revisited: Mutational Studies with Recombinant C1q Variants. *Front. Immunol.* 10, 461. doi:10.3389/fimmu.2019.00461

Baranova, N. S., Inforzato, A., Briggs, D. C., Tilakaratna, V., Enghild, J. J., Thakar, D., et al. (2014). Incorporation of Pentraxin 3 into Hyaluronan Matrices Is Tightly Regulated and Promotes Matrix Cross-Linking. *J. Biol. Chem.* 289 (44), 30481–30498. doi:10.1074/jbc.M114.568154

Behnke, V., Wolf, A., and Langmann, T. (2020). The Role of Lymphocytes and Phagocytes in Age-Related Macular Degeneration (AMD). *Cel Mol Life Sci* 77 (5), 781–788. doi:10.1007/s00018-019-03419-4

Bottazzi, B., Inforzato, A., Messa, M., Barbagallo, M., Magrini, E., Garlanda, C., et al. (2016). The Pentraxins PTX3 and SAP in Innate Immunity, Regulation of Inflammation and Tissue Remodelling. *J. Hepatol.* 64 (6), 1416–1427. doi:10.1016/j.jhep.2016.02.029

Braunschweig, A., and Józsi, M. (2011). Human Pentraxin 3 Binds to the Complement Regulator C4b-Binding Protein. *PLoS One* 6 (8), e23991. doi:10.1371/journal.pone.0023991

Breviario, F., d'Aniello, E. M., Golay, J., Peri, G., Bottazzi, B., Bairoch, A., et al. (1992). Interleukin-1-inducible Genes in Endothelial Cells. Cloning of a New Gene Related to C-Reactive Protein and Serum Amyloid P Component. *J. Biol. Chem.* 267 (31), 22190–22197. doi:10.1016/s0021-9258(18)41653-5

Brown, E. E., DeWeerd, A. J., Ildefonso, C. J., Lewin, A. S., and Ash, J. D. (2019). Mitochondrial Oxidative Stress in the Retinal Pigment Epithelium (RPE) Led to Metabolic Dysfunction in Both the RPE and Retinal Photoreceptors. *Redox Biol.* 24, 101201. doi:10.1016/j.redox.2019.101201

Camozzi, M., Rusnati, M., Bugatti, A., Bottazzi, B., Mantovani, A., Bastone, A., et al. (2006). Identification of an Antiangiogenic FGF2-Binding Site in the N Terminus of the Soluble Pattern Recognition Receptor PTX3. *J. Biol. Chem.* 281 (32), 22605–22613. doi:10.1074/jbc.M601023200

Cavelti-Weder, C., Babians-Brunner, A., Keller, C., Stahel, M. A., Kurz-Levin, M., Zayed, H., et al. (2012). Effects of Gevokizumab on Glycemia and Inflammatory Markers in Type 2 Diabetes. *Diabetes Care* 35 (8), 1654–1662. doi:10.2337/dc11-2219

Ceravolo, I., Oliverio, G. W., Alibrandi, A., Bhatti, A., Trombetta, L., Rejdak, R., et al. (2020). The Application of Structural Retinal Biomarkers to Evaluate the Effect of Intravitreal Ranibizumab and Dexamethasone Intravitreal Implant on Treatment of Diabetic Macular Edema. *Diagnostics (Basel)* 10 (6), 413. doi:10.3390/diagnostics10060413

Cheung, N., Mitchell, P., and Wong, T. Y. (2010). Diabetic Retinopathy. *Lancet* 376 (9735), 124–136. doi:10.1016/S0140-6736(09)62124-3

Chodkowski, A., Nabrdalik, K., Kwiendacz, H., Tomasik, A., Bartman, W., and Gumprecht, J. (2018). Pentraxin 3 and Retinopathy Among Type 2 Diabetic Patients in Relation to Carotid Atherosclerosis and Systolic and Diastolic Cardiac Function - a Pilot Study. *Clin. Diabetol.* 7 (4), 196–202. doi:10.5603/dk.2018.0016

Clark, S. J., Bishop, P. N., and Day, A. J. (2010). Complement Factor H and Age-Related Macular Degeneration: the Role of Glycosaminoglycan Recognition in Disease Pathology. *Biochem. Soc. Trans.* 38 (5), 1342–1348. doi:10.1042/BST0381342

Clark, S. J., and Bishop, P. N. (2018). The Eye as a Complement Dysregulation Hotspot. *Semin. Immunopathol* 40 (1), 65–74. doi:10.1007/s00281-017-0649-6

Clark, S. J., McHarg, S., Tilakaratna, V., Brace, N., and Bishop, P. N. (2017). Bruch's Membrane Compartmentalizes Complement Regulation in the Eye with Implications for Therapeutic Design in Age-Related Macular Degeneration. *Front. Immunol.* 8, 1778. doi:10.3389/fimmu.2017.01778

Clark, S. J., Schmidt, C. Q., White, A. M., Hakobyan, S., Morgan, B. P., and Bishop, P. N. (2014). Identification of Factor H-like Protein 1 as the Predominant Complement Regulator in Bruch's Membrane: Implications for Age-Related

Macular Degeneration. *J. Immunol.* 193 (10), 4962–4970. doi:10.4049/jimmunol.1401613

Costagliola, C., Daniele, A., dell'Omo, R., Romano, M. R., Aceto, F., Agnifili, L., et al. (2013). Aqueous Humor Levels of Vascular Endothelial Growth Factor and Adiponectin in Patients with Type 2 Diabetes before and after Intravitreal Bevacizumab Injection. *Exp. Eye Res.* 110, 50–54. doi:10.1016/j.exer.2013.02.004

Daigo, K., Inforzato, A., Barajon, I., Garlanda, C., Bottazzi, B., Meri, S., et al. (2016). Pentraxins in the Activation and Regulation of Innate Immunity. *Immunol. Rev.* 274 (1), 202–217. doi:10.1111/imr.12476

Deban, L., Jarva, H., Lehtinen, M. J., Bottazzi, B., Bastone, A., Doni, A., et al. (2008). Binding of the Long Pentraxin PTX3 to Factor H: Interacting Domains and Function in the Regulation of Complement Activation. *J. Immunol.* 181 (12), 8433–8440. doi:10.4049/jimmunol.181.12.8433

Deban, L., Russo, R. C., Sironi, M., Moalli, F., Scanziani, M., Zambelli, V., et al. (2010). Regulation of Leukocyte Recruitment by the Long Pentraxin PTX3. *Nat. Immunol.* 11 (4), 328–334. doi:10.1038/ni.1854

Donath, M. Y., and Shoelson, S. E. (2011). Type 2 Diabetes as an Inflammatory Disease. *Nat. Rev. Immunol.* 11 (2), 98–107. doi:10.1038/nri2925

Doni, A., D'Amico, G., Morone, D., Mantovani, A., and Garlanda, C. (2016). Humoral Innate Immunity at the Crossroad between Microbe and Matrix Recognition: The Role of PTX3 in Tissue Damage. *Semin. Cel Dev Biol* 61, 31–40. doi:10.1016/j.semcdb.2016.07.026

Doni, A., Stravalaci, M., Inforzato, A., Magrini, E., Mantovani, A., Garlanda, C., et al. (2019). The Long Pentraxin PTX3 as a Link between Innate Immunity, Tissue Remodeling, and Cancer. *Front. Immunol.* 10, 712. doi:10.3389/fimmu.2019.00712

Elbana, K. A., Salem, H. M., Abdel Fattah, N. R., and Etman, E. (2019). Serum Pentraxin 3 Level as a Recent Biomarker of Diabetic Retinopathy in Egyptian Patients with Diabetes. *Diabetes Metab. Syndr.* 13 (4), 2361–2364. doi:10.1016/j.dsx.2019.06.007

Erdenen, F., Güngel, H., Altunoğlu, E., Şak, D., Müderrisoğlu, C., Koro, A., et al. (2018). Association of Plasma Pentraxin-3 Levels with Retinopathy and Systemic Factors in Diabetic Patients. *Metab. Syndr. Relat. Disord.* 16 (7), 358–365. doi:10.1089/met.2018.0023

Fields, M. A., Bowrey, H. E., Gong, J., Moreira, E. F., Cai, H., and Del Priore, L. V. (2017). Extracellular Matrix Nitration Alters Growth Factor Release and Activates Bioactive Complement in Human Retinal Pigment Epithelial Cells. *PLoS One* 12 (5), e0177763. doi:10.1371/journal.pone.0177763

Forrester, J. V., Kuffova, L., and Delibegovic, M. (2020). The Role of Inflammation in Diabetic Retinopathy. *Front. Immunol.* 11, 583687. doi:10.3389/fimmu.2020.583687

Fritsche, L. G., Igl, W., Bailey, J. N., Grassmann, F., Sengupta, S., Bragg-Gresham, J. L., et al. (2016). A Large Genome-wide Association Study of Age-Related Macular Degeneration Highlights Contributions of Rare and Common Variants. *Nat. Genet.* 48 (2), 134–143. doi:10.1038/ng.3448

Fumagalli, S., Perego, C., Pischiutta, F., Zanier, E. R., and De Simoni, M. G. (2015). The Ischemic Environment Drives Microglia and Macrophage Function. *Front. Neurol.* 6, 81. doi:10.3389/fneur.2015.00081

Garlanda, C., Bottazzi, B., Magrini, E., Inforzato, A., and Mantovani, A. (2018). Ptx3, a Humoral Pattern Recognition Molecule, in Innate Immunity, Tissue Repair, and Cancer. *Physiol. Rev.* 98 (2), 623–639. doi:10.1152/physrev.00016.2017

Goldfine, A. B., Fonseca, V., Jablonski, K. A., Chen, Y. D., Tipton, L., Staten, M. A., et al. (2013). Salicylate (Salsalate) in Patients with Type 2 Diabetes: a Randomized Trial. *Ann. Intern. Med.* 159 (1), 1–12. doi:10.7326/0003-4819-159-1-201307020-00003

Govetto, A., Sarraf, D., Hubschman, J. P., Tadayoni, R., Couturier, A., Chehaibou, I., et al. (2020). Distinctive Mechanisms and Patterns of Exudative versus Tractional Intraretinal Cystoid Spaces as Seen with Multimodal Imaging. *Am. J. Ophthalmol.* 212, 43–56. doi:10.1016/j.ajo.2019.12.010

Güngel, H., Erdenen, F., Pasaoglu, I., Sak, D., Ogreden, T., and Kilic Muftuoglu, I. (2021). New Insights into Diabetic and Vision-Threatening Retinopathy: Importance of Plasma Long Pentraxine 3 and Taurine Levels. *Curr. Eye Res.* 46 (6), 818–823. doi:10.1080/02713683.2020.1836228

Haapasalo, K., and Meri, S. (2019). Regulation of the Complement System by Pentraxins. *Front. Immunol.* 10, 1750. doi:10.3389/fimmu.2019.01750

Hageman, G. S., Anderson, D. H., Johnson, L. V., Hancox, L. S., Taiber, A. J., Hardisty, L. I., et al. (2005). A Common Haplotype in the Complement Regulatory Gene Factor H (HF1/CFH) Predisposes Individuals to Age-Related Macular Degeneration. *Proc. Natl. Acad. Sci. U S A.* 102 (20), 7227–7232. doi:10.1073/pnas.0501536102

Hokazono, K., Belizário, F. S., Portugal, V., Messias-Reason, I., and Nisihara, R. (2018). Mannose Binding Lectin and Pentraxin 3 in Patients with Diabetic Retinopathy. *Arch. Med. Res.* 49 (2), 123–129. doi:10.1016/j.arcmed.2018.06.003

Hwang, N., Kwon, M. Y., Woo, J. M., and Chung, S. W. (2019). Oxidative Stress-Induced Pentraxin 3 Expression Human Retinal Pigment Epithelial Cells Is Involved in the Pathogenesis of Age-Related Macular Degeneration. *Int. J. Mol. Sci.* 20 (23), 6028. doi:10.3390/ijms20236028

Inforzato, A., Baldock, C., Jowitt, T. A., Holmes, D. F., Lindstedt, R., Marcellini, M., et al. (2010). The Angiogenic Inhibitor Long Pentraxin PTX3 Forms an Asymmetric Octamer with Two Binding Sites for FGF2. *J. Biol. Chem.* 285 (23), 17681–17692. doi:10.1074/jbc.M109.085639

Inforzato, A., Peri, G., Doni, A., Garlanda, C., Mantovani, A., Bastone, A., et al. (2006). Structure and Function of the Long Pentraxin PTX3 Glycosidic Moiety: fine-tuning of the Interaction with C1q and Complement Activation. *Biochemistry* 45 (38), 11540–11551. doi:10.1021/bi0607453

Inforzato, A., Rivieccio, V., Morreale, A. P., Bastone, A., Salustri, A., Scarchilli, L., et al. (2008). Structural Characterization of PTX3 Disulfide Bond Network and its Multimeric Status in Cumulus Matrix Organization. *J. Biol. Chem.* 283 (15), 10147–10161. doi:10.1074/jbc.M708535200

Juel, H. B., Faber, C., Munthe-Fog, L., Bastrup-Birk, S., Reese-Petersen, A. L., Falk, M. K., et al. (2015). Systemic and Ocular Long Pentraxin 3 in Patients with Age-Related Macular Degeneration. *PLoS One* 10 (7), e0132800. doi:10.1371/journal.pone.0132800

Khalaf, N., Helmy, H., Labib, H., Fahmy, I., El Hamid, M. A., and Moemen, L. (2017). Role of Angiopoietins and Tie-2 in Diabetic Retinopathy. *Electron. Physician* 9 (8), 5031–5035. doi:10.19082/5031

Kinuthia, U. M., Wolf, A., and Langmann, T. (2020). Microglia and Inflammatory Responses in Diabetic Retinopathy. *Front. Immunol.* 11, 564077. doi:10.3389/fimmu.2020.564077

Kwon, W., and Freeman, S. A. (2020). Phagocytosis by the Retinal Pigment Epithelium: Recognition, Resolution, Recycling. *Front. Immunol.* 11, 604205. doi:10.3389/fimmu.2020.604205

Larsen, C. M., Faulenbach, M., Vaag, A., Vølund, A., Ehses, J. A., Seifert, B., et al. (2007). Interleukin-1-receptor Antagonist in Type 2 Diabetes Mellitus. *N. Engl. J. Med.* 356 (15), 1517–1526. doi:10.1056/NEJMoa065213

Lorenzi, M. (2007). The Polyol Pathway as a Mechanism for Diabetic Retinopathy: Attractive, Elusive, and Resilient. *Exp. Diabetes Res.* 2007, 61038. doi:10.1155/2007/61038

Lueck, K., Busch, M., Moss, S. E., Greenwood, J., Kasper, M., Lommatzsch, A., et al. (2015). Complement Stimulates Retinal Pigment Epithelial Cells to Undergo Pro-inflammatory Changes. *Ophthalmic Res.* 54 (4), 195–203. doi:10.1159/000439596

Lueck, K., Wasmuth, S., Williams, J., Hughes, T. R., Morgan, B. P., Lommatzsch, A., et al. (2011). Sub-lytic C5b-9 Induces Functional Changes in Retinal Pigment Epithelial Cells Consistent with Age-Related Macular Degeneration. *Eye (Lond)* 25 (8), 1074–1082. doi:10.1038/eye.2011.109

Ma, Y. J., Doni, A., Hummelshøj, T., Honoré, C., Bastone, A., Mantovani, A., et al. (2009). Synergy between Ficolin-2 and Pentraxin 3 Boosts Innate Immune Recognition and Complement Deposition. *J. Biol. Chem.* 284 (41), 28263–28275. doi:10.1074/jbc.M109.009225

Ma, Y. J., Doni, A., Romani, L., Jürgensen, H. J., Behrendt, N., Mantovani, A., et al. (2013). Ficolin-1-PTX3 Complex Formation Promotes Clearance of Altered Self-Cells and Modulates IL-8 Production. *J. Immunol.* 191 (3), 1324–1333. doi:10.4049/jimmunol.1300382

Ma, Y. J., Doni, A., Skjoedt, M. O., Honoré, C., Arendrup, M., Mantovani, A., et al. (2011). Heterocomplexes of Mannose-Binding Lectin and the Pentraxins PTX3 or Serum Amyloid P Component Trigger Cross-Activation of the Complement System. *J. Biol. Chem.* 286 (5), 3405–3417. doi:10.1074/jbc.M110.190637

Mutlu, M., Yuksel, N., Takmaz, T., Dincel, A. S., Bilgihan, A., and Altınkaynak, H. (2017). Aqueous Humor Pentraxin-3 Levels in Patients with Diabetes Mellitus. *Eye (Lond)* 31 (10), 1463–1467. doi:10.1038/eye.2017.87

Natoli, R., Fernando, N., Madigan, M., Chu-Tan, J. A., Valter, K., Provis, J., et al. (2017). Microglia-derived IL-1β Promotes Chemokine Expression by Müller Cells and RPE in Focal Retinal Degeneration. *Mol. Neurodegener* 12 (1), 31. doi:10.1186/s13024-017-0175-y

Nauta, A. J., Bottazzi, B., Mantovani, A., Salvatori, G., Kishore, U., Schwaeble, W. J., et al. (2003). Biochemical and Functional Characterization of the Interaction between Pentraxin 3 and C1q. *Eur. J. Immunol.* 33 (2), 465–473. doi:10.1002/immu.200310022

Norata, G. D., Marchesi, P., Pirillo, A., Uboldi, P., Chiesa, G., Maina, V., et al. (2008). Long Pentraxin 3, a Key Component of Innate Immunity, Is Modulated by High-Density Lipoproteins in Endothelial Cells. *Arterioscler Thromb. Vasc. Biol.* 28 (5), 925–931. doi:10.1161/ATVBAHA.107.160606

Ogura, S., Baldeosingh, R., Bhutto, I. A., Kambhampati, S. P., Scott McLeod, D., Edwards, M. M., et al. (2020). A Role for Mast Cells in Geographic Atrophy. *FASEB J.* 34 (8), 10117–10131. doi:10.1096/fj.202000807R

Parente, R., Clark, S. J., Inforzato, A., and Day, A. J. (2017). Complement Factor H in Host Defense and Immune Evasion. *Cel Mol Life Sci* 74 (9), 1605–1624. doi:10.1007/s00018-016-2418-4

Parmeggiani, F., Sorrentino, F. S., Romano, M. R., Costagliola, C., Semeraro, F., Incorvaia, C., et al. (2013). Mechanism of Inflammation in Age-Related Macular Degeneration: an Up-To-Date on Genetic Landmarks. *Mediators Inflamm.* 2013, 435607. doi:10.1155/2013/435607

Pietkiewicz, J., Seweryn, E., Bartyś, A., and Gamian, A. (2008). Receptors for Advanced Glycation End Products and Their Physiological and Clinical Significance. *Postepy Hig Med. Dosw (Online)* 62, 511–523.

Pietras-Baczewska, A., Nowomiejska, K., Brzozowska, A., Toro, M. D., Załuska, W., Sztanke, M., et al. (2021). Antioxidant Status in the Vitreous of Eyes with Rhegmatogenous Retinal Detachment with and without Proliferative Vitreoretinopathy, Macular Hole and Epiretinal Membrane. *Life (Basel)* 11 (5), 453. doi:10.3390/life11050453

Porte, R., Davoudian, S., Asgari, F., Parente, R., Mantovani, A., Garlanda, C., et al. (2019). The Long Pentraxin PTX3 as a Humoral Innate Immunity Functional Player and Biomarker of Infections and Sepsis. *Front. Immunol.* 10, 794. doi:10.3389/fimmu.2019.00794

Presta, M., Foglio, E., Churruca Schuind, A., and Ronca, R. (2018). Long Pentraxin-3 Modulates the Angiogenic Activity of Fibroblast Growth Factor-2. *Front. Immunol.* 9, 2327. doi:10.3389/fimmu.2018.02327

Rask-Madsen, C., and King, G. L. (2013). Vascular Complications of Diabetes: Mechanisms of Injury and Protective Factors. *Cell Metab* 17 (1), 20–33. doi:10.1016/j.cmet.2012.11.012

Ristagno, G., Fumagalli, F., Bottazzi, B., Mantovani, A., Olivari, D., Novelli, D., et al. (2019). Pentraxin 3 in Cardiovascular Disease. *Front. Immunol.* 10, 823. doi:10.3389/fimmu.2019.00823

Rubino, M., Kunderfranco, P., Basso, G., Greco, C. M., Pasqualini, F., Serio, S., et al. (2017). Epigenetic Regulation of the Extrinsic Oncosuppressor PTX3 Gene in Inflammation and Cancer. *Oncoimmunology* 6 (7), e1333215. doi:10.1080/2162402X.2017.1333215

Rusnati, M., Camozzi, M., Moroni, E., Bottazzi, B., Peri, G., Indraccolo, S., et al. (2004). Selective Recognition of Fibroblast Growth Factor-2 by the Long Pentraxin PTX3 Inhibits Angiogenesis. *Blood* 104 (1), 92–99. doi:10.1182/blood-2003-10-3433

Sapieha, P. (2012). Eyeing central Neurons in Vascular Growth and Reparative Angiogenesis. *Blood* 120 (11), 2182–2194. doi:10.1182/blood-2012-04-396846

Scarchilli, L., Camaioni, A., Bottazzi, B., Negri, V., Doni, A., Deban, L., et al. (2007). PTX3 Interacts with Inter-alpha-trypsin Inhibitor: Implications for Hyaluronan Organization and Cumulus Oophorus Expansion. *J. Biol. Chem.* 282 (41), 30161–30170. doi:10.1074/jbc.M703738200

Scholz, R., Caramoy, A., Bhuckory, M. B., Rashid, K., Chen, M., Xu, H., et al. (2015). Targeting Translocator Protein (18 kDa) (TSPO) Dampens Pro-inflammatory Microglia Reactivity in the Retina and Protects from Degeneration. *J. Neuroinflammation* 12, 201. doi:10.1186/s12974-015-0422-5

Schreur, V., de Breuk, A., Venhuizen, F. G., Sánchez, C. I., Tack, C. J., Klevering, B. J., et al. (2020). Retinal Hyperreflective Foci in Type 1 Diabetes Mellitus. *Retina* 40 (8), 1565–1573. doi:10.1097/IAE.0000000000002626

Semeraro, F., Cancarini, A., dell'Omo, R., Rezzola, S., Romano, M. R., and Costagliola, C. (2015). Diabetic Retinopathy: Vascular and Inflammatory Disease. *J. Diabetes Res.* 2015, 582060. doi:10.1155/2015/582060

Semeraro, F., Cancarini, A., Morescalchi, F., Romano, M. R., dell'Omo, R., Ruggeri, G., et al. (2014). Serum and Intraocular Concentrations of Erythropoietin and Vascular Endothelial Growth Factor in Patients with Type 2 Diabetes and Proliferative Retinopathy. *Diabetes Metab.* 40 (6), 445–451. doi:10.1016/j.diabet.2014.04.005

Semeraro, F., Morescalchi, F., Cancarini, A., Russo, A., Rezzola, S., and Costagliola, C. (2019). Diabetic Retinopathy, a Vascular and Inflammatory Disease: Therapeutic Implications. *Diabetes Metab.* 45 (6), 517–527. doi:10.1016/j.diabet.2019.04.002

Shahulhameed, S., Vishwakarma, S., Chhablani, J., Tyagi, M., Pappuru, R. R., Jakati, S., et al. (2020). A Systematic Investigation on Complement Pathway Activation in Diabetic Retinopathy. *Front. Immunol.* 11, 154. doi:10.3389/fimmu.2020.00154

Sharma, Y., Saxena, S., Mishra, A., Saxena, A., and Natu, S. M. (2012). Advanced Glycation End Products and Diabetic Retinopathy. *J. Ocul. Biol. Dis. Infor* 5 (3-4), 63–69. doi:10.1007/s12177-013-9104-7

Sitnilska, V., Enders, P., Cursiefen, C., Fauser, S., and Altay, L. (2021). Association of Imaging Biomarkers and Local Activation of Complement in Aqueous Humor of Patients with Early Forms of Age-Related Macular Degeneration. *Graefes Arch. Clin. Exp. Ophthalmol.* 259 (3), 623–632. doi:10.1007/s00417-020-04910-6

Sivapathasuntharam, C., Hayes, M. J., Shinhmar, H., Kam, J. H., Sivaprasad, S., and Jeffery, G. (2019). Complement Factor H Regulates Retinal Development and its Absence May Establish a Footprint for Age Related Macular Degeneration. *Sci. Rep.* 9 (1), 1082. doi:10.1038/s41598-018-37673-6

Stitt, A. W., Curtis, T. M., Chen, M., Medina, R. J., McKay, G. J., Jenkins, A., et al. (2016). The Progress in Understanding and Treatment of Diabetic Retinopathy. *Prog. Retin. Eye Res.* 51, 156–186. doi:10.1016/j.preteyeres.2015.08.001

Stravalaci, M., Davi, F., Parente, R., Gobbi, M., Bottazzi, B., Mantovani, A., et al. (2020). Control of Complement Activation by the Long Pentraxin PTX3: Implications in Age-Related Macular Degeneration. *Front. Pharmacol.* 11, 591908. doi:10.3389/fphar.2020.591908

Subedi, L., Lee, J. H., Gaire, B. P., and Kim, S. Y. (2020). Sulforaphane Inhibits MGO-AGE-Mediated Neuroinflammation by Suppressing NF-Kb, MAPK, and AGE-RAGE Signaling Pathways in Microglial Cells. *Antioxidants (Basel)* 9 (9), 792. doi:10.3390/antiox9090792

Swinkels, M., Zhang, J. H., Tilakaratna, V., Black, G., Perveen, R., McHarg, S., et al. (2018). C-reactive Protein and Pentraxin-3 Binding of Factor H-like Protein 1 Differs from Complement Factor H: Implications for Retinal Inflammation. *Sci. Rep.* 8 (1), 1643. doi:10.1038/s41598-017-18395-7

Toro, M. D., Nowomiejska, K., Avitabile, T., Rejdak, R., Tripodi, S., Porta, A., et al. (2019). Effect of Resveratrol on *In Vitro* and *In Vivo* Models of Diabetic Retinophathy: A Systematic Review. *Int. J. Mol. Sci.* 20 (14), 3503. doi:10.3390/ijms20143503

Wang, L., Cano, M., Datta, S., Wei, H., Ebrahimi, K. B., Gorashi, Y., et al. (2016). Pentraxin 3 Recruits Complement Factor H to Protect against Oxidative Stress-Induced Complement and Inflammasome Overactivation. *J. Pathol.* 240 (4), 495–506. doi:10.1002/path.4811

Wang, L., Kondo, N., Cano, M., Ebrahimi, K., Yoshida, T., Barnett, B. P., et al. (2014). Nrf2 Signaling Modulates Cigarette Smoke-Induced Complement Activation in Retinal Pigmented Epithelial Cells. *Free Radic. Biol. Med.* 70, 155–166. doi:10.1016/j.freeradbiomed.2014.01.015

Wong, W. L., Su, X., Li, X., Cheung, C. M., Klein, R., Cheng, C. Y., et al. (2014). Global Prevalence of Age-Related Macular Degeneration and Disease burden Projection for 2020 and 2040: a Systematic Review and Meta-Analysis. *Lancet Glob. Health* 2 (2), e106–16. doi:10.1016/S2214-109X(13)70145-1

Woo, J. M., Kwon, M. Y., Shin, D. Y., Kang, Y. H., Hwang, N., and Chung, S. W. (2013). Human Retinal Pigment Epithelial Cells Express the Long Pentraxin PTX3. *Mol. Vis.* 19, 303–310.

Woodell, A., and Rohrer, B. (2014). A Mechanistic Review of Cigarette Smoke and Age-Related Macular Degeneration. *Adv. Exp. Med. Biol.* 801, 301–307. doi:10.1007/978-1-4614-3209-8_38

Wu, J., Zhang, C., Yang, Q., Xie, H., Zhang, J., Qiu, Q., et al. (2021). Imaging Hyperreflective Foci as an Inflammatory Biomarker after Anti-VEGF Treatment in Neovascular Age-Related Macular Degeneration Patients with

Optical Coherence Tomography Angiography. *Biomed. Res. Int.* 2021, 6648191. doi:10.1155/2021/6648191

Yamada, Y., Tian, J., Yang, Y., Cutler, R. G., Wu, T., Telljohann, R. S., et al. (2008). Oxidized Low Density Lipoproteins Induce a Pathologic Response by Retinal Pigmented Epithelial Cells. *J. Neurochem.* 105 (4), 1187–1197. doi:10.1111/j.1471-4159.2008.05211.x

Yang, H. S., Woo, J. E., Lee, S. J., Park, S. H., and Woo, J. M. (2014). Elevated Plasma Pentraxin 3 Levels Are Associated with Development and Progression of Diabetic Retinopathy in Korean Patients with Type 2 Diabetes Mellitus. *Invest. Ophthalmol. Vis. Sci.* 55 (9), 5989–5997. doi:10.1167/iovs.14-14864

Yau, J. W., Rogers, S. L., Kawasaki, R., Lamoureux, E. L., Kowalski, J. W., Bek, T., et al. (2012). Global Prevalence and Major Risk Factors of Diabetic Retinopathy. *Diabetes Care* 35 (3), 556–564. doi:10.2337/dc11-1909

Zhou, W., and Hu, W. (2016). Serum and Vitreous Pentraxin 3 Concentrations in Patients with Diabetic Retinopathy. *Genet. Test. Mol. Biomarkers* 20 (3), 149–153. doi:10.1089/gtmb.2015.0238

Conflict of Interest: AI is inventor of a patent on PTX3 (WO2006037744A1). AM and BB obtain royalties on reagents related to PTX3.

The remaining authors declare that the research was conducted in the absence of any commercial or financial relationships that could be construed as a potential conflict of interest.

The reviewer MDT declared a past co-authorship with one of the authors MRR to the handling editor.

Publisher's Note: All claims expressed in this article are solely those of the authors and do not necessarily represent those of their affiliated organizations, or those of the publisher, the editors, and the reviewers. Any product that may be evaluated in this article, or claim that may be made by its manufacturer, is not guaranteed or endorsed by the publisher.

frontiers in Pharmacology

ORIGINAL RESEARCH
published: 22 February 2022
doi: 10.3389/fphar.2022.824790

Steroid Treatment in Macular Edema: A Bibliometric Study and Visualization Analysis

Yu Lin[1,2†], *Xiang Ren*[1,2†] *and Danian Chen*[1,2*]

[1]Research Laboratory of Ophthalmology and Vision Sciences, State Key Laboratory of Biotherapy, West China Hospital, Sichuan University, Chengdu, China, [2]Department of Ophthalmology, West China Hospital, Sichuan University, Chengdu, China

The use of steroids to treat macular edema (ME) is a research hotspot in ophthalmology. We utilized CiteSpace and VOSviewer software to evaluate the Web of Science Core Collection publications and to build visualizing maps to describe the research progress in this topic. There were 3,252 publications for three decades during 1988–2021. The number of studies was low during the first 14 years but has risen consistently in the following two decades. The average publications per year were only 4.8 during 1988–2002, which jumped to 113 per year during 2003–2012, and 227 per year during 2013–2021. These publications came from 83 countries/regions, with the United States, Germany, and Italy leading positions. Most studies were published in *Investigative Ophthalmology Visual Science*, and *Ophthalmology* was the most cited journal. We found 9,993 authors, with Bandello F having the most publications and Jonas JB being the most frequently co-cited. According to our research, the most popular keyword is triamcinolone acetonide (TA). Macular edema, diabetic macular edema (DME), retinal vein occlusion (RVO), dexamethasone (DEX), fluocinolone acetonide (FA), and some other keywords were commonly studied in this field. In conclusion, the bibliometric analysis provides a comprehensive overview of steroid hotspots and developmental tendencies in the macular edema study. While anti-VEGF therapy is the first-line treatment for DME and RVO-induced macular edema, steroids implant is a valid option for these DME patients not responding to anti-VEGF therapy and non-DME patients with macular edema. Combined therapy with anti-VEGF and steroid agents is vital for future research.

Keywords: steroids, macular edema, intravitreal injection, citespace, VOSviewer, bibliometric study

OPEN ACCESS

Edited by:
Settimio Rossi,
Second University of Naples, Italy

Reviewed by:
Giovanni Luca Romano,
University of Catania, Italy
Ehab Ghoneim,
Portsaid University, Egypt

****Correspondence:***
Danian Chen
danianchen2006@qq.com

†These authors have contributed equally to this work

Specialty section:
This article was submitted to Inflammation Pharmacology, a section of the journal Frontiers in Pharmacology

Received: *29 November 2021*
Accepted: *17 January 2022*
Published: *22 February 2022*

Citation:
Lin Y, Ren X and Chen D (2022) Steroid Treatment in Macular Edema: A Bibliometric Study and Visualization Analysis. Front. Pharmacol. 13:824790. doi: 10.3389/fphar.2022.824790

1 INTRODUCTION

The macula is responsible for central vision and locates at the center of retina, temporal to the optic nerve head (Daruich et al., 2018). Macular diseases can cause blurred vision, distorted vision, and vision loss (Chung, 2020). Macular edema (ME) develops when fluid accumulates in the macular layers due to vascular leakage, causing the macula to swell and thicken, distorting vision (Lang, 2012). It is a complication of several retinal disorders and other diseases, including diabetic retinopathy (DR), age-related macular degeneration (AMD), retinal vein occlusion (RVO), and inflammatory diseases (such as uveitis and retinal necrosis) (Welfer et al., 2011; Smith and Kaiser, 2014; Aksu-Ceylan et al., 2021; Hykin et al., 2021; Tappeiner et al., 2021). The most common causes of macular edema are DR and RVO (Daruich et al., 2018). It affects about 7 million DR patients (Yau et al., 2012), 3 million RVO patients (Rogers et al., 2010), and 40% of uveitis patients (Rothova et al., 1996; Karim et al., 2013).

Several approaches have been developed to treat macular edema and its underlying causes, such as anti-vascular endothelial growth factor (anti-VEGF) therapies, anti-inflammatory treatments, focal laser photocoagulation, carbonic anhydrase inhibitors, and vitrectomy (Mahdy et al., 2010; Supuran, 2019; Shimura et al., 2020; Aref et al., 2021; Mohan et al., 2021). Grid and focal laser photocoagulation, which was once the standard treatment for macular edema, is declining (Romero-Aroca, 2015). On the other hand, intravitreal injections have been commonly utilized to treat macular edema recently (Romero-Aroca, 2015). Anti-VEGF agents and corticosteroids are the most commonly administered drugs intravitreally (Distefano et al., 2017). Anti-VEGF agents can reduce vascular permeability and leakage (Simó et al., 2014). Anti-inflammatory steroids could help repair the blood-retinal barrier and decrease exudation (Cunningham et al., 2008; Sarao et al., 2014). Triamcinolone acetonide (TA), dexamethasone (DEX), and fluocinolone acetonide (FA) are the three most often utilized steroids in the treatment of vitreoretinal disorders (Whitcup et al., 2018). The first steroid to treat AMD and macular edema was TA, which was followed by DEX and FA (Bandello et al., 2014).

Recently sustained-release devices have been developed and approved for intravitreal steroid administration, such as an intravitreal implant that can sustain drug delivery of DEX for up to 6 months (Bucolo et al., 2018). When macular edema is caused by vitreous traction, vitrectomy can relieve the tractional forces pulling on the macula (Yoshizumi et al., 2019). Other new therapeutic agents, such as minocycline and integrin antagonists, are being examined in clinical trials to reverse or even prevent the development of macular edema (Cukras et al., 2012; Shaw et al., 2020).

Bibliometric analysis, which focuses on the literature systems and characteristics, investigates hotspots and developmental trends in the scientific literature, using qualitative and quantitative analysis to describe the relationships between citing and co-cited references and depict the contributions of various authors, countries, and journals (Gu et al., 2021; Ma et al., 2021). This approach can help develop guidelines, identify research hotspots, and predict research trends (Guler et al., 2016). As previously stated, there are many therapeutic options for treating macular edema. New progress has recently been achieved in the study of steroids, particularly in the drug delivery system of these medicines. Thus, we want to use bibliometric analysis software to map out hotspots and developmental trends in using steroids to treat macular edema over the last three decades.

2 METHODS

2.1 Data Collection and Search Strategies

We searched the Web of Science (WOS) Core Collection database for all literature on the treatment of macular edema with steroids. All searches were performed on a single day, 7 October 2021, to avoid biases introduced by daily database updating. The search strategies were integrated as follows: TI = (macular edema) AND TS = (glucocorticoid OR steroid OR dexamethasone OR fluortriamcinolone acetonide OR triamcinolone acetonide). A total of 3,252 records from 1988 to 2021 were identified from WOS. In the WOS citation report, these entries were cited 67,645 times in total. In the following analysis, we used all these 3,252 records, including 2,348 articles, 402 reviews, 295 meeting abstracts, 122 letters, 68 editorial materials, 8 proceedings papers, 8 corrections, and 1 item of news. The retrieved eligible publications were exported and saved as plain text files, including titles, keywords, publication dates, countries and regions, institutions, authors, publishing journals, and sums of citations (**Figure 1**).

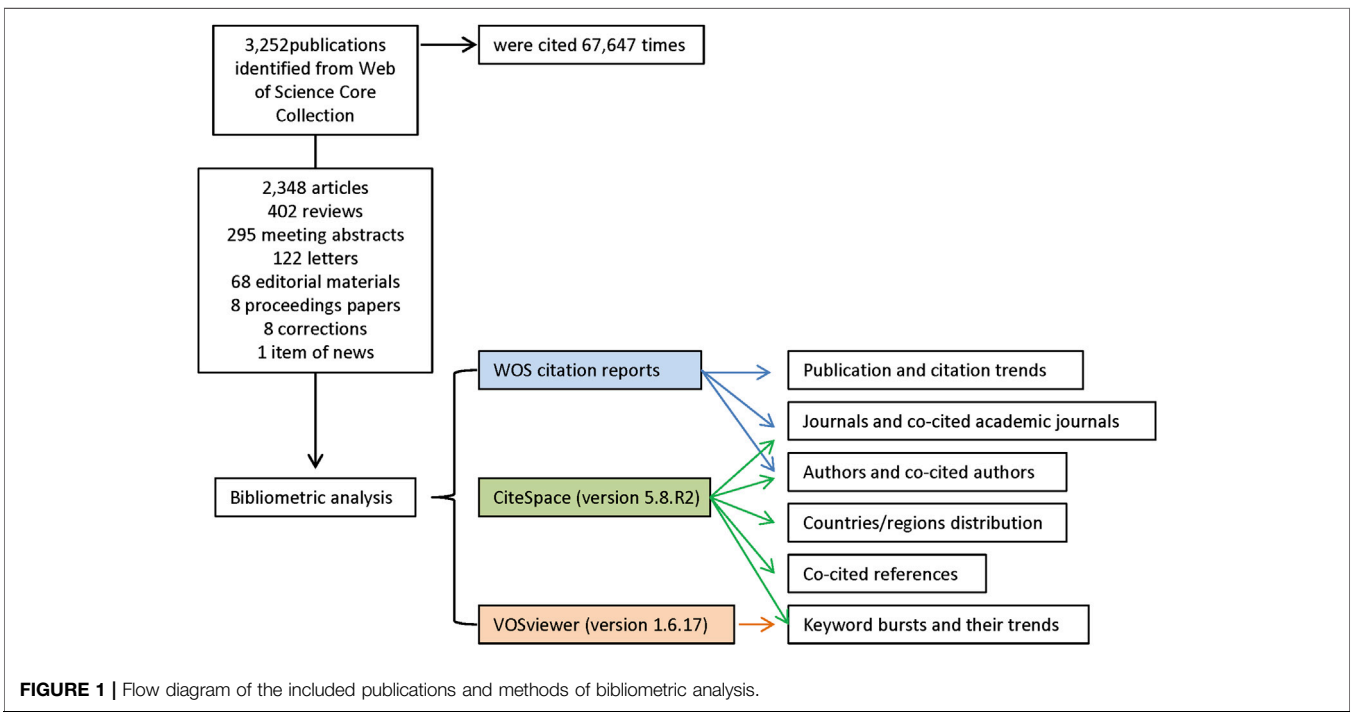

FIGURE 1 | Flow diagram of the included publications and methods of bibliometric analysis.

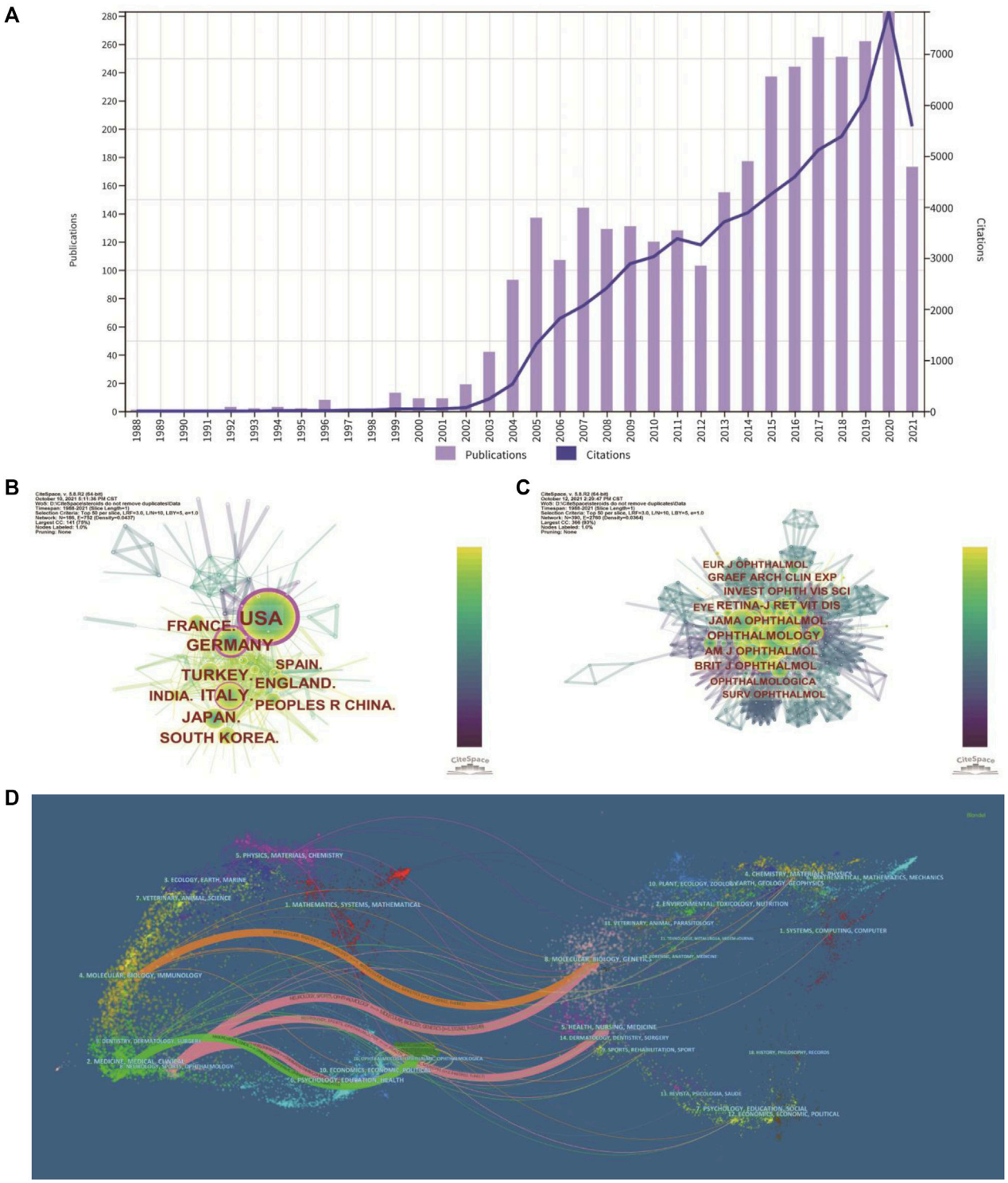

FIGURE 2 | Distribution of publications and citations from different years, countries and journals. **(A)** The distribution of the bibliographic records in Set #7 **(Table 1)**, showing the number of publications and citations during different years. **(B)** Distributions of publications from different countries. **(C)** CiteSpace visualization map of co-cited journals. **(D)** The dual-map overlay of journals. The dual-map shows the relationships between publications and citations, with dots representing citing journals on the left and cited journals on the right.

TABLE 1 | Distribution of publications from different countries/regions.

No.	Country	Counts (%)
1	United States	913 (28.066%)
2	Germany	321 (9.868%)
3	Italy	314 (9.653%)
4	Turkey	242 (7.439%)
5	England	209 (6.425%)
6	France	204 (6.271%)
7	Japan	203 (6.240%)
8	South Korea	179 (5.503%)
9	India	153 (4.703%)
10	Peoples R China	146 (4.488%)

2.2 Bibliometric Analyzing

The exported data were imported into CiteSpace version 5.8.R2 (Drexel University, Philadelphia, United States) (Chen et al., 2012; Chen, 2017) and VOSviewer version 1.6.17 (Leiden University, Leiden, Netherlands) (van Eck and Waltman, 2010) and analyzed both quantitatively and qualitatively. We used the "eliminating duplicates function" in CiteSpace to perform simple literature curation before doing the co-word analysis and document co-citation analysis. Thus the final dataset included no duplicates. The publication and citation trends were generated from the citation reports of WOS. CiteSpace was used to identify countries/regions distribution, journals and co-cited academic journals, authors and co-cited authors, keyword bursts and their trends, and co-cited references. VOSviewer was employed to map and visualize the network of hotspots (keywords) related to macular edema treated with steroids research. Hotspots were classified into disparate clusters according to co-occurrence analysis and simultaneously color-coded by time course. Detailed procedures of the enrolment and analysis are illustrated in **Figure 1**.

3 RESULTS

3.1 The Publication and Citation Trends

The number of publications and citations in a research field shows the evolution of research. The number of publications related to the treatment of macular edema with steroids by year was presented in **Figure 2A**. While there were less than 5 publications per year during 1988–2002, the number of publications increased to about 110 publications per year on average during 2003–2012. The number of publications increased dramatically to about 230 publications per year on average during 2013–2021 (**Figure 2A**). For instance, in 2020, the total number of outputs reached 283, and the number of citations increased to 7,829, which both achieved the climax (**Figure 2A**). In total, 3,252 publications have been cited 67,645 times, and the average number of citations per publication is 20.8 times. Likely, the citation frequency of these studies increased steadily from 1988 to 2021 (**Figure 2A**). These data indicated that the steroids agent is more and more commonly used to treat macular edema.

3.2 Analysis of Leading Countries/Region

These studies were published by researchers in 83 countries and regions worldwide. The top 10 countries/regions contributing to this research field were mainly America, Europe, and Asia (**Table 1**). More than one-quarter of the publications were from the United States (913, 28.066%). Germany (321, 9.868%), Italy (314, 9.653%), Turkey (242, 7.439%), and England (209, 6.425%) also made significant contributions to this topic (**Table 1**). The United States is the largest node on the country network map (**Figure 2B**). In addition, certain countries, such as the United States, Germany, and Italy, showed high centrality and were circled in the purple ring, implying that these countries may have played a crucial role in this research field (**Figure 2B**).

TABLE 2 | Top 8 journals and co-cited journals.

No.	Journal	Count (%)	JCR (2020)	Co-cited Journal	Citation count	JCR (2020)
1	Investigative Ophthalmology Visual Science	306 (9.407%)	Q1	Ophthalmology	2645	Q1
2	Retina - The Journal of Retinal and Vitreous Diseases	247 (7.593%)	Q1	American Journal of Ophthalmology	2327	Q1
3	European Journal of Ophthalmology	146 (4.488%)	Q3	JAMA Ophthalmology (formerly Archives of Ophthalmology)	2249	Q1
4	American Journal of Ophthalmology	136 (4.181%)	Q1	Retina - The Journal of Retinal and Vitreous Diseases	2044	Q1
5	Graefes Archive for Clinical and Experimental Ophthalmology	123 (3.781%)	Q2	British Journal of Ophthalmology	1858	Q1
6	Ophthalmology	120 (3.689%)	Q1	Investigative Ophthalmology Visual Science	1543	Q1
7	Journal of Ocular Pharmacology and Therapeutics	99 (3.043%)	Q2	Graefes Archive for Clinical and Experimental Ophthalmology	1402	Q2
8	Ophthalmologica	94 (2.890%)	Q2	Eye	1254	Q1

Q1: Quartile 1 of JCR 2020.

TABLE 3 | Top 10 authors and co-cited authors.

No.	Author	Country	Count (%)	Co-cited author	Country	Citation count
1	Bandello F	Italy	77 (2.367%)	Jonas JB	Germany	902
2	Jonas JB	Germany	57 (1.752%)	Haller JA	United States	597
3	Loewenstein A	Israel	49 (1.506%)	Campochiaro PA	United States	542
4	Scott IU	United States	38 (1.168%)	Gillies MC	Australia	516
5	Whitcup SM	United States	34 (1.045%)	Ip MS	United States	487
6	Gillies MC	Australia	33 (1.014%)	Boyer DS	United States	476
7	Kodjikian L	France	33 (1.014%)	Martidis A	United States	395
8	Kuppermann BD	United States	31 (0.953%)	Massin P	France	377
9	Kreissig I	Germany	29 (0.891%)	Klein R	United States	370
10	Sakamoto T	Japan	29 (0.891%)	Brown DM	United States	337

TABLE 4 | Top 30 keywords.

No.	Keywords	Count
1	Triamcinolone acetonide	1284
2	Injection	526
3	Bevacizumab	495
4	Macular edema	444
5	Endothelial growth factor	425
6	Ranibizumab	331
7	Retinopathy	317
8	Diabetic macular edema	272
9	Efficacy	265
10	Cystoid macular edema	262
11	Retinal vein occlusion	243
12	Optical coherence tomography	235
13	Safety	227
14	Therapy	197
15	Trial	195
16	Eye	185
17	Visual acuity	167
18	Drug delivery system	167
19	Intraocular pressure	165
20	Management	163
21	Degeneration	146
22	Dexamethasone implant	146
23	Dexamethasone	135
24	Risk factor	125
25	Photocoagulation	117
26	Secondary	116
27	Macular edema secondary	110
28	Pharmacokinetics	106
29	Pars plana vitrectomy	106
30	Outcome	99

3.3 Analysis of Leading Journals and Co-Cited Journals

In total, 345 academic journals have published papers about steroids in macular edema treatment. **Table 2** presented the top 8 journals contributing to this field and *Investigative Ophthalmology Visual Science (IOVS)* as the leading journal published the most papers (306, 9.407%), followed by *Retina - The Journal of Retinal and Vitreous Diseases* (247, 7.593%), *European Journal of Ophthalmology (EJO)* (146, 4.488%), and *American Journal of Ophthalmology (AJO)* (136, 4.181%). These are all major ophthalmological journals (**Table 2**).

The impact factor (IF) represents the importance of journals in particular respective fields, with higher IF indicating publications in that journal with more frequent citations (Mueller et al., 2006). Among these 8 top journals, *Ophthalmology* has the highest IF (12.079). Co-citation analysis can also measure the degree of relationship between articles. The impact of a journal depends on its co-citation frequency. CiteSpace can show co-citations and annotate cited journals based on citation frequency (**Figure 2C**). **Table 2** presented the top eight journals which were cited over 1,000 times, and consistent with the IF, *Ophthalmology* has been the most frequently co-cited journal (2,645 times), followed by *AJO* (2,327 times), *JAMA Ophthalmology* (previously *Archives of Ophthalmology*) (2,249 times), and *Retina - The Journal of Retinal and Vitreous Diseases* (2,044 times). According to the journal citation reports (JCR) in 2020 (Clarivate, United Kingdom), seven of the top eight co-cited journals were in the Quartile 1 (Q1), except for *Graefes Archive for Clinical and Experimental Ophthalmology* (**Table 2**).

CiteSpace can also show the relationships between citing journals and cited journals in the dual-map overlay of journals (**Figure 2D**), with dots representing citing journals on the left and cited journals on the right (Chen et al., 2014). The cited relationships are depicted by the colored lines that run from the left to the right side of the dual map. There are five main citation paths, including three pink paths, one orange path, and one green path (**Figure 2D**). The three pink routes show that Ophthalmology journals mostly cited Molecular or Biology or Genetics, Health or Nursing or Medicine, and Ophthalmology journals. Studies published in Molecular/Biology/Immunology journals frequently cited articles published in Molecular/Biology/Genetics journals, as indicated by the orange path. The green path indicates that research published in Medicine/Medical/Clinical journals cited papers published in Ophthalmology journals frequently.

3.4 Analysis of Authors and Co-Cited Authors

A total of 9,993 authors published papers related to the use of steroids to treat macular edema (**Table 3**). Bandello F from the Department of Ophthalmology, Vita-Salute San Raffaele University, Italy, had the highest number of published papers (77 publications, 2.367%), followed by Jonas JB (57, 1.752%), and Loewenstein A (49, 1.506%). **Table 3** also shows the top 10 most frequently co-cited authors, including Jonas JB (902 times), Haller JA (597 times), and Campochiaro PA (542 times). Jonas JB from the Department of Ophthalmology, Medical Faculty Mannheim of

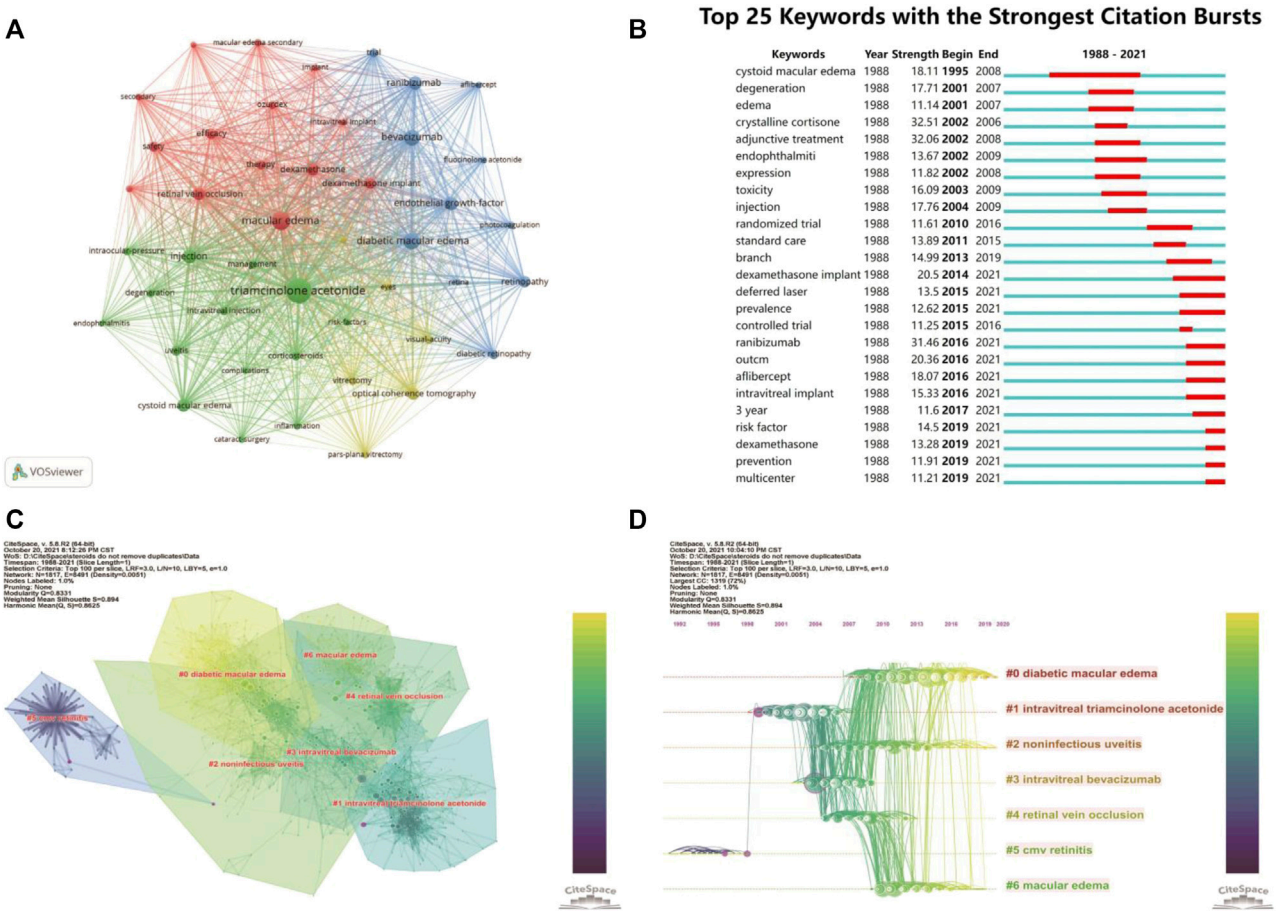

FIGURE 3 | The main keywords and co-citation clusters. **(A)** VOSviewer visualization map of co-occurrence keywords. **(B)** Time trends of burst keywords. **(C)** CiteSpace visualization clusters of co-cited references. **(D)** Timeline view of clusters of co-cited references.

TABLE 5 | Top 12 co-cited references.

No.	Citation count	Author	Reference title	Journal	Year
1	272	Boyer DS	Three-year, randomized, sham-controlled trial of dexamethasone intravitreal implant in patients with diabetic macular edema.	Ophthalmology	2014
2	200	Martidis A	Intravitreal triamcinolone for refractory diabetic macular edema.	Ophthalmology	2002
3	177	Jonas JB	Intravitreal injection of triamcinolone for diffuse diabetic macular edema.	Arch Ophthalmol-Chic	2003
4	153	Haller JA	Randomized, sham-controlled trial of dexamethasone intravitreal implant in patients with macular edema due to retinal vein occlusion.	Ophthalmology	2010
5	149	Haller JA	Dexamethasone intravitreal implant in patients with macular edema related to branch or central retinal vein occlusion.	Ophthalmology	2011
6	141	Massin P	Intravitreal triamcinolone acetonide for diabetic diffuse macular edema - Preliminary results of a prospective controlled trial.	Ophthalmology	2004
7	132	Wells JA	Aflibercept, bevacizumab, or ranibizumab for diabetic macular edema.	New Engl J Med	2015
8	119	Greenberg PB	Intravitreal triamcinolone acetonide for macular oedema due to central retinal vein occlusion.	Brit J Ophthalmol	2002
9	115	Antcliff RJ	Intravitreal triamcinolone for uveitic cystoid macular edema: An optical coherence tomography study.	Ophthalmology	2001
10	111	Jonas JB	Intraocular pressure after intravitreal injection of triamcinolone acetonide.	Brit J Ophthalmol	2003
11	107	Lowder C	Dexamethasone intravitreal implant for noninfectious intermediate or posterior uveitis.	Arch Ophthalmol-Chic	2011
12	102	Campochiaro PA	Sustained delivery fluocinolone acetonide vitreous inserts provide benefit for at least 3 years in patients with diabetic macular edema.	Ophthalmology	2012

TABLE 6 | Cited papers with the highest "betweenness centrality" among the top 7 clusters.

Rank	Centrality	References	Cluster #
1	0.41	Wingate and Beaumont. (1999): Intravitreal triamcinolone and elevated intraocular pressure.	1
2	0.41	Rothova. (1996): Causes and frequency of blindness in patients with intraocular inflammatory disease.	5
3	0.39	Challa et al. (1998): Exudative macular degeneration and intravitreal triamcinolone: 18 months follow up.	5
4	0.16	Jonas et al. (2003b): Intraocular pressure after intravitreal injection of triamcinolone acetonide.	1
5	0.1	Massin. (2004): Intravitreal triamcinolone acetonide for diabetic diffuse macular edema: preliminary results of a prospective controlled trial.	3

the Ruprecht-Karls-University, Heidelberg, Germany, was ranked the second most productive author and the first on the most co-cited list, placing him among the top ten in both lists. Another author ranked highly on both lists was Gillies MC (Sydney Eye Hospital, Sydney, Australia).

3.5 Analysis of Co-Occurring Keywords and Burst Term

Keywords analysis can reveal hotspots in a topic of study. We merged some different versions of the same terms when we analyzed the keywords, including synonyms (e.g., "triamcinolone acetonide" and "triamcinolone"), different spelling versions (e.g., "triamcinolone acetonide" and "triamcinoloneacetonide"), and abbreviated terms (e.g., "DME" and "diabetic macular edema"). **Table 4** shows the top 30 keywords, with most of them falling into two categories. Macular edema and disorders associated with macular edema, such as diabetic macular edema (DME), cystoid macular edema (CME), and RVO, are covered in the disease category. The other group is macular edema therapy, including keywords like TA, injections, and bevacizumab. The rest of the top 30 keywords are related to the efficacy and safety of these treatments. Interestingly, half of the top 6 keywords are VEGF-related terms (Bevacizumab, Endothelial growth factor, and Ranibizumab) (**Table 4**), suggesting anti-VEGF therapy and steroids therapy in macular edema were often connected. In **Figure 3A**, we used VOSviewer software to show the primary keywords more compact and aesthetically pleasing.

We also used CiteSpace's burst detection function to discover the top 25 terms with the most citation bursts (**Figure 3B**). A blue line displays the time interval, whereas a red line segment depicts the burst period time of keywords. Similarly, most of the top 25 burst keywords may be classified as disorders connected to macular edema and its treatment. Keywords associated with macular edema, such as cystoid macular edema, degeneration, and edema, began to burst during the early stages. Following that, keywords like crystalline cortisone and adjunctive treatment began to explode, showing that the study focus had shifted to finding solutions to these perplexing issues. Also worth noting, intravitreal implant and VEGF-related terms only had bursts recently (**Figure 3B**).

3.6 Co-cited References and Burst References

3.6.1 Top-Cited References

The most distinctive feature of CiteSpace is co-cited references analysis, resulting in a broad perspective of a scientific subject by selecting the top 100 most cited publications published over 1 year. We compiled a list of the top 12 co-cited references from 1988 to 2021 (**Table 5**). These references were cited more than 100 times, with the top two receiving more than 200 citations each. The most frequently cited reference was a report on clinical trials (registered with the identifiers NCT00168337 and NCT00168389 at ClinicalTrials.gov), reporting the safety and efficacy of dexamethasone intravitreal implant (Ozurdex, DEX implant) 0.7 and 0.35 mg in the treatment of DME (Boyer et al., 2014). The second most cited paper also reported the results of the intravitreal triamcinolone acetonide (IVTA) clinical trial for treating refractory DME that did not respond well to photocoagulation (Martidis et al., 2002).

3.6.2 Seven Clusters of Co-citation Network

CiteSpace could potentially partition the co-citation network into clusters, displaying firmly related references in one cluster and loosely connected references in another. Words from the titles of the citing articles inside the cluster were used to designate each cluster. The top seven clusters were shown in **Figure 3C**, including #0 diabetic macular edema, #1 intravitreal triamcinolone acetonide, #2 noninfectious uveitis, #3 intravitreal bevacizumab, #4 retinal vein occlusion, #5 cmv retinitis, and #6 macular edema. These included four clusters about the macular edema-related diseases (clusters #0, 2, 4, and 6), one cluster about IVTA, one about anti-VEGF, and one about complications related to steroids treatment (#5 CMV retinitis).

3.6.3 Timeline Cluster Map

The cluster map could be converted into a timeline format, using the cluster number as the *y*-axis (**Figure 3D**). The timeline diagram depicted the progression of research in the general field and its seven sub-fields over time. Notably, cluster #5 CMV retinitis was mainly in the early time, and never overlapped with other clusters (**Figure 3D**); suggesting CMV retinitis is not a major complication of steroids in macular edema treatment. Cluster #0 (DME), #2 (noninfectious uveitis), and #6 (ME, actually mainly about RVO) persisted to recent time, indicating these three ocular diseases are primary indications for steroids therapy of macular edema now (**Figure 3D**)

3.6.4 High Betweenness Centrality Papers

Some nodes in the timeline-cluster map had purple rings around them, indicating that they had high "betweenness centrality" ratings, which is defined as the number of times a node lies on the shortest path between all pairs of nodes (Abbasi et al.,

TABLE 7 | Cited references and citing articles of Cluster #1 intravitreal triamcinolone acetonide.

Cluster #1 intravitreal triamcinolone acetonide			
Cited references			Citing articles
Citation count	Author (Year) Journal Volume, Page	Coverage Count	Author (Year) title
200	Martidis et al. (2002) Ophthalmology, 109, 920	108	Jonas. (2006) Intravitreal triamcinolone acetonide: a change in a paradigm.
177	Jonas et al., 2003a Arch Ophthalmol-Chic, 121, 57	91	Jonas. (2005) Intravitreal triamcinolone acetonide for treatment of intraocular oedematous and neovascular diseases.
119	Greenberg et al. (2002) Brit J Ophthalmol, 86, 247	88	Jonas. (2005) Intravitreal triamcinolone acetonide for treatment of intraocular proliferative, exudative, and neovascular diseases.
115	Antcliff. (2001) Ophthalmology, 108, 765	60	Jonas et al. (2004) Intravitreal triamcinolone acetonide for the treatment of intraocular edematous and neovascular diseases.
111	Jonas et al. (2003b) Brit J Ophthalmol, 87, 24	45	Jonas et al., 2003c Treatment of oedematous, proliferative and neovascular diseases by intravitreal triamcinolone acetonide.
97	Jonas and Söfker. (2001) Am J Ophthalmol, 132, 425	45	Thompson, (2006) Cataract formation and other complications of intravitreal triamcinolone for macular edema.

TABLE 8 | Cited references and citing articles of Cluster #0 diabetic macular edema.

Cluster #0 diabetic macular edema			
Cited references			Citing articles
Citation count	Author (Year) Journal Volume, Page	Coverage Count	Author (Year) title
272	Boyer. (2014) Ophthalmology, 121,1904	40	Cicinelli, Maria Vittoria (2020) The current role of steroids in diabetic macular edema.
132	Wells et al. (2015) New Engl J Med, 372, 1193	36	Bandello, Francesco (2013) Pathophysiology and treatment of diabetic retinopathy.
102	Campochiaro et al. (2012) Ophthalmology, 119, 2125	31	Bandello et al. (2014) Pharmacological approach to diabetic macular edema.
98	Nguyen et al. (2012) Ophthalmology, 119, 789	31	Cebeci, Zafer (2015) Role of implants in the treatment of diabetic macular edema: focus on the dexamethasone intravitreal implant.
92	Chang-Lin et al. (2011) Invest Ophth Vis Sci, 52, 80	29	Urbancic, Mojca (2019) Dexamethasone implant in the management of diabetic macular edema from clinician's perspective.
91	Boyer et al. (2011) Retina-J Ret Vit Dis, 31, 915	29	Lambiase et al. (2014) An update on intravitreal implants in use for eye disorders.

TABLE 9 | Cited references and citing articles of Cluster #2 noninfectious uveitis.

Cluster #2 noninfectious uveitis			
Cited references			Citing articles
Citation count	Author (Year) Journal Volume, Page	Coverage Count	Author (Year) title
107	Lowder et al. (2011) Arch Ophthalmol-Chic, 129, 545	24	Heiligenhaus et al. (2014) Statement of the german ophthalmological society, of the retinological society and the professional association of german oculist for intravitreal therapy for makulaodems in uveitis.
58	Kuppermann et al. (2007) Arch Ophthalmol-Chic, 125, 309	24	Heiligenhaus et al. (2014) Statement of the german ophthalmological society, the retina society and the professional association of eye doctors in germany for intravitreal treatment of macular edema in uveitis.
50	Kiddee et al. (2013) Surv Ophthalmol, 58, 291	19	Lambiase et al. (2014) An update on intravitreal implants in use for eye disorders.
40	Tomkins-Netzer et al. (2014) Ophthalmology, 121, 1649	19	Ossewaarde-van Norel, Annette (2011) Clinical review: update on treatment of inflammatory macular edema.
36	Khurana et al. (2014) Ophthalmology, 121, 67	18	Robinson, Michael R (2012) Pharmacologic and clinical profile of dexamethasone intravitreal implant.

TABLE 10 | Cited references and citing articles of Cluster #4 retinal vein occlusion.

Cluster #4 retinal vein occlusion			
Cited references			Citing articles
Citation count	Author (Year) Journal Volume, Page	Coverage Count	Author (Year) title
92	Ip et al. (2009) Arch Ophthalmol-Chic, 127, 1101	41	Feltgen et al. (2010) Intravitreal drug therapy for retinal vein occlusion - pathophysiological mechanisms and routinely used drugs.
88	Scott et al. (2009) Arch Ophthalmol-Chic, 127, 1115	33	Macdonald, Derek (2014) The abcs of rvo: a review of retinal venous occlusion.
57	Iturralde et al. (2006) Retina-J Ret Vit Dis, 26, 279	33	Chatziralli, Irini P (2014) Branch retinal vein occlusion: treatment modalities: an update of the literature.
43	Jonas. (2005) Eye, 19, 65	26	Siegel, Ruth Axer (2012) Intravitreal bevacizumab treatment for macular edema due to branch retinal vein occlusion in a clinical setting.
34	Rosenfeld et al. (2005) Ophthal Surg Las Im, 36, 336	21	Sarao et al. (2014) Pharmacotherapy for treatment of retinal vein occlusion.
33	Rabena et al. (2007) Retina-J Ret Vit Dis, 27, 419	21	Braithwaite, T (2010) Anti-vascular endothelial growth factor for macular edema secondary to central retinal vein occlusion.
29	Prager et al. (2009) Brit J Ophthalmol, 93, 452	21	Shahsuvaryan, Marianne L (2012) Therapeutic potential of intravitreal pharmacotherapy in retinal vein occlusion.

TABLE 11 | Cited references and citing articles of Cluster #6 macular edema.

Cluster #6 macular edema			
Cited references			Citing articles
Citation count	Author (Year) Journal Volume, Page	Coverage Count	Author (Year) title
153	Haller et al. (2010) Ophthalmology, 117, 1134	27	Macdonald, Derek (2014) The abcs of rvo: a review of retinal venous occlusion.
149	Haller et al. (2011) Ophthalmology, 118, 2453	20	Wang, Jia-Kang (2016) A review of randomized trials of approved pharmaceutical agents for macular edema secondary to retinal vein occlusion.
70	Brown et al. (2011) Ophthalmology, 117, 1124[a]	17	Garweg, Justus G (2016) Retinal vein occlusion and the use of a dexamethasone intravitreal implant (ozurdexa (r)) in its treatment.
65	Campochiaro et al. (2010) Ophthalmology, 117, 1102	17	Ramezani, Alireza (2014) Three intravitreal bevacizumab versus two intravitreal triamcinolone injections in recent onset central retinal vein occlusion.
49	Campochiaro et al. (2011) Ophthalmology, 118, 2041	17	Sarao et al. (2014) Pharmacotherapy for treatment of retinal vein occlusion.
48	Capone et al. (2014) Retina-J Ret Vit Dis, 34, 342	17	Coscas, Gabriel (2014) Retreatment with ozurdex for macular edema secondary to retinal vein occlusion.
47	Brown et al. (2011) Ophthalmology, 118, 1594	17	Maggioa, Emilia (2014) Intravitreal dexamethasone implant for macular edema secondary to retinal vein occlusion: 12-month follow-up and prognostic factors.

[a]*Here, we need to mention that CiteSpace could only analyze the publications in the WOS core collection database, so we only downloaded these publications. However, the references cited by these articles may not be collected in this database, so information on such references would have some discrepancies. In this cluster, the third cited reference was not the one listed in the results of CiteSpace, and it was only collected by the Medline database rather than the WOS Core Collection database. Actually, the primary one given by CiteSpace was a letter by the same author team to reply to some questions about the treatment of age-related macular degeneration by using ranibizumab, which was obviously irrelative with our research topic. Additionally, CiteSpace also gave a DOI number that did not match this article, but the number helped us to find out the matched and right article shown in* ***Table 9*** *with an asterisk. Because this article was published by the same team as the fourth, fifth, and seventh articles in* ***Table 9****, and they were all reports of the efficacy and safety results of the clinical trials about the treatment of RVO-induced macular edema by using ranibizumab, so we used this article to replace the former one instead of straight deleting it in* ***Table 9****.*

2011). The top five papers with higher "betweenness centrality" are shown in **Table 6**. These papers may suggest some emerging trends in this field. Interestingly, two of them published 20 years ago belong to cluster #5 (CMV retinitis). The other three papers are all about IVTA or its complication (glaucoma), suggesting prevention of ocular complications of steroids is still essential now.

3.6.5 Details of Cluster #1 (IVTA)

In cluster #1 (IVTA), Jonas JB was the author of half of the top six co-cited references (**Table 7**), including a case report and two clinical trial articles (Jonas et al., 2003a; Jonas et al., 2003b; Jonas and Söfker, 2001). He was also the author of the top five citing articles, citing most publications in this field (coverage count) (**Table 7**). All these five citing papers were reviews, and two were in German (Jonas et al., 2003c; Jonas et al., 2004; Jonas et al., 2005a; Jonas, 2005; Jonas, 2006). As previously stated, Jonas JB ranked first among the most cited authors, and we now know that he made a significant contribution to the treatment of DME using IVTA. The clinical article by Martidis et al. published in 2002 was the most prominent in cluster #1 (IVTA). Unlike Jonas JB's

clinical trial papers, all of the patients involved in this investigation had received at least two prior sessions of laser photocoagulation yet still showed residual macular edema (Martidis et al., 2002).

3.6.6 Details of Cluster #0 (DME), Cluster #2 (Noninfectious Uveitis), Cluster #4 (RVO) and Cluster #6 (Macular Edema)

Macular edema can be caused by a variety of ocular diseases, including DME, uveitis, and RVO (Cunningham et al., 2008). In cluster #0 (DME) (**Table 8**), the paper about dexamethasone intravitreal implant (Boyer et al., 2014) was the top-cited reference, and it was also the top co-cited reference among all clusters (**Table 5**). In cluster #2 (noninfectious uveitis), the paper about dexamethasone intravitreal implant for uveitis was the most cited reference (Lowder et al., 2011), which indicated that DEX implant was safe and effective for the treatment of intermediate and posterior uveitis (**Table 9**). By employing the DEX implant, they were able to make a significant contribution to the treatment of uveitic macular edema. Regardless of the citing articles or references, all of the publications in cluster #4 (RVO) and cluster #6 (macular edema) were about the treatment of macular edema caused by RVO (**Table 10** and **Table 11**). These two clusters of co-cited references were all clinical trials or case reports examining the efficacy and safety of medications to treat RVO-induced macular edema. Apart from IVTA, two other therapies were used: DEX implant and ranibizumab. DEX implant is a slow-releasing biodegradable implant indicated for injection every 6 months and is a combination of medication and drug delivery mechanisms (Gaballa et al., 2021). Ranibizumab is a recombinant monoclonal antibody that can block VEGF-A (Rosenfeld et al., 2006).

4 DISCUSSION

The first article on this research topic was published in 1988, which described the successful use of steroids drops and sub-Tenon injection to treat cystoid macular edema (CME) following cataract extraction (Suckling and Maslin, 1988), suggesting that local steroids are effective in the treatment of pseudophakic CME. However, only a few studies were published over the next decade, mainly about systemic steroids on uveitis-related macular edema (Nussenblatt et al., 1991), steroid-induced ocular complications in the treatment of aphakic or pseudophakic CME (Melberg and Olk, 1993), and steroids sub-Tenon injections in uveitis patients with cystoid macular edema (Yoshikawa et al., 1995). CME was the top keyword during that time (**Figure 3B**). Steroid research in macular edema was still in its infancy at that time.

The first research wave lasting for one decade began from 2003 (**Figure 2A**), shortly after the first reports of human intravitreal injections of crystalline cortisone in the treatment of DME (Jonas and Söfker, 2001), IVTA for uveitic cystoid macular edema (Antcliff et al., 2001), IVTA for macular edema due to CRVO (Greenberg et al., 2002) and refractory DME (Martidis et al., 2002). These four papers are pioneering works, coming from Europe (Jonas and Söfker, 2001; Antcliff et al., 2001) and the United States (Martidis et al., 2002; Greenberg et al., 2002), and are all top-cited in this field (**Table 5**). At this time, the average publication per year on this topic was more than 110 papers. The second research wave lasting almost another decade began from 2013 to 2014 (**Figure 2A**), the average publication per year on this topic was more than 220 papers. This wave of research may be prompted by good results of the MEAD study demonstrating the efficacy of dexamethasone implant in the treatment of DME (Boyer et al., 2014), and the FDA-approved use of sustained-release biodegradable dexamethasone (Ozurdex) for the treatment of DME in 2014. The paper of the MEAD trial is the top-cited reference among all publications in this field (Boyer et al., 2014).

From the perspective of countries and authors, the United States was the leading contributor in this field with 913 publications, followed by Germany and Italy (**Table 1**). The top three countries were all developed countries in Europe and America. The research output from these countries may be associated with major pioneer researchers in this field and substantial financial support. Indeed, most of the top authors and co-cited authors were from Europe and America (**Table 3**). Europe and American researchers initiated both waves of research in this field. Among the top 10 countries, there are four countries from Asia (Japan, South Korea, India, and China), likely due to the vast number of patients in Asia. Sakamoto T was the only top-productive author from these countries; however, no top-cited authors came from these countries (**Table 3**).

Bandello F published the most papers. His significant contribution to this field is three clinical trials regarding the use of DEX intravitreal implant in macular edema caused by RVO (Haller et al., 2010; Haller et al., 2011) and DME (Boyer et al., 2014). Following Bandello F, Jonas JB, Loewenstein A, Scott IU, Whitcup SM and Gillies MC were the top six most productive authors with cooperative relationships. Jonas JB and Gillies MC were also top-cited authors (**Table 3**). Jonas JB is a comprehensive ophthalmologist and Chairman of the Department of Ophthalmology of the Medical Faculty Mannheim of Heidelberg University. His major contribution to this field is the first report on intravitreal injections of crystalline cortisone in the treatment of DME patients (Jonas and Söfker, 2001), IVTA for DME (Jonas et al., 2003a; Jonas et al., 2006), and IVTA-induced intraocular pressure (Jonas et al., 2003b; Jonas et al., 2005b). Gillies MC is a Professor at Save Sight Institute, University of Sydney. His major contribution to this field is similar to Bandello F, including the use of DEX intravitreal implant in macular edema caused by RVO (Haller et al., 2010; Haller et al., 2011) and DME (Sutter et al., 2004; Gillies et al., 2006). These researchers are considered world leaders in this critical research field and their studies will continue to influence the future development of steroids in the treatment of macular edema.

From the perspective of journals and co-cited journals, *IOVS* published the most papers, followed by *Retina, EJO, and AJO*. The average number of citations for each document is up to 20 times, which fully indicates that researchers obtained international recognition in this field. Co-citation analysis revealed that *Ophthalmology* had been the most co-cited journal (**Table 2**), with the highest impact factor. Indeed, more than half of the 12 top-cited

references in this field were published in *Ophthalmology* (**Table 5**), all about clinical trials regarding DEX implants (Haller et al., 2010; Haller et al., 2011; Boyer et al., 2014), IVTA (Antcliff et al., 2001; Martidis et al., 2002; Massin et al., 2004), and FA inserts (Campochiaro et al., 2012). These studies significantly promote the safety and efficacy of steroids use in treating of macular edema.

Keywords can provide immediate information about hotspots in the field. Word analysis can show how the research concepts evolve during a period. In our study, keywords analysis showed that the high-frequency keywords belong to the disease category (including DME, RVO) and therapy category (including TA, DEX implant, and VEGF-related terms). Interestingly, intravitreal implant and VEGF-related terms were among these top keywords and had bursts recently (**Figure 3B**). These keywords captured this field's current and future direction (Sacconi et al., 2019). Anti-VEGF agents, including bevacizumab, ranibizumab, and aflibercept, are the first-line treatment for DME (Brown et al., 2013; Wells et al., 2015) and macular edema secondary to RVO (Boyer et al., 2012; Holz et al., 2013; Schmidt-Erfurth et al., 2019). While they are more effective and have fewer side effects than steroids (Gao et al., 2019), a significant proportion of patients do not respond well and repeated intravitreal injections are required to maintain the visual benefits (Engman et al., 2011). Steroids generally only have short-term effects, but new DEX and FA sustained-release devices have been developed, such as Ozurdex (DEX implant), Iluvien (FA implant), and YUTIQ (FA implant) (Testi and Pavesio, 2019; McGregor et al., 2021), which offer a longer duration of action and can reduce the number of intravitreal injections required (DEX for 4–6 months; FA for 3 years) (Bandello et al., 2014). These steroids implants or inserts are commonly used as a second-line treatment for DME patients without significant response to anti-VEGF therapies (Tan et al., 2017; He et al., 2018; Fallico et al., 2021), but are also considered as valid therapeutic options in the treatment of RVO-induced macular edema because of their anti-inflammatory, anti-angiogenic, and anti-edema properties (Haller et al., 2010; Haller et al., 2011; Castro-Navarro et al., 2021). Although some patients require repeated steroid injections, the long duration between treatments is still a considerable advantage of these drugs (Scaramuzzi et al., 2015).

Betweenness centrality results from cluster analysis of co-citation network identified important papers about complications of ocular steroids treatment (**Table 6**). Although CMV retinitis was mainly reported almost 20 years ago based on the timeline-cluster map (**Figure 3D**), it was frequently reported recently in patients receiving intravitreal injection of steroids (such as IVTA) or steroids implants (Jaissle et al., 2004; Saidel et al., 2005; Ufret-Vincenty et al., 2007; Witmer and Connolly, 2021). Increased intraocular pressure (IOP) and cataract formation are common side effects of various types of steroids (Jonas et al., 2005b; Yang et al., 2015). According to a Cochrane systematic review, cataracts progressed in 5 or 6 out of 10 patients treated with steroids, and IOP increased in roughly 3 out of 10 patients, which is significantly greater than the control group (Rittiphairoj et al., 2020). These possible side effects must be carefully monitored when using steroids to treat macular edema.

By systematically combining the publications during the past three decades, we show the dynamic development process, hotspots, research trends, and structural relationship of different aspects of steroids treatment of macular edema. There are some limits to this study. First, the analysis of this study is only based on publications in the WOS core collection database. Although this collection includes most of the research publications in this field, other databases may provide broader coverage, such as PubMed and Scopus. Second, the research results of this paper are completed based on CiteSpace and VOSviewer, and the machine algorithm may not be perfect and can induce some bias. For instance, IVTA is a major cluster in the keyword and cluster analysis (**Figures 3C,D**), DEX and FA, on the other hand, are only found on the periphery of the term visualization map and do not even make the top ten in cluster analysis. However, the number of IVTA publications has decreased dramatically, while DEX and FA implants have received increasing attention in recent clinical trials (Castro-Navarro et al., 2021; Fallico et al., 2021). This trend has not been captured in our study.

Combined therapy with anti-VEGF and suprachoroidal corticosteroids may overcome the limits of both agents and increase the therapeutic efficacy (Sacconi et al., 2019). Our study also misses this trend, as many new clinical trials on these strategies are currently being conducted, and results are not published yet. More outcomes from these trials will help us build a better approach for treating macular edema in the future after balancing the benefits and limits of various therapeutic strategies and the patient's medical needs.

5 CONCLUSION

We are at the second research wave of using steroids to treat macular edema with more than 200 publications every year. The United States and Europe led in this field by contributing the most important papers. Papers published in a specialty journal such as *Ophthalmology* will attract more attention than papers published in comprehensive journals. While anti-VEGF therapy is the first-line treatment for DME and RVO-induced macular edema, steroids implant is a valid option for these DME patients not responding to anti-VEGF therapy and non-DME patients with macular edema. Combined therapy with anti-VEGF and steroids agents is essential for future research.

DATA AVAILABILITY STATEMENT

The raw data supporting the conclusions of this article will be made available by the authors, without undue reservation.

AUTHOR CONTRIBUTIONS

YL and DC designed the study. All authors conducted the literature search and analyzed the data. YL, XR, and DC wrote and revised the manuscript. All authors contributed to the article and approved the submitted version.

FUNDING

This work was supported by grants to DC from the National Natural Science Foundation of China (81870665, 82171063).

REFERENCES

Abbasi, A., Altmann, J., and Hossain, L. (2011). Identifying the Effects of Co-authorship Networks on the Performance of Scholars: A Correlation and Regression Analysis of Performance Measures and Social Network Analysis Measures. *J. Informetrics* 5, 594–607. doi:10.1016/j.joi.2011.05.007

Aksu-Ceylan, N., Cebeci, Z., Altinkurt, E., Kir, N., Oray, M., and Tugal-Tutkun, I. (2021). Interferon Alpha-2a for the Treatment of Cystoid Macular Edema Secondary to Acute Retinal Necrosis. *Ocul. Immunol. Inflamm.*, 1–10. [online ahead of print]. doi:10.1080/09273948.2021.1957121

Antcliff, R. J., Spalton, D. J., Stanford, M. R., Graham, E. M., ffytche, T. J., and Marshall, J. (2001). Intravitreal Triamcinolone for Uveitic Cystoid Macular Edema: an Optical Coherence Tomography Study. *Ophthalmology* 108 (4), 765–772. doi:10.1016/s0161-6420(00)00658-8

Aref, A. A., Scott, I. U., VanVeldhuisen, P. C., King, J., Ip, M. S., Blodi, B. A., et al. (2021). Intraocular Pressure-Related Events after Anti-vascular Endothelial Growth Factor Therapy for Macular Edema Due to Central Retinal Vein Occlusion or Hemiretinal Vein Occlusion: SCORE2 Report 16 on a Secondary Analysis of a Randomized Clinical Trial. *JAMA Ophthalmol.* 139, 1285–1291. doi:10.1001/jamaophthalmol.2021.4395

Bandello, F., Preziosa, C., Querques, G., and Lattanzio, R. (2014). Update of Intravitreal Steroids for the Treatment of Diabetic Macular Edema. *Ophthalmic Res.* 52 (2), 89–96. doi:10.1159/000362764

Boyer, D., Heier, J., Brown, D. M., Clark, W. L., Vitti, R., Berliner, A. J., et al. (2012). Vascular Endothelial Growth Factor Trap-Eye for Macular Edema Secondary to central Retinal Vein Occlusion: Six-Month Results of the Phase 3 COPERNICUS Study. *Ophthalmology* 119 (5), 1024–1032. doi:10.1016/j.ophtha.2012.01.042

Boyer, D. S., Faber, D., Gupta, S., Patel, S. S., Tabandeh, H., Li, X. Y., et al. (2011). Dexamethasone Intravitreal Implant for Treatment of Diabetic Macular Edema in Vitrectomized Patients. *Retina* 31 (5), 915–923. doi:10.1097/IAE.0b013e318206d18c

Boyer, D. S., Yoon, Y. H., Belfort, R., Bandello, F., Maturi, R. K., Augustin, A. J., et al. (2014). Three-year, Randomized, Sham-Controlled Trial of Dexamethasone Intravitreal Implant in Patients with Diabetic Macular Edema. *Ophthalmology* 121 (10), 1904–1914. doi:10.1016/j.ophtha.2014.04.024

Brown, D. M., Campochiaro, P. A., Bhisitkul, R. B., Ho, A. C., Gray, S., Saroj, N., et al. (2011). Sustained Benefits From Ranibizumab for Macular Edema Following Branch Retinal Vein Occlusion: 12-Month Outcomes of a Phase III Study. *Ophthalmology* 118 (8), 1594–1602. doi:10.1016/j.ophtha.2011.02.022

Brown, D. M., Campochiaro, P. A., Singh, R. P., Li, Z., Gray, S., Saroj, N., et al. (2010). Ranibizumab for Macular Edema Following Central Retinal Vein Occlusion: Six-Month Primary End Point Results of a Phase III Study. *Ophthalmology* 117 (6), 1124–1133.e1. doi:10.1016/j.ophtha.2010.02.022

Brown, D. M., Nguyen, Q. D., Marcus, D. M., Boyer, D. S., Patel, S., Feiner, L., et al. (2013). Long-term Outcomes of Ranibizumab Therapy for Diabetic Macular Edema: the 36-month Results from Two Phase III Trials: RISE and RIDE. *Ophthalmology* 120 (10), 2013–2022. doi:10.1016/j.ophtha.2013.02.034

Bucolo, C., Gozzo, L., Longo, L., Mansueto, S., Vitale, D. C., and Drago, F. (2018). Long-term Efficacy and Safety Profile of Multiple Injections of Intravitreal Dexamethasone Implant to Manage Diabetic Macular Edema: A Systematic Review of Real-World Studies. *J. Pharmacol. Sci.* 138 (4), 219–232. doi:10.1016/j.jphs.2018.11.001

Campochiaro, P. A., Brown, D. M., Awh, C. C., Lee, S. Y., Gray, S., Saroj, N., et al. (2011). Sustained Benefits From Ranibizumab for Macular Edema Following Central Retinal Vein Occlusion: Twelve-Month Outcomes of a Phase III Study. *Ophthalmology* 118 (10), 2041–2049. doi:10.1016/j.ophtha.2011.02.038

Campochiaro, P. A., Brown, D. M., Pearson, A., Chen, S., Boyer, D., Ruiz-Moreno, J., et al. (2012). Sustained Delivery Fluocinolone Acetonide Vitreous Inserts Provide Benefit for at Least 3 Years in Patients with Diabetic Macular Edema. *Ophthalmology* 119 (10), 2125–2132. doi:10.1016/j.ophtha.2012.04.030

Campochiaro, P. A., Heier, J. S., Feiner, L., Gray, S., Saroj, N., Rundle, A. C., et al. (2010). Ranibizumab for Macular Edema Following Branch Retinal Vein Occlusion: Six-Month Primary End Point Results of a Phase III Study. *Ophthalmology* 117 (6), 1102–1112.e1. doi:10.1016/j.ophtha.2010.02.021

Castro-Navarro, V., Monferrer-Adsuara, C., Navarro-Palop, C., Montero-Hernández, J., and Cervera-Taulet, E. (2021). Effect of Dexamethasone Intravitreal Implant on Visual Acuity and Foveal Photoreceptor Integrity in Macular Edema Secondary to Retinal Vascular Disease. *Ophthalmologica* 244 (1), 83–92. doi:10.1159/000512195

Capone, A., Jr, Singer, M. A., Dodwell, D. G., Dreyer, R. F., Oh, K. T., Roth, D. B., et al. (2014). Efficacy and Safety of Two or More Dexamethasone Intravitreal Implant Injections for Treatment of Macular Edema Related to Retinal Vein Occlusion (Shasta Study). *Retina* 34 (2), 342–351. doi:10.1097/IAE.0b013e318297f842

Challa, J. K., Gillies, M. C., Penfold, P. L., Gyory, J. F., Hunyor, A. B., and Billson, F. A., (1998). Exudative Macular Degeneration and Intravitreal Triamcinolone: 18 Month Follow Up. *Aust. N. Z. J. Ophthalmol.* 26 (4), 277–281. doi:10.1111/j.1442-9071.1998.tb01330.x

Chang-Lin, J. E., Attar, M., Acheampong, A. A., Robinson, M. R., Whitcup, S. M., Kuppermann, B. D., et al. (2011). Pharmacokinetics and Pharmacodynamics of a Sustained-Release Dexamethasone Intravitreal Implant. *Invest. Ophthalmol. Vis. Sci.* 52 (1), 80–86. doi:10.1167/iovs.10-5285

Chen, C., Dubin, R., and Kim, M. C. (2014). Emerging Trends and New Developments in Regenerative Medicine: a Scientometric Update (2000 - 2014). *Expert Opin. Biol. Ther.* 14 (9), 1295–1317. doi:10.1517/14712598.2014.920813

Chen, C., Hu, Z., Liu, S., and Tseng, H. (2012). Emerging Trends in Regenerative Medicine: a Scientometric Analysis in CiteSpace. *Expert Opin. Biol. Ther.* 12 (5), 593–608. doi:10.1517/14712598.2012.674507

Chen, C. (2017). Science Mapping: A Systematic Review of the Literature. *J. Data Inf. Sci.* 2 (2), 1–40. doi:10.1515/jdis-2017-0006

Chung, S. T. L. (2020). Reading in the Presence of Macular Disease: a Mini-Review. *Ophthalmic Physiol. Opt.* 40 (2), 171–186. doi:10.1111/opo.12664

Cukras, C. A., Petrou, P., Chew, E. Y., Meyerle, C. B., and Wong, W. T. (2012). Oral Minocycline for the Treatment of Diabetic Macular Edema (DME): Results of a Phase I/II Clinical Study. *Invest. Ophthalmol. Vis. Sci.* 53 (7), 3865–3874. doi:10.1167/iovs.11-9413

Cunningham, M. A., Edelman, J. L., and Kaushal, S. (2008). Intravitreal Steroids for Macular Edema: the Past, the Present, and the Future. *Surv. Ophthalmol.* 53 (2), 139–149. doi:10.1016/j.survophthal.2007.12.005

Daruich, A., Matet, A., Moulin, A., Kowalczuk, L., Nicolas, M., Sellam, A., et al. (2018). Mechanisms of Macular Edema: Beyond the Surface. *Prog. Retin. Eye Res.* 63, 20–68. doi:10.1016/j.preteyeres.2017.10.006

Distefano, L. N., Garcia-Arumi, J., Martinez-Castillo, V., and Boixadera, A. (2017). Combination of Anti-VEGF and Laser Photocoagulation for Diabetic Macular Edema: A Review. *J. Ophthalmol.* 2017, 2407037. doi:10.1155/2017/2407037

Engman, S. J., Edwards, A. O., and Bakri, S. J. (2011). Administration of Repeat Intravitreal Anti-VEGF Drugs by Retina Specialists in an Injection-Only Clinic for Patients with Exudative AMD: Patient Acceptance and Safety. *Semin. Ophthalmol.* 26 (6), 380–386. doi:10.3109/08820538.2011.622337

Fallico, M., Maugeri, A., Lotery, A., Longo, A., Bonfiglio, V., Russo, A., et al. (2021). Fluocinolone Acetonide Vitreous Insert for Chronic Diabetic Macular Oedema: a Systematic Review with Meta-Analysis of Real-World Experience. *Sci. Rep.* 11 (1), 4800. doi:10.1038/s41598-021-84362-y

Feltgen, N., Pielen, A., Hansen, L., Bertram, B., Agostini, H., Jaissle, G. B., et al. (2010). [Intravitreal Drug Therapy for Retinal Vein Occlusion–Pathophysiological Mechanisms and Routinely Used Drugs]. *Klin. Monbl. Augenheilkd.* 227 (9), 681–693. doi:10.1055/s-0029-1245606

Gaballa, S. A., Kompella, U. B., Elgarhy, O., Alqahtani, A. M., Pierscionek, B., Alany, R. G., et al. (2021). Corticosteroids in Ophthalmology: Drug Delivery Innovations, Pharmacology, Clinical Applications, and Future Perspectives. *Drug Deliv. Transl Res.* 11 (3), 866–893. doi:10.1007/s13346-020-00843-z

Gao, L., Zhou, L., Tian, C., Li, N., Shao, W., Peng, X., et al. (2019). Intravitreal Dexamethasone Implants versus Intravitreal Anti-VEGF Treatment in Treating Patients with Retinal Vein Occlusion: a Meta-Analysis. *BMC Ophthalmol.* 19 (1), 8. doi:10.1186/s12886-018-1016-7

Gillies, M. C., Sutter, F. K., Simpson, J. M., Larsson, J., Ali, H., and Zhu, M. (2006). Intravitreal Triamcinolone for Refractory Diabetic Macular Edema: Two-Year Results of a Double-Masked, Placebo-Controlled, Randomized Clinical Trial. *Ophthalmology* 113 (9), 1533–1538. doi:10.1016/j.ophtha.2006.02.065

Greenberg, P. B., Martidis, A., Rogers, A. H., Duker, J. S., and Reichel, E. (2002). Intravitreal Triamcinolone Acetonide for Macular Oedema Due to central Retinal Vein Occlusion. *Br. J. Ophthalmol.* 86 (2), 247–248. doi:10.1136/bjo.86.2.247

Gu, X., Xie, M., Jia, R., and Ge, S. (2021). Publication Trends of Research on Retinoblastoma during 2001-2021: A 20-Year Bibliometric Analysis. *Front. Med. (Lausanne)* 8, 675703. doi:10.3389/fmed.2021.675703

Guler, A. T., Waaijer, C. J., and Palmblad, M. (2016). Scientific Workflows for Bibliometrics. *Scientometrics* 107, 385–398. doi:10.1007/s11192-016-1885-6

Haller, J. A., Bandello, F., Belfort, R., Blumenkranz, M. S., Gillies, M., Heier, J., et al. (2010). Randomized, Sham-Controlled Trial of Dexamethasone Intravitreal Implant in Patients with Macular Edema Due to Retinal Vein Occlusion. *Ophthalmology* 117 (6), 1134–1146. doi:10.1016/j.ophtha.2010.03.032

Haller, J. A., Bandello, F., Belfort, R., Blumenkranz, M. S., Gillies, M., Heier, J., et al. (2011). Dexamethasone Intravitreal Implant in Patients with Macular Edema Related to branch or central Retinal Vein Occlusion Twelve-Month Study Results. *Ophthalmology* 118 (12), 2453–2460. doi:10.1016/j.ophtha.2011.05.014

He, Y., Ren, X. J., Hu, B. J., Lam, W. C., and Li, X. R. (2018). A Meta-Analysis of the Effect of a Dexamethasone Intravitreal Implant versus Intravitreal Anti-vascular Endothelial Growth Factor Treatment for Diabetic Macular Edema. *BMC Ophthalmol.* 18 (1), 121. doi:10.1186/s12886-018-0779-1

Heiligenhaus, A., Bertram, B., Heinz, C., Krause, L., Pleyer, U., Roider, J., et al. (2014). [Statement of the German Ophthalmological Society, the Retina Society and the Professional Association of German Ophthalmologists for Intravitreal Treatment of Macular Edema in Uveitis: Date: 02/07/2014]. *Ophthalmologe* 111 (8), 740–748. doi:10.1007/s00347-014-3130-0

Holz, F. G., Roider, J., Ogura, Y., Korobelnik, J. F., Simader, C., Groetzbach, G., et al. (2013). VEGF Trap-Eye for Macular Oedema Secondary to central Retinal Vein Occlusion: 6-month Results of the Phase III GALILEO Study. *Br. J. Ophthalmol.* 97 (3), 278–284. doi:10.1136/bjophthalmol-2012-301504

Hykin, P., Prevost, A. T., Sivaprasad, S., Vasconcelos, J. C., Murphy, C., Kelly, J., et al. (2021). Intravitreal Ranibizumab versus Aflibercept versus Bevacizumab for Macular Oedema Due to central Retinal Vein Occlusion: the LEAVO Non-inferiority Three-Arm RCT. *Health Technol. Assess.* 25 (38), 1–196. doi:10.3310/hta25380

Ip, M. S., Scott, I. U., Vanveldhuisen, P. C., Oden, N. L., Blodi, B. A., Fisher, M., et al. (2009). A Randomized Trial Comparing the Efficacy and Safety of Intravitreal Triamcinolone With Observation to Treat Vision Loss Associated With Macular Edema Secondary to Central Retinal Vein Occlusion: The Standard Care vs. Corticosteroid for Retinal Vein Occlusion (SCORE) Study Report 5. *Arch. Ophthalmol.* 127 (9), 1101–1114. doi:10.1001/archophthalmol.2009.234

Iturralde, D., Spaide, R. F., Meyerle, C. B., Klancnik, J. M., Yannuzzi, L. A., Fisher, Y. L., et al. (2006). Intravitreal Bevacizumab (Avastin) Treatment of Macular Edema in Central Retinal Vein Occlusion: A Short-Term Study. *Retina* 26 (3), 279–284. doi:10.1097/00006982-200603000-00005

Jaissle, G. B., Szurman, P., and Bartz-Schmidt, K. U. (2004). Ocular Side Effects and Complications of Intravitreal Triamcinolone Acetonide Injection. *Ophthalmologe* 101 (2), 121–128. doi:10.1007/s00347-003-0975-z

Jonas, J. B., Degenring, R. F., Kreissig, I., Akkoyun, I., and Kamppeter, B. A. (2005). Intraocular Pressure Elevation after Intravitreal Triamcinolone Acetonide Injection. *Ophthalmology* 112 (4), 593–598. doi:10.1016/j.ophtha.2004.10.042

Jonas, J. B. (2005). Intravitreal Triamcinolone Acetonide for Treatment of Intraocular Oedematous and Neovascular Diseases. *Acta Ophthalmol. Scand.* 83 (6), 645–663. doi:10.1111/j.1600-0420.2005.00592.x

Jonas, J. B. (2006). Intravitreal Triamcinolone Acetonide: a Change in a Paradigm. *Ophthalmic Res.* 38 (4), 218–245. doi:10.1159/000093796

Jonas, J. B., Kamppeter, B. A., Harder, B., Vossmerbaeumer, U., Sauder, G., and Spandau, U. H. (2006). Intravitreal Triamcinolone Acetonide for Diabetic Macular Edema: a Prospective, Randomized Study. *J. Ocul. Pharmacol. Ther.* 22 (3), 200–207. doi:10.1089/jop.2006.22.200

Jonas, J. B., Kreissig, I., and Degenring, R. (2003). Intraocular Pressure after Intravitreal Injection of Triamcinolone Acetonide. *Br. J. Ophthalmol.* 87 (1), 24–27. doi:10.1136/bjo.87.1.24

Jonas, J. B., Kreissig, I., and Degenring, R. (2005). Intravitreal Triamcinolone Acetonide for Treatment of Intraocular Proliferative, Exudative, and Neovascular Diseases. *Prog. Retin. Eye Res.* 24 (5), 587–611. doi:10.1016/j.preteyeres.2005.01.004

Jonas, J. B., Kreissig, I., and Degenring, R. F. (2003). Treatment of Oedematous, Proliferative and Neovascular Diseases by Intravitreal Triamcinolone Acetonide. *Klin Monbl Augenheilkd* 220 (6), 384–390. doi:10.1055/s-2003-40272

Jonas, J. B., Kreissig, I., Kamppeter, B., and Degenring, R. F. (2004). Intravitreal Triamcinolone Acetonide for the Treatment of Intraocular Edematous and Neovascular Diseases. *Ophthalmologe* 101 (2), 113–120. doi:10.1007/s00347-003-0982-0

Jonas, J. B., Kreissig, I., Söfker, A., and Degenring, R. F. (2003). Intravitreal Injection of Triamcinolone for Diffuse Diabetic Macular Edema. *Arch. Ophthalmol.* 121 (1), 57–61. doi:10.1001/archopht.121.1.57

Jonas, J. B., and Söfker, A. (2001). Intraocular Injection of Crystalline Cortisone as Adjunctive Treatment of Diabetic Macular Edema. *Am. J. Ophthalmol.* 132 (3), 425–427. doi:10.1016/s0002-9394(01)01010-8

Karim, R., Sykakis, E., Lightman, S., and Fraser-Bell, S. (2013). Interventions for the Treatment of Uveitic Macular Edema: a Systematic Review and Meta-Analysis. *Clin. Ophthalmol.* 7, 1109–1144. doi:10.2147/OPTH.S40268

Khurana, R. N., Appa, S. N., Mccannel, C. A., Elman, M. J., Wittenberg, S. E., Parks, D. J., et al. (2014). Dexamethasone Implant Anterior Chamber Migration: Risk Factors, Complications, and Management Strategies. *Ophthalmology* 121 (1), 67–71. doi:10.1016/j.ophtha.2013.06.033

Kiddee, W., Trope, G. E., Sheng, L., Beltran-Agullo, L., Smith, M., Strungaru, M. H., et al. (2013). Intraocular Pressure Monitoring Post Intravitreal Steroids: A Systematic Review. *Surv. Ophthalmol.* 58 (4), 291–310. doi:10.1016/j.survophthal.2012.08.003

Kuppermann, B. D., Blumenkranz, M. S., Haller, J. A., Williams, G. A., Weinberg, D. V., Chou, C., et al. (2007). Randomized Controlled Study of an Intravitreous Dexamethasone Drug Delivery System in Patients With Persistent Macular Edema. *Arch. Ophthalmol.* 125 (3), 309–317. doi:10.1001/archopht.125.3.309

Lambiase, A., Abdolrahimzadeh, S., and Recupero, S. M., (2014). An Update on Intravitreal Implants in Use for Eye Disorders. *Drugs Today (Barc)* 50 (3), 239–249. doi:10.1358/dot.2014.50.3.2103755

Lang, G. E. (2012). Diabetic Macular Edema. *Ophthalmologica* 227 (Suppl. 1), 21–29. doi:10.1159/000337156

Lowder, C., Belfort, R., Lightman, S., Foster, C. S., Robinson, M. R., Schiffman, R. M., et al. (2011). Dexamethasone Intravitreal Implant for Noninfectious Intermediate or Posterior Uveitis. *Arch. Ophthalmol.* 129 (5), 545–553. doi:10.1001/archophthalmol.2010.339

Ma, D., Guan, B., Song, L., Liu, Q., Fan, Y., Zhao, L., et al. (2021). A Bibliometric Analysis of Exosomes in Cardiovascular Diseases from 2001 to 2021. *Front. Cardiovasc. Med.* 8, 734514. doi:10.3389/fcvm.2021.734514

Mahdy, R. A. R., Saleh, M. M., and Almasalamy, S. M. (2010). Laser Photocoagulation versus Combined Laser Photocoagulation and Posterior Sub-tenon's Triamcinolone Injection for the Primary Treatment of Diffuse Diabetic Macular Edema. *Cutan. Ocul. Toxicol.* 29 (2), 91–97. doi:10.3109/15569521003587335

Martidis, A., Duker, J. S., Greenberg, P. B., Rogers, A. H., Puliafito, C. A., Reichel, E., et al. (2002). Intravitreal Triamcinolone for Refractory Diabetic Macular Edema. *Ophthalmology* 109 (5), 920–927. doi:10.1016/s0161-6420(02)00975-2

Massin, P., Audren, F., Haouchine, B., Erginay, A., Bergmann, J. F., Benosman, R., et al. (2004). Intravitreal Triamcinolone Acetonide for Diabetic Diffuse Macular Edema: Preliminary Results of a Prospective Controlled Trial. *Ophthalmology* 111 (2), 1–5. doi:10.1016/j.ophtha.2003.05.037

McGregor, F., Dick, A. D., and Burke, T. (2021). Achieving Quiescence with Fluocinolone Implants. *Case Rep. Ophthalmol.* 12 (2), 356–362. doi:10.1159/000513221

Melberg, N. S., and Olk, R. J. (1993). Corticosteroid-induced Ocular Hypertension in the Treatment of Aphakic or Pseudophakic Cystoid Macular Edema. *Ophthalmology* 100 (2), 164–167. doi:10.1016/s0161-6420(93)31675-1

Mohan, S., Chawla, G., Surya, J., and Raman, R. (2021). Intravitreal Anti-vascular Endothelial Growth Factor with and without Topical Non-steroidal Anti-inflammatory in centre-involving Diabetic Macular Edema. *Indian J. Ophthalmol.* 69 (11), 3279–3282. doi:10.4103/ijo.IJO_1465_21

Mueller, P. S., Murali, N. S., Cha, S. S., Erwin, P. J., and Ghosh, A. K. (2006). The Effect of Online Status on the Impact Factors of General Internal Medicine Journals. *Neth. J. Med.* 64 (2), 39–44. https://www.njmonline.nl/getpdf.php?id=386

Nguyen, Q. D., Brown, D. M., Marcus, D. M., Boyer, D. S., Patel, S., Feiner, L., et al. (2012). Ranibizumab for Diabetic Macular Edema: Results From 2 Phase III Randomized Trials: RISE and RIDE. *Ophthalmology* 119 (4), 789–801. doi:10.1016/j.ophtha.2011.12.039

Nussenblatt, R. B., Palestine, A. G., Chan, C. C., Stevens, G., Mellow, S. D., and Green, S. B. (1991). Randomized, Double-Masked Study of Cyclosporine Compared to Prednisolone in the Treatment of Endogenous Uveitis. *Am. J. Ophthalmol.* 112 (2), 138–146. doi:10.1016/s0002-9394(14)76692-9

Prager, F., Michels, S., Kriechbaum, K., Georgopoulos, M., Funk, M., Geitzenauer, W., et al. (2009). Intravitreal Bevacizumab (Avastin) for Macular Oedema Secondary to Retinal Vein Occlusion: 12-Month Results of a Prospective Clinical Trial. *Br. J. Ophthalmol.* 93 (4), 452–456. doi:10.1136/bjo.2008.141085

Rabena, M. D., Pieramici, D. J., Castellarin, A. A., Nasir, M. A., and Avery, R. L, (2007). Intravitreal Bevacizumab (Avastin) in the Treatment of Macular Edema

Secondary to Branch Retinal Vein Occlusion. *Retina* 27 (4), 419–425. doi:10.1097/IAE.0b013e318030e77e

Rittiphairoj, T., Mir, T. A., Li, T., and Virgili, G. (2020). Intravitreal Steroids for Macular Edema in Diabetes. *Cochrane Database Syst. Rev.* 11, CD005656. doi:10.1002/14651858.CD005656.pub3

Rogers, S., McIntosh, R. L., Cheung, N., Lim, L., Wang, J. J., Mitchell, P., et al. (2010). The Prevalence of Retinal Vein Occlusion: Pooled Data from Population Studies from the United States, Europe, Asia, and Australia. *Ophthalmology* 117 (2), 313–319. doi:10.1016/j.ophtha.2009.07.017

Romero-Aroca, P. (2015). Is Laser Photocoagulation Treatment Currently Useful in Diabetic Macular Edema? *Med. Hypothesis Discov. Innov. Ophthalmol.* 4 (1), 5–8.

Rosenfeld, P. J., Brown, D. M., Heier, J. S., Boyer, D. S., Kaiser, P. K., Chung, C. Y., et al. (2006). Ranibizumab for Neovascular Age-Related Macular Degeneration. *N. Engl. J. Med.* 355 (14), 1419–1431. doi:10.1056/NEJMoa054481

Rosenfeld, P. J., Fung, A. E., and Puliafito, C. A., (2005). Optical Coherence Tomography Findings After an Intravitreal Injection of Bevacizumab (Avastin) for Macular Edema From Central Retinal Vein Occlusion. *Ophthalmic. Surg. Lasers Imaging* 36 (4), 336–339.

Rothova, A., Suttorp-van Schulten, M. S., Frits Treffers, W., and Kijlstra, A. (1996). Causes and Frequency of Blindness in Patients with Intraocular Inflammatory Disease. *Br. J. Ophthalmol.* 80 (4), 332–336. doi:10.1136/bjo.80.4.332

Sacconi, R., Giuffrè, C., Corbelli, E., Borrelli, E., Querques, G., and Bandello, F. (2019). Emerging Therapies in the Management of Macular Edema: a Review. *F1000Research* 8, F1000 Faculty Rev-1413. doi:10.12688/f1000research.19198.1

Saidel, M. A., Berreen, J., and Margolis, T. P. (2005). Cytomegalovirus Retinitis after Intravitreous Triamcinolone in an Immunocompetent Patient. *Am. J. Ophthalmol.* 140 (6), 1141–1143. doi:10.1016/j.ajo.2005.06.058

Sarao, V., Veritti, D., Boscia, F., and Lanzetta, P. (2014). Intravitreal Steroids for the Treatment of Retinal Diseases. *ScientificWorldJournal* 2014, 989501. doi:10.1155/2014/989501

Scaramuzzi, M., Querques, G., Spina, C. L., Lattanzio, R., and Bandello, F. (2015). Repeated Intravitreal Dexamethasone Implant (Ozurdex) for Diabetic Macular Edema. *Retina* 35 (6), 1216–1222. doi:10.1097/IAE.0000000000000443

Schmidt-Erfurth, U., Garcia-Arumi, J., Gerendas, B. S., Midena, E., Sivaprasad, S., Tadayoni, R., et al. (2019). Guidelines for the Management of Retinal Vein Occlusion by the European Society of Retina Specialists (EURETINA). *Ophthalmologica* 242 (3), 123–162. doi:10.1159/000502041

Scott, I. U., Ip, M. S., Vanveldhuisen, P. C., Oden, N. L., Blodi, B. A., Fisher, M., et al. (2009). A Randomized Trial Comparing the Efficacy and Safety of Intravitreal Triamcinolone With Standard Care to Treat Vision Loss Associated With Macular Edema Secondary to Branch Retinal Vein Occlusion: The Standard Care vs. Corticosteroid for Retinal Vein Occlusion (SCORE) Study Report 6. *Arch. Ophthalmol.* 127 (9), 1115–1128. doi:10.1001/archophthalmol.2009.233

Shaw, L. T., Mackin, A., Shah, R., Jain, S., Jain, P., Nayak, R., et al. (2020). Risuteganib-a Novel Integrin Inhibitor for the Treatment of Non-exudative (Dry) Age-Related Macular Degeneration and Diabetic Macular Edema. *Expert Opin. Investig. Drugs* 29 (6), 547–554. doi:10.1080/13543784.2020.1763953

Shimura, M., Kitano, S., Muramatsu, D., Fukushima, H., Takamura, Y., Matsumoto, M., et al. (2020). Real-world Management of Treatment-Naïve Diabetic Macular Oedema: 2-year Visual Outcome Focusing on the Starting Year of Intervention from STREAT-DMO Study. *Br. J. Ophthalmol.* 104 (12), 1755–1761. doi:10.1136/bjophthalmol-2019-315726

Simó, R., Sundstrom, J. M., and Antonetti, D. A. (2014). Ocular Anti-VEGF Therapy for Diabetic Retinopathy: the Role of VEGF in the Pathogenesis of Diabetic Retinopathy. *Diabetes care* 37 (4), 893–899. doi:10.2337/dc13-2002

Smith, A. G., and Kaiser, P. K. (2014). Emerging Treatments for Wet Age-Related Macular Degeneration. *Expert Opin. Emerg. Drugs* 19 (1), 157–164. doi:10.1517/14728214.2014.884559

Suckling, R. D., and Maslin, K. F. (1988). Pseudophakic Cystoid Macular Oedema and its Treatment with Local Steroids. *Aust. N. Z. J. Ophthalmol.* 16 (4), 353–359. doi:10.1111/j.1442-9071.1988.tb01241.x

Supuran, C. T. (2019). Agents for the Prevention and Treatment of Age-Related Macular Degeneration and Macular Edema: a Literature and Patent Review. *Expert Opin. Ther. Pat* 29 (10), 761–767. doi:10.1080/13543776.2019.1671353

Sutter, F. K., Simpson, J. M., and Gillies, M. C. (2004). Intravitreal Triamcinolone for Diabetic Macular Edema that Persists after Laser Treatment: Three-Month Efficacy and Safety Results of a Prospective, Randomized, Double-Masked, Placebo-Controlled Clinical Trial. *Ophthalmology* 111 (11), 2044–2049. doi:10.1016/j.ophtha.2004.05.025

Tan, G. S., Cheung, N., Simó, R., Cheung, G. C., and Wong, T. Y. (2017). Diabetic Macular Oedema. *Lancet Diabetes Endocrinol.* 5 (2), 143–155. doi:10.1016/S2213-8587(16)30052-3

Tappeiner, C., Bae, H. S., Rothaus, K., Walscheid, K., and Heiligenhaus, A. (2021). Occurrence and Risk Factors for Macular Edema in Patients with Juvenile Idiopathic Arthritis-Associated Uveitis. *J. Clin. Med.* 10 (19), 4513. doi:10.3390/jcm10194513

Testi, I., and Pavesio, C. (2019). Preliminary Evaluation of YUTIQ™ (Fluocinolone Acetonide Intravitreal Implant 0.18 mg) in Posterior Uveitis. *Ther. Deliv.* 10 (10), 621–625. doi:10.4155/tde-2019-0051

Thompson, J. T., (2006). Cataract Formation and Other Complications of Intravitreal Triamcinolone for Macular Edema. *Am. J. Ophthalmol.* 141 (4), 629–637. doi:10.1016/j.ajo.2005.11.050

Tomkins-Netzer, O., Taylor, S. R., Bar, A., Lula, A., Yaganti, S., Talat, L., et al. (2014). Treatment With Repeat Dexamethasone Implants Results in Long-Term Disease Control in Eyes With Noninfectious Uveitis. *Ophthalmology* 121 (8), 1649–1654. doi:10.1016/j.ophtha.2014.02.003

Ufret-Vincenty, R. L., Singh, R. P., Lowder, C. Y., and Kaiser, P. K. (2007). Cytomegalovirus Retinitis after Fluocinolone Acetonide (Retisert) Implant. *Am. J. Ophthalmol.* 143 (2), 334–335. doi:10.1016/j.ajo.2006.09.020

van Eck, N. J., and Waltman, L. (2010). Software Survey: VOSviewer, a Computer Program for Bibliometric Mapping. *Scientometrics* 84 (2), 523–538. doi:10.1007/s11192-009-0146-3

Welfer, D., Scharcanski, J., and Marinho, D. R. (2011). Fovea center Detection Based on the Retina Anatomy and Mathematical Morphology. *Comput. Methods Programs Biomed.* 104 (3), 397–409. doi:10.1016/j.cmpb.2010.07.006

Wells, J. A., Wells, J. A., Glassman, A. R., Ayala, A. R., Jampol, L. M., Aiello, L. P., et al. (2015). Aflibercept, Bevacizumab, or Ranibizumab for Diabetic Macular Edema. *N. Engl. J. Med.* 372 (13), 1193–1203. doi:10.1056/NEJMoa1414264

Whitcup, S. M., Cidlowski, J. A., Csaky, K. G., and Ambati, J. (2018). Pharmacology of Corticosteroids for Diabetic Macular Edema. *Invest. Ophthalmol. Vis. Sci.* 59 (1), 1–12. doi:10.1167/iovs.17-22259

Wingate, R. J., and Beaumont, P. E., (1999). Intravitreal Triamcinolone and Elevated Intraocular Pressure. *Aust. N. Z. J. Ophthalmol.* 27 (6), 431–432. doi:10.1046/j.1440-1606.1999.00238.x

Witmer, M. T., and Connolly, B. P. (2021). Cytomegalovirus Retinitis after an Intravitreal Dexamethasone Implant in an Immunocompetent Patient. *Retin. cases brief Rep.* 15 (6), 670–672. doi:10.1097/icb.0000000000000904

Yang, Y., Bailey, C., Loewenstein, A., and Massin, P. (2015). Intravitreal Corticosteroids in Diabetic Macular Edema: Pharmacokinetic Considerations. *Retina* 35 (12), 2440–2449. doi:10.1097/IAE.0000000000000726

Yau, J. W., Rogers, S. L., Kawasaki, R., Lamoureux, E. L., Kowalski, J. W., Bek, T., et al. (2012). Global Prevalence and Major Risk Factors of Diabetic Retinopathy. *Diabetes care* 35 (3), 556–564. doi:10.2337/dc11-1909

Yoshikawa, K., Kotake, S., Ichiishi, A., Sasamoto, Y., Kosaka, S., and Matsuda, H. (1995). Posterior Sub-tenon Injections of Repository Corticosteroids in Uveitis Patients with Cystoid Macular Edema. *Jpn. J. Ophthalmol.* 39 (1), 71–76.

Yoshizumi, Y., Ohara, Z., Tabuchi, H., Sumino, H., Maeda, Y., Mochizuki, H., et al. (2019). Effects of Kallidinogenase in Patients Undergoing Vitrectomy for Diabetic Macular Edema. *Int. Ophthalmol.* 39 (6), 1307–1313. doi:10.1007/s10792-018-0945-8

Conflict of Interest: The authors declare that the research was conducted in the absence of any commercial or financial relationships that could be construed as a potential conflict of interest.

Publisher's Note: All claims expressed in this article are solely those of the authors and do not necessarily represent those of their affiliated organizations, or those of the publisher, the editors and the reviewers. Any product that may be evaluated in this article, or claim that may be made by its manufacturer, is not guaranteed or endorsed by the publisher.

frontiers in Pharmacology

ORIGINAL RESEARCH
published: 01 March 2022
doi: 10.3389/fphar.2022.811257

Sulforaphane Modulates the Inflammation and Delays Neurodegeneration on a Retinitis Pigmentosa Mice Model

*Antolín Canto, Javier Martínez-González, María Miranda, Teresa Olivar, Inma Almansa and Vicente Hernández-Rabaza**

Department of Biomedical Sciences, Faculty of Health Sciences, Institute of Biomedical Sciences, Cardenal Herrera-CEU University, CEU Universities, Valencia, Spain

OPEN ACCESS

Edited by:
Settimio Rossi,
Second University of Naples, Italy

Reviewed by:
Ana Isabel Arroba,
Fundación Para la Gestión de la Investigación Biomédica de Cádiz, Spain
Haiwei Xu,
Army Medical University, China

***Correspondence:**
Vicente Hernández-Rabaza
vicente.hernandez@uchceu.es

Specialty section:
This article was submitted to Inflammation Pharmacology, a section of the journal Frontiers in Pharmacology

Received: *08 November 2021*
Accepted: *03 January 2022*
Published: *01 March 2022*

Citation:
Canto A, Martínez-González J, Miranda M, Olivar T, Almansa I and Hernández-Rabaza V (2022) Sulforaphane Modulates the Inflammation and Delays Neurodegeneration on a Retinitis Pigmentosa Mice Model. Front. Pharmacol. 13:811257. doi: 10.3389/fphar.2022.811257

The term retinitis pigmentosa (RP) describes a large group of hereditary retinopathies. From a cellular view, retinal degeneration is prompted by an initial death of rods, followed later by cone degeneration. This cellular progressive degeneration is translated clinically in tunnel vision, which evolves to complete blindness. The mechanism underlying the photoreceptor degeneration is unknown, but several mechanisms have been pointed out as main co-stars, inflammation being one of the most relevant. Retinal inflammation is characterized by proliferation, migration, and morphological changes in glial cells, in both microglia and Müller cells, as well as the increase in the expression of inflammatory mediators. Retinal inflammation has been reported in several animal models and clinical cases of RP, but the specific role that inflammation plays in the pathology evolution remains uncertain. Sulforaphane (SFN) is an antioxidant natural compound that has shown anti-inflammatory properties, including the modulation of glial cells activation. The present work explores the effects of SFN on retinal degeneration and inflammation, analyzing the modulation of glial cells in the RP rd10 mice model. A daily dose of 20 mg/kg of sulforaphane was administered intraperitoneally to control (C57BL/6J wild type) and rd10 (Pde6brd10) mice, from postnatal day 14 to day 20. On postnatal day 21, euthanasia was performed. Histological retina samples were used to assess cellular degeneration, Müller cells, and microglia activation. SFN administration delayed the loss of photoreceptors. It also ameliorated the characteristic reactive gliosis, assessed by retinal GFAP expression. Moreover, sulforaphane treatment regulated the microglia activation state, inducing changes in the microglia morphology, migration, and expression through the retina. In addition, SFN modulated the expression of the interleukins 1β, 4, Ym1, and arginase inflammatory mediators. Surprisingly, M2 polarization marker expression was increased at P21 and was reduced by SFN treatment. To summarize, SFN administration reduced retinal neurodegeneration and modified the inflammatory profile of RP, which may contribute to the SFN neuroprotective effect.

Keywords: neuroinflammation, glial cells, rd10, sulforaphane, retinitis pigmentosa

INTRODUCTION

Retinitis pigmentosa (RP) englobes a range of genetic retinal diseases, which cause progressive degeneration of the photoreceptor retinal layer. It has been described that the RP induces first a cellular degeneration of rods, followed by cone degeneration (Hartong et al., 2006). This histopathology pattern produces night blindness, followed by tunnel vision, and finally a total vision loss (Hamel, 2006; Hartong et al., 2006). The RP is the main cause of blindness in young people and the main cause of hereditary blindness all over the world (Hartong et al., 2006). There is no effective cure despite this disease affecting almost 2 million people all over the world (Farrar et al., 2002; Hartong et al., 2006).

Retinal neurodegeneration induces an inflammation reaction, which has been proposed as a crucial mediator of the RP degeneration process. Neuroinflammation is characterized by vascular and glial reactions, which are translated into the production of inflammatory mediators and physiologic and morphologic glial cell activation, including the Müller cells and microglia. Furthermore, chronic inflammation plays a deleterious effect on the retinal function, as has been shown in several studies (Zabel et al., 2016). A genetic disease, such as RP, forces a genetic approach, a possibility that is not currently accessible. The reduction of inflammation research emerges as an interesting field and may provide insights into the mechanisms underlying RP development. It may also help to find new therapeutic targets to reduce the evolution and deleterious effects of RP (Fahim, 2018).

Sulforaphane (SFN) is an antioxidant natural compound (1-isothiocyanate-4-methylsulfonylmethane), found in cruciferous vegetables, that has shown antioxidant properties (Li et al., 2019; Vanduchova et al., 2019). SFN antioxidant properties are mediated by the regulation of the Nrf2 (nuclear factor erythroid 2-related factor 2) pathway. Nrf2 is a transcription factor that modulates the transcription of several antioxidant genes through its interaction with the antioxidant response elements (ARE) complex. SFN induces the Nrf2 action, increasing its cellular expression, as well as the activation and nuclear translocation of Nrf2. Nrf2 cellular level is low in health and unstressed cells, mainly by the action of Kelch-like-ECH-associated protein 1 (KEAP1), which regulates Nrf2 by ubiquitylation and proteasomal degradation. Further to the initial role of SFN as an antioxidant inductor, recent data indicated that the Nrf2/ARE pathway is involved in the regulation of inflammation, including neuroinflammation, and several metabolic derangements (He et al., 2020). These new beneficial actions of Nrf2, have replaced the focus over SFN. Recently, SFN has gained interest as a potential neuroprotective natural agent, including its possible role as an anti-inflammatory target in several neurodegenerative diseases (Li et al., 2019).

Macrophage activation is a hallmark of chronic inflammation. However, the activation of macrophages displays a gradient between proinflammatory and anti-inflammatory states, based on different inflammatory mediator profiles, as well as different proliferation, migration, and cellular morphological patterns. This gradient is dynamic, and the regulation of the macrophage activation states drives the inflammation progression and evolution (Crain et al., 2013).

Microglia cells, resident neural macrophages, show two main poles of activation, the M1 (classical, proinflammatory) and M2 (alternative, anti-inflammatory) (Crain et al., 2013). The anti-inflammatory properties of SFN have been linked with the microglia activation state regulation (Townsend and Johnson, 2016). It has been reported that SFN modulates the microglia activation states in different animal models studies. Specifically, SFN may induce the swap toward the alternative M2 anti-inflammatory state, suggesting that the beneficial SFN effects could be explained, in part, by the regulation of the microglial activation (Townsend and Johnson, 2016).

During the last two decades, SFN effects over the retina have been posted in a shortlist of spotlight studies, through *in vitro* and *in vivo* research, highlighting the SFN neuroprotective features, including beneficial reports in works on epithelial cells and oxidative stress (Dulull et al., 2018), microglial activation (Subedi et al., 2019), photoreceptor degeneration (Pan et al., 2014), retinal pigment epithelial cell degeneration, including human retinal pigment epithelium cells (ARPE-19) (Gao and Talalay, 2004; Ye et al., 2013), and models of retinal ischemia–reperfusion (Pan et al., 2014; Gong et al., 2019), as examples. Mostly all the publications pointed out the neuroprotective SFN potential through the regulation of antioxidant pathways. Recently, new publications have explored the inflammation role of SFN in diabetic retinopathy, highlighting the inhibition of the inflammasome as a mechanism (Li et al., 2019). Regarding RP, SFN has been tested in the rd10 animal model, showing a reduction in cellular degeneration and recovery of cellular retinal response, tested by electroretinography, the inhibition of reticular stress being one of the mechanisms suggested (Kang and Yu, 2017).

All these initial studies tend to confirm the SFN potential as a neuroprotective agent, but still, there are many issues to elucidate, such as the possible SFN role over glia regulation and chronic inflammation progression. In this study, we have explored the SFN effect in an animal model of RP, the rd10 mice (Pde6brd10). We have analyzed the effects of a continuous daily SFN treatment on cellular degeneration and neuroinflammation and focused our cellular analysis on the microglia activation profile. Understanding the modulation of inflammation through the progression of RP, with a special focus on microglia activation, will help to understand the disease and evaluate potential treatments.

MATERIAL AND METHODS

Experimental Design

C57BL/6J wild-type and Pde6brd10 mice were used, as control and RP animal models, respectively. Mice were housed in the facilities of the Research Unit of the Department of Biomedical Sciences of the CEU—Cardenal Herrera University. The animals were kept in cages under controlled conditions of temperature (20°C) and humidity (60%) and constant light–dark cycles of 12 h. The animals had free access to water and a standard diet manufactured and distributed by Harlan Ibérica S.L. (Barcelona, Spain). The body weight of the experimental animals was monitored

FIGURE 1 | Experimental chronogram. Intraperitoneal injections, with sulforaphane (SFN) or saline, were done to the experimental groups, Control, and RD10 during the period illustrated in the figure.

and recorded throughout all the experiments. No differences between the body weight of the experimental groups were observed (data not shown). Handling and care of the animals were approved by the ethical committee of the CEU—Cardenal Herrera Universities (General Department of Agriculture, Livestock and Fisheries, Government of Valencia, Spain, code:2019/VSC/PEA/0040) and followed the "Declaration for the use of animals in ophthalmological and vision research" (ARVO; Association for Research in Vision and Ophthalmology). Day of birth was considered as postnatal day 0 (P0). P14 was chosen as the day to start intraperitoneal SFN treatment (20 mg/kg weight; sulforaphane was dissolved in sterile saline solution and administered using insulin-size syringe). The dose was selected as a result of preliminary experiments performed by our group and revision of the current field (Greaney et al., 2016; Kang and Yu, 2017; Hernández-Rabaza et al., 2019). To evaluate the SFN effect, each mouse received intraperitoneal SFN administration on consecutive days. The last day of treatment was P20. Mice were euthanized on P21, 24 h after the last sulforaphane dose administration. The administration program is presented in **Figure 1**. Note that SFN is quickly metabolized, and its body level decreases significantly around 24 h (Clarke et al., 2011).

All the experimental solutions were administered by intraperitoneal injections. Four experimental mice groups were used, Control Saline (C57BL/6J wild-type mice treated with saline), Control SFN (C57BL/6J wild-type mice treated with sulforaphane), RD10 Saline (Pde6brd10/J mice treated with saline), and RD10 SFN (Pde6brd10/J mice treated with sulforaphane). The number of mice used in each experimental group was at least $n = 5$. Our studies were completed on both male and female populations.

Histological and Immunofluorescence Studies

Eyeballs were fixed by immersion in 4% paraformaldehyde for 2 h, then three washes were performed with 0.1 M phosphate-buffered saline pH 7.2 (PBS) for 10 min. Later, they were cryoprotected using PBS–sucrose in increasing sucrose concentrations (10%–20%–30%) at 4°C.

Afterward, 8-μm-thick retinal sections were obtained by a Leica CM 1850UV Ag protect cryostat, (Leica Microsystems SLU, Barcelona, Spain) on adhesion slides (SuperFrost, Thermo Fisher Scientific, Braunschweig, Germany) and kept at −20°C until their use.

Histological Study of Retinal Degeneration

Retinal degeneration was studied histologically using hematoxylin and eosin (H&E) staining on the four experimental groups.

The quantification method consisted of the measurement of the outer nuclear layer (ONL) thickness in terms of the number of cell rows. To this end, a Leica DM 2000 microscope with ×40 magnification was used, with the software Leica Application Suite version 2.7.0 R1 (Leica Microsystems SLU, Barcelona, Spain) for obtaining the photos of each retina, followed by a manual cell counting by two experienced observers in double-blind conditions.

This procedure was performed in three different retinal histological sections for each eye and three different regions in each section. These regions were central retina (near the optical nerve), mid peripheral retina (between the central retina and far peripheral retina), and far peripheral retina (near the ora serrata). The distance between each retinal region was 500 μm.

Terminal Deoxynucleotidyl Transferase Assay

The TUNEL assay was performed with an *in situ* cell death detection kit (Roche Diagnostics, Mannheim, Germany) as described in Benlloch-Navarro et al. (2019). To analyze retinal TUNEL-positive cells, images were taken with a Nikon DS-Fi1 camera attached to a Leica DM 2000 microscope, with the software Leica Application Suite version 2.7.0 R1 (Leica Microsystems SLU, Barcelona, Spain).

The TUNEL-positive cells were counted manually, by a blind experimenter, in the ONL of three different regions of the retina: central retina, mid peripheral, and far peripheral retina. The distance between each retinal region was 500 μm. TUNEL-positive cells from three retinal sections were counted for each animal of each group, one area per region. The count was taken at ×20 magnification, and the number of cells was referred to the area of the ONL, which was used. This was done with the help of the software ImageJ Fiji 1.5.3.

Retinal Immunofluorescence Studies

Immunofluorescent staining procedures were performed on retinal cryosections that were rehydrated in PBS and merged for 1 h at room temperature (RT) with blocking solution: 10% of normal goat serum in PBS–BSA 1% and Triton 0.1%. Afterward, they were incubated overnight at 4°C with primary antibodies: anti-glial fibrillary acidic protein (anti-GFAP) (1:200, Dako Cytomation, Denmark), anti-ionized calcium-binding adaptor molecule 1 (Iba1; 5 μg/ml, Abcam, Cambridge, United Kingdom), anti-interleukin 4 antibody (IL-4; 5 μg/ml, Abcam, Cambridge, United Kingdom), anti-interleukin-1β (IL1β; 1:100, Abcam, Cambridge, United Kingdom), anti-liver arginase antibody (arginase; 5 μg/ml, Abcam, Cambridge, United Kingdom), and anti-chitinase three-like protein three antibodies (CHI3L3, also named Ym1; 20 μg/ml, Abcam,

Cambridge, United Kingdom). The next day, sections were washed and incubated for 1 h in darkness at RT with the fluorescence-conjugated secondary antibody Alexa Fluor 488 (Invitrogen, Life Technologies, Madrid, Spain). Sections were mounted with Vectashield with DAPI (Vector, Burlingame, CA, United States).

In the case of double immunofluorescence staining, after the incubation with blocking solution, tissue sections were incubated overnight with Iba1 antibody. Next, incubation with a secondary antibody (Alexa Fluor 488 or Alexa Fluor 568) for 1 h was performed. Afterward, incubation overnight with IL1β or IL4 antibodies followed by 1 h of secondary antibody (Alexa Fluor 488 or Alexa Fluor 568) incubation was performed. Ultimately, sections were also mounted with Vectashield with DAPI.

Retinal images were taken with a Nikon DS-Fi1 camera attached to a Leica DM 2000 microscope, with the Leica Application Suite version 2.7.0 R1 program (Leica Microsystem SLU, Barcelona, Spain). Representative images were taken of the central retina, mid peripheral, and far peripheral retina regions (×20 magnification). The distance between each retinal region was 500 μm. Finally, images were quantified with the help of the software ImageJ Fiji 1.5.3. It must be noticed that area is quantified as arbitrary units (AU) (656 AU represents 100 μm).

To evaluate changes in reactive gliosis, the percentage of area occupied by the GFAP antibody labeling was measured throughout the retina. Regarding Iba1 expression, quantification was done in three different ways. First, the number of cells in each layer and the whole retina were measured. Second, it was performed as a migration index. Last, a morphological analysis of the Iba1 cells was performed.

In order to evaluate microglial activation, we counted the total Iba1-positive cells in the whole retina and each layer. This value was divided by the area of each layer. Results were expressed in percentage regarding the maximum value of Iba1 expression in each layer. Regarding the evaluation of microglial migration to the damaged areas, we measured the migration index (MI), which is defined following the method described by Martínez-Fernández de la Cámara et al. (2015), as the number of Iba1-positive cells weighted according to the retinal layer where they are located [MI = ∑ (number of Iba1-positive cells in each layer × layer weighted factor)/total number of Iba1-positive cells in the section]. The layer weighted factor was 1, 25 for the outer nuclear layer (ONL), 1 for the outer plexiform layer (OPL), 0, 75 for the inner nuclear layer (INL), 0, 5 for the inner plexiform layer (IPL), and 0, 25 for the ganglion cell layer (GCL). Finally, regarding the Iba1 morphology study, to quantify the number and length of cellular branches, fluorescence photomicrographs were converted into skeletonized images and analyzed using the ImageJ Fiji 1.5.3. Analyze Skeleton and FracLac were used according to the method described by Young and Morrison, (2018) for this purpose. In this case, data are expressed in arbitrary units (AU) per nucleus.

To evaluate IL1β expression, including both the mature and pro-form of IL1β, the percentage of area occupied by the IL1β antibody labeling was measured throughout the retina. To evaluate IL4 expression, Ym1 expression, and arginase expression, positive cells were counted manually in the retina, by an experimenter in blind conditions. Three retinal sections were counted for each animal of each group, and the number of positive cells was referred to the area of the retina which was used. For the colocalization quantification, the amount of IL1β-Iba1-positive cells was manually counted, and the results were expressed according to the amount of Iba1-positive cells.

Statistical Analysis

The results are presented as mean values ± standard deviation. Each percentage change was performed using the RD10 SFN group reduction/increase in comparison with RD10 SAL results. To ensure the normal distribution of the groups, the Shapiro–Wilk test was performed. Variance homogeneity was determined by Levene's test of variance homogeneity. The two-way analysis of variance (ANOVA) was used. When the ANOVA indicated a significant difference, the Bonferroni test was performed. SPSS software package version 27.0 was used. In every case, it was assumed that a p-value lower than 0.05 is significant.

RESULTS

Sulforaphane Administration Reduces Retina Degeneration

Cellular retinal degeneration was assessed with a double cellular analysis. First, histological analysis of the thickness of the outer photoreceptor layer, stained with H&E, and second a quantification of positive TUNEL cells were performed. The cellular counting was realized in three different retinal regions with the optic nerve position as reference, called far and mid periphery and central nerve regions.

H&E results indicate that all the RD10 groups, treated with or without SFN, show a significant reduction in the number of row cells in the ONL regarding the Control groups (in all the retina areas analyzed, Control Saline vs. RD10 Saline p-value <0.000, Control SFN vs. RD10 SFN, $p < 0.001$). However, the RD10 SFN group suffered a significant minor cellular degeneration, particularly pronounced in the mid and nerve periphery regions, where statistically significant differences were found between the RD10 Saline and RD10 SFN groups ($p < 0.000$), suggesting a delay in the neurodegeneration. The H&E results are illustrated in **Figure 2**, including the mean increase in RD10 SFN in comparison with the RD10 Saline group (**Figure 2C**).

In addition to the H&E data, immunofluorescence analysis of the TUNEL cellular death marker confirms the neuroprotective action of SFN. The results indicate that all the RD10 groups, treated with or without SFN, show a significant increase in TUNEL-positive cells regarding the Control groups (in all the retina areas analyzed, Control Saline vs. RD10 Saline, p-value <0.000, Control-SFN vs. RD10 SFN, $p < 0.000$). However, the RD10 SFN group showed a significant reduction concerning the RD10 Saline group, in the far periphery ($p < 0.000$), in the mid periphery ($p < 0.000$), and in the nerve ($p < 0.000$) regions. The TUNEL results are illustrated in **Figure 3**, including the mean

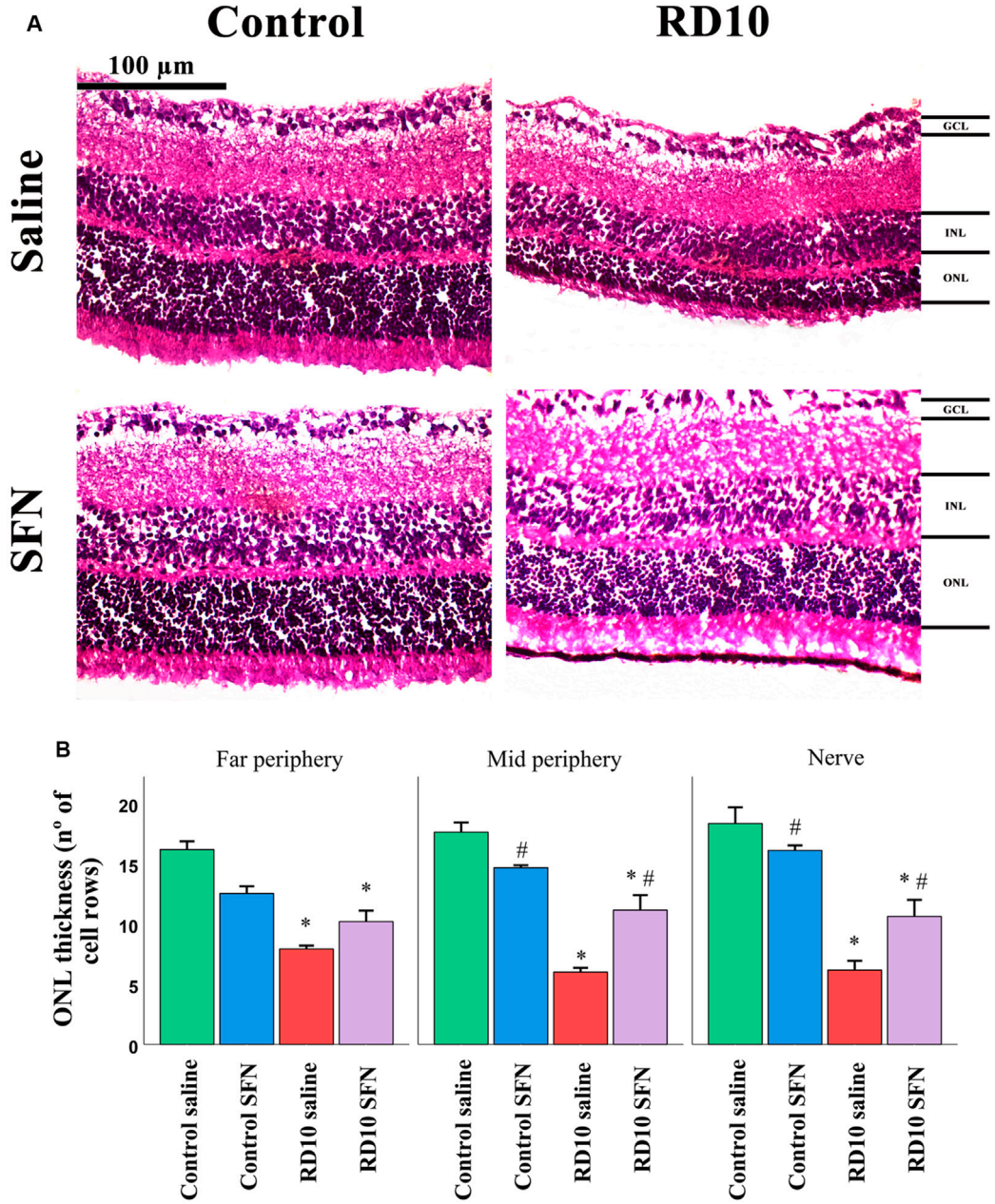

C

Units: n° of cell rows

	Far Periphery			Mid Periphery			Nerve		
	RD10 Saline	RD10 SFN	% H&E increase RD10 saline vs RD10 SFN	RD10 Saline	RD10 SFN	% H&E increase RD10 saline vs RD10 SFN	RD10 Saline	RD10 SFN	% H&E increase RD10 saline vs RD10 SFN
Mean	7.91	10.19	28.82	6.00	11.14	85.66	6.16	10.61	17.24
Standard Deviation	0.28	0.90		0.36	1.24		0.77	1.37	

FIGURE 2 | Hematoxylin and eosin (H&E) cell analysis. **(A)** Nerve region H&E images of the different animal groups in the experiment. **(B)** The number of cell rows in the outer nuclear layer (ONL) in the different studied regions. *Differences between Control Saline vs. RD10 Saline or Control SFN vs. RD10 SFN (p-value <0.05). #Differences between Control Saline vs. Control SFN or RD10 Saline vs. RD10 SFN (*p*-value <0.05). **(C)** Effect of SFN on RD10 mice H&E cell count. RD10 experimental groups: mean and standard deviation and H&E cell percentage expression differences.

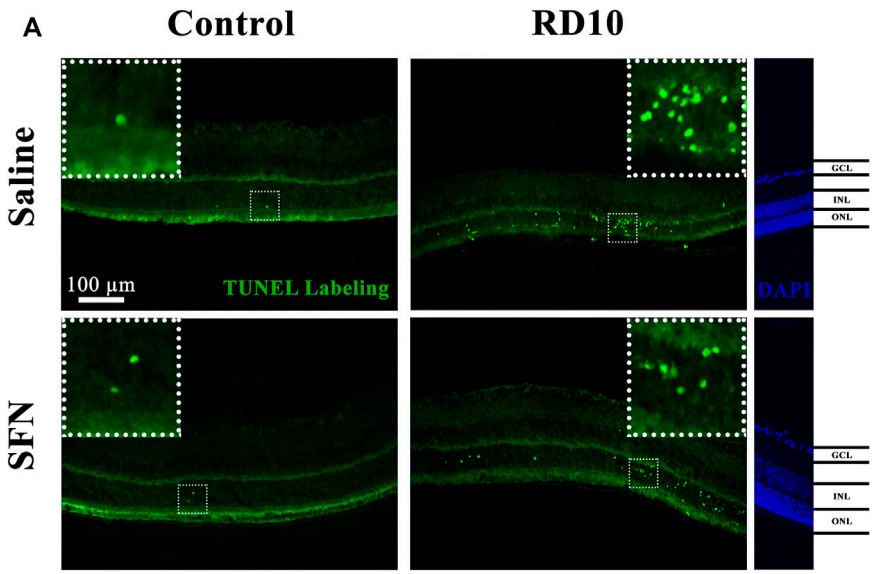

C

Units: n° of positive TUNEL cells / Area x 10^6

	Far Periphery			Mid Periphery			Nerve		
	RD10 Saline	RD10 SFN	% of TUNEL reduction RD10 saline vs RD10 SFN	RD10 Saline	RD10 SFN	% of TUNEL reduction RD10 saline vs RD10 SFN	RD10 Saline	RD10 SFN	% of TUNEL reduction RD10 saline vs RD10 SFN
Mean	151.25	71.20	52.93	171.37	51.43	69.99	121.55	37.38	69.25
Standard Deviation	24.94	12.37		31.16	7.60		21.05	10.28	

FIGURE 3 | Terminal deoxynucleotidyl transferase (TUNEL) cellular stain assessment. **(A)** Nerve region images of TUNEL immunofluorescence of the different groups in the experiment; the positive cells are pointed by white arrows. **(B)** The number of TUNEL-positive cells divided per area and multiplied per 10^6. *Differences between Control Saline vs. RD10 Saline or Control SFN vs. RD10 SFN (p-value <0.05). #Differences between RD10 Saline vs. RD10 SFN (p-value <0.05). **(C)** Effect of SFN on RD10 mice TUNNEL cell count expressed by the mean, standard deviation, and percentage reduction of RD10 SFN with respect to the RD10 Saline.

decrease in RD10 SFN in comparison with the RD10 Saline group (**Figure 3C**).

Sulforaphane Reduces the Glial Cell Activation

Immunohistochemistry data indicated an inflammation process on the RD10 Saline group, which was reverted by the SFN treatment. This affirmation is based on the cellular analysis of the glial cell activation, including both Müller cells and microglial cells.

Müller cell expression was analyzed with the GFAP marker, which was increased in the RD10 Saline in comparison with both control groups (in all the regions analyzed, Control Saline vs. RD10 Saline, p-value <0.000, Control SFN vs. RD10 SFN, $p < 0.000$). This effect was reduced by the SFN treatment in the RD10 group in the three regions analyzed (significant differences with respect to the comparison of RD10 Saline and RD10 SFN groups, $p < 0.000$, far periphery; $p < 0.000$, mid periphery; and $p < 0.000$, nerve region). The GFAP results are illustrated in **Figure 4**, including the mean decrease in RD10 SFN in comparison with the RD10 Saline group (**Figure 4C**).

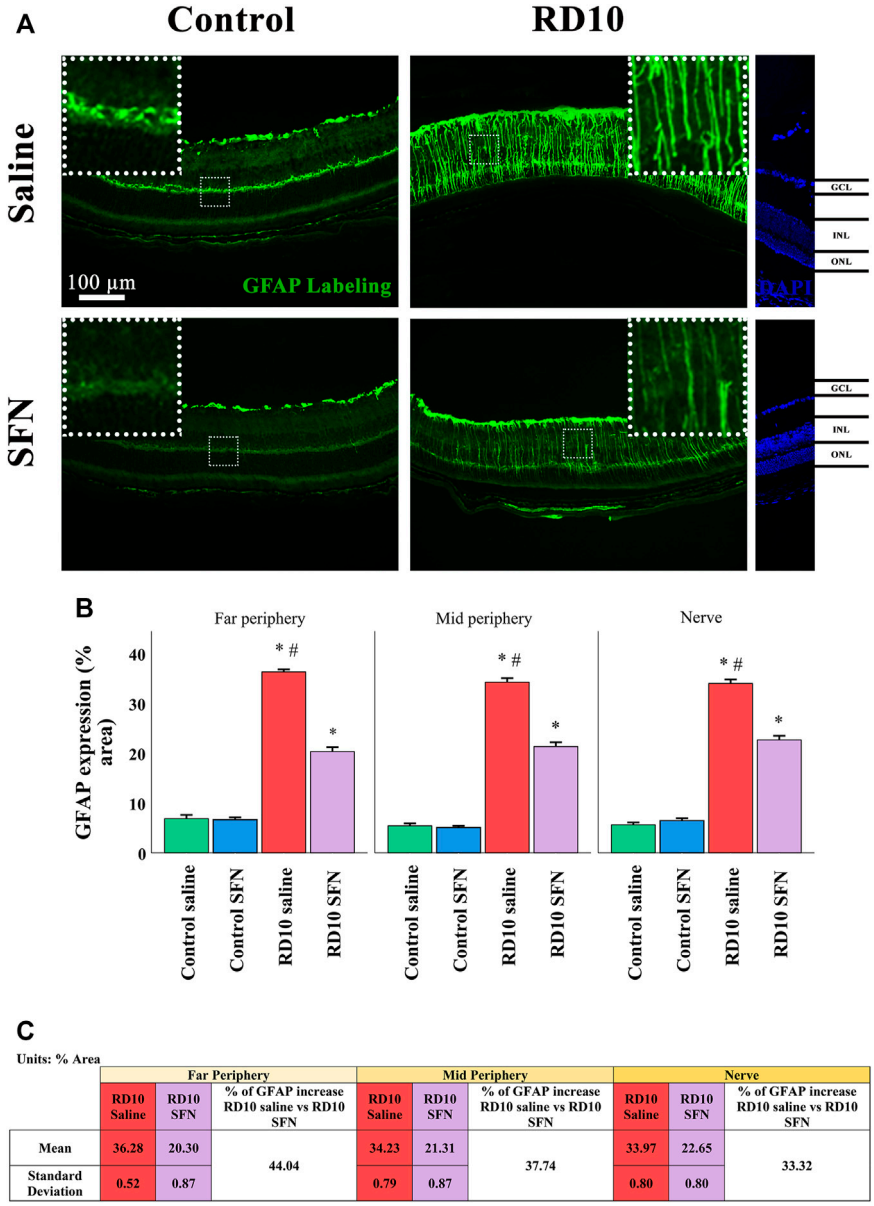

C

Units: % Area

	Far Periphery			Mid Periphery			Nerve		
	RD10 Saline	RD10 SFN	% of GFAP increase RD10 saline vs RD10 SFN	RD10 Saline	RD10 SFN	% of GFAP increase RD10 saline vs RD10 SFN	RD10 Saline	RD10 SFN	% of GFAP increase RD10 saline vs RD10 SFN
Mean	36.28	20.30	44.04	34.23	21.31	37.74	33.97	22.65	33.32
Standard Deviation	0.52	0.87		0.79	0.87		0.80	0.80	

FIGURE 4 | GFAP cellular analysis. **(A)** Nerve images of GFAP immunofluorescence of the different groups in the experiment. **(B)** GFAP percentage. *Differences between Control Saline vs. RD10 Saline or Control SFN vs. RD10 SFN (p-value <0.05). #Differences between RD10 Saline vs. RD10 SFN (p-value <0.05). **(C)** Effect of SFN on RD10 mice GFAP mark expressed by the mean, standard deviation of the RD10 groups, and percentage reduction of RD10 SFN vs. RD10 Saline.

Microglia expression was analyzed with the classical microglia marker Iba1, which expression was elevated in both RD10 groups in the outer nuclear layer (ONL) (Control Saline vs. RD10 Saline, p-value <0.000, Control SFN vs. RD10 SFN, $p < 0.000$). These differences were similar in the outer plexiform layer (OPL) (Control Saline vs. RD10 Saline p-value <0.000, Control SFN vs. RD10 SFN, $p = 0.035$). This effect was reverted by the SFN treatment in the RD10 group, in the three regions analyzed (ONL, significant differences between both RD10 groups, $p < 0.000$ in every studied region, OPL, significant differences between both RD10 groups, $p < 0.000$, in every studied region). In the ONL, no differences were detected between the RD10 SFN and control groups, while in the OPL, a slight increase was found concerning the control values (to see all statistical p-values, please view the **Supplementary Section** of the manuscript). Most of the positive Iba1 marks were found in the ONL and OPL layers, but not all. For example, the inner layers, both nuclear (INL) and plexiform (IPL), and the ganglion cell layers (GCL) were positive also to Iba1, and the analysis reveals no differences in the INL between the RD10 groups and the control groups, except in the nerve region. The tendency showed in the previous layers was swift in the GCL, where both RD10 groups showed significant increase with respect

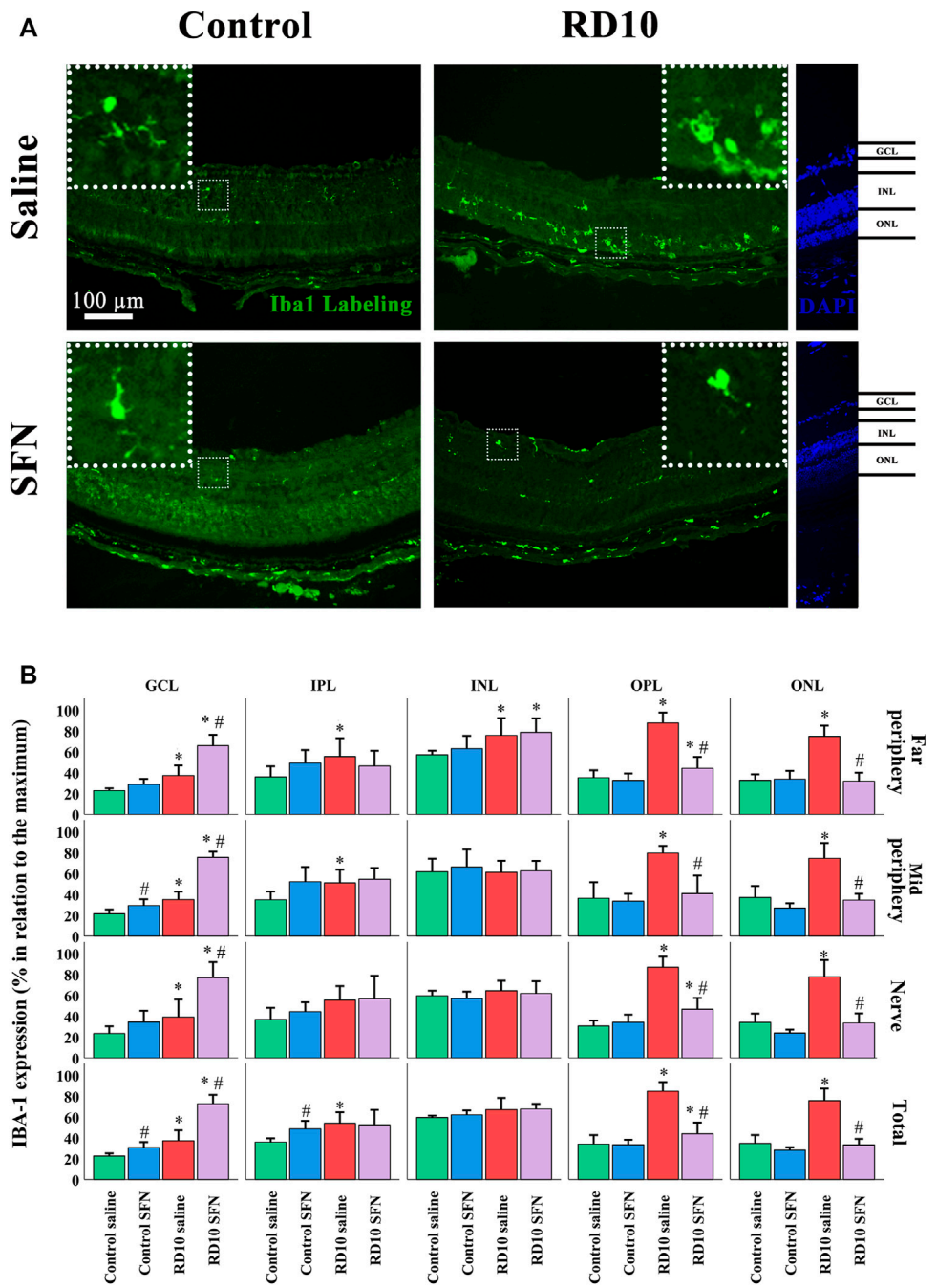

FIGURE 5 | Microglia phenotype analysis **(A)** Nerve region images of Iba1 immunofluorescence of the different groups in the experiment. **(B)** Iba1 cell percentage. *Differences between Control Saline vs. RD10 Saline or Control SFN vs. RD10 SFN (p-value <0.05) #Differences between Control Saline vs. Control SFN or RD10 Saline vs. RD10 SFN (p-value <0.05).

to the control groups, but also between the RD10 groups being the RD10 SFN, the one that showed a higher increase (GCL, significant differences between both RD10 groups, $p < 0.000$, in every studied region). The Iba1 results are illustrated in **Figure 5**.

Further analysis of the Iba1 marker was carried out to assess the activation and migration of the microglia. Microglia activation is characterized by its migration pattern, from the GCL to the ONL, and morphological changes, such as a length reduction of the branches and soma/projections ratio. The migration index indicated significant increases in the RD10 Saline group in comparison with the control groups (in the far periphery $p = 0.010$, mid periphery $p = 0.007$, nerve region $p = 0.016$), which was reverted by SFN treatment (significant differences between both RD10 groups, $p < 0.000$, far

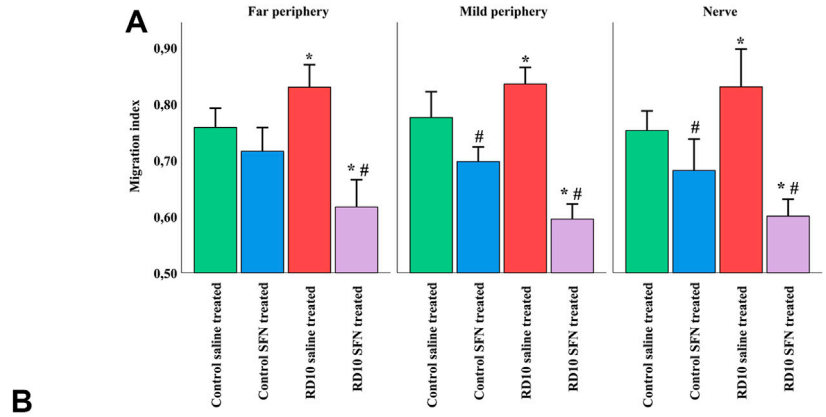

B

Units: Migration index

	Far Periphery			Mid Periphery			Nerve		
	RD10 Saline	RD10 SFN	Migration index decrease RD10 saline vs RD10 SFN	RD10 Saline	RD10 SFN	Migration index decrease RD10 saline vs RD10 SFN	RD10 Saline	RD10 SFN	Migration index decrease RD10 saline vs RD10 SFN
Mean	0.82	0.61	25.60	0.83	0.59	28.91	0.83	0.60	27.71
Standard Deviation	0.03	0.04		0.02	0.02		0.06	0.02	

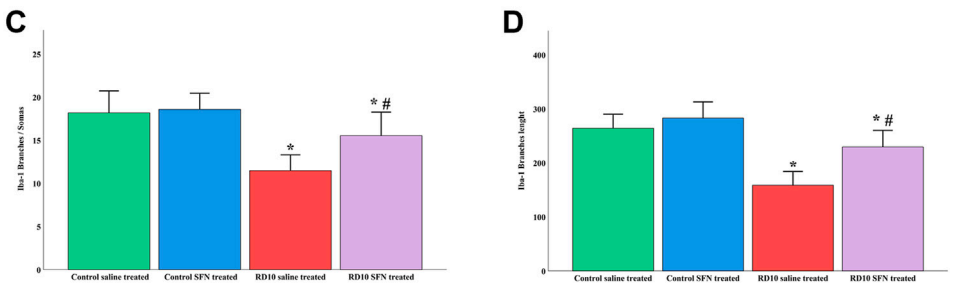

E

		Iba-1 morphology		
Units: nº of branches / soma		RD10 Saline	RD10 SFN	% of Iba-1 branches increase
Iba-1 Branches / Somas	Mean	11.46	15.51	35.34
	Standard Deviation	0.91	1.11	
Units: branches lenght / soma		RD10 Saline	RD10 SFN	% of Iba-1 branches length increase
Iba-1 Branches Lenght	Mean	158.43	229.37	44.77
	Standard Deviation	12.67	12.49	

FIGURE 6 | Microglia activation analysis. **(A)** Migration index. **(B)** Migration index: Mean and standard deviation of RD10 Saline and migration index RD10 SFN groups, and percentage decrease in RD10 SFN with respect to the RD10 Saline. **(C)** Branches of Iba1 cells per soma. **(D)** Branch length of Iba1 cells. *Differences between Control Saline vs. RD10 Saline or Control SFN vs. RD10 SFN (p-value <0.05). #Differences between RD10 Saline vs. RD10 SFN (p-value <0.05). **(E)** Iba1 morphology: Mean and SD of RD10 Saline and RD10 SFN groups, and percentage increase in RD10 SFN vs. RD10 Saline.

periphery; $p < 0.000$, mid periphery; $p < 0.000$, nerve region). The migration index results are illustrated in **Figure 6A**, including the mean decrease in RD10 SFN in comparison with the RD10 Saline group (**Figure 6B**). All the p-values can be seen in the **Supplementary Data** of the manuscript.

The morphological analysis of the microglia indicated a reduction in the microglia branches/soma ratio in the RD10 Saline group (in comparison with the Control Saline group, $p < 0.000$) that was partially reverted by the SFN treatment (significant differences between RD10 groups, $p = 0.013$). These results are presented in **Figure 6C**, including the mean decrease in RD10 SFN in comparison with the RD10 Saline group (**Figure 6E**). Finally, complementary to the previous data, the length assessment of the microglia branches indicated a reduction in the RD10 Saline group, which was partially reversed by the SFN treatment (significant differences between RD10 Saline group and Control Saline group, $p < 0.000$, and between RD10 groups, $p = 0.001$). These data are presented in **Figure 6D**. All

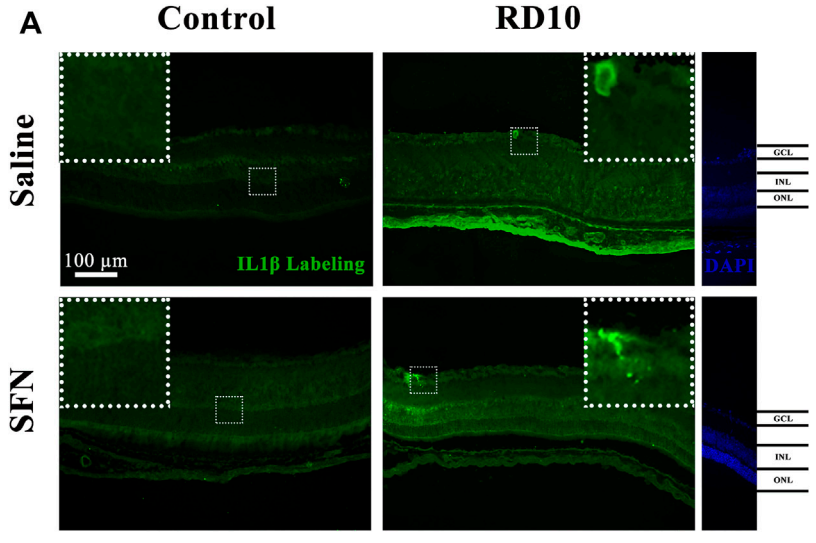

C

Units: % Area

	IL1β		
	RD10 Saline	RD10 SFN	% of IL1β decrease RD10 saline vs RD10 SFN
Mean	1.89	0.55	70.89
Standard Deviation	2.21	0.75	

FIGURE 7 | IL1β expression assessment. **(A)** Nerve region images of IL1β immunofluorescence of the different groups in the experiment; white arrows point out the positive mark. **(B)** IL-1β quantification expressed as area percentage. *Differences between Control Saline vs. RD10 Saline (p-value <0.05). #Differences between RD10 Saline vs. RD10 SFN (p-value <0.05). **(C)** Effect of SFN on RD10 mice IL1β mark expressed by the mean, and standard deviation of the RD10 groups, and percentage increase in RD10 SFN vs. RD10 Saline.

statistical p-values can be seen in the **Supplementary Data** of the manuscript.

Sulforaphane Reduces the Expression of Inflammatory Markers

Microglia and Müller cell activation is characterized by the synthesis and secretion of inflammatory mediators. In this study, we selected and analyzed some of the most relevant inflammatory mediators associated with glial cell activation, including M2 alternative microglia markers. The insight of this analysis was to unveil part of the inflammatory activation pattern of the RD10 Saline group and analyze the SFN effects over this pattern.

IL1β is considered a proinflammatory mediator (Mendiola and Cardona, 2018; Wooff et al., 2019). Immunofluorescence analysis indicated a significant increase in IL1β-positive area in the RD10 Saline group in comparison with the Control Saline group ($p = 0.009$), which was reversed by the SFN treatment (RD10 Saline vs. RD10 SFN, $p = 0.051$). The IL1β results are illustrated in **Figure 7**, including the mean decrease in RD10 SFN in comparison with the RD10 Saline group (**Figure 7C**).

IL1β can be expressed by neurons and glial cells. Colocalization analysis of Iba1 and IL1β was performed to analyze the pattern of microglia IL1β expression based on the recently reported SFN effects as microglia modulator. The analysis reveals that the microglia positive to IL1β was found in the outer layers of the retina. Results indicate a significant

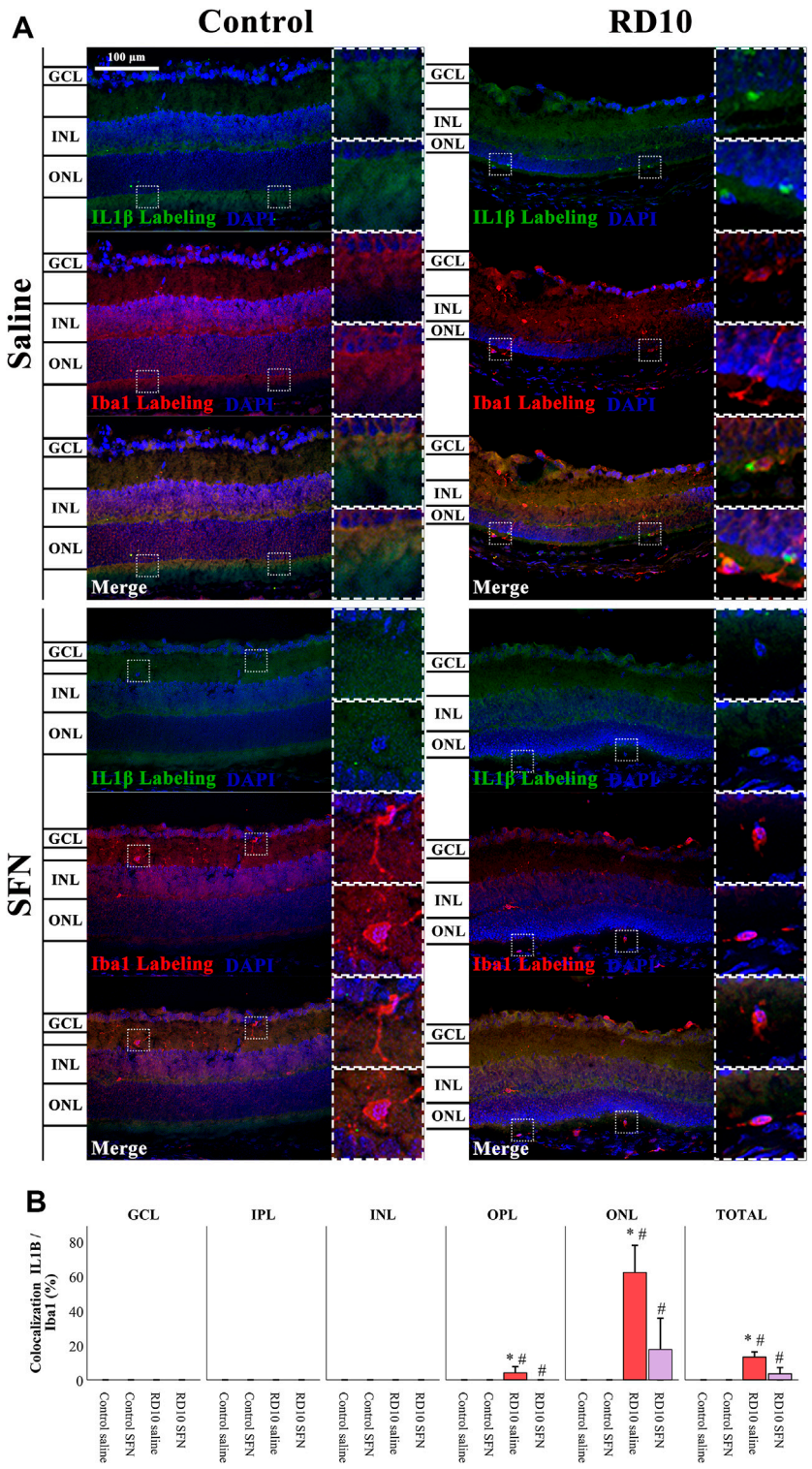

FIGURE 8 | IL1β-Iba1 expression assessment. **(A)** Nerve region images of IL1β-Iba1 immunofluorescence of the different groups in the experiment. **(B)** The percentage of IL1β-Iba1 colocalization was calculated regarding Iba1 total expression. *Differences between Control Saline vs. RD10 Saline or Control SFN vs. RD10 SFN (p-value <0.05). #Differences between RD10 Saline vs. RD10 SFN (p-value <0.05).

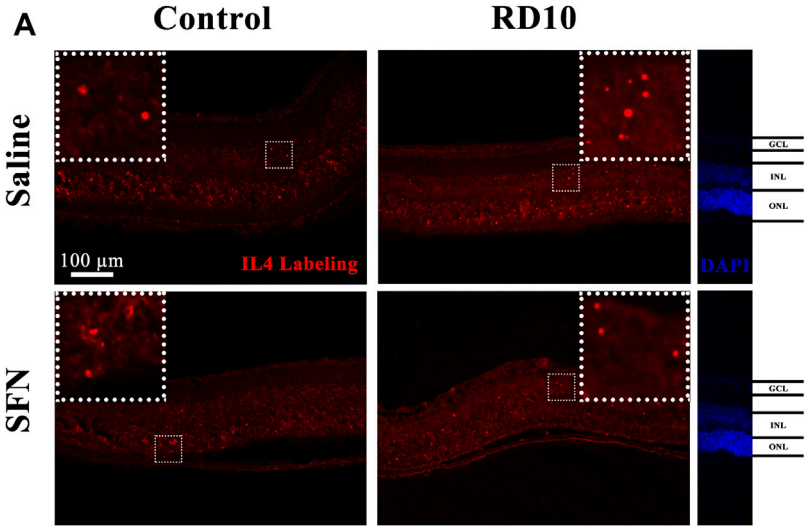

C

Units: IL4 cells / Area x 10^6

	Far Periphery			Mid Periphery			Nerve		
	RD10 Saline	RD10 SFN	% of IL4 reduction RD10 saline vs RD10 SFN	RD10 Saline	RD10 SFN	% of IL4 reduction RD10 saline vs RD10 SFN	RD10 Saline	RD10 SFN	% of IL4 reduction RD10 saline vs RD10 SFN
Mean	77.91	33.87	56.52	68.29	34.47	49.52	66.69	36.91	44.65
Standard Deviation	7.09	6.98		9.28	7.76		12.79	7.51	

FIGURE 9 | IL-4 expression assessment. **(A)** Nerve region images of IL-4 immunofluorescence of the different groups in the experiment; white arrows point out the positive mark. **(B)** The number of IL-4-positive cells was divided per area and multiplied by 10^6. *Differences between Control Saline vs. RD10 Saline or Control SFN vs. RD10 SFN (p-value <0.05). #Differences between RD10 Saline vs. RD10 SFN (p-value <0.05). **(C)** Effect of SFN on RD10 mice IL4 mark expressed by the mean and standard deviation of the RD10 groups, and percentage reduction of RD10 Saline vs. RD10 SFN.

increase in IL1β in the ONL of the RD10 Saline group (with respect to the comparison with the Control Saline group, $p < 0.000$), which was reversed by the SFN (differences between RD10 groups, $p = 0.002$). The same profile, but less evident, was displayed in the OPL. The IL1β-Iba1 colocalization results are illustrated in **Figure 8**. All statistical p-values can be seen in the **Supplementary Data** of the manuscript.

IL4 has been associated with alternative microglia activation. The immunofluorescence analysis indicated a significant increase in the IL4 expression in the RD10 Saline group (in comparison with the Control Saline group, in the far periphery, $p = 0.004$; mid periphery, $p = 0.003$; and nerve region, $p = 0.014$). This effect was partially reversed by the SFN treatment (comparison between both RD10 groups, $p = 0.023$, far periphery; $p = 0.007$, mid periphery; $p = 0.038$, and nerve region). The IL4 results are illustrated in **Figure 9**, including the mean decrease in RD10 SFN in comparison with the RD10 Saline group (**Figure 9C**). All statistical p-values can be seen in the **Supplementary Data** of the manuscript. Further IL4/Iba1 colocalization analysis indicated that IL4-positive cells colocalized with Iba1-positive cells with ameboid shape (**Figure 10**).

YM1 (chitinase 3-like protein 3) recognizes a lectin family, which is secreted by macrophages during inflammation. The immunofluorescence analysis showed a significant increase in the RD10 Saline group that was downregulated in the RD10 SFN group (in comparison with the Control Saline group, $p < 0.001$; in comparison with the RD10 SFN, $p < 0.000$). The YM1 results are

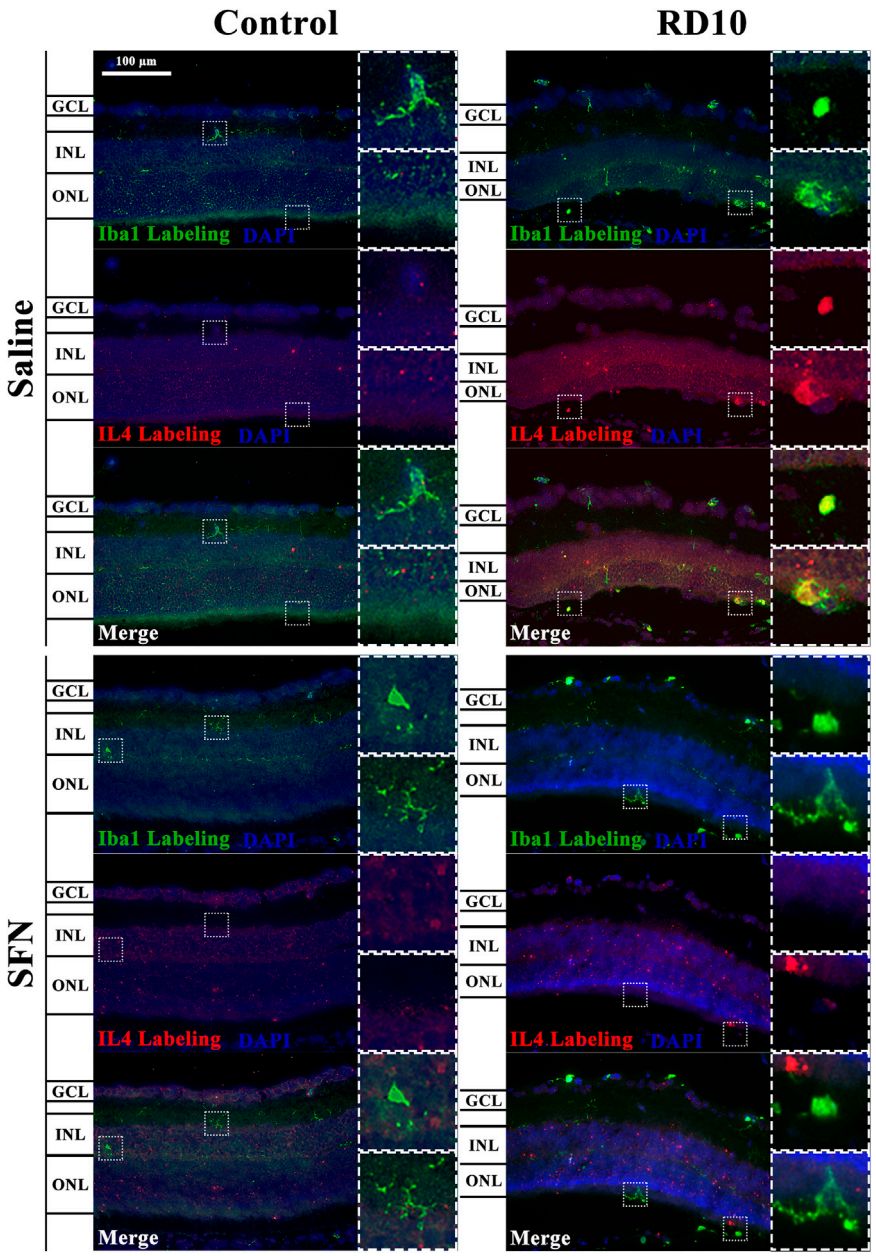

FIGURE 10 | Illustrative IL4-Iba1 immunofluorescent images from the nerve region of the different groups in the experiment.

illustrated in **Figure 11**, including the mean decrease in RD10 SFN in comparison with the RD10 Saline group (**Figure 11C**). All statistical *p*-values can be seen in the **Supplementary Data** of the manuscript.

Finally, the enzyme arginase converts L-arginine to urea and L-ornithine, and its excessive expression has been related to neural toxicity (Caldwell et al., 2015). The immunofluorescence analysis indicated no statistical differences between the RD10 groups and the Control Saline group. However, a significant reduction was found in the Control SFN group in comparison with the Control Saline group (in the mid periphery, $p = 0.016$, and nerve region, $p = 0.024$, but not in the far periphery, $p = 0.343$). The higher mean values were found in the RD10 Saline in the mid periphery (mean = 31.06 cells/area) and nerve region (mean = 29.37 cells/area). The arginase results are illustrated in **Figure 12**. All statistical *p*-values can be seen in the **Supplementary Data** of the manuscript.

DISCUSSION

Our results show that a daily administration of SFN delays the neurodegeneration and reduces the retina inflammation in an animal model of RP. The neuroprotective SFN role on the retina

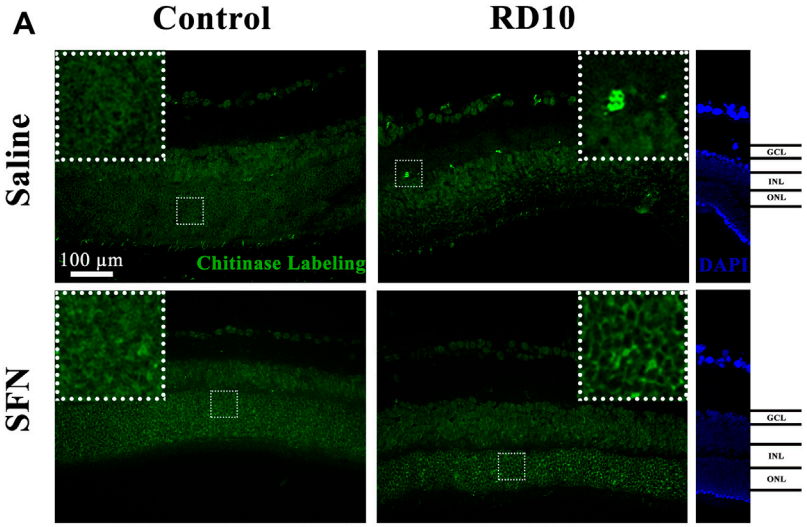

C

Units: n° of positive Chitinase positive cells / Area x 10^6

	Far Periphery			Mid Periphery			Nerve		
	RD10 Saline	RD10 SFN	% of Chitinase reduction RD10 saline vs RD10 SFN	RD10 Saline	RD10 SFN	% of Chitinase reduction RD10 saline vs RD10 SFN	RD10 Saline	RD10 SFN	% of Chitinase reduction RD10 saline vs RD10 SFN
Mean	35.24	5.79	83.57	27.55	5.99	78.27	27.01	5.04	81,34
Standard Deviation	7.89	1.41		6.36	1.44		7.23	1.56	

FIGURE 11 | Chitinase 3-like protein (YM1) expression assessment. **(A)** Nerve region images of chitinase immunofluorescence of the different groups in the experiment; white arrows point out the positive mark. **(B)** The number of chitinase-positive cells was divided per area and multiplied by 10^6. *Differences between Control Saline vs. RD10 Saline or Control SFN vs. RD10 SFN (*p*-value <0.05). #Differences between RD10 Saline vs. RD10 SFN (*p*-value <0.05). **(C)** Effect of SFN on RD10 mice chitinase mark expressed by the mean and standard deviation of the RD10 groups, and percentage reduction of RD10 Saline vs. RD10 SFN.

has been documented by other authors, including the retinal function recovery in an animal model of RP (Kang and Yu, 2017). However, how this action is achieved, and the underlying mechanisms, remain uncertain.

The oxidative stress modulation by SFN is the most recognized action mechanism. Concerning RP research, SFN inhibition of endoplasmic reticulum stress has been proposed as a possible mechanism (Kang and Yu, 2017). The antioxidant properties of SFN are well described, as well as the deleterious relevance of oxidative stress over RP development. The death of the first photoreceptor cells would trigger a sequence of oxidative reactions, which accelerate cellular degeneration (Campochiaro and Mir, 2018). SFN neuroprotective effects will interfere with this xenobiotic cascade, by the induction of the transcription of antioxidant enzymes, through the Nrf2/ARE pathways (Gao and Talalay, 2004). However, oxidative stress is a consequence of specific cellular actions, carried out by specific cells, a process intertwined with other cellular actions, all grouped in a most general and comprehensive concept called inflammation (Medzhitov, 2008). In this line, oxidative stress and inflammation are both cellular defense responses to harmful stimuli, which, under persistent and uncontrolled conditions, may amplify the cellular damage. Our results indicated that SFN administration modulates retinal inflammation, and this effect may reduce the associated neurodegeneration.

Neuroinflammation is characterized by glial cell activation. Our data showed a clear Müller cell reaction that was reduced by SFN administration (see **Figure 4**). Similar results have been

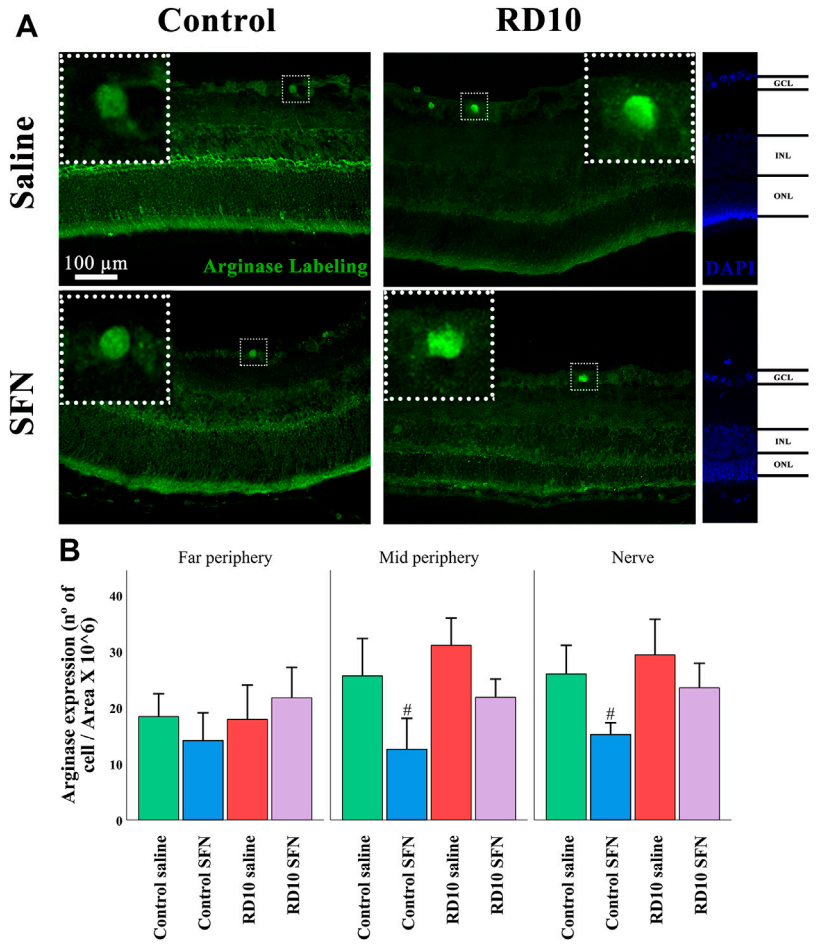

FIGURE 12 | Arginase expression assessment. **(A)** Nerve region images of arginase immunofluorescence of the different groups in the experiment; white arrows point out the positive mark. **(B)** The number of arginase-positive cells was divided per area and multiplied by 10^6. #Differences between Control Saline vs. Control SFN (*p*-value <0.05).

described in diabetic retinopathy (Li et al., 2019), where the SFN protection over the Müller cells was associated with the activation of the Nrf2 pathway and the inhibition of the inflammasome. Moreover, the interplay between Müller cells and microglia has been described in eye pathologies, by which the activation of both glial cells induces continuous activation feedback (Hu et al., 2021). A direct SFN effect over the Müller cells or an indirect effect through the microglia SFN modulation should be considered as underlying mechanisms.

Microglia are macrophages resident in the nervous system, which plays a main role during the inflammation reaction. The activation of the microglia is characterized by the migration, proliferation, morphology changes, and expression and secretion of inflammatory mediators. Our cellular microglia analysis indicates a microglia activation in the RD10 Saline group. This statement is supported by the increased migration index, the increased expression of Iba1, mainly in the ONL, as well as the length reduction of the projections and the soma/projections ratio in the Iba1 cells (see **Figures 5**, **6**). These effects were reduced by the SFN treatment in the RD10 SFN group, but no effect was detected in the Control SFN group. SFN anti-inflammatory properties have been shown in several publications. Proposed mechanisms include the activation of anti-inflammatory genes, the modulation of internal cellular pathways, such as MAP-Kinase p38 (Subedi et al., 2019), or the inhibition of inflammasome (Tufekci et al., 2021). The data suggest that the SFN administration on the Control group does not induce an inflammatory response. The significant H&E reduction induced by the SFN in the Control SFN group is striking in comparison with the Control Saline group. However, the reduction is minimal; in any case, further analysis should explore these data on healthy individuals. Moreover, no differences between Control groups were detected by TUNEL analysis, indicating no SFN noxious effects on cell survival (see **Figures 2**, **3**).

The term inflammation groups cellular and molecular reactions, including the overexpression of several mediators. To complement the neuroinflammation analysis, the expression of a selected group of inflammatory mediators was analyzed. In the animal model of RP, at 21 days of age, the results

indicate an increased expression of IL1β, IL4, and YM-1 that was reduced by SFN.

IL1β has been described as a relevant proinflammatory marker, involved in several processes, such as neutrophil recruitment, inflammatory mediator, inflammasome activator, or even in angiogenesis. The reported IL1β elevation in the rd10 model indicates an inflammatory process, which is reduced by the SFN treatment. The Iba1 colocalization suggests a link between the expression of the cytokine and the activation of the microglia that is not expressed in the group with SFN (see **Figures 7**, **8**). These results indicate that the SFN treatment reduced the inflammatory IL1β pattern shown in the rd10 model, and based on the colocalization data, one of the consequences seems to be the modulation of the microglia activation. It is a highlight that the colocalization analysis indicates a strong colocalization in the ONL, where the Iba1 expression was detected higher. It is relevant to add that the IL1β marker used in this study (Abcam, ab9722) reacts with two IL1β isoforms, the mature and the pro-form. For this reason, it cannot be discriminated which of both isoforms may be affected by SFN This issue should be considered in future studies.

IL4 is a cytokine that displays several functions, which are different based on the glia cell type analyzed and the IL4 concentration (Brodie and Goldreich, 1994). IL4 expression has been associated with M2 microglia polarization, as well as with eye pathological conditions (Zandi et al., 2019; Chen et al., 2021). The results indicate an increased expression of IL4 in the RD10 Saline group, which was reduced by the SFN treatment. IL4 was expressed in microglia cells, although its expression in other cell types cannot be ruled out (see **Figures 9 and 10**). By its side, YM1 is secreted by alternatively activated macrophages. Its elevation has been related to some eye pathologies (Rojas et al., 2014). The YM1 expression analysis shed similar results to previous cytokines. It was elevated in the RP animal model and reduced by the SFN treatment (See **Figure 11**). Finally, arginase is an enzyme that hydrolyzes the amino acid, L-arginine, to ornithine and urea, and is activated during neuroinflammation. It has been reported that a disproportionate arginase activation is associated with neurotoxicity (Caldwell et al., 2015). Our results do not indicate significant differences in arginase expression, except a significant reduction in the Control SFN group. It should be noted that the greater mean value was registered in the RD10 Saline group (See **Figure 12**). Together, these results suggest that RP runs parallel with an inflammation process, which implies glial cell activation, and that the SFN treatment may modulate this inflammation response, a fact connected with its neuroprotective properties. Moreover, based on our data, this modulation seems relevant in microglial cells, without discarding Müller cell regulation.

We are fully aware that IL4, YM1, and arginase are markers of the microglia M2 polarization state. The study of M1/M2 microglia phenotype is not within the scope of this article. However, it is relevant to consider the surprising increased expression of these inflammatory markers. Besides the microglia M2 phenotype, the expression and activity of these molecules have also been related to neuroinflammation and neurotoxicity, suggesting alternative actions to the M2 repair phenotype. Moreover, the M1/M2 phenotypes are conditioned by the disease progression state (Arroba et al., 2016). The SFN treatment modulates the microglia activation and possibly the polarization timing. Without a doubt, future analyses of the microglia polarization in RP will shed light on this issue, but our results indicate a microglia activation, including the upregulation of classical M2 markers in rd10 mice, and its reversion by SFN.

Reaching to this point, the data indicated an inflammatory SFN regulation. However, how does the SFN regulate the microglia and Müller cell activation state? This is a precise and relevant question.

It is logical to propose that the SFN effect over the glia cells would be carried out through the well-described antioxidant Nrf2/ARE pathway, inducing the transcription of genes related to the anti-inflammatory glial cell phenotypes. However, additional and independent Nrf2/ARE SFN intracellular pathways have been described, including inhibition of the inflammasome (Greaney et al., 2016), activation of lysosome and autophagosome programs (Li et al., 2021), and regulation of intracellular architecture (Zhou et al., 2018), which must be considered. Further research is required to unveil the SFN mechanisms alternative to the antioxidant Nrf2/ARE pathway.

Besides acting by direct intracellular pathways, the SFN anti-inflammatory properties, such as microglia phenotype regulation, may be carried out through the astrocyte–microglia homeostasis modulation (Kim and Son, 2021). Our results indicate that the SFN reduces both microglia cell and Müller cell activations. However, are both effects triggered directly by SFN or by glia interactions? Nrf2 is expressed at high levels in astrocytes, pointing out Müller cells as a relevant cellular target of SFN treatment (Navneet et al., 2019; Xu et al., 2019). Moreover, interleukin 1β has been proposed as an intercellular mediator in the regulation of both glial cells (Natoli et al., 2017), and its expression and secretion can be modulated by SFN (Hernandez-Rabaza et al., 2016). Glial cell interactions are required to be understood to further comprehend the SFN mechanism.

To summarize, the main idea that arises from our results is that the SFN reduces retinal neurodegeneration, and this effect would be accomplished, in part, by the anti-inflammatory SFN properties. The regulation of neuroinflammation contributes to achieving neuroprotection in diseases where the harmful stimuli are persistent. Our data supported this statement in the case of SFN and RP. In addition, the microglia activation pattern modulation by SFN treatment emerges as a relevant therapeutic target. In this line, further research is required to understand the underlying SFN mechanism over intracellular and intercellular glia regulations.

DATA AVAILABILITY STATEMENT

The raw data supporting the conclusion of this article will be made available by the authors, without undue reservation.

ETHICS STATEMENT

The animal study was reviewed and approved by the General Department of Agriculture, Livestock and Fisheries, Government of Valencia, Spain, code: 2019/VSC/PEA/0040.

AUTHOR CONTRIBUTIONS

All authors listed have made a substantial, direct, and intellectual contribution to the work and approved it for publication.

FUNDING

This article was funded by the GV/2019/034 project and the Precompetitive project by Fundación San Pablo CEU (FUSP-PPC-19-19F1741D), Productivity indicators UCH-CEU University (INDI21/39), and the grants ACIF/199/2019 and FPU 20/06277.

SUPPLEMENTARY MATERIAL

The Supplementary Material for this article can be found online at: https://www.frontiersin.org/articles/10.3389/fphar.2022.811257/full#supplementary-material

REFERENCES

Arroba, A. I., Alcalde-Estevez, E., García-Ramírez, M., Cazzoni, D., de la Villa, P., Sánchez-Fernández, E. M., et al. (2016). Modulation of Microglia Polarization Dynamics during Diabetic Retinopathy in Db/db Mice. *Biochim. Biophys. Acta* 1862, 1663–1674. doi:10.1016/J.BBADIS.2016.05.024

Benlloch-Navarro, S., Trachsel-Moncho, L., Fernández-Carbonell, Á., Olivar, T., Soria, J. M., Almansa, I., et al. (2019). Progesterone Anti-inflammatory Properties in Hereditary Retinal Degeneration. *J. Steroid Biochem. Mol. Biol.* 189, 291–301. doi:10.1016/J.JSBMB.2019.01.007

Brodie, C., and Goldreich, N. (1994). Interleukin-4 Modulates the Proliferation and Differentiation of Glial Cells. *J. Neuroimmunol.* 55, 91–97. doi:10.1016/0165-5728(94)90150-3

Caldwell, R. B., Toque, H. A., Narayanan, S. P., and Caldwell, R. W. (2015). Arginase: an Old Enzyme with New Tricks. *Trends Pharmacol. Sci.* 36, 395–405. doi:10.1016/J.TIPS.2015.03.006

Campochiaro, P. A., and Mir, T. A. (2018). The Mechanism of Cone Cell Death in Retinitis Pigmentosa. *Prog. Retin. Eye Res.* 62, 24–37. doi:10.1016/J.PRETEYERES.2017.08.004

Chen, S. H., Lin, Y. J., Wang, L. C., Tsai, H. Y., Yang, C. H., Teng, Y. T., et al. (2021). Doxycycline Ameliorates the Severity of Experimental Proliferative Vitreoretinopathy in Mice. *Int. J. Mol. Sci.* 22, 11670. doi:10.3390/IJMS222111670

Clarke, J. D., Hsu, A., Williams, D. E., Dashwood, R. H., Stevens, J. F., Yamamoto, M., et al. (2011). Metabolism and Tissue Distribution of Sulforaphane in Nrf2 Knockout and Wild-type Mice. *Pharm. Res.* 28, 3171–3179. doi:10.1007/S11095-011-0500-Z

Crain, J. M., Nikodemova, M., and Watters, J. J. (2013). Microglia Express Distinct M1 and M2 Phenotypic Markers in the Postnatal and Adult central Nervous System in Male and Female Mice. *J. Neurosci. Res.* 91, 1143–1151. doi:10.1002/JNR.23242

Dulull, N. K., Dias, D. A., Thrimawithana, T. R., and Kwa, F. A. A. (2018). L-sulforaphane Confers Protection against Oxidative Stress in an *In Vitro* Model of Age-Related Macular Degeneration. *Curr. Mol. Pharmacol.* 11, 237–253. doi:10.2174/1874467211666180125163009

Fahim, A. (2018). Retinitis Pigmentosa: Recent Advances and Future Directions in Diagnosis and Management. *Curr. Opin. Pediatr.* 30, 725–733. doi:10.1097/MOP.0000000000000690

Farrar, G. J., Kenna, P. F., and Humphries, P. (2002). On the Genetics of Retinitis Pigmentosa and on Mutation-independent Approaches to Therapeutic Intervention. *EMBO J.* 21, 857–864. doi:10.1093/EMBOJ/21.5.857

Gao, X., and Talalay, P. (2004). Induction of Phase 2 Genes by Sulforaphane Protects Retinal Pigment Epithelial Cells against Photooxidative Damage. *Proc. Natl. Acad. Sci. U. S. A.* 101, 10446–10451. doi:10.1073/PNAS.0403886101

Gong, Y., Cao, X., Gong, L., and Li, W. (2019). Sulforaphane Alleviates Retinal Ganglion Cell Death and Inflammation by Suppressing NLRP3 Inflammasome Activation in a Rat Model of Retinal Ischemia/reperfusion Injury. *Int. J. Immunopathol. Pharmacol.* 33, 2058738419861777. doi:10.1177/2058738419861777

Greaney, A. J., Maier, N. K., Leppla, S. H., and Moayeri, M. (2016). Sulforaphane Inhibits Multiple Inflammasomes through an Nrf2-independent Mechanism. *J. Leukoc. Biol.* 99, 189–199. doi:10.1189/JLB.3A0415-155RR

Hamel, C. (2006). Retinitis Pigmentosa. *Orphanet J. Rare Dis.* 1, 40. doi:10.1186/1750-1172-1-40

Hartong, D. T., Berson, E. L., and Dryja, T. P. (2006). Retinitis Pigmentosa. *Lancet* 368, 1795–1809. doi:10.1016/S0140-6736(06)69740-7

He, F., Ru, X., and Wen, T. (2020). NRF2, a Transcription Factor for Stress Response and beyond. *Int. J. Mol. Sci.* 21, 1–23. doi:10.3390/IJMS21134777

Hernandez-Rabaza, V., Cabrera-Pastor, A., Taoro-Gonzalez, L., Gonzalez-Usano, A., Agusti, A., Balzano, T., et al. (2016). Neuroinflammation Increases GABAergic Tone and Impairs Cognitive and Motor Function in Hyperammonemia by Increasing GAT-3 Membrane Expression. Reversal by Sulforaphane by Promoting M2 Polarization of Microglia. *J. Neuroinflammation* 13, 83–13. doi:10.1186/S12974-016-0549-Z

Hernández-Rabaza, V., López-Pedrajas, R., and Almansa, I. (2019). Progesterone, Lipoic Acid, and Sulforaphane as Promising Antioxidants for Retinal Diseases: A Review. *Antioxidants* 8, 53. doi:10.3390/ANTIOX8030053

Hu, X., Zhao, G.-L., Xu, M.-X., Zhou, H., Li, F., Miao, Y., et al. (20212021). Interplay between Müller Cells and Microglia Aggravates Retinal Inflammatory Response in Experimental Glaucoma. *J. Neuroinflammation* 18, 1–19. doi:10.1186/S12974-021-02366-X

Kang, K., and Yu, M. (2017). Protective Effect of Sulforaphane against Retinal Degeneration in the Pde6rd10 Mouse Model of Retinitis Pigmentosa. *Curr. Eye Res.* 42, 1684–1688. doi:10.1080/02713683.2017.1358371

Kim, S., and Son, Y. (2021). Astrocytes Stimulate Microglial Proliferation and M2 Polarization *In Vitro* through Crosstalk between Astrocytes and Microglia. *Int. J. Mol. Sci.* 22, 8800. doi:10.3390/IJMS22168800

Li, D., Shao, R., Wang, N., Zhou, N., Du, K., Shi, J., et al. (2021). Sulforaphane Activates a Lysosome-dependent Transcriptional Program to Mitigate Oxidative Stress. *Autophagy* 17, 872–887. doi:10.1080/15548627.2020.1739442

Li, S., Yang, H., and Chen, X. (2019). Protective Effects of Sulforaphane on Diabetic Retinopathy: Activation of the Nrf2 Pathway and Inhibition of NLRP3 Inflammasome Formation. *Exp. Anim.* 68, 221–231. doi:10.1538/EXPANIM.18-0146

Martínez-Fernández de la Cámara, C., Hernández-Pinto, A. M., Olivares-González, L., Cuevas-Martín, C., Sánchez-Aragó, M., Hervás, D., et al. (2015). Adalimumab Reduces Photoreceptor Cell Death in A Mouse Model of Retinal Degeneration. *Sci. Rep.* 5, 11764. doi:10.1038/SREP11764

Medzhitov, R. (2008). Origin and Physiological Roles of Inflammation. *Nature* 454, 428–435. doi:10.1038/nature07201

Mendiola, A. S., and Cardona, A. E. (2018). The IL-1β Phenomena in Neuroinflammatory Diseases. *J. Neural Transm. (Vienna)* 125, 781–795. doi:10.1007/S00702-017-1732-9

Natoli, R., Fernando, N., Madigan, M., Chu-Tan, J. A., Valter, K., Provis, J., et al. (2017). Microglia-derived IL-1β Promotes Chemokine Expression by Müller Cells and RPE in Focal Retinal Degeneration. *Mol. Neurodegener.* 12, 31. doi:10.1186/S13024-017-0175-Y

Navneet, S., Cui, X., Zhao, J., Wang, J., Kaidery, N. A., Thomas, B., et al. (2019). Excess Homocysteine Upregulates the NRF2-Antioxidant Pathway in Retinal Müller Glial Cells. *Exp. Eye Res.* 178, 228–237. doi:10.1016/J.EXER.2018.03.022

Pan, H., He, M., Liu, R., Brecha, N. C., Yu, A. C., and Pu, M. (2014). Sulforaphane Protects Rodent Retinas against Ischemia-Reperfusion Injury through the Activation of the Nrf2/HO-1 Antioxidant Pathway. *PLoS One* 9, e114186. doi:10.1371/JOURNAL.PONE.0114186

Rojas, B., Gallego, B. I., Ramírez, A. I., Salazar, J. J., de Hoz, R., Valiente-Soriano, F. J., et al. (2014). Microglia in Mouse Retina Contralateral to Experimental Glaucoma Exhibit Multiple Signs of Activation in All Retinal Layers. *J. Neuroinflammation* 11, 133–224. doi:10.1186/1742-2094-11-133/FIGURES/14

Subedi, L., Lee, J. H., Yumnam, S., Ji, E., and Kim, S. Y. (2019). Anti-Inflammatory Effect of Sulforaphane on LPS-Activated Microglia Potentially through JNK/AP-1/NF-κB Inhibition and Nrf2/HO-1 Activation. *Cells* 8, 194. doi:10.3390/CELLS8020194

Townsend, B. E., and Johnson, R. W. (2016). Sulforaphane Induces Nrf2 Target Genes and Attenuates Inflammatory Gene Expression in Microglia from Brain of Young Adult and Aged Mice. *Exp. Gerontol.* 73, 42–48. doi:10.1016/J.EXGER.2015.11.004

Tufekci, K. U., Ercan, I., Isci, K. B., Olcum, M., Tastan, B., Gonul, C. P., et al. (2021). Sulforaphane Inhibits NLRP3 Inflammasome Activation in Microglia through Nrf2-Mediated miRNA Alteration. *Immunol. Lett.* 233, 20–30. doi:10.1016/J.IMLET.2021.03.004

Vanduchova, A., Anzenbacher, P., and Anzenbacherova, E. (2019). Isothiocyanate from Broccoli, Sulforaphane, and its Properties. *J. Med. Food* 22, 121–126. doi:10.1089/jmf.2018.0024

Wooff, Y., Man, S. M., Aggio-Bruce, R., Natoli, R., and Fernando, N. (2019). IL-1 Family Members Mediate Cell Death, Inflammation and Angiogenesis in Retinal Degenerative Diseases. *Front. Immunol.* 10, 1618. doi:10.3389/FIMMU.2019.01618

Xu, Z., Cho, H., and Duh, E. J. (2019). The Effect of Nrf2 Depletion in Müller Glia on Retinal Angiogenesis in Oxygen-Induced Retinopathy. *Invest. Ophthalmol. Vis. Sci.* 60, 1643.

Ye, L., Yu, T., Li, Y., Chen, B., Zhang, J., Wen, Z., et al. (2013). Sulforaphane Enhances the Ability of Human Retinal Pigment Epithelial Cell against Oxidative Stress, and its Effect on Gene Expression Profile Evaluated by Microarray Analysis. *Oxidative Med. Cell Longevity* 2013, 1–13. doi:10.1155/2013/413024

Young, K., and Morrison, H. (2018). Quantifying Microglia Morphology from Photomicrographs of Immunohistochemistry Prepared Tissue Using Imagej. *JoVE*, 2018 1–9. doi:10.3791/57648

Zabel, M. K., Zhao, L., Zhang, Y., Gonzalez, S. R., Ma, W., Wang, X., et al. (2016). Microglial Phagocytosis and Activation Underlying Photoreceptor Degeneration Is Regulated by CX3CL1-Cx3cr1 Signaling in a Mouse Model of Retinitis Pigmentosa. *Glia* 64, 1479–1491. doi:10.1002/GLIA.23016

Zandi, S., Pfister, I. B., Traine, P. G., Tappeiner, C., Despont, A., Rieben, R., et al. (2019). Biomarkers for PVR in Rhegmatogenous Retinal Detachment. *PLoS One* 14, e0214674. doi:10.1371/JOURNAL.PONE.0214674

Zhou, Y., Yang, G., Tian, H., Hu, Y., Wu, S., Geng, Y., et al. (2018). Sulforaphane Metabolites Cause Apoptosis via Microtubule Disruption in Cancer. *Endocr. Relat. Cancer* 25, 255–268. doi:10.1530/ERC-17-0483

Conflict of Interest: The authors declare that the research was conducted in the absence of any commercial or financial relationships that could be construed as a potential conflict of interest.

Publisher's Note: All claims expressed in this article are solely those of the authors and do not necessarily represent those of their affiliated organizations, or those of the publisher, the editors, and the reviewers. Any product that may be evaluated in this article, or claim that may be made by its manufacturer, is not guaranteed nor endorsed by the publisher.

frontiers in Pharmacology

ORIGINAL RESEARCH
published: 21 March 2022
doi: 10.3389/fphar.2022.839424

Chronic Proinflammatory Signaling Accelerates the Rate of Degeneration in a Spontaneous Polygenic Model of Inherited Retinal Dystrophy

T. J. Hollingsworth[1,2], *Xiangdi Wang*[1], *William A. White*[1], *Raven N. Simpson*[1] *and Monica M. Jablonski*[1,2,3,4]*

[1]Hamilton Eye Institute, Department of Ophthalmology, University of Tennessee Health Science Center, Memphis, TN, United States, [2]Department of Anatomy and Neurobiology, University of Tennessee Health Science Center, Memphis, TN, United States, [3]Department of Pharmaceutical Sciences, University of Tennessee Health Science Center, Memphis, TN, United States, [4]Department of Genetics, Genomics and Informatics, University of Tennessee Health Science Center, Memphis, TN, United States

OPEN ACCESS

Edited by:
Settimio Rossi,
Second University of Naples, Italy

Reviewed by:
Christian Grimm,
University of Zurich, Switzerland
Hideki Hayashi,
Tokyo University of Pharmacy and Life Sciences, Japan

***Correspondence:**
Monica M. Jablonski
mjablonski@uthsc.edu

Specialty section:
This article was submitted to Inflammation Pharmacology, a section of the journal Frontiers in Pharmacology

Received: 20 December 2021
Accepted: 21 February 2022
Published: 21 March 2022

Citation:
Hollingsworth TJ, Wang X, White WA, Simpson RN and Jablonski MM (2022) Chronic Proinflammatory Signaling Accelerates the Rate of Degeneration in a Spontaneous Polygenic Model of Inherited Retinal Dystrophy. Front. Pharmacol. 13:839424. doi: 10.3389/fphar.2022.839424

Collectively, retinal neurodegenerative diseases are comprised of numerous subtypes of disorders which result in loss of a varying cell types in the retina. These diseases can range from glaucoma, which results in retinal ganglion cell death, to age-related macular degeneration and retinitis pigmentosa, which result in cell death of the retinal pigment epithelium, photoreceptors, or both. Regardless of the disease, it's been recently found that increased release of proinflammatory cytokines and proliferation of active microglia result in a remarkably proinflammatory microenvironment that assists in the pathogenesis of the disease; however, many of the details of these inflammatory events have yet to be elucidated. In an ongoing study, we have used systems genetics to identify possible models of spontaneous polygenic age-related macular degeneration by mining the BXD family of mice using single nucleotide polymorphism analyses of known genes associated with the human retinal disease. One BXD strain (BXD32) was removed from the study as the rate of degeneration observed in these animals was markedly increased with a resultant loss of most all photoreceptors by 6 months of age. Using functional and anatomical exams including optokinetic nystamography, funduscopy, fluorescein angiography, and optical coherence tomography, along with immunohistochemical analyses, we show that the BXD32 mouse strain exhibits a severe neurodegenerative phenotype accompanied by adverse effects on the retinal vasculature. We also expose the concurrent establishment of a chronic proinflammatory microenvironment including the TNFα secretion and activation of the NF-κB and JAK/STAT pathways with an associated increase in activated macrophages and phagoptosis. We conclude that the induced neuronal death and proinflammatory pathways work synergistically in the disease pathogenesis to enhance the rate of degeneration in this spontaneous polygenic model of inherited retinal dystrophy.

Keywords: inherited retinal dystrophy, inflammation, microglia, TNFα, JAK/STAT, NF-κB, NLRP3

INTRODUCTION

Progressive retinal dystrophies (RDs) result in the loss of the rod and cone photoreceptors, though, depending on the disease itself, the degeneration observed will occur at varying rates with specific cell types affected more so than others (Cremers et al., 2004; Hunt et al., 2004; Hollingsworth and Gross, 2012; Iannaccone et al., 2015; Rho et al., 2021). For example, diseases like age-related macular degeneration (AMD) and Stargardt's disease primarily or initially affect cone photoreceptors, the retinal pigment epithelium (RPE), or both, with the rates and onsets of degeneration varying dramatically between the two (Cremers et al., 2004; Hunt et al., 2004; Al-Zamil and Yassin, 2017; Fleckenstein et al., 2021; Rho et al., 2021). Contrarily, retinitis pigmentosa (RP) and Leber congenital amaurosis (LCA) both affect rod photoreceptors first, and ultimately the cones as well, while advancing at rates varying from gene to gene and person to person (Rivolta et al., 2002; den Hollander et al., 2008; Ferrari et al., 2011; Hollingsworth and Gross, 2012; O'Neal and Luther, 2021). Although RDs are incredibly heterogenous, some common pathogenetic features have been observed to be conserved amongst them. Regardless of the initial etiology of an RD, proinflammatory signaling has been observed in the retinas of RD models including those for AMD, RP, LCA, and even glaucoma (Brown and Neher, 2012; Soto and Howell, 2014; Iannaccone et al., 2015; Appelbaum et al., 2017; Iannaccone et al., 2017; Silverman and Wong, 2018; Wooff et al., 2019; Hollingsworth and Gross, 2020; Ucgun et al., 2020; Fleckenstein et al., 2021; Hollingsworth et al., 2021). Previously, we have shown upregulation of multiple proinflammatory and autoinflammatory pathways in multiple models of rhodopsin-mediated RP (Hollingsworth and Gross, 2020; Hollingsworth et al., 2021). While these models do recapitulate RP phenotypes, they are hardly representative of a truly natural model of the disease; those mice bear full human rhodopsin genes harboring one single point mutation that was introduced via knock-in methods (Hollingsworth and Gross, 2013; Sandoval et al., 2014). During a study using systems genetics and the BXD family of mice to attempt to elucidate spontaneous high-fidelity models of AMD, we discovered a novel, spontaneous model of a fairly rapid RD, BXD32, which is likely polygenic due to the inherent nature of the BXD family of mice (Geisert and Williams, 2020; Ashbrook et al., 2021). BXD mice are a family of recombinant inbred strains that were derived by crossing a female C57BL/6J and male DBA/2J, two very common mouse strains, and consecutively inbreeding the F2 progeny for more than 20 generations (Geisert and Williams, 2020; Ashbrook et al., 2021). This allowed for homologous recombination to occur at will, making each fully inbred strain genetically distinct. The DBA/2J genome has more than 5 million SNPs, greater than 400,000 insertions/deletions and multiple copy number variants compared to C57BL/6J and these all differentially segregate in each BXD strain due to the natural homologous recombination. Fortunately, each BXD strain has had its genome fully sequenced. It was the purpose of this study to both discern the pathological degenerative phenotypes in the BXD32 mouse strain and determine if chronic proinflammatory activation occurs in the retinas of these mice, allowing for future design of possible therapeutics to intervene in the pathogenesis observed in these mice.

MATERIALS AND METHODS

Animals

C57BL/6J and BXD32 mice were obtained from the Jackson Laboratories. All animals were used in accordance with the Association for Research in Vision and Ophthalmology (ARVO) and University of Tennessee Health Science Center Institutional Animal Care and Use Committee.

Optokinetic Nystagmography

WT and BXD32 mice (n = 3-4 mice/strain) at p63, p84, p105, p126, p147, and p168 were placed onto the pedestal in an OptoDrum OKN machine (Stoelting, 620 Wheat Lane, Wood Dale, IL, United States). The visual acuity (VA) data was collected by fixing the rotation speed on 12°/s and fixing the contrast on 99.72%. The contrast sensitivity (CS) result was collected by fixing the rotation speed on 12°/s and fixing the cycles on 0.103 cycles/degree. Statistical analysis performed using two-tailed student *t* test.

Optical Coherence Tomography

WT and BXD32 mice (n = 3-4mice/strain) at p63, p84, p105, p126, p147, and p168 were anesthetized using ketamine/xylazine (intraperitoneally 71.42 mg/kg ketamine/14.3 mg/kg xylazine in PBS, pH 7.4) and pupils dilated using 1% tropicamide. To keep the eyes lubricated and maintain corneal clarity, artificial tears (Systane Ultra) were applied when needed. The mice were subsequently examined by OCT using an Eyemera OCT (IIScience, 3003 N 1st., San Jose, CA, United States) through the optic nerve head with the purpose of visualizing total retinal and ONL thicknesses non-invasively. Quantification of ONL thickness performed from histological sections through the optic nerve head (ONH).

Funduscopy/Fluorescein Angiography

WT and BXD32 (n = 3-4mice/strain) mice at p63, p84, p105, p126, p147, and p168 were anesthetized using ketamine/xylazine (intraperitoneally 71.42 mg/kg ketamine/14.3 mg/kg xylazine in PBS, pH7.4) and eyes dilated using 1% tropicamide. The animals were then intraperitoneally injected with 100 µl of 4% fluorescein and subsequently imaged with either white light (funduscopy for examining retinal pallor/pigmentation) or 488 nm light (fluorescein angiography for vascular anomalies) emitted from an Eyemera Fundus Camera (IIScience, 3003 N 1st., San Jose, CA, United States).

Fluorescent Immunohistochemistry

Whole eyes from WT and BXD32 (n = 3-4mice/strain, 1 slide/mouse, 3 sections per slide) mice at p63, p84, p105, p126, p147, and p168 were enucleated and fixed in 4% paraformaldehyde in PBS, pH 7.4 overnight at 4°C. Fixation was quenched in 100 mM glycine in PBS, pH 7.4 for 10 min at room temperature and

TABLE 1 | Antibodies used for IHC labeling of retinal sections.

Antibody Target	Catalog #	Host/IgG Isoform	Dilution	Source
GFAP	3670	Mouse IgG_1	1:250	Cell Signaling Tech
GS	610518	Mouse IgG_{2a}	1:500	BD Biosciences
IBA1	17198	Rabbit IgG	1:250	Cell Signaling Tech
RHO	MAB5356	Mouse IgG_1	1:500	EMD Millipore
NF-κB p65	8242	Rabbit IgG	1:400	Cell Signaling Tech
NLRP3	MA5-23919	Rat IgG_{2a}	1:250	ThermoFisher
TNFα	60291-1-Ig	Mouse IgG_{2b}	1:250	ProteinTech
STAT3	9139	Mouse IgG_{2a}	1:200	Cell Signaling Tech
pSTAT3-Tyr705	9145	Rabbit IgG	1:200	Cell Signaling Tech
pSTAT3-Ser727	9134	Rabbit IgG	1:200	Cell Signaling Tech
SOCS3	ab16030	Rabbit IgG	1:100	abcam

subsequently washed in PBS. Eyes were dehydrated with 30 min incubations in a graded ethanol series (50, 70, 85, 95 and 100%) then cleared via a 30 min incubation in graded xylenes (2:1, 1:1, and 1:2 ethanol: xylenes), and two 30 min incubations in 100% xylenes. Eyes were then infiltrated with paraffin using a graded paraffin series with 30 min incubations in 2:1, 1:1, and 1:2 xylenes: paraffin and two subsequent 1 h incubations in 100% paraffin. Paraffin-embedded tissue was then sectioned at 8 μm or 16 μm and sections deparaffinized and rehydrated, treated using heat-mediated antigen retrieval by heating slides at 95°C in sodium citrate buffer (10 mM sodium citrate, 0.05% Tween-20, pH 6.0) for 1 h, washed in PBS twice and subsequently blocked in 10% goat serum/5% BSA/0.5% TritonX-100 in PBS for 30 min at RT. Primary antibodies against markers for glial cells and proinflammatory signaling pathways were then applied at recommended dilutions and incubated overnight at 4°C (**Table 1**). Slides were then washed in PBS, pH 7.4 three times for 10 min each. Post-washing, slides were incubated in secondary antibodies conjugated to either AlexaFluor488, AlexaFluor568, AlexaFluor647, or horseradish peroxidase (A21121, A21241, A11036, A21236, A11006, A21245, A16078, G21234; ThermoFisher; 168 Third Avenue, Waltham, MA, United States) at 1:400 dilutions for 1 h and nuclei stained using a 1:10,000 dilution of 14.3 mM DAPI (D21490; ThermoFisher; 168 Third Avenue, Waltham, MA, United States). For phosphorylated STAT3 (pSTAT3) and STAT3, tyramide signal amplification (TSA) was performed using the TSA with SuperBoost kit with tyramide reagent conjugated to either AlexaFluor 488 or AlexaFluor568 (B40926, B40953, B40956; ThermoFisher; 168 Third Avenue, Waltham, MA, United States) following the manufacturer's instructions. Slides were then washed in PBS, pH 7.4 four times and mounted using Prolong Diamond Antifade mountant (P36961; ThermoFisher; 168 Third Avenue, Waltham, MA, United States). For TUNEL labeling, the Click-It Plus TUNEL Kit (C10647; ThermoFisher; 168 Third Avenue, Waltham, MA, United States) was used to label apoptotic nuclei with AlexFluor488 following the manufacturer's instructions. After drying overnight, sections were imaged using a Zeiss 710 laser scanning confocal microscope (LSM) using a 40X objective with 1.3 numerical aperture (NA) or 63X objective with 1.4 NA with an associated 1.6X zoom (100X). Fluorescent intensities analyzed using ImageJ. Statistical analysis performed using two-tailed Welch's *t* test (unequal variance).

RESULTS

OKN Reveals a Loss of Visual Acuity and Contrast Sensitivity in the BXD32 Mouse

Using screens with passing alternating black and white bars of varying thicknesses and at varying speeds, OKN data output allows for quantification of both the visual acuity (VA) and contrast sensitivity (CS) of the subject, both of which decrease with age normally. BXD32 mice, while initially having similar VA (**Figure 1A**) and CS (**Figure 1B**) as WT, gradually lose both with age more rapidly than observed in WT, correlating to a loss of photoreceptors in the outer retina.

OCT Analysis Reveals a Rapid Loss of Photoreceptor Cells in the BXD32 Mouse Retina

By utilizing infrared light passing through the cornea, OCT can generate an image of the retinal tissue through interpolation of the photons reflected back to the lens by the tissue, the amount of which is determined by the density of the retinal layers. Using OCT imaging (**Figures 2A,B**), we are able to visualize a rapid, early onset loss of the outer layers of the retina, namely the photoreceptor outer nuclear layer (ONL) and inner and outer segments, resulting in a loss of total retinal thickness. This finding strongly correlates to a severe form of inherited retinal dystrophy (IRD). Using histological sections through the ONH, ONL measurements show the retinal degeneration in the BXD32 mouse occurs superiorly to inferiorly and centrally to peripherally with the peak rate of degeneration occurring around p105 (**Figures 2C,D**).

Funduscopy and Fluorescein Angiography Reveal Hallmarks of Severe IRD

To observe the overall health of the retina visually, funduscopy is used by shining a white light into the eye, allowing for full retinal visualization. By injecting a subject with fluorescein and

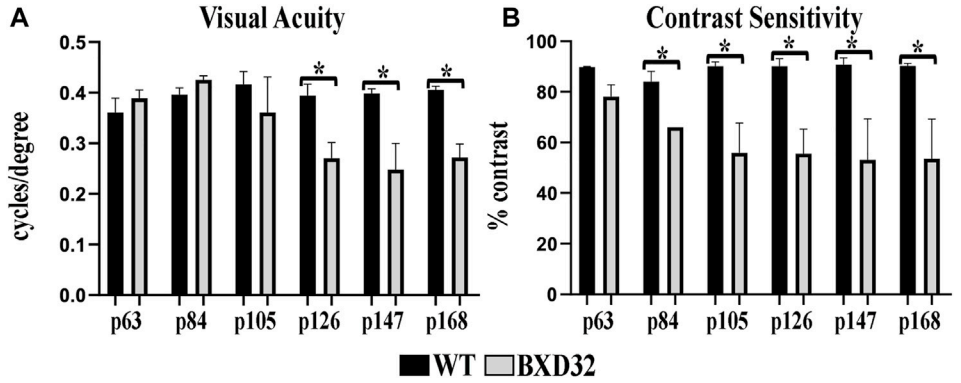

FIGURE 1 | The BXD32 mouse retina exhibits diminished visual ability by OKN. WT and BXD32 mice were examined using OKN to assess for visual acuity **(**VA, **A)** and contrast sensitivity **(**CS**, B)**, respectively. BXD32 mice exhibit a loss of visual acuity beginning around p105 and dropping significantly by p168. Similarly, but beginning much earlier at p63, the BXD32 mice lose contrast sensitivity compared to WT mice to levels roughly half of WT animals by p168. Error bars = ±SEM. *, $p < 0.05$.

visualizing the retina with a blue (~488 nm) light, one is also capable of examining the retinal vasculature. The BXD32 mouse retina shows strong dissimilarity to WT retinas, which will tend toward a healthy bluish pallor. The BXD32 retina, instead, exhibits distinct features of RP with a loss of retinal thickness allowing for the RPE to be visualized (**Figure 3A**). Observation of the retinal vasculature reveals vessel attenuation with age, indicative of an RP phenotype as well (**Figure 3B**). No vascular leakage was witnessed at any age; however, an apparent loss of visible intermediate and deep vascular plexi can be observed with age.

BXD32 Mouse Retinas Exhibit Markedly Up-Regulated Levels of Both Monocytic Activation and Invasion and Proinflammatory Pathway Proteins

Previously, we and other labs have shown that as RDs progress, proinflammatory pathways are upregulated due to release of various cytokines including TNFα, IL-6, IL-1β, and others (Ten Berge et al., 2019; Wooff et al., 2019; Yi et al., 2019; Hollingsworth et al., 2021). To investigate whether the BXD32 mouse retina propagates the formation of a proinflammatory microenvironment, we paraffin embedded eyes, sectioned, and immunolabeled them for retinal stress markers, multiple proinflammatory cytokines/pathway proteins. Under normal physiological conditions, glial fibrillary acidic protein (GFAP) is expressed primarily in the nerve fiber layer regions of the retina and is localized to astrocytes. Under disease conditions, however, GFAP expression is increased and in turn localized to the Müller glial cells of the retina (Lewis and Fisher, 2003). This upregulation has been linked to both hypertrophy and gliosis in the retina. To test for GFAP upregulation, we performed fIHC on retinal sections from BXD32 and WT mice (**Figure 4** and **Supplementary Figure S1**). GFAP upregulation starts from the earliest time point tested in the BXD32 mice and levels never diminish, indicating a highly stressed, detrimental retinal state. In addition to GFAP, we immunolabeled for glutamine synthetase (GS), a marker for Müller glia (as well as other glial cells), and IBA1, a marker for macrophages, or in the case of the central nervous system, microglia, the resident macrophages in the retina and brain. Normally, microglia are found resting in the inner retinal layers and present with a ramified morphology of filamentous projections that extend to the outer retina seeking out dying cells or foreign invaders (Li et al., 2015; Silverman and Wong, 2018; Rashid et al., 2019; Kinuthia et al., 2020). We observed a dramatic increase in the number of macrophages not only present in the retina, but migrating to the outer retina and RPE, something these cells only tend to do under disease conditions (Li et al., 2015; Rashid et al., 2019). In addition to labeling for these glial and microglial cells, we performed fIHC for rhodopsin in conjunction with IBA1 and TUNEL labeling to indicate apoptosing cells (**Figure 5** and **Supplementary Figure S2**). TUNEL labeling increased with age, peaking at p105 and decreasing up to p168 where significantly fewer photoreceptors are observed (**Supplementary Figure S3**). We visualized both phagocytosis of TUNEL-labeled cells as well as the aberrant phagocytosis of living cells, known as phagoptosis (**Figure 6** and **Supplementary Figure S4)**, recently discovered to be an underlying cause of cell death in RD (Brown and Neher, 2014; Zhao et al., 2015; Hollingsworth et al., 2021).

TNFα is released from multiple retinal cell types under normal and diseased physiological conditions. When TNFα is upregulated, such as in proinflammatory conditions, it initiates a cascade through its cognate receptors to ultimately cause upregulation of inflammatory pathways including NF-κB and NLRP3 upregulation and activation (Hohmann et al., 1990; Meichle et al., 1990; Bauernfeind et al., 2009; Toma et al., 2010; Qiao et al., 2012; Hollingsworth et al., 2021). We observed that TNFα is upregulated in the BXD32 retina compared to WT and both NF-κB and NLRP3 are grossly upregulated indicating heavy proinflammatory signaling in the degenerating retina (**Figure 7** and **Supplementary Figure S5**). This upregulation is high regardless of age.

The Janus kinase/signal transducer and activator of transcription (JAK/STAT) pathway is known to be activated by proinflammatory cytokines such as interleukins 1 and 6 as

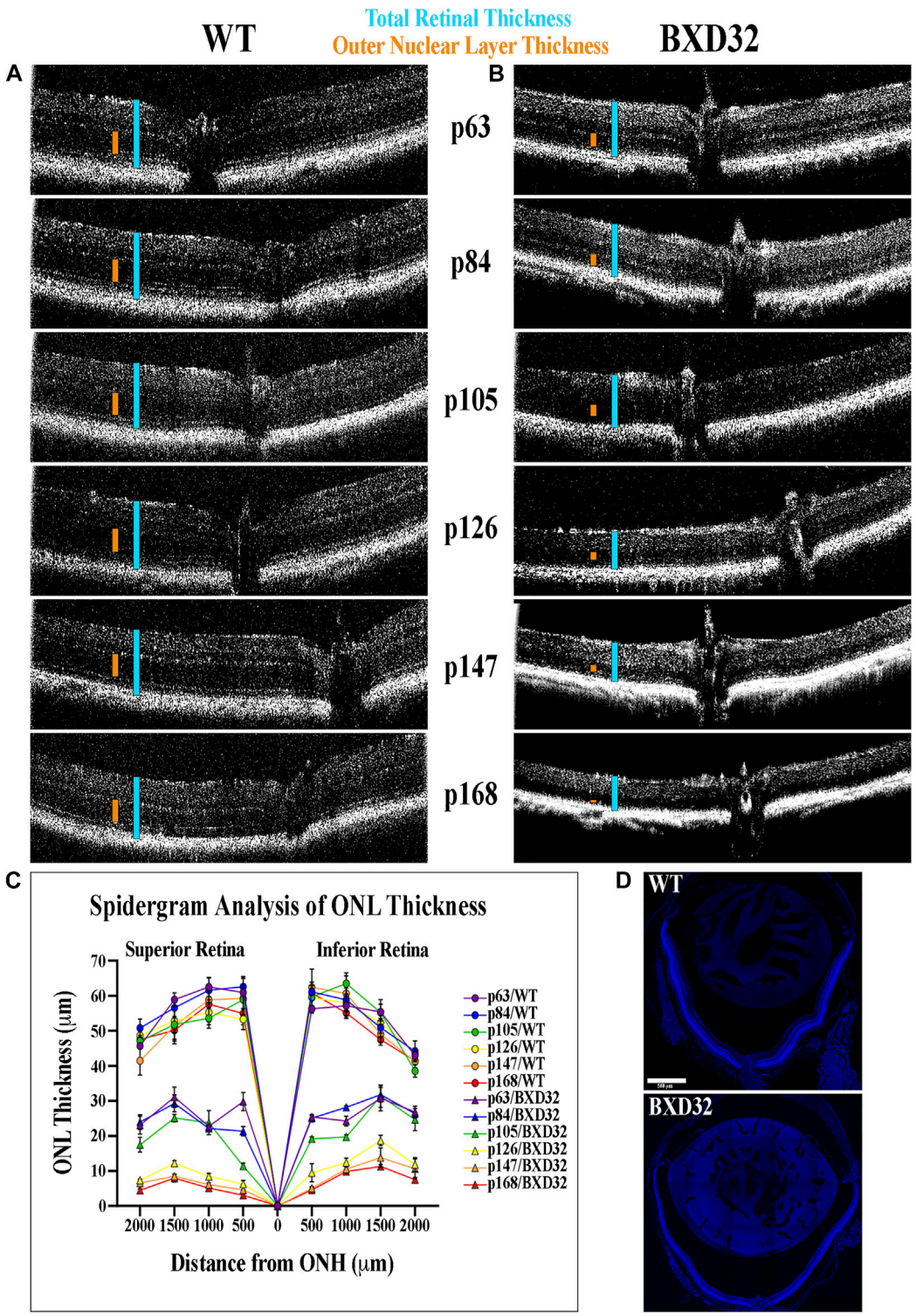

FIGURE 2 | BXD32 retinas degenerate rapidly when observed by OCT. WT **(A)** and BXD32 **(B)** mice were anesthetized and had their retinas imaged by OCT. p63 BXD32 mice already demonstrate thinning of both the ONL (orange caliper) and the total retina (light blue caliper) compared to WT. This thinning increases rapidly until almost no ONL exists by p168. **(C)** ONL measurements were taken from tiled DAPI stained retinal sections through the ONH at distances of 500, 1,000, 1,500, and 2000 μm superiorly and inferiorly to the ONH and graphed as a spidergram. Examples of typical retinal tiled images are shown in **(D)**.

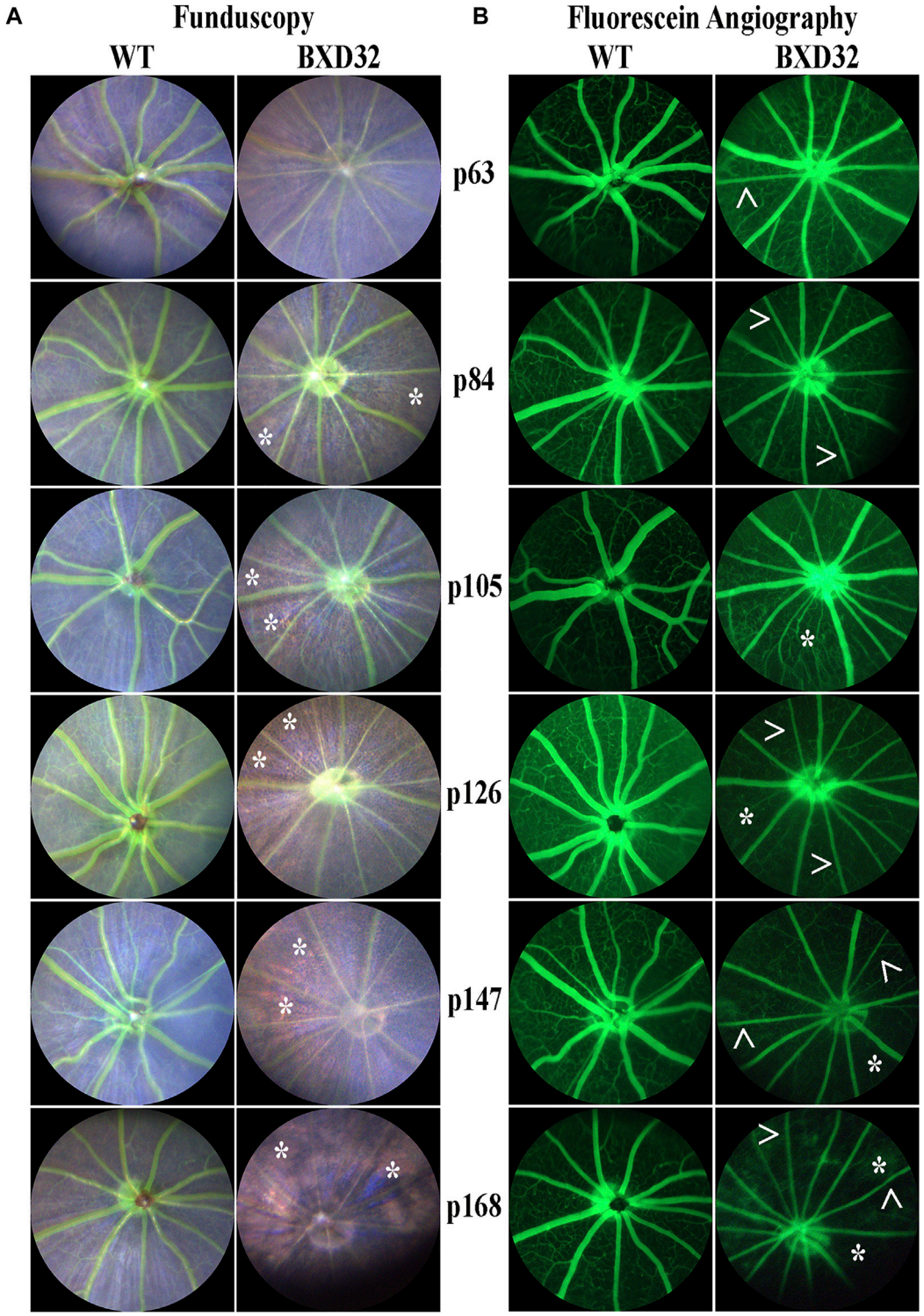

FIGURE 3 | Funduscopy and fluorescein angiography reveal retinal phenotypes consistent with RP. WT and BXD32 retinas were observed under white light for funduscopy **(A)** and using 488 nm for fluorescein angiography **(B)** light post-fluorescein injection. By funduscopy, BXD32 mice as early as p84 begin showing RPE through the neural retina (asterisks, *) indicating a major loss of photoreceptors in these regions. Fluorescein angiography reveals vessel attenuation in the superficial vascular plexus (arrowheads, >) beginning around p63 with some regions exhibiting vaso-obliteration, mostly in the intermediate and deep vascular plexi (asterisk, *).

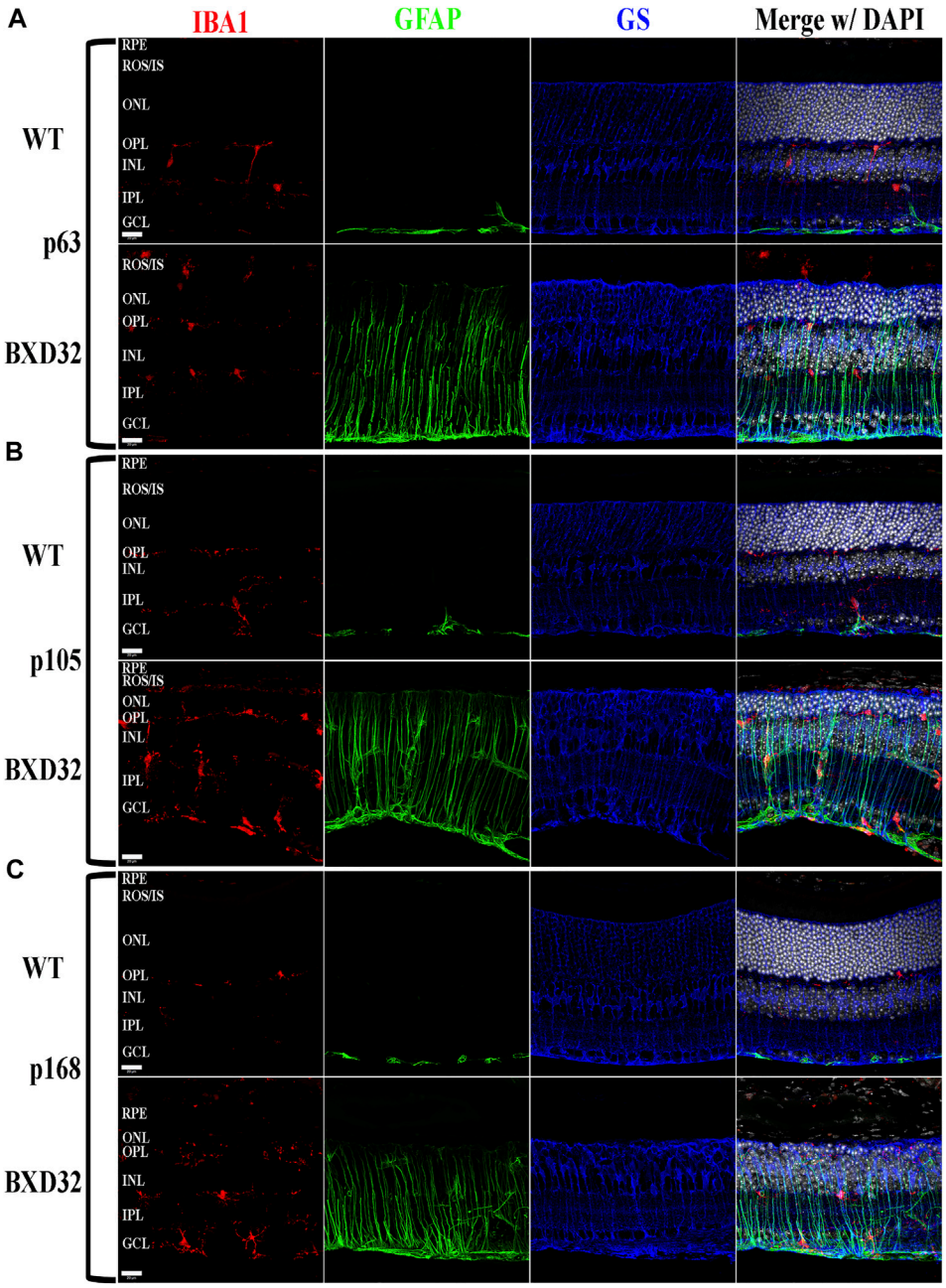

FIGURE 4 | BXD32 mouse retinas have advanced glial hypertrophy and an increased presence of monocytes in the outer retina. WT and BXD32 retinal sections were immunolabeled for glial cells using IBA1 (red), GFAP (green), and GS (blue). Beginning at the earliest timepoint examined p63 **(A)**, BXD32 retinas exhibit dramatic upregulation of GFAP and a larger number of monocytes, presumably microglia, both in the outer retina and the retina as a whole. By p105 **(B)**, no decrease in GFAP is observed and monocyte numbers are even higher than at p63. At p168 **(C)**, the outer retina is mostly degenerated and while monocyte numbers are lesser from p105, GFAP is still upregulated, indicating continued retinal stress. GS levels remained relatively similar amongst WT mice and BXD32 mice, with occasional variations with age. Nuclei stained with DAPI (white/grey). RPE, retinal pigment epithelium; ROS/IS, rod outer segments/inner segments; ONL, outer nuclear layer; OPL, outer plexiform layer; INL, inner nuclear layer; IPL, inner plexiform layer; GCL, ganglion cell layer. Scale bars = 20 μm.

well as pro-survival/cell division factors such as leukemia inhibitory factor (LIF) and, depending on the ligand, the pathway serves different functions (Nakashima and Taga, 1998). STAT3, which is phosphorylated by JAK, is capable of being phosphorylated at Tyr705 and Ser727, with the two sites serving varying functions. The Tyr705 site tends to induce activation, dimerization, and transcriptional activity, whereas the S727 site has been implicated in the deactivation of the dimerized STAT3, as well as other functions such as immunity and cell division (Lim and Cao, 1999; Murray, 2007; Wakahara

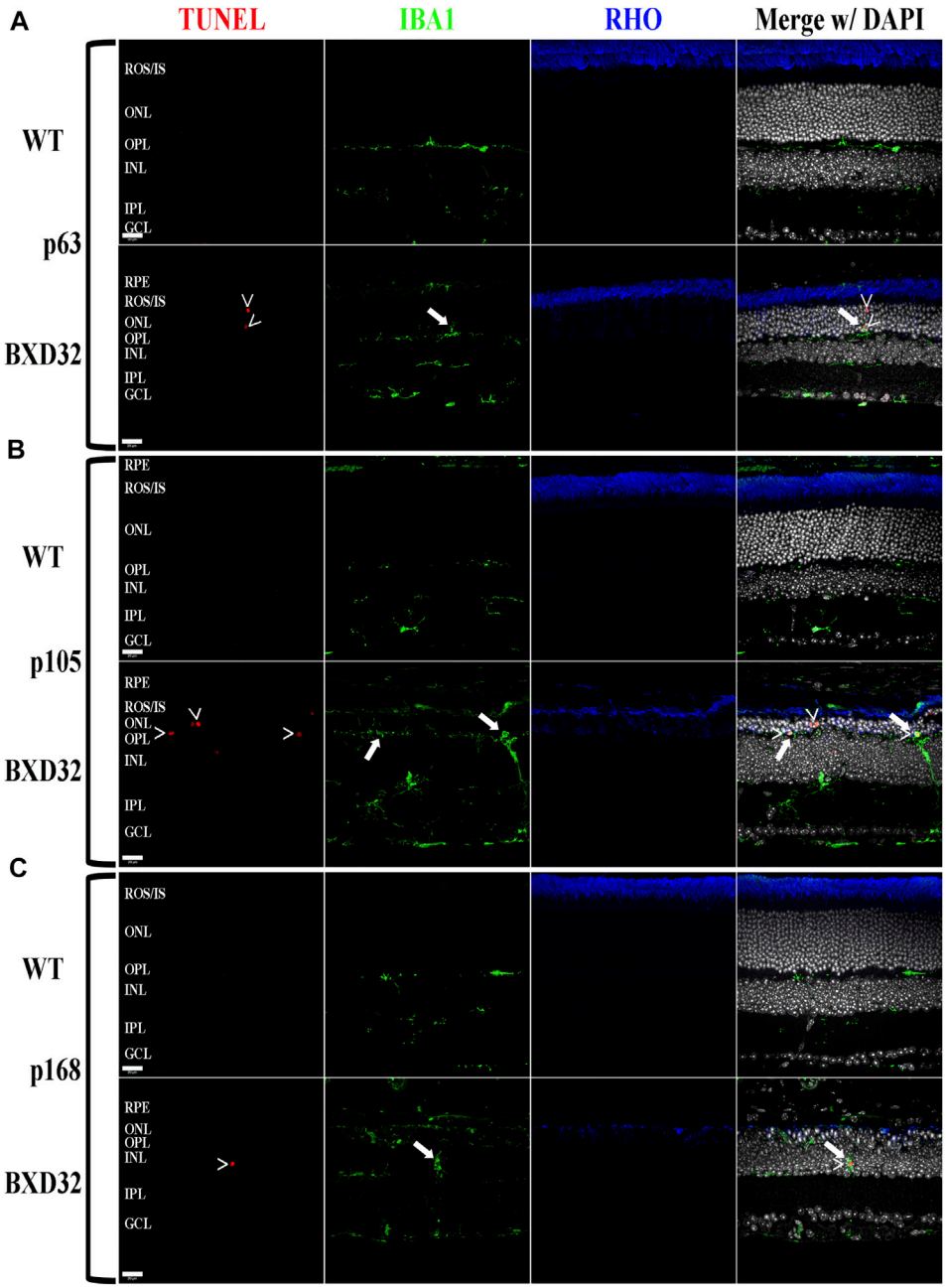

FIGURE 5 | The BXD32 retina exhibits cell death by apoptosis and proper function of microglia. Using TUNEL labeling (red) for apoptotic nuclei (arrowheads, >) and immunolabeling for monocytes (IBA1, green) and photoreceptors (RHO, blue) at p63 **(A)**, p105 **(B)** and p168 **(C)**, presumed microglia can be observed migrating to the ONL and phagocytosing apoptotic photoreceptor nuclei (arrows) the normal function of microglial cells in the retina under degenerative conditions. Nuclei stained with DAPI (white/grey). RPE, retinal pigment epithelium; ROS/IS, rod outer segments/inner segments; ONL, outer nuclear layer; OPL, outer plexiform layer; INL, inner nuclear layer; IPL, inner plexiform layer; GCL, ganglion cell layer. Scale bars = 20 μm.

et al., 2012; Balic et al., 2020; Yang et al., 2020). To examine for activation of the JAK/STAT signaling pathway, we performed fIHC for both pSTAT3-Tyr705 and pSTAT3-Ser727 along with total STAT3 and the negative regulator of the pathway, SOCS3. We observed dramatic upregulation of pSTAT3-Tyr705 with age (**Figure 8** and **Supplementary Figure S6**) and a concurrent phosphorylation at S727 (**Figure 9** and **Supplementary Figure S7**). As expected, the pSTAT3-Tyr705 localizes to the nuclei of the various retinal cell types while the pSTAT3-Ser727 can be found in both the nuclei as well as other non-nuclear regions such as the IPL. Interestingly, the total STAT3 and pSTAT3-Ser727 do not co-label unless present in the nucleus. As the epitope for the STAT3 antibody (peptide surrounding Gln692) is prior to the Ser727 site, the lack of co-labeling seems confounding; however,

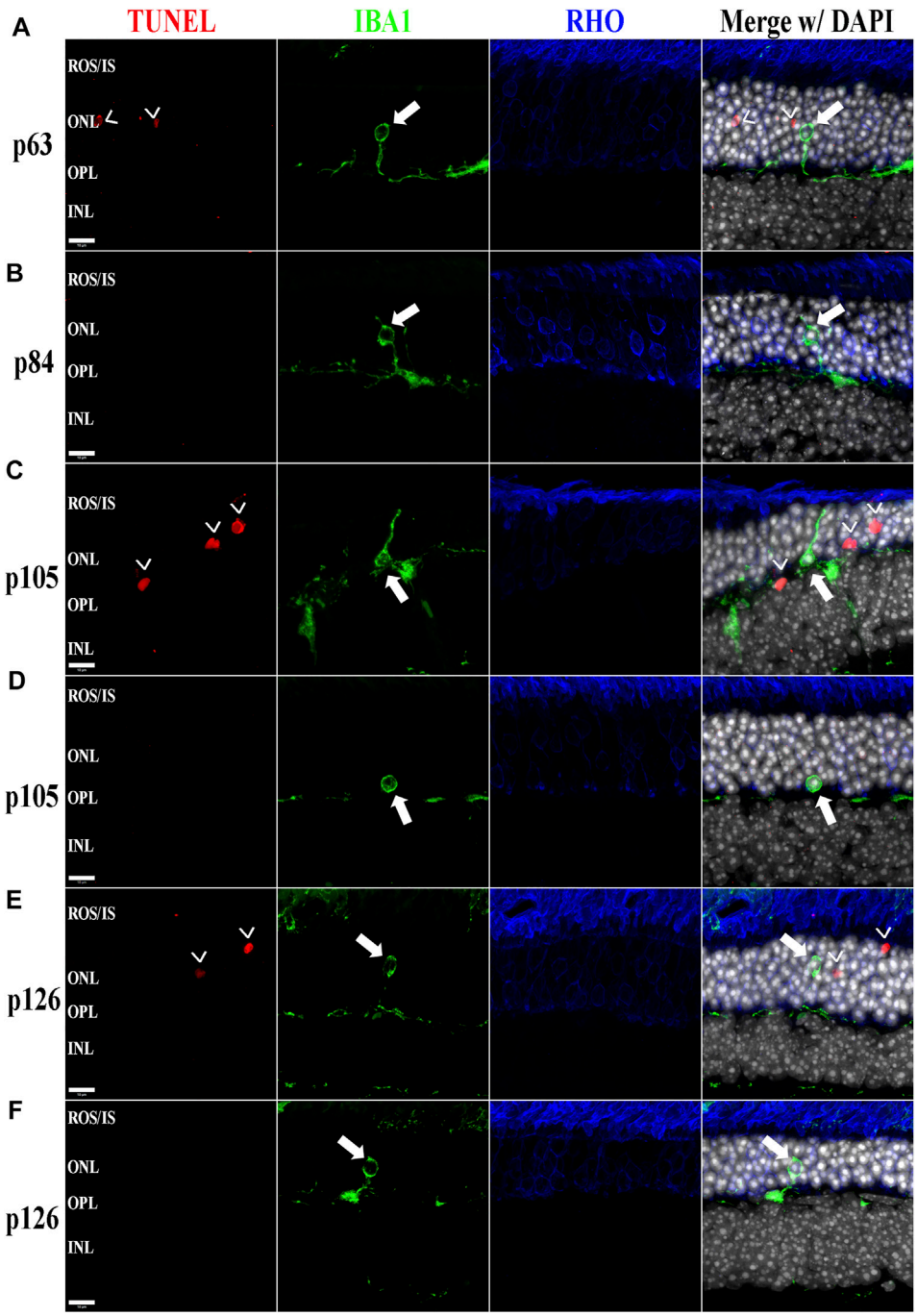

FIGURE 6 | The BXD32 mouse retina shows aberrant phagocytosis of living photoreceptors by monocytes. Using TUNEL labeling (red) for apoptotic nuclei (arrowheads, >) and immunolabeling for monocytes (IBA1, green) and photoreceptors (RHO, blue) at p63 **(A)**, p84 **(B)**, p105 **(C,D)**, **and** p126 **(E,F)**, monocytes of either microglial or bloodborne origins can be observed phagocytosing non-apoptotic photoreceptors (arrows), a process known as phagoptosis. Nuclei stained with DAPI (white/grey). ROS/IS, rod outer segments/inner segments; ONL, outer nuclear layer; OPL, outer plexiform layer; INL, inner nuclear layer. Scale bars = 10 μm.

previous works have shown that STAT3 is proteolyzed by multiple caspases, enzymes which we know are involved in apoptosis and inflammation, both processes of which appear heavily active in the BXD32 mouse retina (Darnowski et al., 2006; Matthews et al., 2007). As there are three recognized isoforms of STAT3 (α, β, and γ, though a δ form has also been observed), but only one of them has the Ser727 site, the Ser727 labeling must be on STAT3α. As shown in Danowski, *et al,* six putative caspase recognition sites are present in the STAT3α protein, with an xxxD motif present from residues 720 to 723, immediately prior to the

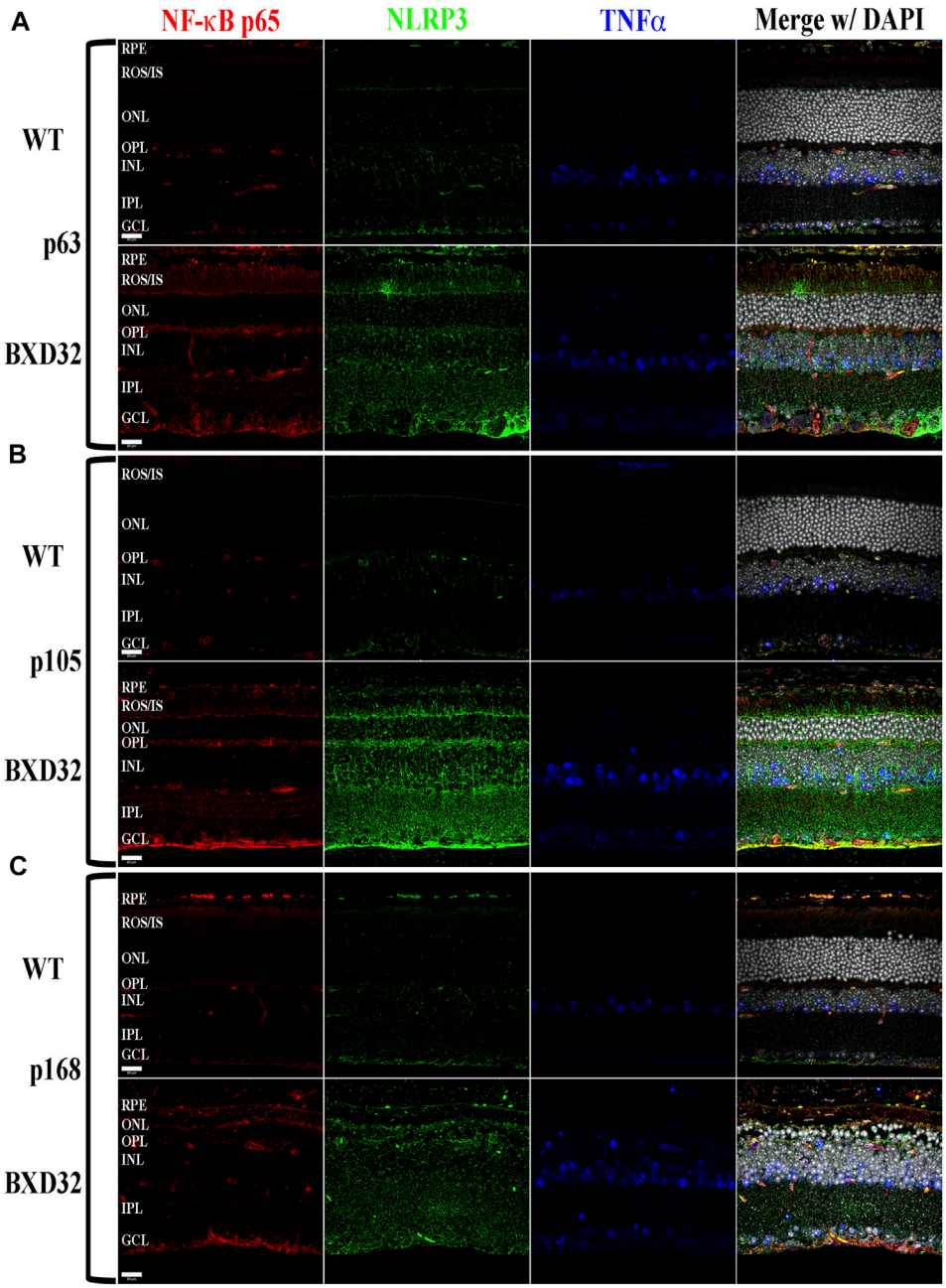

FIGURE 7 | The proinflammatory cytokine TNFα and one of its cognate pathways, the NF-κB/NLRP3 inflammasome, are substantially upregulated and activated in the BXD32 mouse retina. Using immunolabeling for NF-κB p65 (red), NLRP3 (green), and TNFα (blue), the BXD32 mouse retina displays upregulated levels of all three proteins examined beginning as early as p63 **(A)** and continuing through p105 **(B)** and p168 **(C)**, indicating a chronic proinflammatory retinal environment. Nuclei stained with DAPI (white/grey). RPE, retinal pigment epithelium; ROS/IS, rod outer segments/inner segments; ONL, outer nuclear layer; OPL, outer plexiform layer; INL, inner nuclear layer; IPL, inner plexiform layer; GCL, ganglion cell layer. Scale bars = 20 μm.

Ser727 site but after the STAT3 epitope. This is a quite plausible explanation for the large quantity of pSTAT3-Ser727 labeling observed outside of the nuclei. This is the first time we have observed such an intense and copious amount of STAT3 activation in a mouse model of RP as, in the rhodopsin mouse models, the pSTAT3-Tyr705 labeling was confined or mostly confined to the Müller cells and photoreceptors; however, as observed in the BXD32 retina, the STAT3 activation broadens to nearly every retinal cell type as early as p63 with a concomitant propagation across the entire retinal section by p147. We also observe, in contrast to what was observed in the rhodopsin-mediated RP mouse models, a substantial increase in the levels of

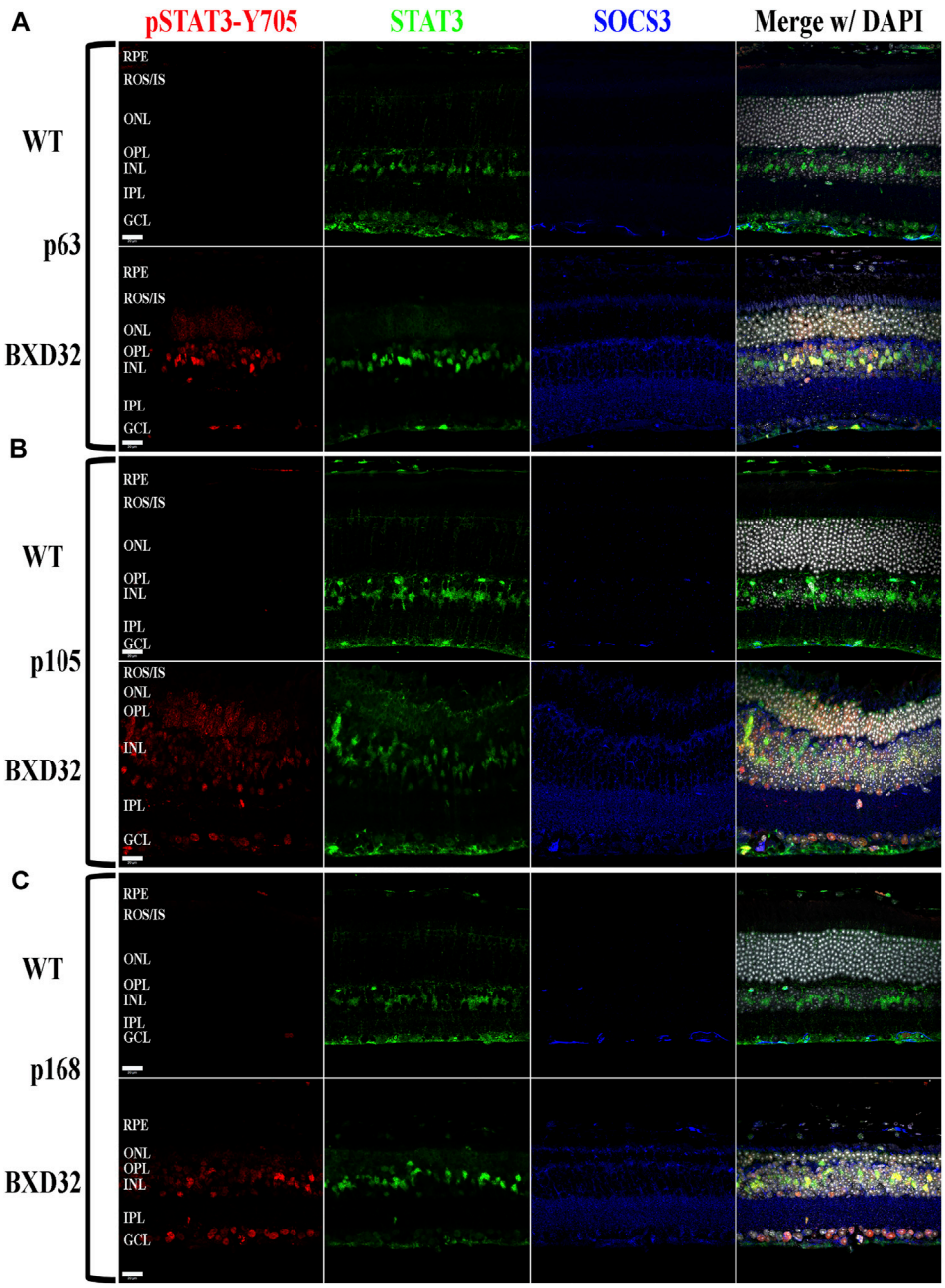

FIGURE 8 | Activation of STAT3 by JAK phosphorylation is observed in the BXD32 mouse retina. Using immunolabeling for pSTAT3 at tyrosine 705 (pSTAT3-Y705, red), total STAT3 (green) and the inhibitory protein SOCS3 (blue), the BXD32 mouse retina exhibits both increased expression of total STAT3 and the inhibitory protein SOCS3, while also having substantial STAT3-Y705 phosphorylation which increases with age from p63 **(A)** to p105 **(B)** up through p168 **(C)**. This pSTAT3 labeling is observed in multiple cell layers of the retina including the ONL, INL and GCL. Nuclei stained with DAPI (white/grey). RPE, retinal pigment epithelium; ROS/IS, rod outer segments/inner segments; ONL, outer nuclear layer; OPL, outer plexiform layer; INL, inner nuclear layer; IPL, inner plexiform layer; GCL, ganglion cell layer. Scale bars = 20 μm.

SOCS3 in the BXD32 mouse retina compared to WT retinas, indicating, in conjunction with phosphorylation at Ser727, a possible attempt to lessen or control the proinflammatory signaling. Using ImageJ, fluorescent intensities were quantified from confocal images for all immunolabels and the results expressed as the means ± SEM (**Figure 10**).

DISCUSSION

Progressive RDs affect a myriad of diverse populations. For instance, AMD preferentially afflicts elderly white females from western cultures while RP and LCA primarily affect young and middle-aged adults and children/teenagers,

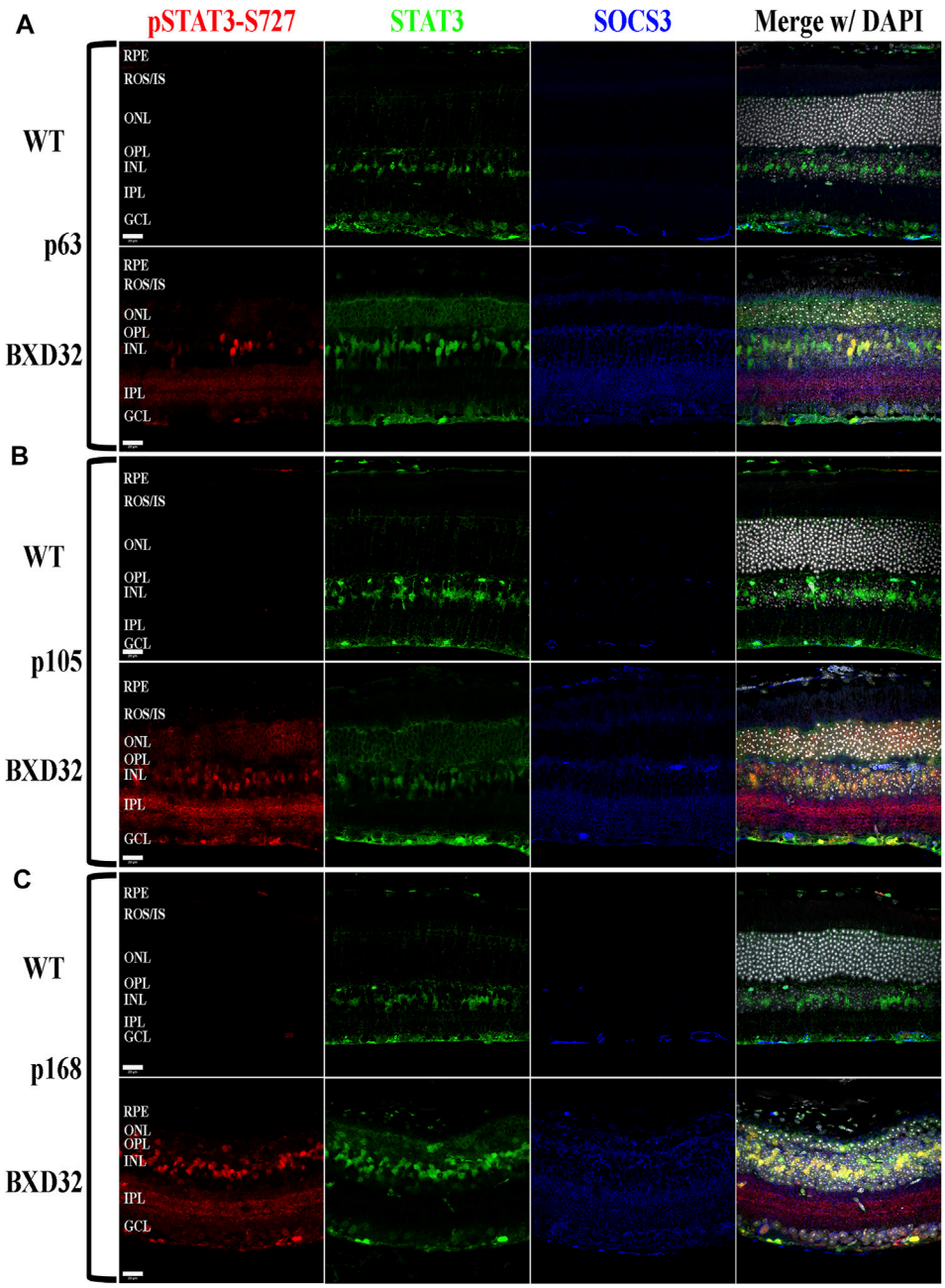

FIGURE 9 | BXD32 mouse retinas also exhibit STAT3 phosphorylation at serine 727, a multifunctional phosphorylation site. Using immunolabeling for pSTAT3 at serine 727 (pSTAT3-S727, red), total STAT3 (green), and SOCS3 (blue), it is observed that BXD32 retinas have excessive phosphorylation on STAT3-S727, a phosphorylation site serving multiple functions, two of which are the initiation of dephosphorylation of Y705, the inactivation step of STAT3, and upregulation of the mRNA for SOCS3. This upregulation can be observed in p63 **(A)**, p105 **(B)**, and p168 **(C)** retinas. The upregulation of both STAT3 and SOCS3 can also be observed in these sections. Nuclei stained with DAPI (white/grey). RPE, retinal pigment epithelium; ROS/IS, rod outer segments/inner segments; ONL, outer nuclear layer; OPL, outer plexiform layer; INL, inner nuclear layer; IPL, inner plexiform layer; GCL, ganglion cell layer. Scale bars = 20 μm.

respectively, from regions with more consanguineous families (den Hollander et al., 2008; Jordan et al., 2021; Rho et al., 2021). The heterogeneity of RDs has, to date, been one of the most in surmountable factors in producing therapeutics capable of tackling multiple types of RDs. The primarily genetic etiologies and age of disease onsets of RP and LCA make gene therapy for these diseases an arduous, complicated task. To exemplify this, one can examine the variety of modes of inheritance associated with RP. While autosomal recessive or X-linked recessive RP can be somewhat straightforward (i.e.

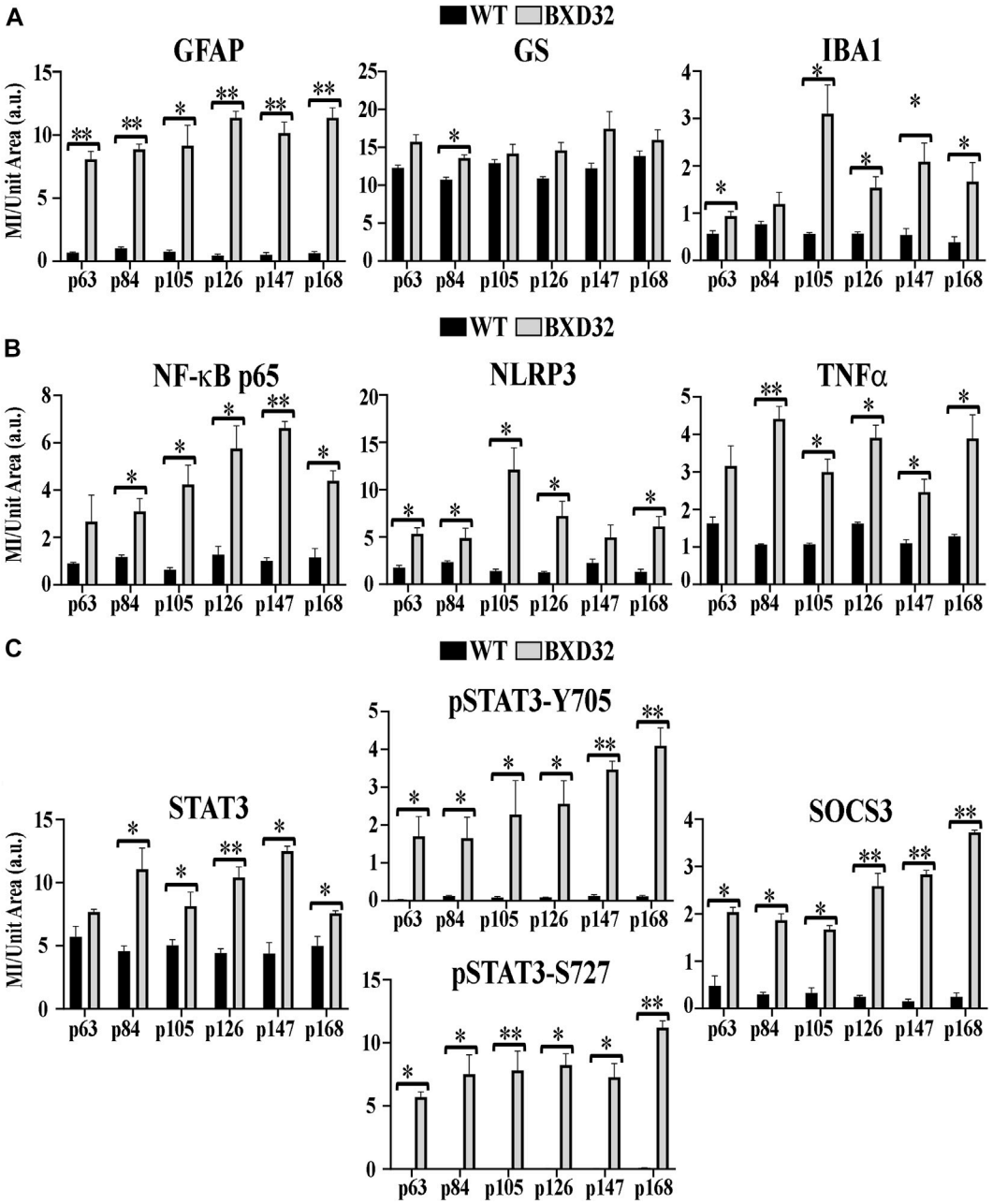

FIGURE 10 | Quantification of fIHC. Using ImageJ, mean intensity (MI) per unit area in arbitrary units (a.u.) was assessed for fIHC labeling of GFAP, GS, and IBA1 **(A)**; NF-κB, NLRP3, and TNFα **(B)**; and STAT3, pSTAT3-Y705 and S727, and SOCS3 **(C)** in WT (black) and BXD32 (grey) mouse retinas with age. Error bars = ±SEM. *, $p < 0.05$; **, $p < 0.005$.

replacing the mutated gene product with the correct gene product), treating the autosomal dominant or maternally inherited forms becomes significantly more challenging as supplying the correct protein product doesn't correct the issue as one copy of the mutated gene is enough to cause the degeneration (Dryja et al., 1990; Rivolta et al., 2002; Ferrari et al., 2011; Gorbatyuk et al., 2012; Hollingsworth and Gross, 2012; Orlans et al., 2020; O'Neal and Luther, 2021). Thus, a more intricate and sophisticated therapy is necessary to reduce expression of the mutated gene, while possibly also enhancing expression of the correct gene. LCA, though always recessively inherited, presents a different problem. While gene therapy for one form LCA has already been FDA-approved (LCA caused by *RPE65* mutations), one must now consider the age of the subjects that need to be treated (Acland et al., 2001; Narfstrom et al., 2003). For LCA to be effectively countered and the

highest amount of vision preserved for the patients, they would need to be treated as infants/young children or even *in utero* as LCA has a disease onset of birth and often a high rate of progression (den Hollander et al., 2008). In the case of AMD, patients may not even know they have an RD until the degeneration has already set in. By this point, the lost vision cannot be restored as the photoreceptors and/or RPE in that region have already degenerated and the disease progression cannot, as of yet, be halted or even hindered in many cases, especially in the dry form (Chintalapudi et al., 2019; Rho et al., 2021).

In describing the many pitfalls associated with RD heterogeneity, one can easily lose hope in the prospects of treating these debilitating diseases; nevertheless, RDs do, in fact, have common factors. One of these, and currently one of the most promising targets, is retinal inflammation. All RDs present with some form of inflammatory phenotype, be it association with the complement system in AMD, upregulation of cytokine release and their downstream pathways in RP and LCA, or overactive aberrantly functioning monocytes, RDs are now seemingly always associated with a proinflammatory retinal uptick (Iannaccone et al., 2015; Iannaccone et al., 2017; Hollingsworth and Gross, 2020; Hollingsworth et al., 2021; Jordan et al., 2021; Rho et al., 2021). Targeting these molecules, cells and pathways could likely allow for the ability to slow the progression of the degenerative phenotypes associated with progressive RDs. The fact that many of the proinflammatory cytokines and chemokines observed in RD retinas are also found to be associated with cancer and autoinflammatory conditions, finding already FDA-approved therapeutics targeting these molecules can be as simple as doing an Internet search such as on DrugCentral.com. For example, in the mouse models of RP referenced previously (as well as the BXD32 mouse described in this work), upregulation of the JAK/STAT pathway was observed and this fell heavily in the Müller cells (Hollingsworth and Gross, 2020; Hollingsworth et al., 2021). By searching DrugCentral.com, our group discovered the drug upadacitinib, an FDA-approved JAK inhibitor produced by Abbvie, that we tested with positive results on LIF-activated rat retinal Müller cells (rMC-1 cells) (Hollingsworth et al., 2021).

Within this manuscript, we describe a novel polygenic model of IRD, the BXD32 mouse strain. As we have shown, the retinas of these mice degenerate at varied rates in different geographic regions of the retina with regions from the central to peripheral and superior to inferior retina degenerating more rapidly with an onset as early as p63. Further preliminary work looking at a younger age has shown that apoptosis of photoreceptors is already occurring at p42 (n = 1, **Supplementary Figure S8**). As we continue to investigate the pathogenetic mechanisms governing the degeneration observed in these mice, younger ages will be inspected to determine the specific age of onset. As these mice represent a spontaneous IRD, they could make a more accurate model of the human condition, especially in cases of polygenic IRDs, which have been shown to occur in human patients (Bergsma and Brown, 1975; Kajiwara et al., 1994; Katsanis et al., 2001; Burkard et al., 2018), when compared to the more artificial transgenic and knock-in models of IRDs. In the BXD32 mouse retina, we documented numerous markers of proinflammatory pathway activation, of which one striking observation was macrophages performing both proper and aberrant phagocytosis of retinal cells. Some of these cells were labeled for TUNEL, a marker for apoptosis; however, several cells observed being phagocytosed at all ages lacked TUNEL labeling, indicating the process of phagoptosis, previously described in other models of RP (Brown and Neher, 2012; Brown and Neher, 2014; Li et al., 2015; Zhao et al., 2015; Hollingsworth et al., 2021). This process is likely a strong underlying cause of the rapid pace of degeneration. We have, in addition, shown upregulation of numerous proinflammatory factors and pathways. TNFα is secreted by multiple cell types including macrophages and glial cells. This allows for initiation of pathways involving activation of NF-κB and the NLRP3 inflammasome (Collart et al., 1990; Hohmann et al., 1990; Meichle et al., 1990). Interestingly, these pathways can create a positive feedback loop which ultimately causes more secretion of TNFα (Collart et al., 1990; Hohmann et al., 1990; Meichle et al., 1990; Shannon et al., 1990). We also show that the JAK/STAT signaling pathway is activated in the BXD32 mouse retina and that this activation ultimately spans the entire retina. At this time, we are uncertain as to which cytokine(s) are initiating this pathway as many can, including IL-6, LIF, and others (Levy and Lee, 2002; Murray, 2007). We have future experiments planned to pin down the cytokine(s) in order to better understand the purpose of STAT3 activation. In addition to the Tyr705 phosphorylation which activates STAT3, we also observed a dramatic increase in phosphorylation at Ser727, a site conferring multiple different properties. Ser727 is typically only phosphorylated after Tyr705 as Ser727 phosphorylation is an initiation step to deactivate STAT3 by dephosphorylating Tyr705 and inducing upregulation of the SOCS3 mRNA, the inhibitor of this pathway (Lim and Cao, 1999; Wakahara et al., 2012; Yang et al., 2020). We also found it quite interesting that the Ser727 phosphorylation labeling existed outside of the nucleus and did not colocalize with total STAT3 in these regions. As we mentioned, this could be explained by caspase activity targeting an xxxD caspase cleavage motif near the C-terminus of STAT3 (Darnowski et al., 2006; Matthews et al., 2007). Future plans for the BXD32 mouse include experiments to pin down the exact genetic etiologies resulting in the degenerative phenotype to assess its applicability as a preclinical model for testing of therapeutics.

Utilizing pre-clinical animal models of RDs such as the BXD32 mouse and the therapeutic resources already available to the scientific community, treating RDs by targeting inflammation has become a pivotal and highly explored area of basic and clinical research in ophthalmology. Thus, it is our goal, to use our pre-clinical mouse models including BXD32 to better understand the pathophysiology of these diseases and discover more efficacious treatments and ultimately, cures, for progressive RDs.

DATA AVAILABILITY STATEMENT

The raw data supporting the conclusions of this article will be made available by the authors, without undue reservation.

ETHICS STATEMENT

The animal study was reviewed and approved by University of Tennessee Health Science Center IACUC.

AUTHOR CONTRIBUTIONS

Conceptualization, TJH and MMJ; methodology, TJH; investigation, TJH, XW, RS, and WW; resources, MMJ; data curation, TJH and XW; writing—original draft preparation, TJH; writing—review and editing, TJH and MMJ; visualization, TJH and MMJ; project administration, TJH and MMJ; funding acquisition, MMJ All authors have read and agreed to the published version of the manuscript.

FUNDING

This research was funded by the National Institutes of Health (NIH), National Eye Institute (NEI; EY021200 to MMJ), and Research to Prevent Blindness (RPB) Catalyst Award for Innovative Research Approaches for Age-Related Macular Degeneration (to MMJ) and RPB Challenge Award (to the Hamilton Eye Institute at UTHSC).

ACKNOWLEDGMENTS

We would like to thank the Neuroscience Institute for the use of the Zeiss 710 LSM.

SUPPLEMENTARY MATERIAL

The Supplementary Material for this article can be found online at: https://www.frontiersin.org/articles/10.3389/fphar.2022.839424/full#supplementary-material

REFERENCES

Acland, G. M., Aguirre, G. D., Ray, J., Zhang, Q., Aleman, T. S., Cideciyan, A. V., et al. (2001). Gene Therapy Restores Vision in a Canine Model of Childhood Blindness. *Nat. Genet.* 28 (1), 92–95. doi:10.1038/ng0501-92

Al-Zamil, W. M., and Yassin, S. A. (2017). Recent Developments in Age-Related Macular Degeneration: a Review. *Clin. Interv. Aging* 12, 1313–1330. doi:10.2147/CIA.S143508

Appelbaum, T., Santana, E., and Aguirre, G. D. (2017). Strong Upregulation of Inflammatory Genes Accompanies Photoreceptor Demise in Canine Models of Retinal Degeneration. *PLoS One* 12 (5), e0177224. doi:10.1371/journal.pone.0177224

Ashbrook, D. G., Arends, D., Prins, P., Mulligan, M. K., Roy, S., Williams, E. G., et al. (2021). A Platform for Experimental Precision Medicine: The Extended BXD Mouse Family. *Cell Syst* 12 (3), 235. doi:10.1016/j.cels.2020.12.002

Balic, J. J., Albargy, H., Luu, K., Kirby, F. J., Jayasekara, W. S. N., Mansell, F., et al. (2020). STAT3 Serine Phosphorylation Is Required for TLR4 Metabolic Reprogramming and IL-1β Expression. *Nat. Commun.* 11 (1), 3816. doi:10.1038/s41467-020-17669-5

Bauernfeind, F. G., Horvath, G., Stutz, A., Alnemri, E. S., MacDonald, K., Speert, D., et al. (2009). Cutting Edge: NF-kappaB Activating Pattern Recognition and Cytokine Receptors License NLRP3 Inflammasome Activation by Regulating NLRP3 Expression. *J. Immunol.* 183 (2), 787–791. doi:10.4049/jimmunol.0901363

Bergsma, D. R., and Brown, K. S. (1975). Assessment of Ophthalmologic, Endocrinologic and Genetic Findings in the Bardet-Biedl Syndrome. *Birth Defects Orig Artic Ser.* 11 (2), 132–136.

Brown, G. C., and Neher, J. J. (2012). Eaten Alive! Cell Death by Primary Phagocytosis: 'phagoptosis'. *Trends Biochem. Sci.* 37 (8), 325–332. doi:10.1016/j.tibs.2012.05.002

Brown, G. C., and Neher, J. J. (2014). Microglial Phagocytosis of Live Neurons. *Nat. Rev. Neurosci.* 15 (4), 209–216. doi:10.1038/nrn3710

Burkard, M., Kohl, S., Krätzig, T., Tanimoto, N., Brennenstuhl, C., Bausch, A. E., et al. (2018). Accessory Heterozygous Mutations in Cone Photoreceptor CNGA3 Exacerbate CNG Channel-Associated Retinopathy. *J. Clin. Invest.* 128 (12), 5663–5675. doi:10.1172/JCI96098

Chintalapudi, S. R., Wang, X., Wang, X., Shi, Y., Kocak, M., Palamoor, M., et al. (2019). NA3 Glycan: a Potential Therapy for Retinal Pigment Epithelial Deficiency. *FEBS J.* 286 (24), 4876–4888. doi:10.1111/febs.15006

Collart, M. A., Baeuerle, P., and Vassalli, P. (1990). Regulation of Tumor Necrosis Factor Alpha Transcription in Macrophages: Involvement of Four Kappa B-like Motifs and of Constitutive and Inducible Forms of NF-Kappa B. *Mol. Cel Biol* 10 (4), 1498–1506. doi:10.1128/mcb.10.4.1498-1506.1990

Cremers, F. P., Maugeri, A., den Hollander, A. I., and Hoyng, C. B. (2004). The Expanding Roles of ABCA4 and CRB1 in Inherited Blindness. *Novartis Found. Symp.* 255, 68–178. doi:10.1002/0470092645.ch6

Darnowski, J. W., Goulette, F. A., Guan, Y. J., Chatterjee, D., Yang, Z. F., Cousens, L. P., et al. (2006). Stat3 Cleavage by Caspases: Impact on Full-Length Stat3 Expression, Fragment Formation, and Transcriptional Activity. *J. Biol. Chem.* 281 (26), 17707–17717. doi:10.1074/jbc.M600088200

den Hollander, A. I., Roepman, R., Koenekoop, R. K., and Cremers, F. P. (2008). Leber Congenital Amaurosis: Genes, Proteins and Disease Mechanisms. *Prog. Retin. Eye Res.* 27 (4), 391–419. doi:10.1016/j.preteyeres.2008.05.003

Dryja, T. P., McGee, T. L., Hahn, L. B., Cowley, G. S., Olsson, J. E., Reichel, E., et al. (1990). Mutations within the Rhodopsin Gene in Patients with Autosomal Dominant Retinitis Pigmentosa. *N. Engl. J. Med.* 323 (19), 1302–1307. doi:10.1056/NEJM199011083231903

Ferrari, S., Di Iorio, E., Barbaro, V., Ponzin, D., Sorrentino, F. S., and Parmeggiani, F. (2011). Retinitis Pigmentosa: Genes and Disease Mechanisms. *Curr. Genomics* 12 (4), 238–249. doi:10.2174/138920211795860107

Fleckenstein, M., Keenan, T. D. L., Guymer, R. H., Chakravarthy, U., Schmitz-Valckenberg, S., Klaver, C. C., et al. (2021). Age-related Macular Degeneration. *Nat. Rev. Dis. Primers* 7 (1), 31. doi:10.1038/s41572-021-00265-2

Geisert, E. E., and Williams, R. W. (2020). Using BXD Mouse Strains in Vision Research: A Systems Genetics Approach. *Mol. Vis.* 26, 173–187.

Gorbatyuk, M. S., Gorbatyuk, O. S., LaVail, M. M., Lin, J. H., Hauswirth, W. W., and Lewin, A. S. (2012). Functional rescue of P23H Rhodopsin Photoreceptors by Gene Delivery. *Adv. Exp. Med. Biol.* 723, 191–197. doi:10.1007/978-1-4614-0631-0_26

Hohmann, H. P., Remy, R., Pöschl, B., and van Loon, A. P. (1990). Tumor Necrosis Factors-Alpha and -beta Bind to the Same Two Types of Tumor Necrosis Factor Receptors and Maximally Activate the Transcription Factor NF-Kappa B at Low Receptor Occupancy and within Minutes after Receptor Binding. *J. Biol. Chem.* 265 (25), 15183–15188. doi:10.1016/s0021-9258(18)77239-6

Hollingsworth, T. J., and Gross, A. K. (2012). Defective Trafficking of Rhodopsin and its Role in Retinal Degenerations. *Int. Rev. Cel Mol Biol* 293, 1–44. doi:10.1016/B978-0-12-394304-0.00006-3

Hollingsworth, T. J., and Gross, A. K. (2020). Innate and Autoimmunity in the Pathogenesis of Inherited Retinal Dystrophy. *Cells* 9 (3), 630. doi:10.3390/cells9030630

Hollingsworth, T. J., and Gross, A. K. (2013). The Severe Autosomal Dominant Retinitis Pigmentosa Rhodopsin Mutant Ter349Glu Mislocalizes and Induces

Rapid Rod Cell Death. *J. Biol. Chem.* 288 (40), 29047–29055. doi:10.1074/jbc.M113.495184

Hollingsworth, T. J., Hubbard, M. G., Levi, H. J., White, W., Wang, X., Simpson, R., et al. (2021). Proinflammatory Pathways Are Activated in the Human Q344X Rhodopsin Knock-In Mouse Model of Retinitis Pigmentosa. *Biomolecules* 11 (8), 1163. doi:10.3390/biom11081163

Hunt, D. M., Wilkie, S. E., Newbold, R., Deery, E., Warren, M. J., Bhattacharya, S. S., et al. (2004). Dominant Cone and Cone-Rod Dystrophies: Functional Analysis of Mutations in retGC1 and GCAP1. *Novartis Found. Symp.* 255, 37177–38178. discussion 49-50. doi:10.1002/0470092645.ch4

Iannaccone, A., Giorgianni, F., New, D. D., Hollingsworth, T. J., Umfress, A., Alhatem, A. H., et al. (2015). Circulating Autoantibodies in Age-Related Macular Degeneration Recognize Human Macular Tissue Antigens Implicated in Autophagy, Immunomodulation, and Protection from Oxidative Stress and Apoptosis. *PLoS One* 10 (12), e0145323. doi:10.1371/journal.pone.0145323

Iannaccone, A., Hollingsworth, T. J., Koirala, D., New, D. D., Lenchik, N. I., Beranova-Giorgianni, S., et al. (2017). Retinal Pigment Epithelium and Microglia Express the CD5 Antigen-like Protein, a Novel Autoantigen in Age-Related Macular Degeneration. *Exp. Eye Res.* 155, 64–74. doi:10.1016/j.exer.2016.12.006

Jordan, K. E., Jablonski, M. M., and Hollingsworth, T. J. (2021). Inflammation in the Pathogenesis of Progressive Retinal Dystrophies. *J. Ophthalmic Res. Vis. Care* 1 (1). doi:10.54289/JORVC2100103

Kajiwara, K., Berson, E. L., and Dryja, T. P. (1994). Digenic Retinitis Pigmentosa Due to Mutations at the Unlinked Peripherin/RDS and ROM1 Loci. *Science* 264 (5165), 1604–1608. doi:10.1126/science.8202715

Katsanis, N., Ansley, S. J., Badano, J. L., Eichers, E. R., Lewis, R. A., Hoskins, B. E., et al. (2001). Triallelic Inheritance in Bardet-Biedl Syndrome, a Mendelian Recessive Disorder. *Science* 293 (5538), 2256–2259. doi:10.1126/science.1063525

Kinuthia, U. M., Wolf, A., and Langmann, T. (2020). Microglia and Inflammatory Responses in Diabetic Retinopathy. *Front. Immunol.* 11, 564077. doi:10.3389/fimmu.2020.564077

Levy, D. E., and Lee, C. K. (2002). What Does Stat3 Do? *J. Clin. Invest.* 109 (9), 1143–1148. doi:10.1172/JCI15650

Lewis, G. P., and Fisher, S. K. (2003). Up-regulation of Glial Fibrillary Acidic Protein in Response to Retinal Injury: its Potential Role in Glial Remodeling and a Comparison to Vimentin Expression. *Int. Rev. Cytol.* 230, 263–290. doi:10.1016/s0074-7696(03)30005-1

Li, L., Eter, N., and Heiduschka, P. (2015). The Microglia in Healthy and Diseased Retina. *Exp. Eye Res.* 136, 116–130. doi:10.1016/j.exer.2015.04.020

Lim, C. P., and Cao, X. (1999). Serine Phosphorylation and Negative Regulation of Stat3 by JNK. *J. Biol. Chem.* 274 (43), 31055–31061. doi:10.1074/jbc.274.43.31055

Matthews, J. R., Watson, S. M., Tevendale, M. C., Watson, C. J., and Clarke, A. R. (2007). Caspase-dependent Proteolytic Cleavage of STAT3alpha in ES Cells, in Mammary Glands Undergoing Forced Involution and in Breast Cancer Cell Lines. *BMC Cancer* 7, 29. doi:10.1186/1471-2407-7-29

Meichle, A., Schütze, S., Hensel, G., Brunsing, D., and Krönke, M. (1990). Protein Kinase C-independent Activation of Nuclear Factor Kappa B by Tumor Necrosis Factor. *J. Biol. Chem.* 265 (14), 8339–8343. doi:10.1016/s0021-9258(19)39077-5

Murray, P. J. (2007). The JAK-STAT Signaling Pathway: Input and Output Integration. *J. Immunol.* 178 (5), 2623–2629. doi:10.4049/jimmunol.178.5.2623

Nakashima, K., and Taga, T. (1998). gp130 and the IL-6 Family of Cytokines: Signaling Mechanisms and Thrombopoietic Activities. *Semin. Hematol.* 35 (3), 210–221.

Narfström, K., Katz, M. L., Ford, M., Redmond, T. M., Rakoczy, E., and Bragadóttir, R. (2003). *In Vivo* gene Therapy in Young and Adult RPE65-/- Dogs Produces Long-Term Visual Improvement. *J. Hered.* 94 (1), 31–37. doi:10.1093/jhered/esg015

O'Neal, T. B., and Luther, E. E. (2021). *Retinitis Pigmentosa*. Treasure Island (FL): StatPearls.

Orlans, H. O., Barnard, A. R., Patrício, M. I., McClements, M. E., and MacLaren, R. E. (2020). Effect of AAV-Mediated Rhodopsin Gene Augmentation on Retinal Degeneration Caused by the Dominant P23H Rhodopsin Mutation in a Knock-In Murine Model. *Hum. Gene Ther.* 31 (13-14), 730–742. doi:10.1089/hum.2020.008

Qiao, Y., Wang, P., Qi, J., Zhang, L., and Gao, C. (2012). TLR-induced NF-Kb Activation Regulates NLRP3 Expression in Murine Macrophages. *FEBS Lett.* 586 (7), 1022–1026. doi:10.1016/j.febslet.2012.02.045

Rashid, K., Akhtar-Schaefer, I., and Langmann, T. (2019). Microglia in Retinal Degeneration. *Front. Immunol.* 10, 1975. doi:10.3389/fimmu.2019.01975

Rho, J., Percelay, P., Pilkinton, S., Hollingsworth, T. J., Kornblau, I., and Jablonski, M. M. (2021). "An Overview of Age-Related Macular Degeneration: Clinical, Pre-clinical Animal Models and Bidirectional Translation," in *Animal Models in Medicine and Biology* (London, United Kingdom: InTechOpen). doi:10.5772/intechopen.96601

Rivolta, C., Sharon, D., DeAngelis, M. M., and Dryja, T. P. (2002). Retinitis Pigmentosa and Allied Diseases: Numerous Diseases, Genes, and Inheritance Patterns. *Hum. Mol. Genet.* 11 (10), 1219–1227. doi:10.1093/hmg/11.10.1219

Sandoval, I. M., Price, B. A., Gross, A. K., Chan, F., Sammons, J. D., Wilson, J. H., et al. (2014). Abrupt Onset of Mutations in a Developmentally Regulated Gene during Terminal Differentiation of post-mitotic Photoreceptor Neurons in Mice. *PLoS One* 9 (9), e108135. doi:10.1371/journal.pone.0108135

Shannon, M. F., Pell, L. M., Lenardo, M. J., Kuczek, E. S., Occhiodoro, F. S., Dunn, S. M., et al. (1990). A Novel Tumor Necrosis Factor-Responsive Transcription Factor Which Recognizes a Regulatory Element in Hemopoietic Growth Factor Genes. *Mol. Cel Biol* 10 (6), 2950–2959. doi:10.1128/mcb.10.6.2950-2959.1990

Silverman, S. M., and Wong, W. T. (2018). Microglia in the Retina: Roles in Development, Maturity, and Disease. *Annu. Rev. Vis. Sci.* 4, 45–77. doi:10.1146/annurev-vision-091517-034425

Soto, I., and Howell, G. R. (2014). The Complex Role of Neuroinflammation in Glaucoma. *Cold Spring Harb Perspect. Med.* 4 (8). doi:10.1101/cshperspect.a017269

Ten Berge, J. C., Fazil, Z., van den Born, I., Wolfs, R. C. W., Schreurs, M. W. J., Dik, W. A., et al. (2019). Intraocular Cytokine Profile and Autoimmune Reactions in Retinitis Pigmentosa, Age-Related Macular Degeneration, Glaucoma and Cataract. *Acta Ophthalmol.* 97 (2), 185–192. doi:10.1111/aos.13899

Toma, C., Higa, N., Koizumi, Y., Nakasone, N., Ogura, Y., McCoy, A. J., et al. (2010). Pathogenic Vibrio Activate NLRP3 Inflammasome via Cytotoxins and TLR/nucleotide-binding Oligomerization Domain-Mediated NF-Kappa B Signaling. *J. Immunol.* 184 (9), 5287–5297. doi:10.4049/jimmunol.0903536

Ucgun, N. I., Zeki-Fikret, C., and Yildirim, Z. (2020). Inflammation and Diabetic Retinopathy. *Mol. Vis.* 26, 718–721.

Wakahara, R., Kunimoto, H., Tanino, K., Kojima, H., Inoue, A., Shintaku, H., et al. (2012). Phospho-Ser727 of STAT3 Regulates STAT3 Activity by Enhancing Dephosphorylation of Phospho-Tyr705 Largely through TC45. *Genes Cells* 17 (2), 132–145. doi:10.1111/j.1365-2443.2011.01575.x

Wooff, Y., Man, S. M., Aggio-Bruce, R., Natoli, R., and Fernando, N. (2019). IL-1 Family Members Mediate Cell Death, Inflammation and Angiogenesis in Retinal Degenerative Diseases. *Front. Immunol.* 10, 1618. doi:10.3389/fimmu.2019.01618

Yang, J., Kunimoto, H., Katayama, B., Zhao, H., Shiromizu, T., Wang, L., et al. (2020). Phospho-Ser727 Triggers a Multistep Inactivation of STAT3 by Rapid Dissociation of pY705-SH2 through C-Terminal Tail Modulation. *Int. Immunol.* 32 (2), 73–88. doi:10.1093/intimm/dxz061

Yi, Q. Y., Wang, Y. Y., Chen, L. S., Li, W. D., Shen, Y., Jin, Y., et al. (2019). Implication of Inflammatory Cytokines in the Aqueous Humour for Management of Macular Diseases. *Acta Ophthalmol.* 98, e309–e315. doi:10.1111/aos.14248

Zhao, L., Zabel, M. K., Wang, X., Ma, W., Shah, P., Fariss, R. N., et al. (2015). Microglial Phagocytosis of Living Photoreceptors Contributes to Inherited Retinal Degeneration. *EMBO Mol. Med.* 7 (9), 1179–1197. doi:10.15252/emmm.201505298

Conflict of Interest: The authors declare that the research was conducted in the absence of any commercial or financial relationships that could be construed as a potential conflict of interest.

Publisher's Note: All claims expressed in this article are solely those of the authors and do not necessarily represent those of their affiliated organizations, or those of the publisher, the editors and the reviewers. Any product that may be evaluated in this article, or claim that may be made by its manufacturer, is not guaranteed or endorsed by the publisher.

frontiers | Frontiers in Pharmacology

ORIGINAL RESEARCH
published: 06 April 2022
doi: 10.3389/fphar.2022.832448

Efficacy and Safety of Subthreshold Micropulse Yellow Laser for Persistent Diabetic Macular Edema After Vitrectomy: A Pilot Study

Vincenza Bonfiglio[1], Robert Rejdak[2], Katarzyna Nowomiejska[2], Sandrine Anne Zweifel[3], Maximilian Robert Justus Wiest[3], Giovanni Luca Romano[4,5], Claudio Bucolo[4,5], Lucia Gozzo[5], Niccolò Castellino[6], Clara Patane[6], Corrado Pizzo[6], Michele Reibaldi[7], Andrea Russo[6], Antonio Longo[5,6], Matteo Fallico[6], Iacopo Macchi[6], Maria Vadalà[1], Teresio Avitabile[5,6], Ciro Costagliola[8], Kamil Jonak[9,10] and Mario Damiano Toro[2,11]**

[1]Department of Experimental Biomedicine and Clinical Neuroscience, Ophthalmology Section, University of Palermo, Palermo, Italy, [2]Chair and Department of General and Pediatric Ophthalmology, Medical University of Lublin, Lublin, Poland, [3]Department of Ophthalmology, University of Zurich, Zurich, Switzerland, [4]Department of Biomedical and Biotechnological Sciences, Section of Pharmacology, University of Catania, Catania, Italy, [5]Center for Research in Ocular Pharmacology—CERFO, University of Catania, Catania, Italy, [6]Department of Ophthalmology, University of Catania, Catania, Italy, [7]Department of Surgical Sciences, Eye Clinic Section, University of Turin, Turin, Italy, [8]Eye Clinic Department of Neuroscience, Reproductive and Odontostomatological Sciences, University of Naples Federico II, Naples, Italy, [9]Department of Clinical Neuropsychiatry, Medical University of Lublin, Lublin, Poland, [10]Department of Computer Science, Lublin University of Technology, Lublin, Poland, [11]Eye Clinic, Public Health Department, University of Naples Federico II, Naples, Italy

Aim: To examine the effect of subthreshold micropulse yellow laser (SMYL) on best-corrected visual acuity (BCVA), central macular thickness (CMT), and optical coherence tomography angiography (OCT-A) changes in eyes with persistent diabetic macular edema (DME) after pars plana vitrectomy (PPV) for tractional DME (TDME).

Patients and Methods: In a comparative study, 95 eyes of 95 consecutive patients with persistent DME were prospectively enrolled. The SMYL group (54 eyes) was treated with SMYL 6 months after PPV, while the control group (41 eyes) was followed up without treatment. BCVA and CMT by OCT were analyzed at baseline and 3 and 6 months. Additionally, parameters such as the vessel density (VD) in the superficial capillary plexus (SCP) and deep capillary plexus (DCP), respectively, and the area of the foveal avascular zone (FAZ) were also evaluated on OCT-A.

Results: There were no significant differences between both groups in demographic data. In the SMYL group, mean BCVA was significantly increased [$F(2,106) = 17.25$; $p < 0.001$; $\eta_p^2 = 0.246$] from 51.54 ± 13.81 ETDRS letters at baseline to 57.81 ± 12.82 ETDRS letters at 3 months ($p < 0.001$) and 57.83 ± 13.95 EDTRS letters at 6 months ($p < 0.001$), respectively. In comparison to the control group, BCVA values were statistically significantly higher in the SMYL group at 3 and 6 months, respectively. Mean CMT significantly decreased [$F(2,106) = 30.98$; $p < 0.001$; $\eta_p^2 = 0.368$] from the baseline value 410.59 ± 129.91 µm to 323.50 ± 89.66 µm at 3 months ($p < 0.001$) and to 283.39 ± 73.45 µm at 6 months ($p < 0.001$). CMT values were significantly lower in the SMYL group ($p < 0.001$), especially at 6 months follow-up time ($p < 0.001$) compared with the control

Edited by:
Galina Sud'ina,
Lomonosov Moscow State University, Russia

Reviewed by:
Yusuke Ichiyama,
Shiga University of Medical Science, Japan
Tommaso Verdina,
University Hospital of Modena, Italy
Honghua Yu,
Guangdong Provincial People's Hospital, China

***Correspondence:**
Claudio Bucolo
claudio.bucolo@unict.it
Mario Damiano Toro
toro.mario@email.it

Specialty section:
This article was submitted to Inflammation Pharmacology, a section of the journal Frontiers in Pharmacology

Received: 09 December 2021
Accepted: 28 February 2022
Published: 06 April 2022

Citation:
Bonfiglio V, Rejdak R, Nowomiejska K, Zweifel SA, Justus Wiest MR, Romano GL, Bucolo C, Gozzo L, Castellino N, Patane C, Pizzo C, Reibaldi M, Russo A, Longo A, Fallico M, Macchi I, Vadalà M, Avitabile T, Costagliola C, Jonak K and Toro MD (2022) Efficacy and Safety of Subthreshold Micropulse Yellow Laser for Persistent Diabetic Macular Edema After Vitrectomy: A Pilot Study. Front. Pharmacol. 13:832448. doi: 10.3389/fphar.2022.832448

group. Parafoveal VD in the SCP and DCP was significantly higher in the SMYL group in comparison to the control group, respectively, at 3-month (SCP $p < 0.001$; DCP $p < 0.001$) and 6-month follow-up (SCP $p < 0.001$; DCP $p < 0.001$). FAZ area was also significantly smaller in the SMYL group at 6-month follow-up ($p = 0.001$). There were no adverse SMYL treatment effects.

Conclusion: SMYL therapy may be a safe and effective treatment option in eyes with persistent macular edema following PPV for TDME.

Keywords: subthreshold micropulse laser, tractional DME, OCT angiography, inflammation, diabetic retinopathy

INTRODUCTION

Diabetic macular edema (DME) is a major disorder with increasing public health importance across the world (Klein et al., 1995).

The pathogenesis of DME is complex and multifactorial, and it is the result of the disruption of the blood–retinal barrier (BRB) (Bandello et al., 2017; Ceravolo et al., 2020). A study by optical coherence tomography (OCT) has shown abnormalities in the vitreomacular interface (VMI) up to 75% of eyes with DME (Ophir et al., 2010). In particular, vitreomacular traction (VMT), reported from 4 to 25% (Thomas et al., 2005), is a relevant factor in the development and persistence of DME. Indeed, the retina interface can be distorted by attached vitreous, epiretinal membranes and abnormal taut vitreomacular adhesions (Hartley et al., 2008).

To date, intravitreal therapy (IVT) with anti-vascular endothelial growth factor (VEGF) agents or steroids is considered a first-line treatment of DME (Bucolo et al., 2018; Kodjikian et al., 2019; Arumuganathan et al., 2021; Elfalah et al., 2021). However, the treatment of tractional DME (TDME) with IVT of anti-VEGF or corticosteroids may be poorly effective due to a possible influence of tractional forces (Sadiq et al., 2016; Chang et al., 2017). In such cases, pars plana vitrectomy (PPV) has been proven to be an effective therapeutic option in the resolution of DME, removing the tractional cause that is involved in its pathogenesis (Flikier et al., 2019). Despite surgery, persistent or recurrent DME can occur, and it is difficult to treat due to the increased clearance of medications in the vitreous cavity of vitrectomized eyes (Gunay and Erdogan, 2021). Previous studies (Yanyali et al., 2007; Pessoa et al., 2018; Pessoa et al., 2019; Arumuganathan et al., 2021) observed the persistence of DME up to 22% of eyes with TDME treated with PPV.

Currently, no treatment algorithm exists for recurrent or persistent DME in vitrectomized eyes although the use of dexamethasone (DEX) (Reibaldi et al., 2012; Bonfiglio et al., 2017) or fluoroquinolone acetonide (FA) implants (Meireles et al., 2017; Pessoa et al., 2018) has been proved to be effective in these cases, playing an anti-inflammatory role, even if a risk of cataract progression, ocular hypertension, and endophthalmitis was reported (Bonfiglio et al., 2017; Bucolo et al., 2018; Pessoa et al., 2018). Laser photocoagulation has been historically represented as the main option for the treatment of DME. Subthreshold micropulse yellow laser (SMYL) is a new treatment option that turns out to be safe and effective in the treatment of macular edema induced by different retinal diseases, including DME in naïve eyes. SMYL uses a photo-stimulation process with repetitive short pulses at low temperatures through which the tissue is preserved (Frizziero et al., 2021). Yellow light has an excellent absorption rate for O2 Hb and is not absorbed by foveal pigments such as lutein and zeaxanthin, thus allowing central macular edema treatment without foveal damage (Gawecki 2019). This method is a revolutionary alternative when compared to a conventional continuous wavelength laser. Previous studies have demonstrated that, in eyes with naïve DME, SMYL treatment plays an anti-inflammatory effect, reducing the aqueous humor (AH) concentration of inflammatory cytokines secreted by retinal glial cells (GLCs), both Müller cells (MCs) and microglial cells (MGCs), and the number of hyper-reflective retinal spots (HRS) (Midena et al., 2019; Midena et al., 2020; Vujosevic et al., 2020).

This pilot study aimed to evaluate the functional and anatomical outcomes and the rate of side effects of SMYL for the treatment of persistent DME after PPV for TDME in comparison with a control group observed after PPV.

PATIENTS AND METHODS

In this perspective, comparative non-randomized pilot study, all consecutive pseudophakic patients with a persistent DME after PPV for TDME at the Retina Division of the Chair and Department of General and Pediatric Ophthalmology at the University of Lublin, Poland between March 2019 and September 2020 were evaluated. The study, compliant with the tenets of the Declaration of Helsinki, was approved by our Institutional Review Board (n° KE-0254/132/2019). Every patient signed written informed consent for the treatment of personal data.

In the present study, the included eyes with persistent DME after PPV were divided into two groups: DME eyes who received micropulse subthreshold laser treatment (SMYL group) and matched DME eyes observed after PPV without treatment (control group). All the eyes with persistent DME after PPV, included in the study, underwent a 25-gauge PPV, associated with epiretinal membrane (ERM) peeling and gas injection performed by the same surgeon (R.R.) under local anesthesia. If necessary, a posterior capsulotomy was performed at the beginning of PPV. The staining of the ERM was performed in all patients by brilliant blue G (BBG).

Persistent DME was defined as a persistent central macular thickness (CMT) ≥ 300 μm by spectral-domain (SD) OCT for at least 6 months after PPV, and no response to conventional treatments (steroid and non-steroidal anti-inflammatory eye drops, and tablets such as oral indomethacin) (Elkayal et al., 2021).

The inclusion criteria for eyes with persistent DME were: a confirmed diagnosis of diabetes mellitus Type 2 as defined by the World Health Organization (WHO) criteria; an age of ≥18 years; best-corrected visual acuity (BCVA) between 70 and 35 ETDRS letters; an absence of macular ischemia assessed with fluorescein angiography (FFA) and a follow-up of at least 6 months after SMYL laser treatment.

The exclusion criteria were co-existence of any eye disease that may affect the visual outcome including glaucoma, macular hole, age-related macular degeneration, vascular occlusion, axial length >26 mm, amblyopia, active proliferative diabetic retinopathy, and vitreous hemorrhage. The patients affected by chorioretinal atrophy in the macular area or lipid exudative disorders and grid or focal laser treatments, or IVT of any anti-VEGF agents or steroids during 6 months before PPV were also excluded. In the SMYL group, laser treatment with 577 nm SMYL photo-stimulation (IRIDEX IQ 577TM, IRIDEX, Mountain View, CA, United States) was performed on the macula by the same ophthalmologist (KN). The Area-Centralis lens (Volk Optical, Mentor, OH, United States) was used and the micropulse laser power was obtained for each eye after a continuous wave test burn that was located more than 3-disc diameters from the foveal center outside the vascular arcades in a non-edematous area. A 200 μm diameter spot was tested with a pulse duration of 200 msec and a power of 50 mW in a non-edematous area. The power was increased at 10 mW increments (whilst advancing the laser to non-edematous areas immediately beside the previous test site) until a barely visible tissue reaction (white color) was observed. The SMYL treatment was performed on the edema site, switching on a 5% duty cycle and adjusting the power to four times the test spot threshold. Two hundred milliseconds of exposure and 4 grids (7 × 7) with confluent spots of 200 μm (0.00 spacing), including the foveal center were used. The setting, including the spot size, lens, and duration remained the same as it was in the test spot (Verdina et al., 2020).

Retreatment was performed at 3 months from the first treatment, using the same power setting, if CMT was >300 μm, or the retinal thickness decrease in the treated ETDRS quadrant (on OCT map) was less than 20% of the baseline value (Vujosevic et al., 2020).

After SMYL treatment non-steroidal anti-inflammatory eye drops were administered twice a day for 1 month in all cases.

In both groups, functional and anatomical findings were recorded at baseline, 3 and 6 months, including autofluorescence.

A single, independent, well-trained, experienced ophthalmologist measured the BCVA using the Early Treatment Diabetic Retinopathy Study (ETDRS) charts at a 4 m distance. For statistical analysis, visual acuity was scored as the total number of letters read correctly (ETDRS score).

OCT angiography (OCT-A) was performed using an XR Avanti AngioVue OCT-A (version 2017.1.0.151AngioVue Phase 7 software with PAR) in the Angio Retina mode and a scanning area of 6 × 6 mm. The retinal vascular layers were visualized and segmented based on the default settings of the automated software algorithm embedded in the XR Avanti AngioVue OCT-A.

The three-dimensional projection artifacts removal (3D-PAR) algorithm was applied to simplify the OCT-A imaging interpretation by enhancing the depth resolution of vascular layers. This new algorithm retains the flow signal from real blood vessels, while suppressing the projected flow signal in deeper layers, avoiding downward tails on cross-sectional angiograms, and duplicated vascular patterns on *en* face angiograms (Iafe et al., 2016).

The images were reviewed by two retinal specialists for the correctness of segmentation; if segmentation errors were observed, they were corrected using the segmentation editing and propagation tool embedded in the AngioVue system.

The updated AngioVue software automatically calculates a single foveal avascular zone (FAZ) value as automated FAZ boundary detection provided by the AngioVue software, applied on a retinal slab that includes both superficial and deep vascular plex [from the internal limiting membrane (ILM) to outer plexus layer +10 μm]. This protocol was used based on the recent studies validating a single merged quantitative measurement of the FAZ (Coscas et al., 2016; Bonfiglio et al., 2019).

The vessel density (VD) was defined as the percentage area occupied by vessels in a circular region of interest (ROI) centered on the center of the FAZ with a diameter of 3 mm included inside the 6 × 6 mm scan area (Wiest et al., 2021). The AngioVue software automatically splits the ROI into three fields: the foveal area, a central circle with a diameter of 1 mm; and the parafoveal area and perifoveal area of 3.0 and 6.0 mm, respectively. The foveal and parafoveal density of superficial and deep capillary plex (SCP and DCP) were analyzed. Low-quality OCT-A images with signal strength index <50 were excluded from the analysis (Bonfiglio et al., 2019).

CMT was assessed by the same OCT system (version 2017.1.0.151 AngioVue Phase 7 software with PAR) at the same time as the retinal vasculature using the retinal map mode, which covered a 6 × 6 mm area centered at the fovea. CMT was automatically measured as the average macular thickness within a scope of 1 mm in diameter, centered around the fovea (Bonfiglio et al., 2019).

At the baseline examination, each radial SD-OCT scan and each OCT-A scan were marked as the patient's baseline and it was used as a reference for the subsequent scans using the "follow-up" function, assuring that the scans would be performed in the same position. Two masked expert investigators interpreted the SD-OCT images. When there was disagreement, a third investigator was consulted for the final decision.

Statistical Analysis

For statistical analysis, BCVA, CMT, and FAZ detected at baseline (6 months after PPV) and after SMYL laser treatment (3 and 6 months) were evaluated and presented as means ± standard deviations (SD) in both groups. The mixed model repeated measures analysis of variance (ANOVA) with η_p^2 as

TABLE 1 | Demographics and clinical characteristics of the SMYL and control group at baseline.

	SMYL group (n = 54 eyes)	Control group (n = 41 eyes)	p value
Mean age (years) ±SD	69.65 ± 11.30	67.81 ± 12.82	0.366
Gender (male/female ratio)	24/30	19/22	0.215
Mean duration of diabetes ±SD	13.67 ± 6.63	18.65 ± 3.72	0.291
Mean hemoglobin A1c level (%) ±SD	8.1 ± 2.1%	7.70 ± 0.81%	0.136

Abbreviations: SMYL, subthreshold micropulse yellow laser; SD, standard deviation.

TABLE 2 | Comparison of mean BCVA, CMT, and OCT-A parameters over the SMYL group.

	Baseline	3 months	6 months	ANOVA	
				p value	η_p^2
Mean BCVA (ETDRS letters) ±SD	51.54 ± 13.81	57.81 ± 12.82	57.83 ± 13.95	< 0.001*	0.246
Mean CMT (μm) ±SD	410.59 ± 129.91	331.01 ± 89.66	283.39 ± 73.45	< 0.001†	0.368
Mean foveal VD SCP (%) ±SD	25.51 ± 5.96	25.41 ± 5.16	27.53 ± 4.97	0.055	0.054
Mean foveal VD DCP (%) ±SD	25.38 ± 7.15	25.76 ± 7.48	27.09 ± 4.98	0.373	0.018
Mean parafoveal VD SCP (%) ±SD	42.17 ± 3.42	42.50 ± 3.75	43.43 ± 4.48	0.136	0.036
Mean parafoveal VD DCP (%) ±SD	47.69 ± 3.39	48.91 ± 3.86	47.98 ± 3.44	0.227	0.027
Mean FAZ (mm^2) ±SD	0.29 ± 0.09	0.29 ± 0.10	0.31 ± 0.12	0.478	0.014

**Post hoc baseline vs. 3 months:* p < *0.001; baseline vs. 6 months:* p < *0.001; 3 vs. 6 months:* p = *1*
†Post hoc baseline vs. 3 months: p < *0.001; baseline vs. 6 months:* p < *0.001; 3 vs. 6 months:* p = *0.012.*
Abbreviations: BCVA, best-corrected visual acuity; CMT, central macular thickness; OCT-A, optical coherence tomography angiography; SMYL, subthreshold micropulse yellow laser; ANOVA, analysis of variance; η_p^2 partial etha squared; ETDRS, Early Treatment Diabetic Retinopathy Study; SD, standard deviation; μm, micrometers; VD, vessel density; SCP, superficial capillary plexus; DCP, deep capillary plexus; FAZ, foveal avascular zone; mm^2, millimeter squared.

an effect size indicator was used to determine whether there were any significant differences between the baseline, 3 and 6 months of the follow-up. For post hoc comparison, Bonferroni test was used. A p value less than 0.003 was considered statistically significant (including correction for multiple comparisons). For statistical analysis of the data, the Statistical Package for the Social Sciences, v.17.0 for Windows (SPSS, Chicago, Ill., United States) has been applied.

RESULTS

In our study, 97 eyes of 97 patients with persistent DME after PPV for TDME met the inclusion criteria. Fifty-six eyes of 56 patients in the SMYL group were treated by SMYL (SMYL Group), while 41 eyes of 41 patients in the control group were observed. Two, out of 56 patients of the SMYL group, were excluded because lost at the 3 months follow-up. Therefore, 54 consecutive eyes of 54 patients were used for the data analysis.

Baseline demographics and clinical characteristics of both SMYL and control groups are shown in **Table 1**.

No statistically significant differences were observed between both groups at the baseline.

In the SMYL Group, the post hoc comparison showed that mean BCVA increased significantly from 51.54 ± 13.81 ETDRS letters (baseline) to 57.81 ± 12.82 ETDRS letters (p < 0.001) at 3 months and 57.83 ± 13.95 (p < 0.001) ETDRS letters at 6 months, respectively. No statistically significant differences were found between 3 and 6 months (p = 1, **Table 2**).

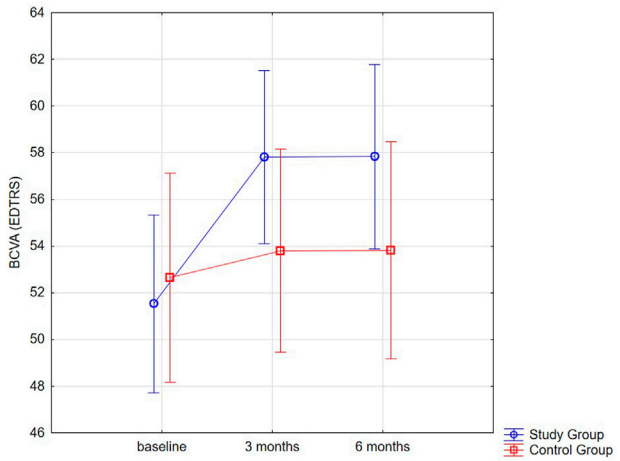

FIGURE 1 | Distribution plot for BCVA (EDTRS letters) mean values in both groups at baseline and 3 and 6 month.

In comparison to the control group, BCVA values were statistically significantly higher in the SMYL group (**Figure 1**).

After SMYL treatment, the mean CMT significantly decrease from the baseline value 410.59 ± 129.91 μm to 323.50 ± 89.66 μm at 3 months (p < 0.001) and to 283.39 ± 73.45 μm at 6 months (p < 0.001) (**Figure 2**; **Table 2**).

Additionally, in comparison to the control group, the CMT values were significantly lower in the SMYL group (interaction

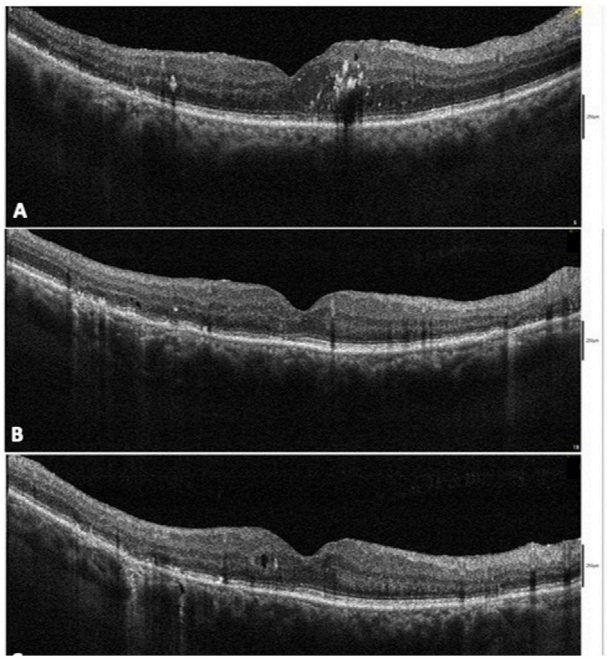

FIGURE 2 | Case of persistent diabetic macular edema (DME) after pars plana vitrectomy (PPV) for tractional diabetic macular edema (TDME) treated with subthreshold micropulse yellow laser (SMYL) **(A)**. At 3 months after SMYL treatment, a reduction in the macular thickness with a normalization of the outer retinal layer was seen **(B)**. A macular thickness within the normal limits and the presence of a microcysts in the macular area at 6-month follow-up were seen **(C)**.

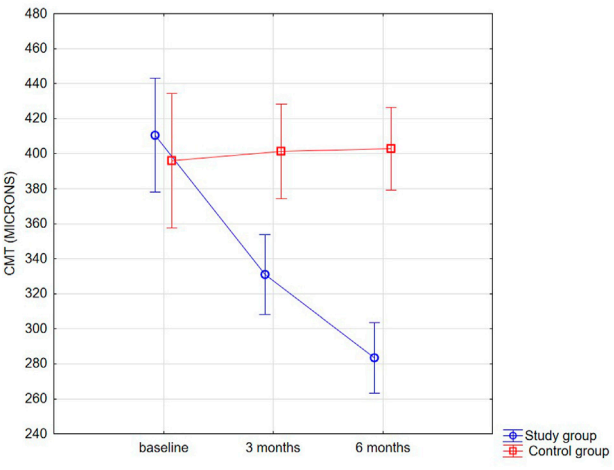

FIGURE 3 | Distribution plot for CMT (*μm*) mean values in both groups at baseline and 3 and 6 months.

effect $p < 0.001$), especially at 6 months follow-up time ($p < 0.001$; **Figure 3** and **Table 3**).

Regarding FAZ area, in SMYL Group, no statistically significant changes were seen between baseline (0.29 ±

TABLE 3 | BCVA, CMT, and OCT-A parameters of both SMYL and control groups at baseline and 3- and 6-month follow-up.

	Mean BCVA (ETDRS letters) ±SD			Mean CMT (μm) ±SD			Mean foveal VD SCP (%) ±SD			Mean foveal VD DCP (%) ±SD			Mean parafoveal VD SCP (%) ±SD			Mean parafoveal VD DCP (%) ±SD			Mean FAZ (mm^2) ±SD		
	Baseline	3 months	6 months	Baseline	3 months	6 months	Baseline	3 months	6 months	Baseline	3 months	6 months	Baseline	3 months	6 months	Baseline	3 months	6 months	Baseline	3 months	6 months
SMYL group	51.54 ± 13.81	57.81 ± 12.82	57.83 ± 13.95	410.59 ± 129.91	331.01 ± 89.66	283.39 ± 73.45	25.51 ± 5.96	25.41 ± 5.16	27.53 ± 4.97	25.38 ± 7.15	25.76 ± 7.48	27.09 ± 4.98	42.17 ± 3.42	42.50 ± 3.75	43.43 ± 4.48	47.69 ± 3.39	48.91 ± 3.86	47.98 ± 3.44	0.29 ± 0.09	0.29 ± 0.10	0.31 ± 0.12
Control group	52.64 ± 14.64	53.81 ± 14.81	53.82 ± 15.48	396.05 ± 106.98	401.28 ± 76.36	402.84 ± 75.55	25.27 ± 6.32	24.39 ± 4.28	23.49 ± 4.08	25.34 ± 6.99	23.43 ± 4.48	24.49 ± 4.04	41.71 ± 2.41	35.44 ± 3.82	31.17 ± 3.81	47.29 ± 1.87	40.09 ± 2.78	39.94 ± 1.91	0.32 ± 0.08	0.34 ± 0.09	0.38 ± 0.09
p-value	1	1	1	1	0.008	<0.001	1	1	0.004	1	1	0.671	1	<0.001	<0.001	1	<0.001	<0.001	1	0.036	0.001

Abbreviations: BCVA, best-corrected visual acuity; CMT, central macular thickness; SMYL, subthreshold micropulse yellow laser; OCT-A, optical coherence tomography angiography; ETDRS, Early Treatment Diabetic Retinopathy Study; SD, standard deviation; μm, micrometers; VD, vessel density; SCP, superficial capillary plexus; DCP, deep capillary plexus; FAZ, foveal avascular zone; mm^2, millimeter squared.

0.09 mm^2) and 3 (0.29 ± 0.10 mm^2—p = 0.478; ANOVA) and 6 months follow-up, respectively (0.31 ± 0.12 mm^2—p = 0.478; ANOVA). Similarly, no significant differences were found in the foveal and parafoveal VD in the SCP [F(2,106) = 2.973; p = 0.055; η_P^2 = 0.054] and DCP, respectively [F(2,106) = 0.973 p = 0.373; η_P^2 = 0.018]. Nevertheless, parafoveal VD in the SCP and DCP were significantly higher (interaction effect for both VD parameters $p < 0.001$) in the SMYL group when compared with the control group, respectively at 3 months (SCP $p < 0.001$; DCP $p < 0.001$) and 6 months follow-up (SCP $p < 0.001$; DCP $p < 0.001$). FAZ area was also significantly smaller in the SMYL group with respect to the control Group at 6 months follow-up (p = 0.001). The comparison of mean BCVA, CMT, and OCTA parameters over the follow-up course is shown in **Table 3**. No subjective symptoms such as visual field defects or scotoma were observed. None of the eyes experienced complications related to the SMYL treatment. A single SMYL treatment was performed in 18 eyes (33%), while 36 eyes (67%) needed a second retreatment after 3 months.

DISCUSSION

PPV associated with the ERM peeling is a highly effective procedure to treat patients with TDME. PPV could decrease DME through multiple mechanisms, including the release of tractional elements, improvement of intravitreal oxygenation, removal of pathological cytokines from the vitreous cavity, and acceleration of the half-life of intravitreal cytokines (Flikier et al., 2019). However, despite a functional improvement and a reduction of macular thickening, DME may not resolve completely up to 55% of treated eyes (Gunay and Erdogan, 2021) or reoccur up to 22% of patients after PPV (Pessoa et al., 2019; Fallico et al., 2021). The persistence or recurrence of macular edema can be explained by the vascular and inflammatory nature of the disease. In fact, while PPV releases the tractional component, the macular edema can be sustained by the dysfunction/breakdown of the inner and outer blood–retinal barrier (Parodi Battaglia et al., 2018).

The present prospective comparative pilot study has shown that SMYL treatment seems to be an effective and safe therapy to handle persistent DME in vitrectomized eyes following PPV for TDME leading to an improvement of both BCVA and retinal thickness after 6 months follow-up. Due to the possibility that DME may resolve slowly after PPV, SMYL therapy was deferred for up to 6 months after surgery (Behera et al., 2021), and long-term visual and anatomical outcomes in the SMYL group were compared with eyes observed after PPV without treatment (control group).

For 6 months follow-up, eyes treated with SMYL have shown both functional (from 51.54 ± 13.81 to 57.83 ± 13.95 ETDRS letters) and anatomical (from 410.59 ± 129.91 μm to 283.39 ± 73.45 μm) improvement with a single treatment in 33% and two treatments in 67% of eyes in comparison with either no visual acuity recovery either reduced macula thickness in Control group eyes.

These results suggest that in case of the persistent DME after PPV long-term follow-up did not show any significant restored visual and anatomical outcomes. Additionally, it is important to underline that SMYL is repeatable without foveal damage (Elfalah et al., 2021).

Beneficial results on the use of SMYL in the treatment of DME have been already reported by several authors in the literature (Bucolo et al., 2015; Verdina et al., 2020; Donati et al., 2021). Vujosevic et al. showed a significant improvement of BCVA from 69.7 ± 12.0 to 74.3 ± 9.5 ETDRS letters 6 months after treatment, although retinal thickness did not change during the follow-up (Vujosevic et al., 2020). This study included only naive DME eyes, which explain better visual acuity at the baseline and final follow-up.

Our results are in line with Donati et al. (Donati et al., 2021) who reported a reduction of CMT from 371.06 ± 37.8 to 326.70 ± 81.08 μm after 6 months follow-up in naïve DME eyes.

The previous authors have been already demonstrated the efficacy of micropulse laser in the treatment of macular edema in vitrectomized eyes.

Lutrull et al. (Luttrull, 2020) have reported better functional (from 0.6 ± 0.3 to 0.4 ± 0.3 logMar) and anatomical (from 364.6 ± 155.7 to 342.5 ± 112.7 μm) results after subthreshold diode micropulse laser treatment for persistent macular thickening after epiretinal membrane peeling.

In their study, the laser treatment was performed with an average of 41 months after PPV with a possible poor recovery. However, the authors stated that improvements in macular thickness and VA were not related to the natural history of progressive long-term post-membrane peeling, but to the efficacy of subthreshold diode laser macular treatment.

As regards the OCT-A parameters, our study has shown no alterations in SCP and DCP VDs in foveal and parafoveal areas, respectively, at 3 and 6 months after SMYL treatment. No modifications of the size of the FAZ were detected as well during the follow-up.

In addition, the control group eyes had significantly lower VD values at the level of the deep and superficial retinal plexi (in the parafoveal areas) and significant larger FAZ area when compared with the SMYL group. These OCT-A biomarkers confirmed progression in impaired macular perfusion in persistent DME eyes observed without treatment. It has been demonstrated that hypertension, blood pressure (BP) levels, and kidney function can affect OCTA metrics (Peng et al., 2020; Zeng et al., 2021). In the future, it would be interesting to verify the impact of hypertension, BP levels, and kidney function on OCTA metrics after SMYL treatment.

Similarly, Vujosevic et al. (Vujosevic et al., 2020) have demonstrated that micropulse laser does not alter vascular parameters such as superficial and deep VD in naïve eyes with macular edema even if they reported enlargement of the FAZ in DCP 6 months after the treatment. This could be due to a different OCT-A devise used. Indeed, the software of OCTA, used in our study, did not let to measure separately FAZ area into the SCP and DCP giving only one value measured in one slab and including superficial and deep plexi.

Currently, there are no guidelines for the treatment of persistent DME after PPV, although IVTs of anti-VEGF, corticosteroids such as DEX (Reibaldi et al., 2012; Bonfiglio

et al., 2017; Fallico et al., 2021) or FA (Meireles et al., 2017; Ong et al., 2021) implants have been proved to be effective. It should be considered that the efficacy of IVTs of anti-VEGF drugs in vitrectomized eyes is significantly reduced due to the increased clearance of the drug in the vitreous cavity (Edington et al., 2017), while DEX and FA implants have shown strong anti-inflammatory activity and good efficacy due to similar clearance in vitrectomized and non-vitrectomized eyes (Edington et al., 2017; Augustin et al., 2021). However, corticosteroids implants may lead to side effects, such as an increase in IOP, cataract progression, and endophthalmitis (Vie et al., 2017), and its use is contraindicated in glaucomatous eyes (Chou et al., 2018; Celik et al., 2020). Conversely, the main advantage of the treatment with a micropulse laser is represented by its safety profile. Indeed, as already demonstrated by previous studies, it does not cause any chorioretinal foveal damage (Midena et al., 2019; Elfalah et al., 2021; Fallico et al., 2021). In our study no modifications on autofluorescence or on FFA have been detected, supporting its safety even when used on the macular area (Gawecki, 2019; Midena et al., 2021). These results confirm that SMYL therapy acts on the outer blood–retinal barrier and on the pigmented epithelium (RPE) (Gawecki 2019; Frizziero et al., 2021; Midena et al., 2021). RPE layer is considered to be the main site of action of SMYL. RPE plays an important role in the pathogenesis of DME, in outer blood–retinal barrier regulation, in homeostasis, and the integrity and survival of retinal cells. It also regulates the transport of nutrients, ions, oxygen, and water between the retina and choroid. Therefore, SMYL can reduce macular edema by acting directly on the RPE through a photostimulating effect (Gawecki, 2019). Additionally, Midena et al. (Midena et al., 2020) reported the efficacy of SMYL in the reduction of VEGF concentration and aqueous humor muller cells biomarkers in diabetic eyes.

Recently, it has been reported that subthreshold micropulse laser reduces the aqueous humor concentration of inflammatory cytokines secreted by retinal glial cells, both Müller cells, and microglial cells in eyes with DME (Midena et al., 2019; Midena et al., 2020). Inflammatory cytokines, mainly produced by the retinal microglia, were significantly reduced after treatments, suggesting that subthreshold micropulse laser may act by deactivating microglial cells, and reducing local inflammatory diabetes-related response. (Midena et al., 2019). Additionally, some authors have shown that SMYL treatment plays an anti-inflammatory role in reducing the number of HRS (a sign of activated microglia cells in the retina) (Vujosevic et al., 2020).

Recently, it has been shown that B cell activation is involved in the pathogenesis of diabetic retinopathy (Liu et al., 2020) and RPE cells can inhibit B cell activation (Sugita et al., 2010). Therefore, it could be possible that subthreshold micropulse laser could also activate RPE cells to suppress B cell activation.

The main limitations of our study are the non-randomized design and the short-term follow-up (6 months). In addition, to conclude that there is no effect on visual field sensitivity, tests such as micro perimeter should be performed.

In conclusion, this pilot study has shown the efficacy and safety of SMYL laser in vitrectomized eyes in comparison with observed eyes, suggesting its early use in the management of persistent macular edema following PPV for TDME.

A further prospective randomized study could evaluate if different anatomical features of DME, such as subretinal fluid or HRS, could have a different response to SMYL treatment.

In addition, prospective randomized studies are required to compare the efficacy of SMYL treatment with other treatment procedures, such as IVT of anti-VEGF drugs or steroids, used to treat DME in vitrectomized eyes.

DATA AVAILABILITY STATEMENT

The raw data supporting the conclusion of this article will be made available by the authors without undue reservation.

ETHICS STATEMENT

The studies involving human participants were reviewed and approved by the Institutional Review Board (n° KE-0254/132/2019). The patients/participants provided their written informed consent to participate in this study.

AUTHOR CONTRIBUTIONS

VB, MT, SZ, CPa, CC, and GR made substantial contributions to conception, design, and interpretation of data. LG, VB, AL, AR, MF, NC, and MT carried out formal analysis of data. VB, GR, NC, MT, CPa, KN, RR, CB, and MT wrote the initial draft of the manuscript. CB, LG, CPi, MJ, KN, TA, MV, KJ, CC, and IM reviewed the manuscript critically for important intellectual content and gave final approval of the version to be submitted.

FUNDING

This research was funded by the University of Catania research grant PIAno inCEntivi RIcerca (PIACERI) Ateneo 2020/2022 (NanoRET). GR was supported by the PON AIM R&I 2014–2020—E66C18001260007.

REFERENCES

Arumuganathan, N., Wiest, M. R. J., Toro, M. D., Hamann, T., Fasler, K., and Zweifel, S. A. (2021). Acute and Subacute Macular and Peripapillary Angiographic Changes in Choroidal and Retinal Blood Flow post-intravitreal Injections. *Sci. Rep.* 11, 19381. doi:10.1038/s41598-021-98850-8

Augustin, A. J., Bopp, S., Fechner, M., Holz, F. G., Sandner, D., Winkgen, A. M., et al. (2021). The Impact of Vitrectomy on Outcomes Achieved with 0.19 Mg Fluocinolone Acetonide Implant in Patients with Diabetic Macular Edema. *Eur. J. Ophthalmol.* 4, 11206721211014728. doi:10.1177/11206721211014728

Bandello, F., Battaglia Parodi, M., Lanzetta, P., Loewenstein, A., Massin, P., Menchini, F., et al. (2017). Diabetic Macular Edema. *Dev. Ophthalmol.* 58, 102–138. doi:10.1159/000455277

Behera, U. C., Das, T., Sivaprasad, S., Rani, P. K., Raman, R., Agarwal, M., et al. (2021). Is Immediate Treatment Necessary for Diabetic Macular Edema after Pars Plana Vitrectomy for Tractional Complications of Proliferative Diabetic Retinopathy? *Int. Ophthalmol.* 41, 3607–3614. doi:10.1007/s10792-021-01923-w

Bonfiglio, V., Reibaldi, M., Fallico, M., Russo, A., Pizzo, A., Fichera, S., et al. (2017). Widening Use of Dexamethasone Implant for the Treatment of Macular Edema. *Drug Des. Devel. Ther.* 11, 2359–2372. doi:10.2147/DDDT.S138922

Bonfiglio, V., Ortisi, E., Scollo, D., Reibaldi, M., Russo, A., Pizzo, A., et al. (2019). 'Vascular Changes after Vitrectomy for Rhegmatogenous Retinal Detachment: Optical Coherence Tomography Angiography Study. *Acta Ophthalmol.* 98. doi:10.1111/aos.14315

Bucolo, C., Gozzo, L., Longo, L., Mansueto, S., Vitale, D. C., and Drago, F. (2018). Long-term Efficacy and Safety Profile of Multiple Injections of Intravitreal Dexamethasone Implant to Manage Diabetic Macular Edema: A Systematic Review of Real-World Studies. *J. Pharmacol. Sci.* 138, 219–232. doi:10.1016/j.jphs.2018.11.001

Bucolo, C., Musumeci, M., Salomone, S., Romano, G. L., Leggio, G. M., Gagliano, C., et al. (2015). Effects of Topical Fucosyl-Lactose, a Milk Oligosaccharide, on Dry Eye Model: An Example of Nutraceutical Candidate. *Front. Pharmacol.* 6, 280. doi:10.3389/fphar.2015.00280

Celik, N., Khoramnia, R., Auffarth, G. U., Sel, S., and Mayer, C. S. (2020). Complications of Dexamethasone Implants: Risk Factors, Prevention, and Clinical Management. *Int. J. Ophthalmol.* 13, 1612–1620. doi:10.18240/ijo.2020.10.16

Ceravolo, I., Oliverio, G. W., Alibrandi, A., Bhatti, A., Trombetta, L., Rejdak, R., et al. (2020). The Application of Structural Retinal Biomarkers to Evaluate the Effect of Intravitreal Ranibizumab and Dexamethasone Intravitreal Implant on Treatment of Diabetic Macular Edema. *Diagnostics (Basel)* 10, 413. doi:10.3390/diagnostics10060413

Chang, C. K., Cheng, C. K., and Peng, C. H. (2017). The Incidence and Risk Factors for the Development of Vitreomacular Interface Abnormality in Diabetic Macular Edema Treated with Intravitreal Injection of Anti-VEGF. *Eye (Lond)* 31, 762–770. doi:10.1038/eye.2016.317

Chou, T. H., Musada, G. R., Romano, G. L., Bolton, E., and Porciatti, V. (2018). Anesthetic Preconditioning as Endogenous Neuroprotection in Glaucoma. *Int. J. Mol. Sci.* 19, 237. doi:10.3390/ijms19010237

Coscas, F., Sellam, A., Glacet-Bernard, A., Jung, C., Goudot, M., Miere, A., et al. (2016). Normative Data for Vascular Density in Superficial and Deep Capillary Plexuses of Healthy Adults Assessed by Optical Coherence Tomography Angiography. *Invest. Ophthalmol. Vis. Sci.* 57, OCT211. doi:10.1167/iovs.15-18793

Donati, M. C., Murro, V., Mucciolo, D. P., Giorgio, D., Cinotti, G., Virgili, G., et al. (2021). Subthreshold Yellow Micropulse Laser for Treatment of Diabetic Macular Edema: Comparison between Fixed and Variable Treatment Regimen. *Eur. J. Ophthalmol.* 31, 1254–1260. doi:10.1177/1120672120915169

Edington, M., Connolly, J., and Chong, N. V. (2017). Pharmacokinetics of Intravitreal Anti-VEGF Drugs in Vitrectomized versus Non-vitrectomized Eyes. *Expert Opin. Drug Metab. Toxicol.* 13, 1217–1224. doi:10.1080/17425255.2017.1404987

Elfalah, M., AlRyalat, S. A., Toro, M. D., Rejdak, R., Zweifel, S., Nazzal, R., et al. (2021). Delayed Intravitreal Anti-VEGF Therapy for Patients during the COVID-19 Lockdown: An Ethical Endeavor. *Clin. Ophthalmol.* 15, 661–669. doi:10.2147/OPTH.S289068

Elkayal, H., Bedda, A. M., El-Goweini, H., Souka, A. A., and Gomaa, A. R. (2021). Pars Plana Vitrectomy versus Intravitreal Injection of Ranibizumab in the Treatment of Diabetic Macular Edema Associated with Vitreomacular Interface Abnormalities. *J. Ophthalmol.* 2021, 6699668. doi:10.1155/2021/6699668

Fallico, M., Maugeri, A., Romano, G. L., Bucolo, C., Longo, A., Bonfiglio, V., et al. (2021). Epiretinal Membrane Vitrectomy with and without Intraoperative Intravitreal Dexamethasone Implant: A Systematic Review with Meta-Analysis. *Front. Pharmacol.* 12, 635101. doi:10.3389/fphar.2021.635101

Flikier, S., Wu, A., and Wu, L. (2019). Revisiting Pars Plana Vitrectomy in the Primary Treatment of Diabetic Macular Edema in the Era of Pharmacological Treatment. *Taiwan J. Ophthalmol.* 9, 224–232. doi:10.4103/tjo.tjo_61_19

Frizziero, L., Calciati, A., Midena, G., Torresin, T., Parrozzani, R., Pilotto, E., et al. (2021). Subthreshold Micropulse Laser Modulates Retinal Neuroinflammatory Biomarkers in Diabetic Macular Edema. *J. Clin. Med.* 10, 1–10. doi:10.3390/jcm10143134

Gawecki, M. (2019). Micropulse Laser Treatment of Retinal Diseases. *J. Clin. Med.* 8, 1–18. doi:10.3390/jcm8020242

Gunay, B. O., and Erdogan, G. (2021). Evaluation of Macular Changes in the Long Term after Pars Plana Vitrectomy with Internal Limiting Membrane Peeling for Diabetic Macular Edema. *Ophthalmologica* 244, 237–244. doi:10.1159/000514992

Hartley, K. L., Smiddy, W. E., Flynn, H. W., Jr., and Murray, T. G. (2008). Pars Plana Vitrectomy with Internal Limiting Membrane Peeling for Diabetic Macular Edema. *Retina* 28, 410–419. doi:10.1097/IAE.0b013e31816102f2

Iafe, N. A., Phasukkijwatana, N., Chen, X., and Sarraf, D. (2016). Retinal Capillary Density and Foveal Avascular Zone Area Are Age-dependent: Quantitative Analysis Using Optical Coherence Tomography Angiography. *Invest. Ophthalmol. Vis. Sci.* 57, 5780–5787. doi:10.1167/iovs.16-20045

Klein, R., Klein, B. E., Moss, S. E., and Cruickshanks, K. J. (1995). The Wisconsin Epidemiologic Study of Diabetic Retinopathy. XV. The Long-Term Incidence of Macular Edema. *Ophthalmology* 102, 7–16. doi:10.1016/s0161-6420(95)31052-4

Kodjikian, L., Bellocq, D., Bandello, F., Loewenstein, A., Chakravarthy, U., Koh, A., et al. (2019). First-line Treatment Algorithm and Guidelines in center-involving Diabetic Macular Edema. *Eur. J. Ophthalmol.* 29, 573–584. doi:10.1177/1120672119857511

Liu, B., Hu, Y., Wu, Q., Zeng, Y., Xiao, Y., Zeng, X., et al. (2020). Qualitative and Quantitative Analysis of B-Cell-Produced Antibodies in Vitreous Humor of Type 2 Diabetic Patients with Diabetic Retinopathy. *J. Diabetes Res.* 2020, 4631290. doi:10.1155/2020/4631290

Luttrull, J. K. (2020). Subthreshold Diode Micropulse Laser (SDM) for Persistent Macular Thickening and Limited Visual Acuity after Epiretinal Membrane Peeling. *Clin. Ophthalmol.* 14, 1177–1188. doi:10.2147/OPTH.S251429

Meireles, A., Goldsmith, C., El-Ghrably, I., Erginay, A., Habib, M., Pessoa, B., et al. (2017). Efficacy of 0.2 μg/day Fluocinolone Acetonide Implant (ILUVIEN) in Eyes with Diabetic Macular Edema and Prior Vitrectomy. *Eye (Lond)* 31, 684–690. doi:10.1038/eye.2016.303

Midena, E., Bini, S., Martini, F., Enrica, C., Pilotto, E., Micera, A., et al. (2020). Changes of Aqueous Humor Müller Cells' Biomarkers in Human Patients Affected by Diabetic Macular Edema after Subthreshold Micropulse Laser Treatment. *Retina* 40, 126–134. doi:10.1097/IAE.0000000000002356

Midena, E., Micera, A., Frizziero, L., Pilotto, E., Esposito, G., and Bini, S. (2019). Sub-threshold Micropulse Laser Treatment Reduces Inflammatory Biomarkers in Aqueous Humour of Diabetic Patients with Macular Edema. *Sci. Rep.* 9, 10034. doi:10.1038/s41598-019-46515-y

Midena, E., Torresin, T., Longhin, E., Midena, G., Pilotto, E., and Frizziero, L. (2021). Early Microvascular and Oscillatory Potentials Changes in Human Diabetic Retina: Amacrine Cells and the Intraretinal Neurovascular Crosstalk. *J. Clin. Med.* 10, 4035. doi:10.3390/jcm10184035

Ong, S. S., Walter, S. D., Chen, X., Thomas, A. S., Finn, A. P., and Fekrat, S. (2021). Bilateral Intravitreal 0.19-Mg Fluocinolone Acetonide Implant for Persistent Nondiabetic Cystoid Macular Edema after Vitrectomy. *Retin. Cases Brief. Rep.* 15, 261–265. doi:10.1097/ICB.0000000000000779

Ophir, A., Martinez, M. R., Mosqueda, P., and Trevino, A. (2010). Vitreous Traction and Epiretinal Membranes in Diabetic Macular Oedema Using Spectral-Domain Optical Coherence Tomography. *Eye (Lond)* 24, 1545–1553. doi:10.1038/eye.2010.80

Parodi Battaglia, M., Iacono, P., Cascavilla, M., Zucchiatti, I., and Bandello, F. (2018). A Pathogenetic Classification of Diabetic Macular Edema. *Ophthalmic Res.* 60, 23–28. doi:10.1159/000484350

Peng, Q., Hu, Y., Huang, M., Wu, Y., Zhong, P., Dong, X., et al. (2020). Retinal Neurovascular Impairment in Patients with Essential Hypertension: An Optical Coherence Tomography Angiography Study. *Invest. Ophthalmol. Vis. Sci.* 61 (8), 42. doi:10.1167/iovs.61.8.42

Pessoa, B., Coelho, J., Correia, N., Ferreira, N., Beirão, M., and Meireles, A. (2018). Fluocinolone Acetonide Intravitreal Implant 190 μg (ILUVIEN®) in

Vitrectomized versus Nonvitrectomized Eyes for the Treatment of Chronic Diabetic Macular Edema. *Ophthalmic Res.* 59, 68–75. doi:10.1159/000484091

Pessoa, B., Dias, D. A., Baptista, P., Coelho, C., Beirão, J. N. M., and Meireles, A. (2019). Vitrectomy Outcomes in Eyes with Tractional Diabetic Macular Edema. *Ophthalmic Res.* 61, 94–99. doi:10.1159/000489459

Reibaldi, M., Russo, A., Zagari, M., Toro, M., Grande De, V., Cifalinò, V., et al. (2012). Resolution of Persistent Cystoid Macular Edema Due to Central Retinal Vein Occlusion in a Vitrectomized Eye Following Intravitreal Implant of Dexamethasone 0.7 Mg. *Case Rep. Ophthalmol.* 3, 30–34. doi:10.1159/000336273

Sadiq, M. A., Soliman, M. K., Sarwar, S., Agarwal, A., Hanout, M., Demirel, S., et al. (2016). Effect of Vitreomacular Adhesion on Treatment Outcomes in the Ranibizumab for Edema of the Macula in Diabetes (READ-3) Study. *Ophthalmology* 123, 324–329. doi:10.1016/j.ophtha.2015.09.032

Sugita, S., Horie, S., Yamada, Y., and Mochizuki, M. (2010). Inhibition of B-Cell Activation by Retinal Pigment Epithelium. *Invest. Ophthalmol. Vis. Sci.* 51 (11), 5783–5788. doi:10.1167/iovs.09-5098

Thomas, D., Bunce, C., Moorman, C., and Laidlaw, A. H. (2005). Frequency and Associations of a Taut Thickened Posterior Hyaloid, Partial Vitreomacular Separation, and Subretinal Fluid in Patients with Diabetic Macular Edema. *Retina* 25, 883–888. doi:10.1097/00006982-200510000-00011

Verdina, T., D'Aloisio, R., Lazzerini, A., Ferrari, C., Valerio, E., Mastropasqua, R., et al. (2020). The Role of Subthreshold Micropulse Yellow Laser as an Alternative Option for the Treatment of Refractory Postoperative Cystoid Macular Edema. *J. Clin. Med.* 9, 1066. doi:10.3390/jcm9041066

Vié, A. L., Kodjikian, L., Malclès, A., Agard, E., Voirin, N., El Chehab, H., et al. (2017). Tolerance of Intravitreal Dexamethasone Implants in Patients with Ocular Hypertension or Open-Angle Glaucoma. *Retina* 37, 173–178. doi:10.1097/IAE.0000000000001114

Vujosevic, S., Gatti, V., Muraca, A., Brambilla, M., Villani, E., Nucci, P., et al. (2020). Optical Coherence Tomography Angiography Changes after Subthreshold Micropulse Yellow Laser in Diabetic Macular Edema. *Retina* 40, 312–321. doi:10.1097/IAE.0000000000002383

Wiest, M. R. J., Toro, M. D., Nowak, A., Baur, J., Fasler, K., Hamann, T., et al. (2021). Globotrioasylsphingosine Levels and Optical Coherence Tomography Angiography in Fabry Disease Patients. *J. Clin. Med.* 10, 1–12. doi:10.3390/jcm10051093

Yanyali, A., Horozoglu, F., Celik, E., and Nohutcu, A. F. (2007). Long-term Outcomes of Pars Plana Vitrectomy with Internal Limiting Membrane Removal in Diabetic Macular Edema. *Retina* 27, 557–566. doi:10.1097/01.iae.0000249390.61854.d5

Zeng, X., Hu, Y., Chen, Y., Lin, Z., Liang, Y., Liu, B., et al. (2021). Retinal Neurovascular Impairment in Non-diabetic and Non-dialytic Chronic Kidney Disease Patients. *Front. Neurosci.* 15, 703898. doi:10.3389/fnins.2021.703898

Conflict of Interest: The authors declare that the research was conducted in the absence of any commercial or financial relationships that could be construed as a potential conflict of interest.

Publisher's Note: All claims expressed in this article are solely those of the authors and do not necessarily represent those of their affiliated organizations, or those of the publisher, the editors, and the reviewers. Any product that may be evaluated in this article, or claim that may be made by its manufacturer, is not guaranteed or endorsed by the publisher.

Advantages of publishing in Frontiers

OPEN ACCESS
Articles are free to read for greatest visibility and readership

FAST PUBLICATION
Around 90 days from submission to decision

HIGH QUALITY PEER-REVIEW
Rigorous, collaborative, and constructive peer-review

TRANSPARENT PEER-REVIEW
Editors and reviewers acknowledged by name on published articles

Frontiers
Avenue du Tribunal-Fédéral 34
1005 Lausanne | Switzerland

Visit us: www.frontiersin.org
Contact us: frontiersin.org/about/contact

REPRODUCIBILITY OF RESEARCH
Support open data and methods to enhance research reproducibility

DIGITAL PUBLISHING
Articles designed for optimal readership across devices

FOLLOW US
@frontiersin

IMPACT METRICS
Advanced article metrics track visibility across digital media

EXTENSIVE PROMOTION
Marketing and promotion of impactful research

LOOP RESEARCH NETWORK
Our network increases your article's readership